

UNIVERSITÀ
DI TORINO

Department of Molecular Biotechnology and Health Sciences

PhD School in Molecular Medicine

XXXVI Cycle
Academic years 2020/2024

Evaluation of TLR2 targeting approaches for improvement of breast cancer therapies

Supervisors:
Prof. Federica Cavallo
Prof. Laura Conti

PhD Candidate:
Antonino Di Lorenzo

TABLE OF CONTENTS

Abstract **pag. 3**

INTRODUCTION **5**

1. Breast cancer 6

1.1 General overview 6

1.2 Risk factors 6

1.3 Diagnosis 8

1.4 Breast cancer subtypes 8

2. Breast cancer therapies 10

2.1 Clinical strategies 10

2.2 Chemotherapy and targeted therapies for breast cancer treatment 12

2.3 Breast cancer immunotherapy 13

2.4 Resistance to therapies 16

2.5 Tumor heterogeneity and cancer stem cells in resistance to therapies 19

3. Toll-like Receptor 2 (TLR2) 23

3.1 TLR2 in the immune system 23

3.2 TLR2 in the anti-tumor immune response 25

3.3 TLR2 in immunosuppression 26

3.4 Cancer-cell intrinsic pro-tumoral role of TLR2 27

AIMS OF THE THESIS **30**

RESULTS

Chapter I **33**

Investigating the role of TLR2 in breast cancer progression and resistance to chemotherapy

Paper I: Toll-like receptor 2 promotes breast cancer progression and resistance to chemotherapy 38

Chapter II **68**

Development and characterization of RGD-functionalized nanoparticles for the delivery of chemotherapy and TLR2 inhibitors

Paper II: RGD_PLGA nanoparticles with Docetaxel: a route for improving drug efficiency and reducing toxicity in breast cancer treatment 74

Chapter III **115**

Exploiting TLR2 inhibition to improve pharmacological and immunological breast cancer treatment

CONCLUSIONS **126**

MATERIALS AND METHODS **130**

REFERENCES **139**

List of publications related to this thesis **153**

List of publications not related to this thesis **154**

List of activities performed during the PhD program **154**

Acknowledgements **158**

Abstract

Breast cancer is the major cause of cancer-related death in women worldwide, despite substantial advancements in its diagnosis and treatment. Routine screening and improved therapeutic interventions have significantly enhanced early detection and survival rates. However, therapy resistance and poor outcomes persist, underscoring the urgent need for continued research to address these challenges.

Among the key contributors to therapy resistance, breast cancer stem cells (CSCs) have a crucial role. CSCs possess unique phenotypic plasticity, metabolic reprogramming, and resistance mechanisms, which makes them able to drive metastasis and evade conventional treatments. The aim of my thesis is to set up new therapies able to effectively target CSCs, thus overcoming therapy resistance.

Building on prior research by our group, this work explores the therapeutic targeting of Toll-like receptor 2 (TLR2), a molecule expressed in breast cancer and upregulated in breast CSCs. TLR2 plays a dual role in cancer progression, activating pro-tumorigenic pathways while promoting immune evasion. This thesis identifies a novel non-immunological role for TLR2 in breast cancer. Public dataset analyses revealed that high TLR2 expression correlates with poor prognosis and chemoresistance, establishing it as a promising therapeutic target. When activated by damage-associated molecular patterns (DAMPs) such as High Mobility Group Box 1 (HMGB1) within the tumor microenvironment, TLR2 triggers NF-κB signaling and induces pro-tumoral cytokine production. These cytokines establish cancer cell-intrinsic survival loops, drive neoangiogenesis, and recruit immunosuppressive cells such as regulatory T cells (Tregs). Furthermore, chemotherapeutic agents like doxorubicin inadvertently hyperactivate TLR2 via DAMPs release, exacerbating therapy resistance.

To counteract these effects, this thesis demonstrates the efficacy of TLR2 inhibition using the small molecule CU-CPT22. In preclinical models, TLR2 inhibition reverses doxorubicin resistance, enhances therapeutic efficacy, and synergistically reduces tumor progression and CSC frequency. To refine this approach, targeted nanoparticle-based drug delivery systems were developed. Poly lactic-co-glycolic acid (PLGA) nanoparticles encapsulating CU-CPT22 and liposomes delivering doxorubicin were coated with an integrin $\alpha_v\beta_3$-targeting cyclic Arg-Gly-Asp (RGD) tripeptide. This strategy enhances tumor-specific drug accumulation, while minimizing off-target effects, thus significantly reducing chemotherapy-associated toxicity.

Additionally, this thesis explores a multi-targeted approach by combining TLR2 inhibition and chemotherapy with a vaccination-based immunotherapy targeting xCT, a protein implicated in CSC

maintenance and metastasis. This combinatorial strategy exhibited remarkable therapeutic efficacy in preclinical models, aligning with emerging trends that integrate diverse pharmacological approaches. In conclusion, the findings presented in this thesis highlight TLR2 as a critical driver of breast cancer progression and resistance, providing a robust foundation for novel therapeutic interventions. The development of multi-disciplinary, multi-targeted strategies holds promise for improving breast cancer treatment and patient outcomes. Future research will extend the applicability of TLR2 and xCT targeting to other tumor types, advancing the clinical potential of this approach.

Introduction

1. Breast cancer

1.1 General overview

Breast cancer is the first cause of cancer in women and, every year, more than 1 in 10 women receive a diagnosis of breast cancer worldwide. Despite the mortality of breast cancer patients has been reduced thanks to the progresses in early diagnosis and in the therapeutic options, breast cancer remains the second cause of cancer death in women. Breast cancer normally evolves without evident symptoms. The presence of the malignancy is usually detected by specific screenings in western countries, or as a palpable mass in the breast [1].

The mammary glands contain cells that can produce milk and are structured in lobules. Different lobules form lobes dispersed in a fat tissue. The milk secreted by mammary cells is collected through lactiferous ducts that converge in the nipple [2]. Breast carcinogenesis mostly occurs in the ductal epithelium (ductal carcinoma) but, in some cases, can be developed also in the lobules (lobular carcinoma). Both ductal and lobular carcinoma can be *"in situ"*, when the tumor mass is localised in a specific area, or *"invasive"* if cancer cells easily spread to adjacent tissues, lymph nodes or other organs [1].

1.2 Risk factors

Several risk factors associated with an increased probability of developing breast cancer have been identified. Among them, the first two are surely gender and age. Indeed, women have higher chances than man of facing a breast cancer diagnosis during their life. This risk increases with age, and most breast cancer cases occur in women between the age of 50 and 69 years [3].

Besides gender and age, the other most common risk factors are personal and family history. Many women who already had breast cancer can receive a second diagnosis, even after several years from the first one, and the tumor can arise in the same or opposite breast. In addition, a history of breast or other types of cancer in the family can underline the presence of some inheritable risk factors and the susceptibility to the development of the disease [4,5].

Correlated to the last point, genetic predisposition to an increased risk of breast cancer exists. As for many types of cancer, also breast cancer can be caused by inherited mutations in specific genes. In breast cancer, only between 5 and 10% of the cases are caused by inherited genetic variations. There are two main genes involved in breast cancer regulation, named breast cancer 1 and 2 (BRCA1 and BRCA2). BRCA1 and BRCA2 are tumor suppressor genes that prevent breast cancer development.

Genetic mutations of these genes can cause their loss-of-function and an impaired ability of inhibiting tumor growth. These mutations are rare, as only 1 in 500 people inherit them. Women with inherited mutations in BRCA1 or BRCA2 genes have 85% risk of developing breast cancer during their life and compared to other women, the appearance of the tumor can occur earlier. BRCA gene mutations also predispose to the chance of having tumors in both breasts. In addition, women who carry BRCA mutations can be affected by ovarian cancer at any age [6].

The dimension of breasts and their density can play a role as risk factors. Women with larger and more dense breasts have a higher risk of developing breast cancer as compared to those with smaller and less dense breasts. Brest density is influenced by genetic factors and can be detected and analysed by mammograms. However, a dense breast tissue makes harder the interpretation of the results of mammography, since in this case the healthy tissue appears very similar to the tumor, thus limiting the possibility of early diagnosis [7].

Breast carcinogenesis is also influenced by the levels of hormones, in particular estrogen and progesterone. Normally, these hormones regulate several physiological processes in women. With age, ovaries stop their production, resulting in the arrest of menstrual cycle and the beginning of menopause. If this event occurs later than normal in women's life (after 55 years of age), the longer exposure to the hormones raises the possibility of breast cancer. Indeed, early menopause is associated with a lower risk of breast cancer due to shorter hormone exposure [8]. For the same reason of menopause, also pregnancy slightly decreases the risk of developing breast cancer, as the production of estrogen is discontinued during this period. Women with late or no pregnancies have a higher exposure of breast cells to estrogen, which marginally increases the risk of breast cancer. On the contrary, in women who had at least one pregnancy before 30 years, or more pregnancies during life, this risk is reduced [9].

Similarly to what happens for other diseases, obesity can increase the possibility of breast cancer onset. This is because fat tissue produces small amounts of estrogen. Therefore, even in post-menopausal women, a gain in the amount of fat tissues leads to prolonged estrogen exposure that can increase the risk of breast cancer [10]. Since estrogen is one of the main factors involved in the risk of breast cancer development, also exogenous estrogen sources can increase this risk. Hormonal replacement treatments or oral contraceptives, which can contain estrogen, are positively correlated to the risk of breast cancer [11,12].

1.3 Diagnosis

Breast cancer can be diagnosed through several methods. Usually, the diagnosis occurs during routine screenings or with specific analysis prompted by suspicion arisen during an initial clinical examination [1].

Mammography is the most common exam used for the screenings. It is a x-ray-based technique that uses low-energy radiations to produce an image of the breast tissue. Mammography allows to visualise the tumor mass inside the breast. Similarly, ultrasounds are high-frequency sound waves that can be used to discriminate between a solid tumor and a cyst or other non-malignant structures. Normally, mammography and echography are used together with biopsies to localise the primary tumor site or to identify the presence of metastases in woman with advanced breast cancer [13].

Despite imaging techniques and palpation are the first-line diagnostic exams, they allow only to detect the presence of abnormal masses in the breast. To obtain an accurate breast cancer diagnosis in case of suspect masses, bioptic analyses are required. Breast biopsies can be performed by collecting several tissue samples from different parts of the breast or from a specific area near the suspect tumor mass. Biopsies can be collected by vacuum aspiration or using the fine needle aspiration (FNA) technique. The latter enables the clinicians to isolate cancer cells from the primary tumor mass. These cells can be subsequently analysed to determine their main features and make a precise diagnosis of the breast cancer subtypes and the stage of the disease [3].

The identification of the breast cancer subtypes, and the stage of advancement is a crucial part of the diagnosis, as it provides not only some information about the possible prognosis but also indications about the therapeutic treatments that are required.

1.4 Breast cancer subtypes

Breast cancer is not a unique disease and due to its heterogeneity, different subtypes have been classified. The differences between the subtypes significantly influence the choice of the treatments and the clinical outcomes [14]. Normally, to identify the subtype and make a clear diagnosis, histological and molecular analysis of tumor biopsies are performed. The classification of the breast cancer subtypes is based on the expression of some specific markers. The most commonly used are the estrogen receptor (ER), the progesterone receptor (PR) and the human epidermal growth factor receptor 2 (HER2). According to the differential expression of these three receptors, breast cancer can be classified as Luminal A, Luminal B, HER2 positive and triple negative breast cancer (TNBC) [15].

Luminal A

Luminal A tumors are defined by the expression of ER and/or PR, the absence of HER2 expression, and low levels of the cell proliferation marker Ki-67 (below 20%). Luminal A constitutes the 80-90% of luminal tumors. From the clinical point of view, they are slow-growing tumors associated with the most favorable prognosis, a lower risk of recurrence, and higher survival rates. These carcinomas exhibit a strong response to hormone therapy (tamoxifen or aromatase inhibitors) but have limited response to chemotherapy [1,16]. Consequently, both the European Society for Medical Oncology (ESMO) and the National Comprehensive Cancer Network (NCCN) guidelines recommend the use of tools in this group to determine which patients might benefit from adjuvant chemotherapy, based on recurrence risk and survival rates. For instance, it is commonly used the ESMO-Magnitude of Clinical Benefit Scale (ESMO-MCBS), a validated platform that allows to evaluate anti-cancer therapies for solid tumors, assigning grades and predicting which therapeutic strategy can have higher chances of obtaining positive outcomes [17,18]. Recurrences are more commonly observed in the bone and rarely in visceral or central nervous system (CNS) [1,16].

Luminal B

Representing 10-20% of luminal tumors, luminal B tumors display moderately low ER expression alongside a high expression of genes associated with cell proliferation and the cell cycle, including Ki-67, while they can be PR-negative. Typically, these tumors are of intermediate to high histological grade. The elevated Ki-67 levels (greater than 20%) contribute to faster tumor growth and a worse overall prognosis compared to Luminal A tumors [19]. While responsive to hormonal treatments, they derive greater benefit from chemotherapy relative to Luminal A tumors, and therefore they are often treated with a combination of hormonal therapy and chemotherapy. Although bone metastases are common, these tumors exhibit a higher frequency of visceral recurrences, and the survival time from diagnosis to relapse is shorter than in luminal A cancers [1,16].

HER2 positive

The HER2-positive subgroup accounts for 10–15% of breast cancers and is defined by high levels of HER2 expression. These tumors exhibit faster growth rates and are more aggressive compared to luminal subtypes, though prognosis has significantly improved with the advent of HER2-targeted therapies. The HER2-positive group can be further divided into two subtypes: luminal HER2 (ER+,

PR+, HER2+, Ki-67: 15-30%) and HER2-enriched (HER2+, ER-, PR-, Ki-67: > 30%) [20]. These tumors have a less favourable prognosis than luminal subtypes and require specialized HER2-targeted treatments, such as the monoclonal antibodies Trastuzumab and Pertuzumab, the antibody-drug conjugate Trastuzumab-Emtansine (T-DM1), and tyrosine kinase inhibitors like Lapatinib and Neratinib. These therapies are typically combined with surgery and tailored chemotherapy regimens [21], to which HER2-positive tumors show a strong response. While bone metastases remain the most common site for disease dissemination, this subgroup also exhibits a higher incidence of visceral relapses compared to luminal tumors [1,16].

Triple negative

Triple-negative breast cancer (TNBC) is defined by the absence of ER, PR, and HER2 expression. This subtype accounts for approximately 20% of all breast cancers and is more prevalent in women under 40 and in African American women. Histologically, TNBC is a poorly differentiated and highly proliferative neoplasm with substantial heterogeneity, resulting in subsets with varying prognoses [1,16]. Immunohistochemically, TNBC is categorized into basal and non-basal types. Basal TNBC is characterized by the expression of cytokeratins (CK5/6) and epidermal growth factor receptor 1 (EGFR1), while non-basal TNBC lacks CK5/6 expression. According to the molecular profile, TNBC can be further divided into distinct subtypes, including basal-like (BL)1 and BL2, claudin-low, mesenchymal (MES), luminal androgen receptor (LAR), and immunomodulatory (IM). Among these, the basal-like subtypes are the most common, representing 50-70% of TNBC, followed by claudin-low (20-30% of TNBC) [22]. Each subtype exhibits unique phenotypes, clinical behaviors, and responses to therapy. TNBC is known for its aggressive nature, high proliferation rates, and early recurrence, often presenting in advanced stages. This subtype is marked by significant genomic instability and alterations in DNA repair genes. Around 80% of breast tumors associated with BRCA1 and BRCA2 mutations fall within this group. Several factors influence the risk of developing TNBC, including genetics, ethnicity, age, obesity and breastfeeding practices [1].

2. Breast cancer therapies

2.1 Clinical strategies

The treatment of breast cancer often requires multidisciplinary approaches and may differ depending on the tumor stage and subtype, and the available resources. Generally, therapeutic approaches to

breast cancer are categorized into three main types: treatment for early breast cancer, treatment for locally advanced breast cancer, and treatment for metastatic breast cancer [1].

Early breast cancer comprises tumors smaller than 5 cm and without lymph node metastases. In this case, the treatment includes surgery through partial mastectomy for breast conservation, where possible, or total mastectomy. The axillary lymph nodes are analyzed to assess the possible presence of micrometastases, and plan interventions if necessary. In case of hormone receptor (HR) positive tumors, patients will receive hormonal therapy, which is combined with neoadjuvant chemotherapy when the risk classification is high. All the HER2-positive patients receive HER2-targeted therapies, while TNBC patients only receive chemotherapy. Radiotherapy is used in neoadjuvant regimens to reduce the tumor bed in case of breast conservation surgery but is avoided if a complete mastectomy is performed. Recently, the use of chemotherapy before surgery, as a neoadjuvant therapy aimed at decreasing the tumor mass and targeting micrometastases, has been widely used in case of TNBC and HER-positive breast cancer, due to the benefits observed, especially for breast conservation approaches [23,24].

Locally advanced breast cancer (LABC) includes tumors bigger than 5 cm or with lymph node metastases. Tumor-positive lymph nodes are removed or treated with radiations, while the primary tumor is normally removed by surgery. However, breast conservation is not always possible in this clinical scenario due to the larger volume of the tumor and the possible involvement of the adjacent tissues. The use of systemic neoadjuvant chemotherapy is evaluated depending on several factors, such as type of tumor, age and physical condition. Also in this case, the aim of chemotherapy is to reduce the primary tumor mass and eliminate potential micrometastases before surgery interventions. In case of HR-positive tumors, hormonal therapy is always included in the treatment. After surgery, adjuvant radiotherapy, hormonal or targeted therapy, or chemotherapy are often used to decrease the risk of local or distal relapse. Taxane-based, non-anthracycline regimens are used for lower-risk disease, and anthracyclines are included in regimens that target TNBC with lymph node involvement [1].

Metastatic breast cancer is managed differently from the previously described types. In this case, surgery is avoided most of the times. Depending on the molecular profile of the tumor, the treatment options can include chemotherapy, hormonal therapies, targeted therapies and immunotherapies. Radiotherapy is used to control the symptoms and the metastatic spreading. The median survival rate for patients with metastatic breast cancer has improved over the past decades thanks to advances in

therapies. However, the disease is rarely curable, and most therapeutic interventions are just palliatives, with a median survival time of 24-40 months from diagnosis [25].

2.2 Chemotherapy and targeted therapies for breast cancer treatment

As mentioned in the previous section, there is a large variety of systemic therapies that are currently used to treat breast cancer. The choice of the drugs and of the therapeutic approaches strictly depends on specific aspects, like the tumor molecular subtype and the stage [1].

Chemotherapy is largely used as adjuvant and neoadjuvant therapy. Tumors that are poorly differentiated and highly proliferating, such as HER2-positive and TNBC, are the most sensitive to chemotherapy [26]. One of the first adjuvant treatments to be developed was a combination of cyclophosphamide, methotrexate, and 5-fluorouracil (CMF). Currently, the first-line treatment is constituted by anthracyclines (i.e. doxorubicin or epirubicin) or taxanes, such as docetaxel, combined with other drugs. An example is the Taxotere, Adriamycin, and Cyclophosphamide (TAC) regimen composed by docetaxel, doxorubicin and cyclophosphamide [27,28].

HR-positive breast cancer patients will primarily benefit from hormonal therapy. In particular, ER inhibitors (i.e. tamoxifen) or aromatase inhibitors (i.e. exemestane and letrozole) are the most common. Hormonal therapies limit the risk of breast cancer recurrence and are indicated for up to 10 years after surgery [29].

During the last decades, several drugs have been developed to target specific molecules in cancer cells. The use of targeted therapies for breast cancer is rapidly increasing due to the benefits observed in clinics. For instance, the treatment of HER2-positive breast cancer has made great strides after the introduction of anti-HER2 therapies. The first approved drug was Trastuzumab, a monoclonal antibody that targets the HER2 protein. The combination of Trastuzumab and chemotherapy for HER2-positive, early breast cancer reduces by 52% the risk of recurrence and by 33% the risk of death as compared to chemotherapy alone. Recently, the dual blocking of HER2 using Trastuzumab and Pertuzumab, another monoclonal antibody against HER2, has been proposed to improve the response to therapy [1,30,31].
Small molecule inhibitors, such as Olaparib and Talazoparib, are used to inhibit the activation of the DNA repair enzyme poly (ADP-ribose) polymerase (PARP) and thus increase cell death. PARP inhibitors are mainly used as adjuvant therapy in patients with BRCA mutations and HER2-negative

breast cancer, which are more sensitive to this treatment as they display vulnerabilities in DNA repair mechanisms [32].

Cyclin-dependent kinases 4 and 6 (CDK4/6) inhibitors, such as Palbociclib, act by targeting the CDK4/6 proteins responsible for driving cell division. Blocking this pathway enhances tumor cell destruction, particularly in HR-positive, HER2-negative cancers. These inhibitors are approved for use in metastatic HR-positive, HER2-negative cancers and are also considered for specific patients with early-stage HR-positive tumors [33].

2.3 Breast cancer immunotherapy

Immunotherapy has entered the clinical practice for breast cancer patients as early as 1998, with the FDA-approval of Trastuzumab, followed by other HER2 targeting antibodies. Besides these passive immunotherapies, active immunotherapy has been extensively studied.

Indeed, throughout the evolutionary trajectory of a tumor, a complex and dynamic interplay is established between tumor cells and the cells within the tumor microenvironment (TME), which contributes to shaping several hallmark characteristics of cancer. A critical aspect of this interaction is the specific role played by various immune cell types, which form an intricate communication network with cancer cells. In this context, tumor immunoediting mediated by innate and adaptive immune cell populations in the TME plays a pivotal role in influencing tumor progression [34]. Immunoediting is a dynamic process occurring in three distinct phases: Elimination, Equilibrium, and Escape. The initial phase, Elimination, also referred to as immunosurveillance, involves the destruction of transformed cells by a fully functional immune system capable of mounting a robust anti-cancer response. In the subsequent Equilibrium phase, tumor cells that survived Elimination interact with immune cells, leading to reciprocal shaping. This phase establishes a balance between the tumor and the immune system, exerting selection pressure on tumor cells, which are inherently genetically unstable and prone to rapid mutation. Tumor cell variants that acquire resistance to immune-mediated destruction progress to the Escape phase, the final step in the process. During this phase, the tumor proliferates uncontrollably and becomes clinically evident, accompanied by the establishment of a progressively immunosuppressive TME [35].

Based on their roles in the immunoediting process, immune cells can be broadly categorized into two major groups: immunosuppressive and immunostimulating cells. Evidence indicates that the composition of these immune cell populations within the TME significantly influences breast cancer progression and treatment outcomes. Notably, the infiltration of tumors by immunostimulating cells,

including certain macrophages, lymphocytes, natural killer (NK) cells, innate lymphoid cells (ILCs), dendritic cells (DCs), and eosinophils, is critical for tumor suppression. However, the anti-cancer immune response mediated by these cells is counteracted by immunosuppressive cells, such as myeloid-derived suppressor cells (MDSCs), regulatory T cells (Tregs), mast cells (MCs), and type 2-polarized tumor-associated macrophages (M2-like TAMs), which are intrinsically linked to the evolving TME [36] (Fig. 1). Moreover, the presence of an immunosuppressive TME can impair the effector function of T cells, rendering them exhausted. Thus, reverting the immunosuppressive function of the TME by means of immunotherapy would impair tumor progression [34].

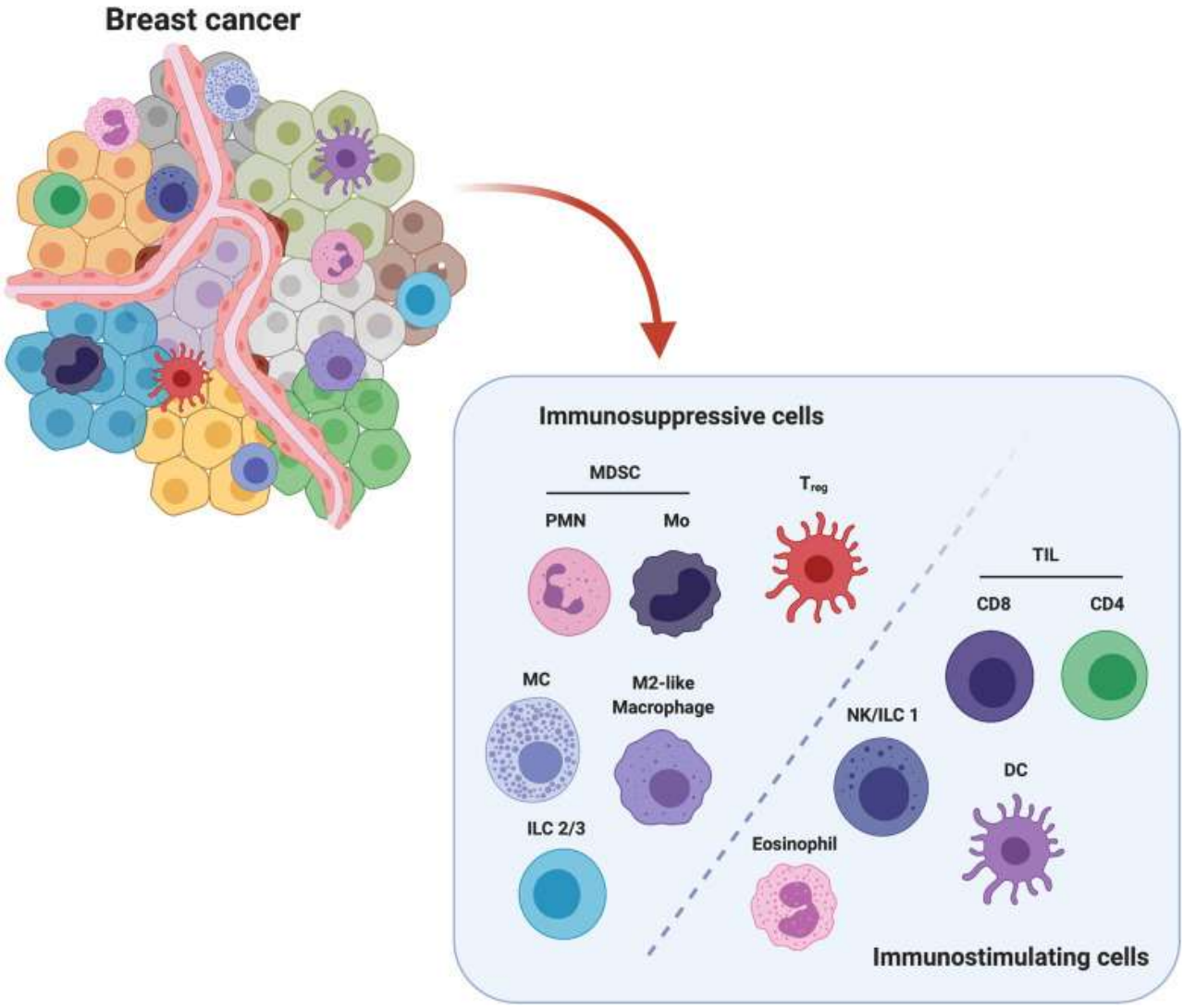


Figure 1. Major components of the tumor immune ecosystem. Principal immune cell populations in the breast tumor microenvironment (TME) include those with immunosuppressive and anti-tumor roles. Among the immunosuppressive cells are polymorphonuclear (PMN) and monocytic (Mo) myeloid-derived suppressor cells (MDSCs), mast cells (MCs), type 2 and 3 innate lymphoid cells (ILC2/3), M2-like tumor-associated macrophages (TAMs), and FoxP3+ regulatory T cells (Tregs). Conversely, cells such as tumor-infiltrating CD4+ and CD8+ lymphocytes (TILs), natural killer (NK) cells

or type 1 innate lymphoid cells (ILC1), dendritic cells (DCs), and eosinophils are linked to anti-tumor activity. (Vincenzo Salemme et al., Front. Oncol. 2021) [34]

According to their immune state, tumors can be defined as “cold” or “hot”. Cold tumors have high levels of immune suppressive cells and low or totally absent infiltration of T cells, which are confined to the tumor periphery or completely excluded. Hot tumors, instead, have high mutational burden, T cell infiltration and programmed death-ligand 1 (PD-L1) expression. PD-L1 is an immune checkpoint, a class of molecules that block the immune response. In particular, PD-L1 is the ligand for the receptor programmed cell death 1 (PD-1) expressed by exhausted T cells. This axis suppresses T cell activity by inhibiting their effector function. In the last years, a new class of immunotherapies, called immune checkpoint inhibitors (ICI), has been developed. ICI are monoclonal antibodies that block immunosuppressive receptors or their ligands, such as PD-1, PD-L1, and cytotoxic T-lymphocyte–associated protein 4 (CTLA-4), in order to unleash the anti-tumor immune response. Due to their high PD-L1 expression and the presence of intratumor T lymphocytes, hot tumors are the best responders to ICI, while cold tumors are often poorly sensitive [37]. Although breast cancer is often a cold tumor, in the last years the use of the anti-PD-1 monoclonal antibodies Pembrolizumab and Nivolumab has been introduced for the treatment of TNBC and HER2-positive breast cancer patients in combination with chemotherapy or Trastuzumab, respectively [1,38]. These combination therapies have shown promising results, improving therapy response rate in metastatic breast cancer patients [38]. Moreover, recent clinical trials have demonstrated the efficacy of ICI as neoadjuvant therapy in early-stage TNBC and HER2-positive breast cancer with a sufficient safety. However, less promising results were obtained in the adjuvant setting, suggesting that the use of ICI has some limitations and that their benefits may be dependent on the specific clinical contexts [39].

If several immunotherapeutic approaches for breast cancer treatment have been successful, others unfortunately have not yet obtained great results, despite the initial enthusiasm. Breast cancer vaccines are part of this last category. The principle of vaccination against cancer is to revert the immune suppressive environment created by the tumor into an immune permissive one. The vaccination against specific tumor antigens is supposed to elicit an immune response directed towards cancer cells. While theoretically this approach seems strongly promising, practically the many pre-clinical and clinical studies have indicated how difficult is to obtain encouraging results using this strategy [40]. For instance, after the advent of HER2-targeted therapies, different vaccines against HER2 were developed and tested. Many of these vaccines were based on HER2-derived peptides with immunogenic properties. However, poor results were obtained. HER2 vaccines were also tested

in HER2-low and TNBC, with no significant results. This also reflected some sort of confusion among the clinicians and a kind of frustration due to the inability to finding effective tools for the treatment of TNBC and metastatic breast cancer [38]. Other types of vaccines are based on DCs pulsed with cancer cell lysates or with tumor peptides. Some of them have shown minimal activity and others are currently under clinical trial. Besides these, a few other attempts have been made using DNA vaccines against one or more tumor antigens. Some of these studies are currently on going [41]. During the past years, also our group has developed and tested different types of DNA vaccination platforms, obtaining promising results in pre-clinical models of breast cancer [42–46]. In particular, one of these vaccines, utilizing a viral vector platform [43], was employed in a portion of the experiments detailed in Chapter III of this Thesis.
In the next few years, the combination of anti-cancer vaccines with ICI is expected to improve the efficacy of the single treatments, hopefully ameliorating breast cancer patients' prognosis.

Another type of immunotherapy that is increasingly studied in virtue of its promising therapeutic potential is the adoptive cell therapy. This strategy consists in the isolation of T cells from a patient and their modification, activation and expansion before they are reinfused into the patient [38]. CAR-T cells are an example of adoptive cell therapies. This strategy involves the genetic modification of T lymphocytes to express a chimeric antigen receptor (CAR). The CAR is engineered to recognize a specific antigen expressed by cancer cells and produce an intracellular signal transduction that activates the T cell response against the tumor. CAR-T cells are currently used for haematological malignancies with good results. Currently, some studies are focused on the development of CAR-T targeting antigens expressed by solid tumors, including breast cancer [47]. However, this approach presents some limitations such as the development of resistance, the toxicity due to adverse immune reactions, the complexity of the manufacturing process and its elevated costs [38,47].
Altogether, although data from the literature and clinical practice offer definitive evidence that immunotherapy is efficacious for a subset of breast cancer patients, they also highlight the need to develop new combination strategies for patients who have metastatic breast cancer endowed with low immunogenicity.

2.4 Resistance to therapies

In cancer, up to 90% of fatalities are attributed to drug resistance [48]. Multidrug resistance (MDR) significantly reduces the effectiveness of chemotherapeutic drugs, often leading to cancer relapse and metastasis. Both intrinsic and acquired resistance contribute equally to cases of drug resistance, with

each accounting for approximately 50% of affected patients. Intrinsic resistance, present before treatment begins, can arise from factors such as genetic mutations, the presence of pre-existing drug-insensitive subpopulations like cancer stem cells (see next section), and the activation of natural defence mechanisms against toxic substances. In contrast, acquired resistance develops post-treatment and may involve the activation of proto-oncogenes, alterations in gene expression driven by mutations or epigenetic changes, and modifications in the TME. In breast cancer, resistance mechanisms include increased drug efflux, improved DNA repair capabilities, escape from senescence, epigenetic changes, tumor heterogeneity, shifts in the TME, and epithelial-to-mesenchymal transition (EMT) [49].

A major cause of chemotherapy resistance is the reduced intracellular accumulation of drugs caused by increased drug efflux [50]. This phenomenon is mostly mediated by the ATP-binding cassette (ABC) transporters family members [51]. The ABCB1 gene is typically expressed in normal tissues but is overexpressed in various cancers, including breast, kidney, colon, and others. In breast cancer, paclitaxel-resistant tumor cells show high ABCB1 expression, and silencing this gene partially restores sensitivity to the drug; on the other hand, epigenetic mechanisms, such as CpG island hypermethylation in the ABCB1 promoter, are associated with lower ABCB1 expression and improved survival in breast (and ovarian) cancer patients [49].

Many cancer therapies, including cisplatin, 5-fluorouracil, gemcitabine, and methotrexate, work by inducing DNA damage. However, the DNA damage response (DDR) can repair these lesions, contributing to treatment resistance. Targeting key components of the DDR pathway offers a promising strategy to overcome resistance. As mentioned in the previous sections, PARP, a critical enzyme in DDR, has been effectively targeted using PARP inhibitors, particularly for the treatment of BRCA-deficient tumors, highlighting the potential of novel DNA repair protein inhibitors [52,53]. Unfortunately, also PARP inhibitors can be subjected to drug resistance [54]. A way to overcome this issue is to use drugs targeting different actors in the DDR, such as DNA repair kinases inhibitors. However, DDR is fundamental for the maintenance of genomic stability. Therefore, targeting DDR can be complex, and more specific inhibitors are required to limit the adverse effects on healthy tissues [49].

Besides mutations in the drug target proteins, acquired resistance to targeted therapies can arise from changes in their expression levels driven by epigenetic modifications. These mechanisms can include CpG hypermethylation to silence a gene - as in the case of the ABCB1 promoter - or hypomethylations

to overexpress an oncogene, histone modifications and changing in non-coding RNA expression [53]. For example, demethylation in oncogene promoter regions can increase gene expression, contributing to resistance, while hypermethylation of DNA repair genes can inhibit cell cycle arrest. Tamoxifen, a widely used therapy for ER-positive breast cancer, often encounters resistance. This resistance, which varies among patients, is frequently associated with reduced ER expression caused by mutations or epigenetic changes [55]. MicroRNAs (miRNAs) are small non-coding RNAs that act as epigenetic regulators by modulating gene expression through post-transcriptional modifications. In breast cancer, miRNAs such as miRNA-27b-3p, miRNA-21, and miRNA-134 contribute to drug resistance by affecting genes involved in resistance mechanisms, cell cycle regulation, cell proliferation, and apoptosis [49,53].

Besides cancer cell-intrinsic factors, also the TME can contribute to drug resistance. Hypoxia, a key feature of the TME, plays a crucial role in cancer progression by driving mechanisms such as angiogenesis, drug efflux through increased ABCC1 and ABCG2 expression, senescence modulation, apoptosis resistance, metastasis, and genomic instability. Hypoxia triggers the production of hypoxia-induced factors (HIFs), transcription factors that mediate responses to low oxygen levels. In particular, HIF-1 promotes EMT, typical of TNBC. Additionally, HIF-1α is implicated in drug resistance in ER-positive breast cancer cell lines [56,57]. Hypoxia can also contribute to drug resistance by creating a "reversed pH gradient," where cancer cells develop a more acidic extracellular environment (pH 6.5–7.1) compared to normal tissues. This acidic environment causes ion trapping of weak-base anticancer drugs, reducing their distribution and effectiveness. Therapeutic strategies such as proton pump inhibitors, which increase extracellular pH, have been explored as potential solutions to overcome this resistance [49].

Furthermore, cancer cells can express receptors, normally present in healthy tissues, which can detect a variety of ligands present in the TME. In particular, many molecules released after chemo- and radiotherapy activate signaling pathways, like that of the nuclear factor kappa B (NF-κB), responsible to produce growth factors and cytokines, such as transforming growth factor-beta (TGF-β), IL-6 and vascular endothelial growth factor (VEGF), that in turns upregulate several pro-tumoral pathways. These pathways can confer to the tumor higher resistance to therapy-induced apoptosis, increased invasive properties and promote phenotyping changes of cancer cells that facilitates their escape from immune surveillance and anti-cancer therapies [58]. These mechanisms will be further described in the following parts of this Thesis.

Despite HER2-positive tumors have been generally associated with a poor prognosis, the development of targeted therapies has given a new hope for patients affected by these tumors. However, patients often have recurrences due to acquired resistance [49]. Resistance to HER2-targeted therapies can occur through mechanisms like mutations or alterations that reduce the capability of the drugs to bind to HER2 or to induce its downregulation, disruptions in apoptosis and cell cycle regulation, and upregulation of alternative growth factor receptors or signaling pathways. Indeed, several studies have demonstrated that resistance to anti-HER2 therapies can be caused by an increased expression of CDK4/6-cyclin D1. Thus, the use of CDK4/6 inhibitors restores breast cancer sensitivity to anti-HER2 therapy [59,60]. Moreover, in aggressive forms of breast cancer and other type of tumors, constitutive or acquired expression of different tyrosine kinase receptors is often present. This leads to dysregulation or hyperactivation of PI3K/AKT/mTOR, Ras and MAPK pathways, which can promote cancer resistance to various therapies, including anti-HER2 treatments in case of HER2-positive breast cancer [49].

Additionally, immunodeficiency can play a critical role in therapy resistance. For instance, some genetic defects that alter NK cell activity can significantly limit the efficacy of Trastuzumab by weakening antibody-dependent cellular cytotoxicity (ADCC), one of its main mechanisms of action [61].

New strategies able to overcome resistance mechanisms and optimize therapeutic outcomes are urgently needed.

2.5 Tumor heterogeneity and cancer stem cells in resistance to therapies

In all tumors, including breast cancers, the population of cancer cells constituting the tumor mass is far to be homogeneous. It is instead a mosaic of various subclonal populations that exhibit significant differences in their genetic, epigenetic and biological characteristics. This well-known phenomenon is defined as tumor heterogeneity and represents the main reason for failure of cancer therapies. Indeed, the complete eradication of a tumor is limited by the fact that some subpopulations of cancer cells may be less responsive than others to a certain therapy. Moreover, cancer cells are able to rapidly evolve to counteract adverse stimuli. This means that therapies themselves can exert a selection of the more resistant cancer cells, which can cause tumor recurrence [49,62].

A crucial role in tumor heterogeneity, survival and therapy resistance is played by a particular population of cancer cells called cancer stem cells (CSCs). CSCs exhibit self-renewal properties, the ability to escape therapies through several mechanisms, and the capability to give rise to metastases [62] (Fig. 2).

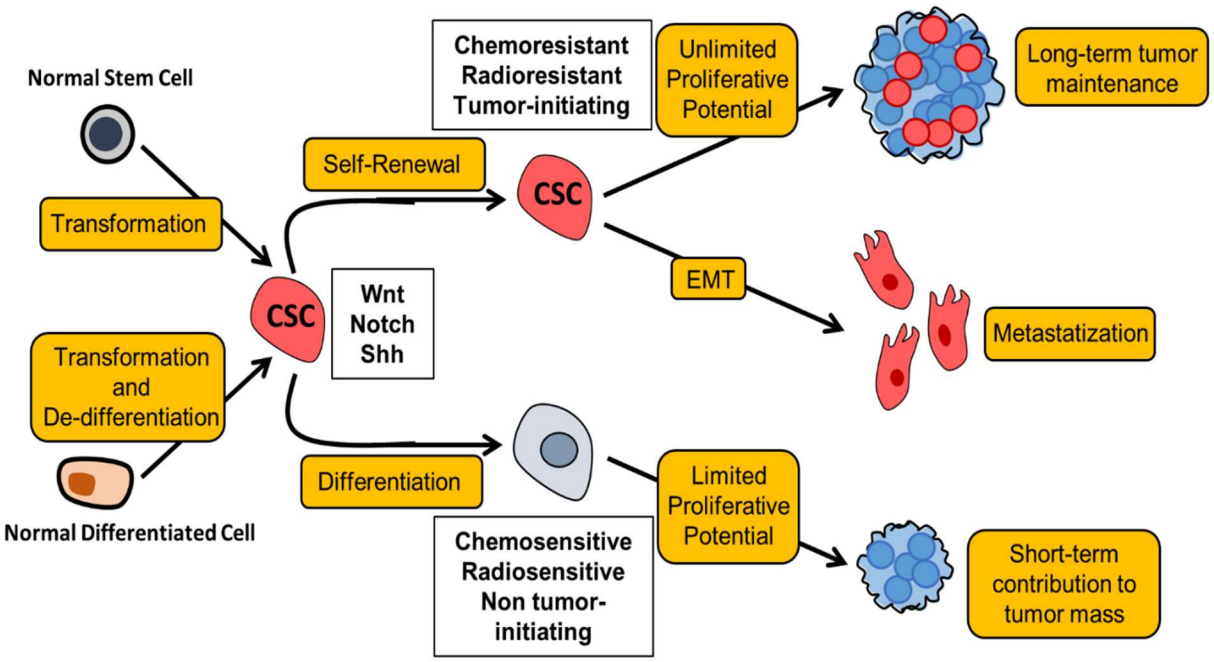


Figure 2. Main features of CSCs. CSCs can originate from either the malignant transformation of normal stem cells or differentiated cells that acquire stem cell-like properties. The activation of signaling pathways such as Notch, Sonic Hedgehog (Shh), and Wnt grants CSCs the ability to self-renew over long periods and differentiate into the diverse populations that comprise a tumor. CSCs, which are resistant to chemotherapy and radiation, possess unlimited proliferative capacity, enabling sustained tumor growth. These cells can also undergo epithelial-to-mesenchymal transition (EMT), contributing to metastasis. In contrast, differentiated cells are more sensitive to chemotherapy and radiation, exhibit limited proliferative capacity, and lack the ability to initiate tumors. (Roberto Ruiu et al. Prog Mol Biol Transl Sci 2019) [63]

For instance, chemotherapy can push some cancer cells towards senescence (a state of irreversible growth arrest) or dormancy (a temporary quiescent state) conditions by arresting their cell cycle in the G0 phase. These states allow cancer cells to evade the effects of chemo- and radiotherapy, which mainly target proliferating cells. In addition, chemotherapy can promote the acquisition of CSC properties, which contribute to tumor progression [64–66]. CSCs can mediate many of the previously described mechanisms of therapy resistance. For example, CSCs can upregulate ABC transporters, and ABCG2 is considered a marker of CSCs. This is particularly frequent in TNBC [62].

Moreover, cancer cells often exploit EMT to be more resistant to therapies and promote metastases. During EMT, the epithelial phenotype is lost through downregulation of E-cadherin and other cell-cell adhesion molecules. EMT makes cancer cells resistant to apoptosis and increases their invasiveness [57]. It is still not fully understood what triggers EMT, but it seems that CSCs can promote this process through the activation of specific pathways, such as the Wnt/β-catenin [56]. Wnt signaling is active in embryonic development and regulates a few normal functions in adult

individuals. In normal tissues, Wnt regulates stemness [67]. In breast cancer, this pathway is known to promote EMT and cancer cell migration through the upregulation of Twist [68]. Twist and Snail, another common EMT factor, upregulate the CSC markers [69]. Additional Wnt targets, including ABCB1, CD44, CD24, and CD133 are linked to CSC properties and therapy resistance [70–72]. Of note, it has been shown that the Wnt pathway can be constitutively active in TNBC and HER2-positive breast cancer, which therefore result enriched in CSCs [73].

The complex role of CSCs in tumor progression highlights their significance as a major challenge in the treatment of breast cancer. Therefore, effective therapies must successfully target and eradicate this population. To achieve this, numerous studies have been conducted to better understand the biology and the specific markers of breast CSCs, with the aim of identifying potential therapeutic targets to enhance breast cancer treatments.

Over the years, our group has dedicated substantial effort to this objective. Specifically, a pipeline to identify and characterize genes differentially expressed in breast CSCs was developed. High-throughput transcription analyses were performed on various human and murine mammary cancer cell lines to characterize the transcription profile of CSCs. As CSCs can be enriched by culturing cells under non-adherent conditions and in the absence of serum, conditions that lead to the generation of multicellular spheroids called tumorspheres, the gene expression profiles of cells cultured in standard 2D conditions and of tumorspheres were compared to identify a gene expression signature characteristic of breast CSCs [45,74] (Fig. 3).

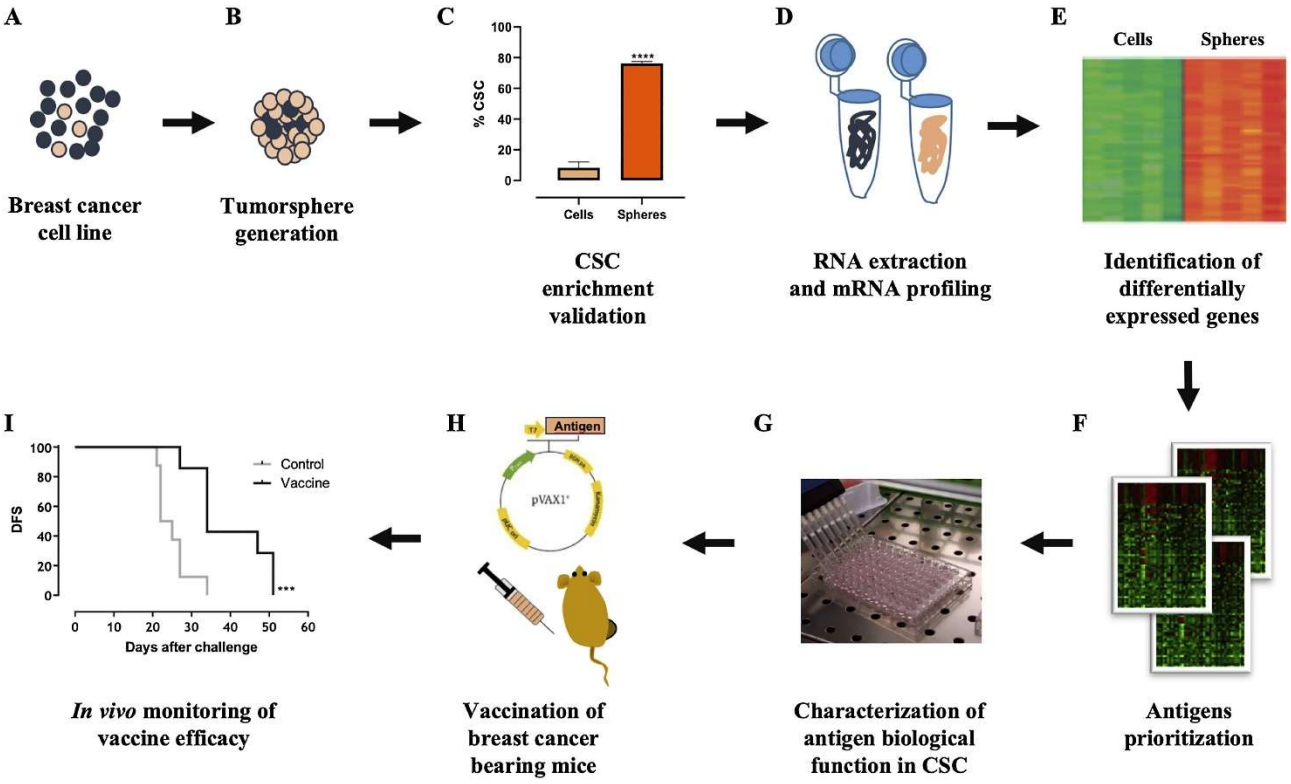


Figure 3. Workflow for breast CSC antigens identification. Culture of breast cancer cell lines as epithelial monolayers (A) or as tumorspheres (B), enriched with cancer stem cells (CSCs), as confirmed by flow cytometric analysis of various CSC markers (C). A high-throughput transcriptomic analysis is conducted on both breast cancer cells and tumorspheres (D), leading to the identification of differentially expressed genes (E). Genes with increased expression in tumorspheres are considered potential BCSC-associated antigens and are prioritized based on their correlation with poor prognosis in breast cancer patients using public datasets (F). The most promising antigens are validated through in vitro experiments to confirm their relevance to CSC biology (G). Subsequently, mammary tumor-bearing mice are immunized with DNA vaccines targeting these selected antigens (H), and their therapeutic effects are evaluated (I). (Adopted from Elena Quaglino et al. Semin Immunol. 2020) [75]

Of the transcripts upregulated in CSCs, only those that have an orthologue in humans, low expression in normal human tissues, and whose high expression is linked to poor prognosis in breast cancer patients were selected as putative targets for CSCs elimination. They were then validated by testing their role in CSC survival and self-renewal *in vitro* and *in vivo*. Among the genes upregulated in CSCs, we focused on Toll-like Receptor 2 (TLR2) due to its functional relevance and potential as therapeutic target for breast cancer [75]. TLR2 is the primary focus of this Thesis, and the following section will provide an introduction and a detailed description of this receptor and its functions.

The same transcriptional analysis revealed another upregulated gene of potential interest, SLC7A11, coding for the cystine/glutamate antiporter xCT. A detailed discussion on its role in breast cancer and its relevance to this research will be presented in Chapter III.

3. Toll-like Receptor 2

3.1 TLR2 in the immune system

TLR2, as some other members of the TLR family, was identified and characterized for the first time in 1998 [76]. TLRs are the mammalian homologous of the Toll receptor, previously discovered in Drosophila. Both Toll and TLRs are an ancient and evolutionary conserved mechanism of defence against microbial infections [58,77].
In mammals, TLRs are part of a larger receptor class called Pattern Recognition Receptors (PRRs) [78]. PRRs are a fundamental component of the innate immune system. They are transmembrane proteins located on cellular and endosomal membranes or within the cytoplasm. PRRs detect pathogen-associated molecular patterns (PAMPs), which are common molecular signatures of pathogens. This recognition activates intracellular signaling cascades that stimulate the production of inflammatory cytokines, type I interferons (IFNs), and other mediators. These responses play a crucial role in initiating inflammation, modulating adaptive immunity, and promoting elimination of the pathogens [79]. In addition to recognizing PAMPs, PRRs also play a critical role in detecting damage-associated molecular patterns (DAMPs), a concept first introduced by Polly Matzinger in her "Danger Theory." Matzinger proposed that tissue stress or damage leads to the release or activation of endogenous molecules that trigger an inflammatory response. This process enhances the activity of antigen-presenting cells, thereby facilitating the activation of the adaptive immune system [80]. Additionally, the innate immune system can sense, through PRRs, disruptions in cellular homeostasis caused by infections or other pathological conditions by recognizing homeostasis-altering molecular processes (HAMPs) [81].

Up to now, 10 human and 13 murine TLRs have been identified. They are expressed by all the innate immune cells and can also be expressed by T and B lymphocytes. Surprisingly, TLR expression is not confined to the immune system. Indeed, they are present in a large variety of tissues across the different organs and are expressed by different types of cells, such as epithelial and endothelial cells and fibroblasts. TLRs are distributed between the extracellular membrane and the intracellular compartments, depending on their affinity for the different ligands. In particular, TLRs on the extracellular membrane recognize proteins and lipids belonging to the microbial world, and tissue components that are exposed in the extracellular environment after tissue damage. Intracellular TLRs detect nucleic acids deriving from viral or bacterial infections. Once activated, TLRs can trigger two different intracellular pathways that promote inflammation and immune response. One is the myeloid

differentiation primary response protein 88 (MyD88)-dependent, and the other is the toll-interleukin 1 receptor (TIR) domain containing adaptor inducing IFN-β (TRIF)-dependent pathway. These signaling pathways converge on key transcription factors, including MAPK, activating protein-1 (AP-1), (NF-κB), and interferon regulatory factors (IRFs). Their activation ultimately drives the production of pro-inflammatory cytokines such as tumor necrosis factor-alpha (TNF-α), interleukin-1β (IL-1β), and IL-6; type I IFNs; chemokines like CXCL8 and CXCL10; and antimicrobial peptides. Most TLRs rely on the MyD88-dependent pathway to stimulate inflammatory cytokine production, while the TRIF-dependent pathway, utilized by TLR3 and TLR4, primarily promotes the production of type I IFNs [58] (Fig. 4).

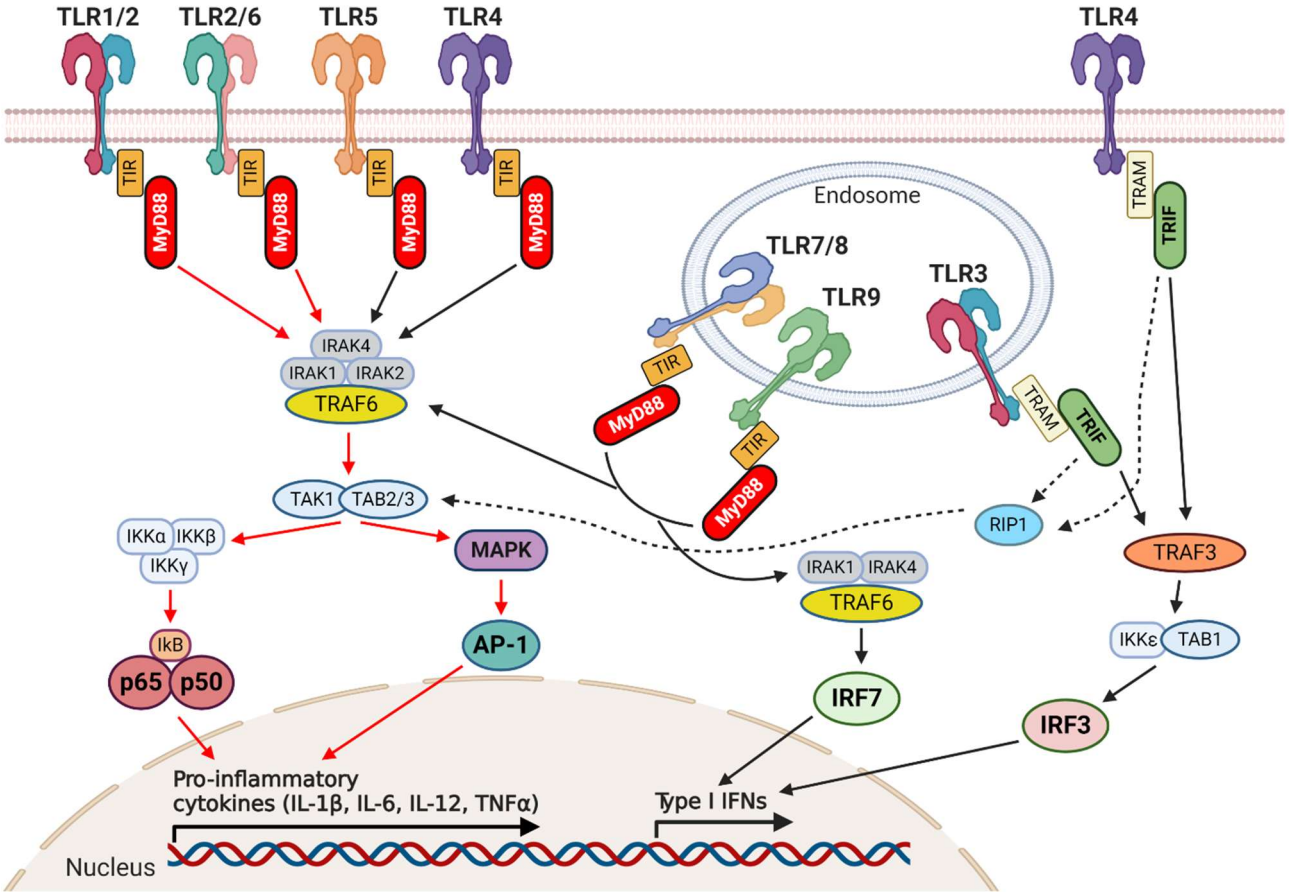


Figure 4. TLRs cellular localization and signaling pathways. Toll-like receptors (TLRs) are strategically located to detect specific pathogen-associated molecular patterns (PAMPs) and damage-associated molecular patterns (DAMPs). TLR2, along with TLR1, TLR4, TLR5, and TLR6, is expressed on the external cellular membrane, where it recognizes extracellular PAMPs/DAMPs. In contrast, TLR3, TLR7, TLR8, and TLR9 reside within endosomal compartments, where they interact with nucleic acids. All TLRs, except TLR3, signal through the myeloid differentiation primary response protein 88 (MyD88) pathway. TLR3 exclusively relies on the TIR-domain-containing adapter-inducing IFN-β (TRIF) pathway for signal transduction. TLR2 dimers, indicated by red arrows, initiate the canonical MyD88-dependent pathway, recruiting the IL-1 receptor-associated kinase (IRAK) complex and TNF receptor-associated factor (TRAF)6. This leads to the activation of nuclear factor kappa-light-chain-enhancer of activated B cells (NF-κB), mitogen-activated protein

kinase (MAPK), and activating protein-1 (AP-1), promoting the production of pro-inflammatory cytokines. Intracellular TLRs predominantly contribute to type I interferon responses. TLR7, TLR8, and TLR9 activate interferon regulatory factor 7 (IRF7) through the recruitment of IRAK and TRAF6. Since these intracellular TLRs utilize the MyD88 pathway, they can also activate the canonical signaling cascade. Meanwhile, the TRIF-dependent pathway, engaged by TLR3 and, in certain cases, TLR4, activates TRAF3, subsequently inducing interferon regulatory factor 3 (IRF3). This results in type I interferon (IFN) production. The schematic employs red arrows to denote TLR2-specific signaling, while black and dashed arrows indicate other TLR signaling pathways. All arrows represent activation events. (Antonino Di Lorenzo et al. Int. J. Mol. Sci. 2020) [58]

TLR2 is the only TLR able to form functional heterodimers with multiple other TLRs, including TLR1, TLR6, and occasionally TLR4 and TLR10. Additionally, TLR2 interacts with various non-TLR molecules, enabling it to detect a wide range of PAMPs across microbial groups, including viruses, fungi, bacteria, and parasites. Notably, TLR2 recognizes conserved lipoproteins found on the outer membranes of Gram-positive bacteria and, in coordination with its co-receptor CD14, can also identify membrane antigens of certain Gram-negative bacteria, such as lipopolysaccharide (LPS). Regardless of the specific dimerization partner, the resulting downstream signaling is mediated through the MyD88-dependent pathway, culminating in cytokine production [82].
TLR2 is expressed by various cell types, including immune cells, endothelial cells, and epithelial cells. This broad expression pattern highlights the diverse TLR2's roles and functions in immune response and pathogen recognition [83]. TLR2 signaling plays a dual role in maintaining mucosal homeostasis and defending against pathogens. Nevertheless, TLR2 stimulation by certain pathogens or some endogenous ligands can have opposite effects potentially exacerbating infectious and inflammatory diseases. Moreover, TLR2 mediates critical interactions between hosts and the microbiota, supporting tissue health. TLR2 is also activated by DAMPs, including extracellular matrix components, cytoplasmic proteins (e.g., S100, HSPs), and nuclear proteins (e.g., histones, HMGB1), highlighting its importance in both pathogen response and homeostasis. Disruptions in the balance of tissue cells, immune cells, and microbiota, due to factors like aggressive therapies or cancer, can shift TLR2's role toward either promoting or suppressing tumorigenesis. Understanding these mechanisms is crucial for developing innovative anti-cancer therapies [58].

3.2 TLR2 in the anti-tumor immune response

Lymphoid and myeloid cells within the TME play dual roles, acting as either immune suppressors or stimulators, thereby significantly influencing cancer progression, survival, and resistance to therapy. Dying cells in the TME release DAMPs, which activate myeloid cells through their PRRs [84,85].

For example, HMGB1, a nuclear protein released into the TME following cell damage or death, can activate multiple PRR signaling pathways, including TLR2 [86].

DCs activated by DAMPs and other stimuli like TNF-α and type I IFNs enhance antigen presentation, promoting adaptive immunity. Some studies on TLR2 activation in murine cancer models showed its potential to stimulate anti-cancer responses [87]. For instance, synthetic or bacterial TLR2 ligands in lung cancer models induce monocytic MDSCs to differentiate into anti-tumoral M1 macrophages, producing IFN-γ, nitric oxide (NO), and pro-inflammatory cytokines. In melanoma models, the TLR1/2 ligand diprovocim enhances leukocyte infiltration and boosts systemic immune responses when combined with anti-PD-L1 immunotherapy. However, TLR2 effects can vary. In fibrosarcoma models, the TLR2/6 ligand FSL-1 promotes tumor growth by increasing Tregs. Nevertheless, anti-tumoral effects of the synthetic lipoprotein FSL-1, such as increased cytotoxic T lymphocytes and ADCC, are observed when combined with tumor-associated antigen immunization. TLR2 also influences NK cell-mediated immunity. In lung cancer, TLR2 stimulation by the natural polysaccharide SEP induces NK cell activation, cytotoxicity, and cytokine release. Similarly, the polysaccharide krestin (PSK) activates human NK cells, enhances trastuzumab efficacy, and boosts ADCC in HER2/Neu models. Thus, TLR2's role in cancer immunity can be context-dependent, with both pro- and anti-tumor effects [58,88].

3.3 TLR2 in immunosuppression

As discussed previously, TLR2 plays a pivotal role in the activation of innate immune cells, promoting anti-tumor responses through the activation of antigen-presenting cells and subsequent stimulation of tumor-specific T lymphocytes. Conversely, TLR2 is also expressed on immunosuppressive cells such as Tregs, MDSCs, macrophages, and neutrophils. Its activation in these cells fosters their immunosuppressive functions, contributing to tumor growth, the creation of an immunosuppressive microenvironment, and the establishment of a metastatic niche [58].

Indeed, the stimulation of TLR2 signaling in Tregs promotes their expansion. Furthermore, TLR2 activation on macrophages induces the release of cytokines that recruit Tregs [89,90]. In cancer, the immunosuppressive activity of Tregs through the release of cytokines, like IL-10, inhibits the anti-tumoral $CD8^+$ T cell response [58]. In a similar way, upon TLR2 activation, B lymphocytes can differentiate in B regulatory cells (Bregs) and secrete IL-10, suppressing the T cell response [91]. Moreover, the activation of TLR2 in $CD4^+$ T cells, stimulated by heat shock protein (HSP)90 and other DAMPs released by breast cancer cells, triggers an IL-6 signaling loop that promotes the production of IL-10 and IL-21, contributing to immune suppression, and hindering anti-tumor

immunity [92]. TLR2 activation in bone marrow precursors drives their differentiation into MDSCs, which accumulate within the TME and secrete pro-tumoral cytokines. This process also facilitates the polarization of macrophages toward the M2 pro-tumoral phenotype and promotes the release of NO, an inhibitor of effector T-cell activity. Additionally, DAMPs like HMGB1 and serum amyloid A1 protein, which are secreted by breast cancer cells and found in elevated levels in the plasma and tumor biopsies of patients with TNBC, mediate an immunosuppressive effect on neutrophils via TLR2 activation [93,94].

Together, these mechanisms contribute to the establishment of an immunosuppressive microenvironment that facilitates tumor progression. Indeed, as discussed above, TLR2 activation in immune cells drives the secretion of factors that suppress anti-tumor immune responses, thereby supporting tumor growth and metastasis. Exploring these pathways can uncover therapeutic targets to counteract the immunosuppressive TME and enhance anti-tumor immunity.

3.4 Cancer-cell intrinsic pro-tumoral role of TLR2

Breast cancer cells overexpress TLR2, which can be stimulated by endogenous ligands such as HSPs, HMGB1, and other DAMPs, or by PAMPs like bacterial lipoproteins. TLR2 activation drives signaling pathways that enhance tumor growth and survival. One key downstream effector is NF-κB, which initiates the transcription of numerous genes associated with inflammation and cell survival [58].

A study from Wenjie Xie and colleagues has demonstrated that TLR2 expression is 10-fold higher in the human highly metastatic TNBC cell line MDA-MB-231 compared to the poorly metastatic ER^+ MCF-7 breast cancer cells [95]. In MMTV–Wnt1 transgenic mice that spontaneously develop ER^- mammary tumors, TLR2 deletion impairs tumorigenesis. Moreover, TLR2 modulates Wnt downstream genes, such as CD44 and Lgr5, which are mediators of NF-κB pro-tumoral activity [96,97].

Our research group has shown that the stimulation of TLR2 by its endogenous ligand HMGB1 triggers the activation of the NF-κB signaling pathway. This activation leads to the release of pro-tumorigenic cytokines, including IL-6 and TGF-β, which subsequently activate the STAT3 and Smad3 signaling cascades in an autocrine or paracrine manner. These pathways are known to exert potent pro-tumoral effects, such as sustaining the CSC population. Notably, TLR2 activation has been found to significantly increase the expression of CSC markers in breast cancer cells, underscoring its pivotal role in maintaining CSC self-renewal and plasticity [74].

Beyond activating NF-κB, TLR2 signaling also engages the MAPK pathway, which promotes cell proliferation and migration. In gastric cancer, this activation drives EMT, thus stimulating cancer migration and invasion. By enabling cancer cells to adopt migratory and invasive traits, TLR2-mediated EMT facilitates metastasis. Additionally, TLR2 contributes to angiogenesis by increasing the production of VEGF and other pro-angiogenic molecules by breast cancer cells, promoting the development of blood vessels to sustain tumor growth [88].

TLR2 acts as a sensor of both DAMPs and PAMPs, linking TLR2-expressing cells with the microbial environment. While this mechanism has primarily been studied in the immune system for its role in protecting against infections, recent research has shifted towards exploring the influence of the microbiota in various diseases. Changes in microbiota composition and its interactions with host cells may play a significant role in pathological processes, including carcinogenesis and cancer recurrence, [58,98]. Numerous studies have highlighted the link between specific bacterial species and tumor development, particularly in the gastrointestinal tract. For example, *Helicobacter pylori* plays a role in gastric and colon carcinogenesis through multiple mechanisms, including TLR2-mediated activation of NF-κB and Wnt pathways, as well as the induction of EMT in epithelial cells [99,100]. A distinct microbiota has been identified in the mammary gland, with alterations observed in breast cancer. *Bacteroides fragilis* has been detected in tumor biopsies of breast cancer patients, where it promotes tumorigenesis. *Fusobacterium nucleatum* (*F. nucleatum*), a commensal bacterium typically found in the oral cavity, can migrate to other organs and become pathogenic. *F. nucleatum* has been detected in both colon and breast cancer tissues. In colo-rectal cancer it contributes to tumor progression by activating TLR2 signaling in cancer cells and inducing immunosuppression. Therefore, it is reasonable to hypothesis that similar mechanisms can occur in breast cancer [101–103]. Beyond the pro-tumoral effects of individual bacterial species, broader alterations in microbiota, known as dysbiosis, play a critical role in cancer. Dysbiosis can contribute to carcinogenesis or support tumor progression by promoting therapy resistance and metastasis. Studies have shown a correlation between antibiotic use prior to or during the early stages of cancer and poorer outcomes in breast cancer patients, likely due to dysbiosis and an increased prevalence of pro-tumoral bacteria. Additionally, chemotherapy-induced dysbiosis and opportunistic infections can elevate TLR2 ligand availability, potentially undermining treatment effectiveness [104–106].

Taken together, all these information indicate that in breast cancer the presence of TLR2 and its endogenous or exogenous ligands could result in several pro-tumoral effects. This may accelerate cancer progression and limit the efficacy of anti-tumor therapies, leading to a worse prognosis for the patients. Therefore, investigating the role of TLR2 in breast cancer can be fundamental to obtain information that will allow to improve breast cancer therapies.

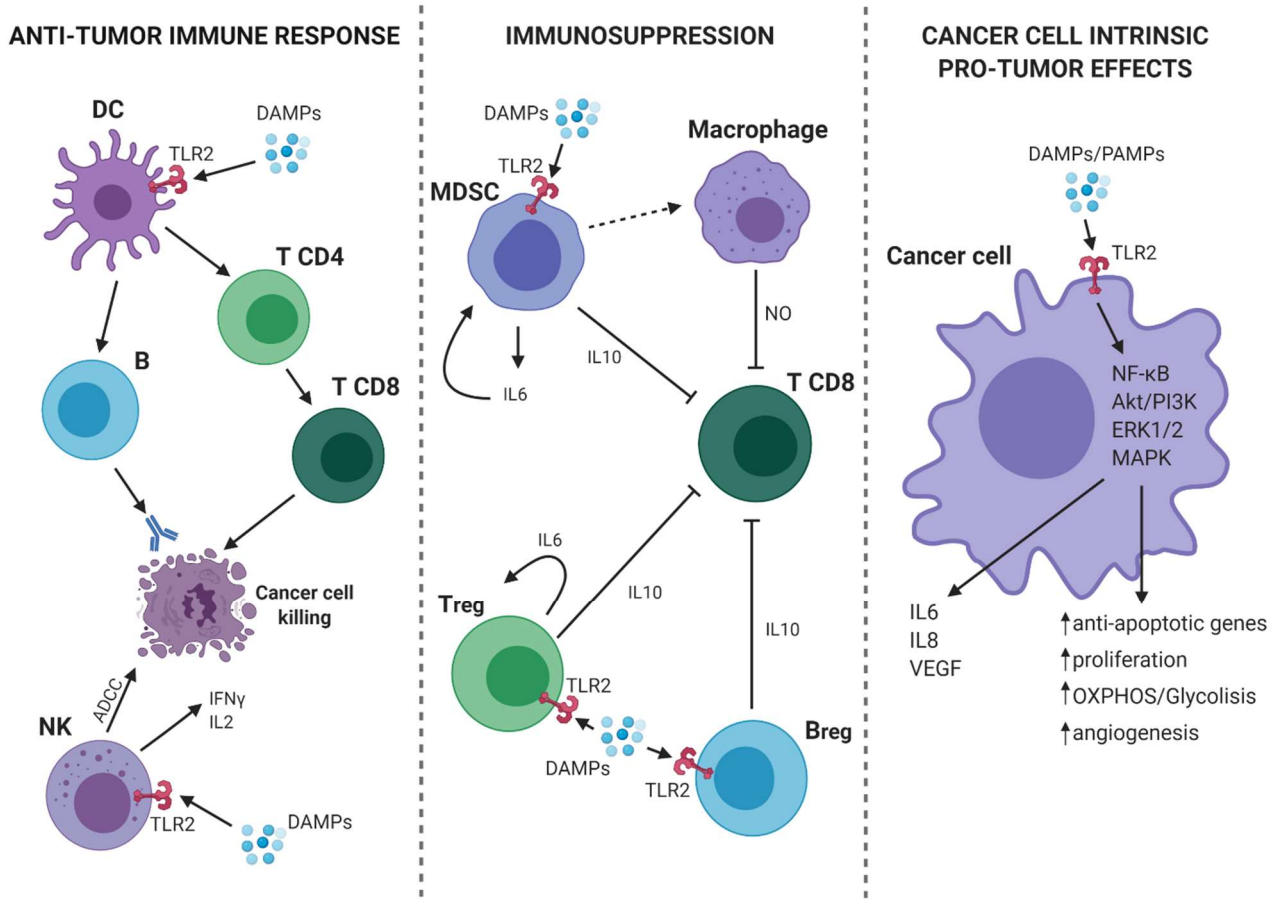


Figure 5. TLR2-mediated pro- and anti-tumoral mechanisms. (Left) Within the tumor microenvironment (TME), damage-associated molecular patterns (DAMPs) activate dendritic cells (DCs) via TLR2. Activated DCs then present tumor antigens, triggering a specific anti-tumor T cell response. Simultaneously, TLR2 on natural killer (NK) cells facilitates their activation, promoting antibody-dependent cell-mediated cytotoxicity (ADCC) against cancer cells. This activation also leads to the release of interferon-gamma (IFN-γ) and interleukin-2 (IL-2), which further bolster anti-tumor immunity. (Center) TLR2 activation on myeloid-derived suppressor cells (MDSCs), regulatory B cells (Bregs), and regulatory T cells (Tregs) exerts an immunosuppressive effect. MDSCs stimulate macrophages to produce nitric oxide (NO), which suppresses the activity of cytotoxic CD8+ T lymphocytes. Additionally, activated MDSCs, Bregs, and Tregs release interleukins IL-6 and IL-10, which synergistically inhibit CD8+ T cell activity, further dampening the immune response. (Right) On cancer cells, TLR2 interacts with DAMPs or pathogen-associated molecular patterns (PAMPs), initiating intracellular signaling pathways, including nuclear factor kappa-light-chain-enhancer of activated B cells (NF-κB), Akt/PI3K, extracellular signal-regulated kinase (ERK)1/2, and mitogen-activated protein kinase (MAPK). These pathways drive a pro-tumor response characterized by the secretion of IL-6, IL-8, and vascular endothelial growth factor (VEGF). This promotes cancer cell proliferation, enhanced metabolism, angiogenesis, and protection from apoptosis. The diagram uses continuous and dashed arrows to illustrate the respective pathways and effects. (Antonino Di Lorenzo et al. Int. J. Mol. Sci. 2020) [58]

Aims of the thesis

Breast cancer remains one of the leading causes of death worldwide, primarily due to relapses and distal metastases, underscoring the limitation of current therapies in many patients. Indeed, resistance to chemotherapy and immunotherapy is common challenge in breast cancer patients, highlighting the urgent need for novel therapeutic strategies.

Since breast CSCs play a key role in therapy resistance, over the past years our group developed a pipeline to identify molecules overexpressed in CSCs that sustain their self-renewal and survival, providing promising targets for anti-cancer therapies. Using this approach, our group discovered that TLR2 is expressed in $HER2^+$ and TN breast cancer cells of human and mouse origin and is upregulated in CSC-enriched tumorspheres. This finding suggested a previously unrecognized role for TLR2 in breast cancer biology, particularly in CSCs.

Subsequent studies revealed an autocrine TLR2-mediated loop in breast CSCs. Specifically, breast CSCs actively release the TLR2 ligand HMGB1, which stimulate TLR2 activating the NF-κB pathway. This activation leads to the release of pro-tumoral cytokines, including IL-6 and TGF-β, and to the downstream activation of STAT3 and Smad3 pathways, promoting CSC self-renewal and tumor progression. Activation of TLR2 also upregulates CSC markers, underscoring its pivotal role in maintaining the CSC pool [74].

HMGB1, along with other DAMPs, can be released into the TME by cancer cells, either actively or passively as a result of cell death induced by anti-cancer therapies. This release fuels TLR2 activation, promoting tumor progression. Notably, elevated serum HMGB1 levels are correlated with metastasis and poor prognosis in TNBC patients [107]. These findings suggest that TLR2 inhibitors or other targeted strategies could improve the efficacy of breast cancer treatments.

The primary objective of my PhD project was to investigate the role of TLR2 role in breast cancer and to develop innovative combination therapeutic strategies based on its targeting.

To achieve this aim, I pursued three research lines, which form the structure of this thesis:

Chapter I

This chapter investigates the role of TLR2 in spontaneous $HER2^+$ mammary tumor progression using transgenic mouse models. It examines cancer cell-intrinsic and extrinsic mechanisms through which TLR2 drives breast cancer progression and resistance to chemotherapy, and the therapeutic potential of TLR2 inhibition to enhance chemotherapy efficacy. Results from this work are detailed in **Paper I** [108].

Chapter II

This chapter addresses translational challenges in combining TLR2 inhibitors with chemotherapy. Collaborating with Prof. Giuseppe Ferrauto's team (Department of Molecular Biotechnology and Health Science, University of Torino), I contributed to the development of targeted nanoparticles for precise intra-tumor delivery of TLR2 inhibitors and chemotherapeutic agents. Initial studies validated the nanoparticle design and efficacy, as described in **Paper II** [109]. Further experiments evaluated in vitro and in vivo efficacy of combining nanoparticles loaded with TLR2 inhibitors and chemotherapeutic drugs.

Chapter III

This chapter investigates the synergistic potential of combining TLR2 inhibition and chemotherapy to enhance immunotherapy efficacy. This chapter focuses on a viral vector-based vaccine targeting the xCT cystine/glutamate antiporter, previously shown by our group to have significant anti-cancer potential [42,43]. Combination therapies were tested in transplantable mammary cancer mouse models and complemented by *in vitro* experiments with xCT inhibitors, TLR2 inhibitors, and chemotherapy.

Overall, this thesis provides new insights into the role of TLR2 in breast cancer, demonstrating its potential as a therapeutic target. It highlights the benefits of TLR2 inhibition in combination with chemotherapy and immunotherapy, offering promising strategies to improve breast cancer treatment outcomes.

Chapter I

Investigating the role of TLR2 in breast cancer progression and resistance to chemotherapy

This Chapter represents the starting point of the work described in this Thesis. The results obtained were propaedeutic for designing and executing subsequent parts of the project.
(For detailed Results and Materials & Methods, please refer to Paper I).

To investigate the role of TLR2 in breast cancer onset and progression, we began by assessing whether its expression levels correlate with patients' prognosis. Analysing public datasets, we identified a significant correlation between high TLR2 expression and poor prognosis in breast cancer patients. To further explore the role of TLR2 in mammary carcinogenesis and tumor progression, we utilized pre-clinical models specifically developed for this purpose. These models are based on neuT mice, which harbor an active form of the rat HER2 oncogene (*neuT*) under the control of a strong mammary gland-specific promoter of the mouse mammary tumor virus (MMTV), leading to the spontaneous development of mammary tumors in female neuT mice. Specifically, in neuT female mice on BALB/c background (BALB-neuT mice), starting from the fourth week of life, cells in the incompletely developed mammary gland ducts express the r-p185^{neu} protein, a product of the *neuT* oncogene. These protein-expressing cells proliferate, forming side buds along the majority of the mammary ducts. Over time, these side buds enlarge and coalesce, leading to atypical hyperplasia and carcinoma *in situ*. By the 19th week, these lesions become invasive and palpable through the skin, occupying much of the subcutaneous fibroadipose tissue extending from the armpits to the ten mammary gland regions. By the 30th week, lung metastases are frequently observed. BALB-neuT mice have been extensively used to study the key features of aggressive HER2^{+} mammary carcinoma and to test various pharmacological and immunological therapeutic approaches. Notably, some interventions, such as anti-cancer vaccines, can partially control and slow cancer progression when administered during the early stages of the disease. However, treatment initiated at later stages show limited efficacy [110].
Despite challenges such as the time required to recruit mice and monitor their cancer progression, the carcinogenesis and tumor development observed in neuT mice closely mirror the characteristics of human breast cancer. These aspects make neuT mice a valuable model for our studies. To evaluate the impact of TLR2, we crossed TLR2^{KO} C57Bl6 mice with C57Bl6-neuT mice (TLR2^{WT} mice), previously generated in Prof. Cavallo's laboratory from BALB-neuT mice. This new model – TLR2^{KO} neuT mice - allowed us to study mammary tumor progression in the presence or absence of TLR2.
Since TLR2 is a crucial component of the innate immune system, we considered potential concers about defects in the immune response against both pathogens and cancer resulting from TLR2 deletion. However, studies on TLR2^{KO} mice have demonstrated that, while TLR2 signaling pathway

and its target gene products play an important role in the innate immunity, inflammatory processes and acquired immunity can still occur in the absence of TLR2 [111]. This evidence supports the hypothesis that TLR2 deletion in cancer models allows for the evaluation of TLR2's role in tumor progression without compromising the anti-tumor immune response, thereby ensuring the reliability of the observations. Moreover, these findings, together with the promising data that we obtained from $TLR2^{KO}$ neuT mice, suggest that TLR2 could be a viable therapeutic targeted without impairing the immune system.

By monitoring cancer progression in $TLR2^{WT}$ and $TLR2^{KO}$ neuT mice, we demonstrated that TLR2 deletion significantly delayed tumor onset, impaired tumor progression, reduced the number of tumors per mouse, and improved survival. Immunophenotypic analysis of tumors and other compartments, such as blood and spleen, revealed no major changes in overall immune cell populations due to TLR2 deletion, except for a notable reduction in the frequency of Tregs. Further investigations confirmed that TLR2 is critical for Treg expansion, indicating that TLR2 deletion limits the immunosuppressive effects mediated by Tregs.

Additionally, tumors from $TLR2^{KO}$ neuT mice exhibited lower percentages of CSCs, supporting the hypothesis that TLR2 plays a pivotal role in CSC biology. These findings highlight TLR2 as a potential target for therapeutic intervention in breast cancer.

To further explore the role of TLR2 in breast cancer, we established breast cancer cell lines derived from both $TLR2^{WT}$ and $TLR2^{KO}$ neuT tumors. Transplantation experiments using these cell lines in mice with either $TLR2^{WT}$ or $TLR2^{KO}$ backgrounds revealed that TLR2 expression in cancer cells is essential for efficient tumor engraftment and growth, independent of the TLR2 status of the recipient mice. Additionally, we observed that $TLR2^{WT}$ cancer cells grow faster when injected into $TLR2^{WT}$ than into $TLR2^{KO}$ mice, suggesting that TLR2 expressed in non-cancer cells promotes tumor progression. These findings suggest that TLR2-driven, cancer cell-intrinsic mechanisms play a critical role in cancer progression, although TLR2-dependent, cancer cell-extrinsic mechanisms also contribute. Our investigations also demonstrated that TLR2 activation in breast cancer cells induces the release of pro-tumoral cytokines and enhances cancer cell stemness. Consequently, we assessed the effects of TLR2 inhibition on breast cancer cells.

According to public literature, no clinical trials with TLR2 inhibitors have been conducted in breast cancer. Nevertheless, monoclonal antibodies or inhibitors targeting TLR2 have shown promise in clinical trials for haematological malignancies [112–114]. Research using mouse models of various cancers, including gastric and pancreatic cancers, has demonstrated that tumorigenesis can be impeded by genetically deleting TLR2 or employing blocking antibodies such as OPN-301 [115].

Additionally, recent studies have highlighted the role of natural compounds, such as Robinin, in slowing pancreatic cancer progression by modulating the TLR2-PI3K-Akt signaling pathway [116]. Experiments involving head and neck squamous cell carcinoma have also shown that TLR2-blocking antibodies effectively suppress the growth of organoids and patient-derived xenografts [117].

In our study we used the small molecule CU-CPT22, an inhibitor of the TLR2/TLR1 dimer, which also inhibits the TLR2/TLR6 dimer with a lower efficiency. Other commercially available inhibitors are more selective for different dimers. One of our future goals is to determine whether specific TLR2 dimers are more strongly associated with pro-tumoral or immunological activities.

In *in vitro* dose-response experiments using CU-CPT22, we observed that pharmacological inhibition of TLR2 reduced viability of different breast cancer cell lines, underscoring the therapeutic potential of targeting TLR2 in breast cancer.

Analysis of public datasets revealed that TLR2 expression is linked to chemotherapy resistance in breast cancer patients. To investigate this aspect, we utilized our mouse models. *In vitro* studies showed that $TLR2^{KO}$ breast cancer cells exhibit greater sensitivity to doxorubicin compared to their $TLR2^{WT}$ counterparts. Mechanistically, we demonstrated that doxorubicin treatment increases the release of HMGB1 from breast cancer cells, which, in turn, activates the TLR2 downstream signaling pathway converging on NF-κB and promoting chemotherapy resistance. Importantly, pharmacological inhibition of TLR2 with CU-CPT22 reduced NF-κB activation and synergistically enhanced doxorubicin efficacy. This finding highlights a dual mechanism where TLR2 inhibition not only mitigates chemoresistance but also amplifies the therapeutic potential of doxorubicin. Furthermore, we identified this mechanism of chemoresistance as being specifically associated with TLR2 expression and treatments that induce the release of DAMPs within the TME, thereby activating TLR2 signaling. Notably, TLR2 deletion or inhibition did not increase sensitivity to drugs that do not induce immunogenic cell death in breast cancer cells. These insights underscore the potential of targeting TLR2 to overcome chemotherapy resistance in breast cancer.

To evaluate whether TLR2 represents a viable therapeutic target for breast cancer, we tested the synergistic effect of CU-CPT22 and doxorubicin in transplantable mouse models. BALB/c mice bearing palpable mammary tumors were treated with doxorubicin and CU-CPT22, administered intra-tumorally to avoid systemic TLR2 inhibition. Combined therapy significantly inhibited tumor progression compared to the single treatments. Additionally, the combination reduced the proportion of CSCs within the tumors while reshaping the TME to support anti-tumor immunity. This remodeling included reductions in immunosuppressive cells, such as Tregs and MDSCs, and increases in cytotoxic T cells and pro-inflammatory macrophages.

Overall, this study describes for the first time a pro-tumoral role of TLR2 in breast cancer, emphasizing its implications for tumor progression, chemoresistance, and potential as a therapeutic target. Chemotherapy remains the first-line treatment for breast cancer, including aggressive forms like TNBC, but chemoresistance remains a significant obstacle to successful outcomes. This underscores the need for combination therapies that enhance the efficacy of existing protocols. Our data demonstrate that TLR2 targeting can enhance breast cancer cell vulnerability to standard therapies. These results provide strong justification for further exploration of TLR2 inhibitors as part of combination therapeutic strategies for breast cancer treatment.

Paper I



OncoImmunology

ISSN: (Print) (Online) Journal homepage: www.tandfonline.com/journals/koni20

Toll-like receptor 2 promotes breast cancer progression and resistance to chemotherapy

Antonino Di Lorenzo, Elisabetta Bolli, Roberto Ruiu, Giuseppe Ferrauto, Enza Di Gregorio, Lidia Avalle, Aurora Savino, Pietro Poggio, Irene Fiore Merighi, Federica Riccardo, Mara Brancaccio, Elena Quaglino, Federica Cavallo & Laura Conti

To cite this article: Antonino Di Lorenzo, Elisabetta Bolli, Roberto Ruiu, Giuseppe Ferrauto, Enza Di Gregorio, Lidia Avalle, Aurora Savino, Pietro Poggio, Irene Fiore Merighi, Federica Riccardo, Mara Brancaccio, Elena Quaglino, Federica Cavallo & Laura Conti (2022) Toll-like receptor 2 promotes breast cancer progression and resistance to chemotherapy, OncoImmunology, 11:1, 2086752, DOI: 10.1080/2162402X.2022.2086752

To link to this article: https://doi.org/10.1080/2162402X.2022.2086752

© 2022 The Author(s). Published with license by Taylor & Francis Group, LLC.

View supplementary material

Published online: 15 Jun 2022.

Submit your article to this journal

Article views: 2904

View related articles

View Crossmark data

Citing articles: 19 View citing articles

Full Terms & Conditions of access and use can be found at
https://www.tandfonline.com/action/journalInformation?journalCode=koni20

ONCOIMMUNOLOGY
2022, VOL. 11, NO. 1, e2086752 (18 pages)
https://doi.org/10.1080/2162402X.2022.2086752

Taylor & Francis
Taylor & Francis Group

ORIGINAL RESEARCH

OPEN ACCESS Check for updates

Toll-like receptor 2 promotes breast cancer progression and resistance to chemotherapy

Antonino Di Lorenzo[a], Elisabetta Bolli[a], Roberto Ruiu[a], Giuseppe Ferrauto[a], Enza Di Gregorio[a], Lidia Avalle[a], Aurora Savino[b], Pietro Poggio[a], Irene Fiore Merighi[a], Federica Riccardo[a], Mara Brancaccio[a], Elena Quaglino[a], Federica Cavallo[a]§, and Laura Conti[a]§

[a]Department of Molecular Biotechnology and Health Sciences, University of Turin, Turin, Italy; [b]Human Technopole, Milan, Italy

ABSTRACT

Cancer stem cells (CSCs) are the main drivers of disease progression and chemotherapy resistance in breast cancer. Tumor progression and chemoresistance might then be prevented by CSC-targeted therapies. We previously demonstrated that Toll-like Receptor (TLR)2 is overexpressed in CSCs and fuels their self-renewal. Here, we show that high TLR2 expression is linked to poor prognosis in breast cancer patients, therefore representing a candidate target for breast cancer treatment. By using a novel mammary cancer-prone $TLR2^{KO}$ mouse model, we demonstrate that TLR2 is required for CSC pool maintenance and for regulatory T cell induction. Accordingly, cancer-prone $TLR2^{KO}$ mice display delayed tumor onset and increased survival. Transplantation of $TLR2^{WT}$ and $TLR2^{KO}$ cancer cells in either $TLR2^{WT}$ or $TLR2^{KO}$ hosts shows that tumor initiation is mostly sustained by TLR2 expression in cancer cells. TLR2 host deficiency partially impairs cancer cell growth, implying a pro-tumorigenic effect of TLR2 expression in immune cells. Finally, we demonstrate that doxorubicin-induced release of HMGB1 activates TLR2 signaling in cancer cells, leading to a chemotherapy-resistant phenotype. Unprecedented use of TLR2 inhibitors *in vivo* reduces tumor growth and potentiates doxorubicin efficacy with no negative impact on the host immune system, opening new perspectives for the treatment of breast cancer patients.

ARTICLE HISTORY
Received 8 December 2021
Revised 1 June 2022
Accepted 1 June 2022

KEYWORDS
Breast cancer; Toll-like receptor 2; HER2; HMGB1; chemoresistance

Introduction

Breast cancer (BC) is the most prevalent tumor in women, and its incidence is progressively increasing.[1] Remarkable advances in diagnosis and adjuvant and neoadjuvant treatments have improved patient outcomes. However, BC is still the first cause of cancer-associated mortality in women in more than 100 countries.[1] More than 30% of patients experience local or distal relapse after surgery, and about 80% of deaths occur in patients whose BC progressed to metastatic disease despite treatment.[2]

Although endocrine and HER2-targeted therapies are commonly used for estrogen receptor (ER)- and HER2-positive early BCs, respectively, systemic chemotherapy with anthracyclines or cyclophosphamide is the cornerstone of treatment for triple negative (TN) BC, high-risk luminal cancers, and advanced BC. Neoadjuvant chemotherapy using a doxorubicin-based schedule has recently become a common therapeutic option for operable BC.[3] However, the emergence of chemoresistance is a common event that often leads to treatment failure and metastasis.[4]

Resistance to chemotherapy can be attributed to several cancer-cell-intrinsic mechanisms, including altered drug absorption, efflux, or metabolism, the increased activation of pro-survival pathways, enhanced DNA repair, and tumor stemness.[4] Furthermore, many chemotherapeutic drugs induce the release of several molecules by dying or injured cancer cells. One class of molecules released or exposed on the cell surface following chemotherapy-induced cell death is represented by damage-associated molecular patterns (DAMPs), which are a wide-ranging group of biomolecules that include (but are not limited to) High Mobility Group Box (HMGB)1, ATP, Heat Shock Protein (HSP)70 and HSP90, Calreticulin, and Annexin A1. Such DAMPs can act as signals by interacting with pattern recognition receptors (PRRs), leading to functional alterations in cells composing the tumor microenvironment (TME).[5] Physiologically, PRRs are expressed in immune cells and promote inflammatory responses.[6] In this scenario, dying or injured cancer cells release or expose on their surface DAMPs that help recruiting and activating cells of the immune system, including dendritic cells (DCs) that engulf them and initiate an adaptive immune response against the tumor. This type of cell death is called immunogenic cell death (ICD). However, some DAMPs may switch immune cells toward an anti-inflammatory response, depending on the type of cell death that induced their release, with which kinetic (acute vs chronic), and the PRR they engage.[7,8] Therefore, surviving tumor cells can exploit TME alterations induced by cancer cell death to stimulate their survival and proliferation, resulting in cancer progression.[4,9] In addition, several PRRs have

CONTACT Laura Conti laura.conti@unito.it; Federica Cavallo federica.cavallo@unito.it Department of Molecular Biotechnology and Health Sciences - Molecular Biotechnology Center "Guido Tarone", University of Turin, Via Nizza, 52, Turin, 10126, Italy
*These authors equally contributed
§These are co-last authors
Supplemental data for this article can be accessed online at https://doi.org/10.1080/2162402X.2022.2086752

© 2022 The Author(s). Published with license by Taylor & Francis Group, LLC.
This is an Open Access article distributed under the terms of the Creative Commons Attribution-NonCommercial License (http://creativecommons.org/licenses/by-nc/4.0/), which permits unrestricted non-commercial use, distribution, and reproduction in any medium, provided the original work is properly cited.

recently been observed in cancer cells as well, where they can activate pro-tumor pathways, and thus act as a double-edge sword in cancer.[6,10]

We have previously demonstrated that BC cells express Toll-like receptor (TLR)2, a PRR playing a key role in the survival and self-renewal of cancer stem cells (CSCs). CSCs are a small population of cancer cells able to self-renew, differentiate into all the cell lineages that form the tumor bulk and initiate the metastatic cascade.[11,12] Breast CSCs are resistant to most current therapies, including chemotherapy, being thus responsible for local or distal relapse after treatment.[13–15] Therefore, high levels of CSCs in breast tumors are associated with poor prognosis.[16] TLR2 activation in breast CSCs is autocrinally induced by the secretion of the DAMP HMGB1, which leads to the activation of the NF-κB, AKT, and MAPK pathways and the subsequent production of Interleukin (IL)-6, tumor growth factor (TGF)-β, granulocytic-colony stimulating factor (G-CSF), and vascular endothelial growth factor (VEGF).[6,13] IL-6 and TGF-β induce STAT3- and Smad3-pathway activation in CSCs, promoting their survival, proliferation, self-renewal, and invasion.[13]

Besides being actively secreted by CSCs,[13] HMGB1 can be released into the TME as a consequence of treatment with chemotherapeutic drugs, including doxorubicin and taxanes, that induce ICD.[17] High HMGB1 levels have been associated with clinical progressive disease during neoadjuvant chemotherapy in TNBC patients.[18] We therefore hypothesize that ICD-inducing chemotherapy triggers the release of HMGB1 that, engaging TLR2, fosters the appearance of CSC-related features, including chemoresistance. TLR2 inhibition may therefore prevent the tumor-promoting effect of HMGB1, thus preserving the anti-tumor function of ICD-inducing chemotherapy.

Herein, we show that TLR2 promotes BC growth and chemoresistance, mainly via tumor cell-intrinsic mechanisms, and that its inhibition improves the efficacy of doxorubicin in preclinical models of BC. This study therefore identifies TLR2 as a new potential target for combined therapies.

Materials and methods

Cell cultures

MDA-MB-231 and 4T1 cell lines were purchased from American Type Culture Collection (ATCC) in 2018, aliquoted, frozen, and then used within 10 passages after resuscitation in DMEM or RPMI 1640 (ThermoFisher Scientific) 10% FBS (Sigma-Aldrich), respectively. TUBO cell line was derived from a BALB-neuT primary tumor and cultured in DMEM 20% FBS.[19] WT-874, WT-879, WT-880, KO-C26, KO-M26, and KO-E26 cell lines were derived, as described in the study of Liu and Chen,[20] from mammary tumors isolated from C57Bl6-neuT mice either TLR2 wild-type (neuT-TLR2^{WT}) or TLR2 knock-out (neuT-TLR2^{KO}), respectively, and cultured in DMEM-F12 (ThermoFisher Scientific) with 20% FBS. All cells were negative for mycoplasma.[21]

Meta-analysis using patient databases

The prognostic value of TLR2 mRNA expression in the 5-y-relapse-free (RFS) and overall survival (OS) of patients with BC, either treated with chemotherapy or not, was analyzed using the 32 breast cancer transcriptomic datasets available through the open access online software Kaplan-Meier Plotter.[22] Patients were stratified into two groups according to TLR2 expression using the "auto select best cutoff" function. Removal of redundant samples, exclusion of biased arrays and proportional hazard assumptions check were included in quality control. Hazard ratios and p-values obtained with each dataset, either considering all patients or separating them by molecular subtype, were merged with Fisher's method[23] from the metap package (https://CRAN.R-project.org/package=metap).

The expression levels of TLR2 across BC molecular subtypes were obtained from the transcriptomic datasets collected in the MetaGxBreast R package,[24] and PAM50 subtyping was performed through the molecular subtyping function of the genefu R package ("pam50" model).[25] Since the log-rank tests were two-sided, one-sided p-values were obtained with the two2one function from the metap package, taking the hazard ratio into account, before applying Fisher's method. A total of 32 datasets had a probe for TLR2 and allowed the inference of the molecular subtype. TLR2 mRNA expression levels in BC patients that responded to adjuvant chemotherapy and those that did not were analyzed using the datasets and tools available;[22,26] patients who relapsed within 5 y of treatment were compared with patients who did not, excluding those censored before the 5 y had passed.

The correlation between TLR2 expression and a CSC signature was computed using the transcriptomic datasets in MetaGxBreast and the cor.test function in R, collapsing the expression of CSC markers[16] with single sample GSEA (GSVA R package).[27] Correlations' p-values were merged similarly to log-rank survival tests' p-values. A total of 33 datasets had probes for TLR2 and for the CSC signature.

Mice

Mice were bred and maintained under saprophytic and pathogen-free conditions at the animal facility of the Molecular Biotechnology Center and treated in accordance with EU and institutional guidelines, with the approval of the Animal Care and Use Committee of the University of Turin and the Italian Ministry of Health (authorizations N° 107/2020-PR and 500/2017-PR).

NeuT-TLR2^{WT} mice were generated by crossing male BALB-neuT[19] with C57Bl6 female mice, and then backcrossing neuT male offspring with C57Bl6 mice for 12 generations. NeuT-TLR2^{WT} males were then crossed with B6.129-*Tlr2*^{tm1Kir}/J female mice (The Jackson Laboratory), and the *Tlr2*^{Het} offspring intercrossed to obtain neuT-TLR2^{KO} mice. Mice were screened with primers to *neuT* (Fwd: 5'-GTAACACAGGCAGATGTAGGA-3'; Rev: 5'-ATCGGTGATGTCGGCGATAT-3'), *Tlr2* (Fwd: 5'-CTTCCTGAATTTGTCCAGTACA-3'; RevWT: 5'-GGGCCAGCTCATTCCTCCCAC-3'; Rev*Tlr2*^{tm1Kir}5'-GAAACGGAATGTTGTGGAGT-3'), and *β-casein* (Fwd: 5'-GATGTGCTCCAG

GCTAAAGTT-3'; Rev: 5'-AGAAACGGAATGTTGTGGAGT-3'), according to Jackson Laboratory website protocols. Tumor growth was monitored twice per week with a caliper (N = 21 neuT-TLR2^{WT} and N = 22 neuT-TLR2^{KO} mice) until all 10 mammary glands displayed a tumor, or a tumor exceeded 10 mm mean diameter.

1×10^6 WT-874, WT-879, WT-880, KO-C26, KO-E26, and KO-M26 cells were injected orthotopically into the fourth mammary gland of 8-week-old syngeneic C57Bl6 mice either TLR2^{WT} or TLR2^{KO} or in NOD/SCID/IL-2 receptor gamma chain deficient (NSG, Charles River Laboratories) female mice (N = 6 per group). Cells were dissociated from 5 to 6 mm mean diameter tumors explanted from neuT-TLR2^{WT} (N = 4) and neuT-TLR2^{KO} (N = 4) mice, using the protocol described in the study of Lanzardo et al.[28] Then, 1×10^4 or 1×10^5 cells were injected orthotopically into the fourth mammary gland of 8-week-old C57Bl6 mice (N = 16). Tumor growth was monitored twice per week by caliper. All mice were culled when the WT-874 tumors reached 10 mm in mean diameter.

1×10^4 4T1 cells were transfected with a pool of TLR2-specific or scrambled siRNAs, injected orthotopically, 24 hours later, into 6-week-old female BALB/c mice (Charles River Laboratories), and tumor growth was monitored. In the therapeutic model, 1×10^4 4T1 cells were injected orthotopically into 6-week-old female BALB/c mice (N = 40). When the tumors reached 2 mm mean diameter, mice were blindly randomized into four groups, which received intratumor and intraperitoneal (i.p.) injections of the vehicle (control); 50 µg CU-CPT22 (Tocris Bioscience, Cat#4884) intratumorally and vehicle i.p. (CU-CPT22-treated); 3 mg/Kg doxorubicin (Sigma-Aldrich, Cat#D1515) i.p. and vehicle intratumorally (doxorubicin-treated); or 50 µg CU-CPT22 intratumorally and 3 mg/Kg doxorubicin i.p. (CU-CPT22 + doxorubicin-treated) twice per week. When control tumors reached 10 mm mean diameter, mice were culled, tumors removed and processed for FACS, and lungs fixed in 4% formaldehyde, paraffin embedded, sectioned into four sections spaced by 50 µm and H&E stained. Pictures were acquired using a Nikon SMZ1000 stereomicroscope (Mager Scientific) and metastases counted with ImageJ.[28]

Ex vivo T regulatory cell (Treg) analysis

Blood of tumor-bearing neuT-TLR2^{WT} mice was collected and processed, and T cells were activated as in the study of Conti et al.,[29] and either treated or not with 20 µg/ml peptidoglycan from *S. aureus* (PGN-SA; InvivoGen, Cat#tlrl-pgns2) or 10 µg/ml HMGB1 (Sigma-Aldrich, Cat#SRP6265). The percentage of Tregs was analyzed 6 d later by FACS.

FACS analysis

Single-cell suspensions were obtained from fresh primary tumors, spleens, and heparinized blood as in the study of Conti et al.[30] 1×10^6 cells were treated with Fc-receptor blocker (BD Bioscience, Cat#01245B) and stained for 20 min at 4°C with anti-mouse CD45-VioGreen (Cat#130-110-803), CD11b-FITC (Cat#130-110-803), CD3-FITC (Cat#130-119-135), CD4-APC-Vio770 (Cat#130-119-134), CD8-VioBlue (Cat#130-123-865), CD49b-PE (Cat#130-123-702), B220-PE-Vio770 (Cat#130-123-702), γδ TCR-PE/Cy7 (Cat#130-123-290), CD19-PE (Cat#130-123-272), Gr1-VioBlue (Cat#130-102-830), F4/80-PE-Vio770 (Cat#130-118-320) and MHC-II-APC (Cat#130-102-139) from Miltenyi Biotec, and CD44-PE (Cat#103007), CD24-PE/Cy7 (Cat#101822), Sca1-AlexaFluor647 (Cat#122518), CD206-PE (Cat#141706), CD4-PE/Cy7 (Cat#100528), GITR-PE (Cat#126310), TLR2-PE (Cat#148604) and CD25-APC (Cat#101910) from Biolegend, the Aldefluor kit (Stem Cell Technologies, Cat#01700) or the anti-FoxP3-FITC kit (eBioscience, Cat#10191071-5775-40).[31] At least 50,000 CD45$^+$ events were acquired per sample on BD-FACSVerse and analyzed with FlowJO10.5.3. Cells were gated according to their physical parameters, and dead cells were excluded following propidium iodide (Sigma-Aldrich, Cat#P4864) or LIVE/DEAD™ Fixable Violet Dead Cell Stain Kit 450 nm (Thermo Fisher Cat#L34963,) staining. The CD45$^+$ leucocytes and CD45$^-$ cells were gated, and cell populations analyzed as follows: NK: CD3$^-$ CD49b$^+$; CD4$^+$ T cells: CD3$^+$ CD49b$^-$ CD4$^+$; CD8$^+$ T cells: CD3$^+$ CD49b$^-$ CD8$^+$; γδ TCR$^+$ T cells: CD3$^+$ CD49b$^-$ γδ TCR$^+$; Tregs: CD3$^+$ CD4$^+$ CD25^{high} GITR$^+$ Foxp3$^+$; B cells: CD3$^-$ B220$^+$; MDSCs: CD11b$^+$ Gr1$^+$; M1 macrophages: CD11b$^+$ F4/80$^+$ MHC-II$^+$ CD206$^-$; M2 macrophages: CD11b$^+$ F4/80$^+$ CD206$^+$;[32,33] CSCs: CD45$^-$ Sca1$^+$, CD45$^-$ CD44$^+$ CD24$^-$ and CD45$^-$ Aldefluor$^+$.[30] Cell lines were characterized by staining with anti-mouse HER2 (Ab4, Cat#OP16, Calbiochem), α smooth muscle actin-FITC (Abcam Cat#ab8211), CD44-PE, CD24-PE/Cy7, Sca1-AlexaFluor647, TLR2-PE (Biolegend, Cat#148604 and Cat#392306), Aldeafluor, Oct-4 (Abcam Cat#ab19857), Musashi-1 (Abcam Cat#ab52865) or cytokeratin (CK)19-FITC (Abcam Cat#ab15463), followed by either rabbit anti-mouse Ig-PE (Cat# R043901), swine anti-rabbit Ig-FITC (Cat#F0205) from Dako or goat anti-rabbit IgG-PE (Thermo Fisher, Cat# P-2771MP). For the staining of intracellular proteins, cells were fixed and permeabilized with the BD Cytofix Cytoperm kit (BDBioscience, Cat# BD 554714). Tumor cells were either treated with 5 or 0.2 µM doxorubicin, 15 µM docetaxel (Hikma) or 12.5 µM cisplatin (Sandoz) and/or with 5 µM CU-CPT22 or 10 µg/ml of the HMGB1 inhibitor BOX-A (HMGBIotech, Cat#HM-014) or 8 µM of the NF-κB inhibitor BAY 11–7082 (Sigma-Aldrich, Cat#B5556) for 48 hours, or left untreated, and then stained with AnnexinV-Apoptosis Kit-APC (eBioscience, Cat#88-8007-72).[34] To analyze NF-κB activation, cells were either treated with 5 µM doxorubicin and/or 5 µM CU-CPT22 for 48 hours or starved in serum-free medium for 4 hours and then stimulated for 30 min with or without 10 µg/ml HMGB1. Cells were fixed with 4% formaldehyde and 90% methanol (Sigma-Aldrich), permeabilized and stained for 30 min at 4°C with Alexa Fluor 647-conjugated anti-pNF-κB p65-S536 (Cell Signaling Technology, Cat#4887).[13]

3-(4,5-Dimethylthiazol-2-yl)-2,5-Diphenyl Tetrazolium Bromide (MTT) assay

5×10^3 cells were cultured overnight in 96-well plates, and scalar doses of either docetaxel, cisplatin, CU-CPT22 or doxorubicin, alone or with 5 µM CU-CPT22, were then added. Viability was measured 48 hours after by MTT (0.5 mg/ml;

Sigma Aldrich, Cat#M2128).[30] The combined effect of doxorubicin and CU-CPT22 was determined as in the study of She et al.,[35] by Bliss independence analyses, using the equation: $C = (A + B) - (A \times B)$, where A and B are the fractional growth inhibitions of doxorubicin and CU-CPT22, respectively, at a given dose. "Delta Bliss" scores (the difference between the observed growth inhibition and the Bliss expectation at the same dose) of the different doses were summed to generate a Bliss score. Bliss score = 0: additive effect, Bliss score > 0: synergy, Bliss score < 0: antagonism.

Tumorsphere-generation assays

Tumorspheres were generated from cell lines or cells dissociated from tumors.[13] Dissociated tumorspheres were transfected with a pool of TLR2-specific (MSS216272, MSS216273, MSS280579) or scrambled (Cat#12935110) siRNAs using Lipofectamine 2000 (all from ThermoFisher Scientific). Twenty-four hours later, cells were treated with 20 μg/ml PGN-SA or 10 μg/ml HMGB1 or left untreated. After 4 d, contrast phase images were acquired (10X) and the number of spheres counted (4X) using Zeiss Axio Observer or Leica DMi1 inverted microscope connected to DC120 digital camera.[30]

ELISA

Supernatants of cells treated with 5 μM or 0.2 μM doxorubicin or left untreated were harvested after 48 hours, and HMGB1, IL-6, TGF-β and VEGF were quantified using ELISA (IBL International GmbH, Cat#ST51011 and R&D Systems, Cat#DY406, DY1679, DY493).

RNA extraction and real-time quantitative PCR (qPCR)

Total RNA was isolated from siRNA-transfected tumorspheres, 48 hours after transfection, using TriZol (ThermoFisher Scientific) according to the manufacturer's instructions. RNA quality was assessed with the Agilent 2100 Bioanalyzer and quantified with a NanoDrop 2000 Spectrophotometer (ThermoFisher Scientific). Genomic DNA contaminations were removed with a DNA-free kit (Ambion), RNA was retrotranscribed with RETROscript reagents (Ambion), and qPCRs were carried out using gene-specific primers (QuantiTect Primer Assay; Qiagen), SYBR green, and a 7900HT RT-PCR system (Applied Biosystems). Quantitative normalization was performed on the expression of GAPDH. The expression levels in siTLR2-transfected tumorspheres relative to siSCR-transfected tumorspheres were calculated using the comparative ΔCt (threshold cycle number) method and reported as fold changes, as in the study of Conti et al.[13]

Magnetic resonance imaging

MR images were acquired at 7.1 T on a Bruker Avance300 spectrometer equipped with the Micro2.5 microimaging probe at room temperature. T_{2W} morphological images were acquired using a standard RARE (Rapid Acquisition with Refocused Echoes) sequence with the following parameters: TR = 4000 ms, TE = 40.57 ms, RARE factor = 24, flip angle = 180°, number of averages = 4, FOV = 30 mm x 30 mm, slice thickness 1 mm, matrix size 256 x 256, and spatial resolution = 0.117 × 0.117 mm/pixel. Diffusion-Weighted MR Images (DWI-MRI) were acquired using Spin Echo sequences with TE = 27 ms, TR = 750 ms, number of averages = 1, FOV = 30 x 30 mm, slice thickness = 1 mm, matrix size 128 x 128, spatial resolution = 0.234 × 0.234 mm/pixel. Six different B-values were used (0, 150, 250, 500, 755, and 1000 s/mm^2). Apparent diffusion constant (ADC) maps were calculated by fitting DW-MRI signal intensity as a function of B-values using Bruker ParaVision360 software.[36] ADC maps were obtained by superimposing the ADC values of the tumor ROI onto T_{2w} MRI (Fiji-Image software).

Statistical analysis

Statistical significance was evaluated using GraphPad8 software. Differences in tumor-free mice and survival were analyzed using Mantel-Cox log-rank test. Differences in sphere formation, FACS and ELISA data, and tumor multiplicity were analyzed using two-tailed unpaired Student's t test (with Welch's correction for samples with different variance) and non-parametric Mann–Whitney or Kruskal–Wallis test when the distribution calculated using Shapiro-Wilk or Kolmogorov Smirnov test was not normal. Differences in cell viability and tumor growth were analyzed using two-way ANOVA with Bonferroni posttest. $P < 0.05$ was considered significant.

Results

TLR2 expression is linked to poor prognosis in BC patients

To investigate whether TLR2 expression correlates with prognosis in BC patients, we performed a meta-analysis on public gene-expression data from human breast tumors.[22,26] Patients with high TLR2 expression showed significantly lower RFS (Figure 1a) and a trend in decreased OS (Figure 1b) than those with low TLR2, suggesting that TLR2 may play a role in BC progression, as also confirmed by a meta-analysis in 32 individual datasets (Supplementary Table 1, Fisher's collapsed p-value = 6.35 x 10^{-9}). We did not find a significant difference in survival analyzing each BC subtype separately, probably due to the lower statistical power in smaller sets of samples. However, using an extensive set of transcriptomic data (33 datasets from the MetaGxBreast database[24]), we observed that TLR2 displays higher expression in the most aggressive Basal-like subtype with respect to the other subtypes (one-sided Wilcoxon signed-rank test p-value <0.05 in 27/33 datasets; data not shown).

TLR2 deletion hinders HER2-driven mammary carcinogenesis

To study the role of TLR2 in mammary carcinogenesis and progression, we generated neuT-TLR2^{WT} and neuT-TLR2^{KO} mice, which carry the activated rat HER2/neu oncogene under the MMTV promoter and spontaneously develop mammary tumors. Tumor onset was significantly delayed in neuT-TLR2^{KO} mice (Figure 1c), which displayed significantly

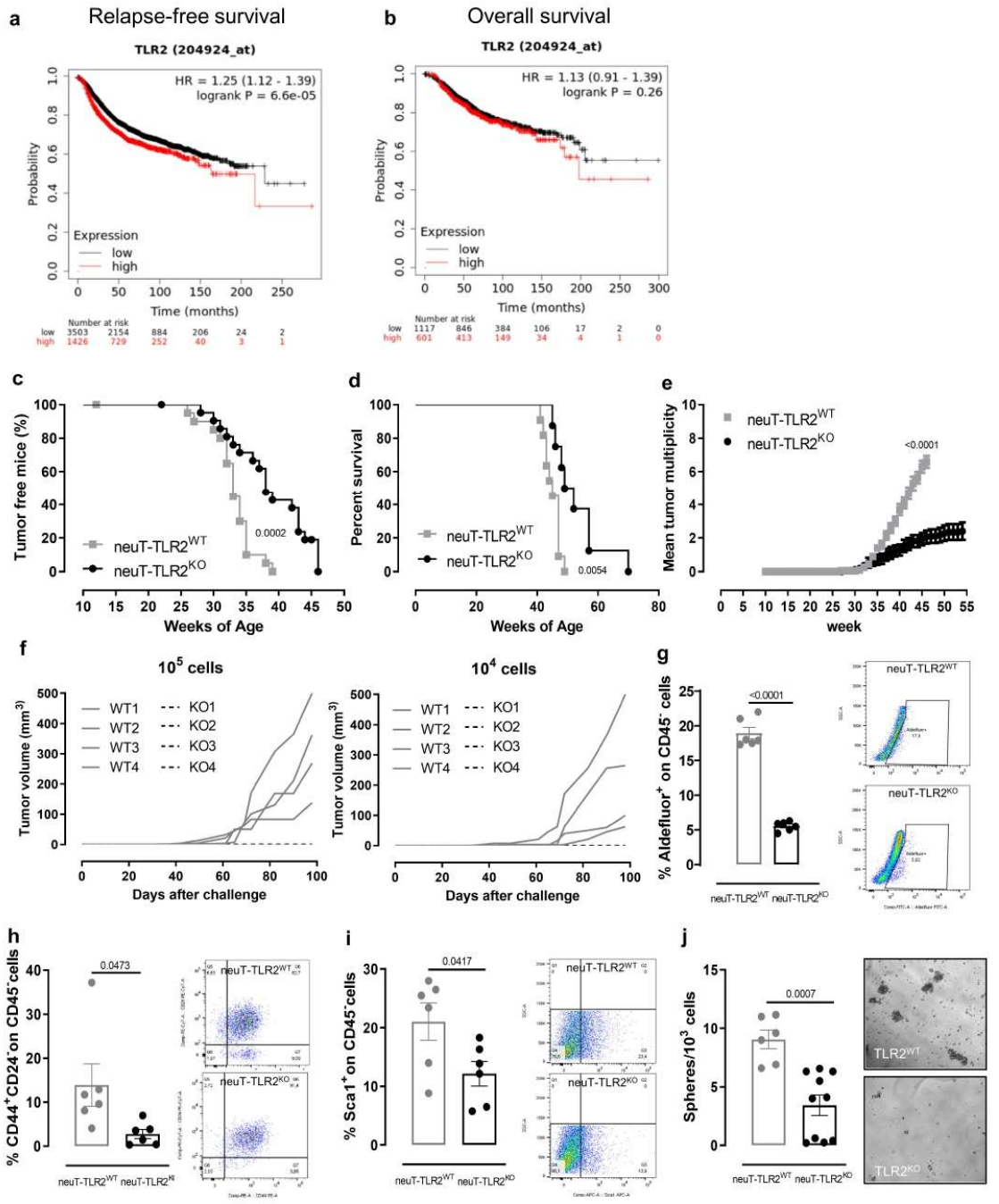


Figure 1. TLR2 correlates with poor prognosis in BC patients, and its deletion hinders HER2-driven mammary carcinogenesis and affects CSCs (a, b) Kaplan–Meier plots displaying (a) RFS and (b) OS in BC patients from all the datasets included in the KMPlotter website, stratified according to TLR2 mRNA expression (N = 4929 and N = 1728 in A and B, respectively). (c) Tumor-free survival, (d) OS, (e) mean tumor multiplicity of neuT-TLR2^{WT} (N = 21) and neuT-TLR2^{KO} (N = 22) mice. (f) Mean tumor volume of C57Bl6 mice injected orthotopically with 1 x 10^4 or 1 x 10^5 cells dissociated from tumors explanted from 4 neuT-TLR2^{WT} (solid lines) or 4 neuT-TLR2^{KO} (dashed lines) mice. (g-i) FACS analysis of (g) Aldefluor$^+$ (h) CD44$^+$ CD24$^-$ and (i) Sca1$^+$ CSCs in tumors explanted from neuT-TLR2^{WT} or neuT-TLR2^{KO} mice. Representative density plots are shown. Graphs show mean ± SEM of the percentage of CSCs from among CD45$^-$ cells (each dot represents a mouse). N = 6 per group. (l) Sphere-generating ability (number of tumorspheres generated every 10^3 plated cells) of cells dissociated from the tumors of neuT-TLR2^{WT} (N = 6) and neuT-TLR2^{KO} (N = 10) mice. Results come from at least 3 independent experiments. (c-d) Log-rank Mantel-Cox, (e) Mann Whitney, and (g-j) unpaired Student's t tests with Welch's correction.

higher survival (Figure 1d) and a decrease in tumor multiplicity compared to neuT-TLR2^{WT} mice (Figure 1e). This was accompanied by a lower frequency of CSCs functionally defined as tumor-initiating cells, as demonstrated by the inability of cells dissociated from four different neuT-TLR2^{KO} tumors to generate progressively growing masses when injected orthotopically at different amounts (either 1 x 10^5 or 1 x 10^4 cells) in syngeneic mice. Cells dissociated from four different neuT-TLR2^{WT} tumors gave rise to tumors with a 100% penetrance at both dilutions (Figure 1f). Moreover, the lower frequency of CSCs in neuT-TLR2^{KO} tumors was confirmed by the lower percentage of cells stained with the Aldefluor reagent, which measures the activity of aldehyde dehydrogenase 1, typically increased in breast CSCs,[15] and of cells displaying the prototypical breast CSC phenotype CD44$^+$ CD24$^-$[15] or expressing Sca1, a marker of CSCs in the neuT mouse model,[37,38] observed in neuT-TLR2^{KO} than in neuT-TLR2^{WT} tumors (Figure 1g-i and Supplementary Fig 1a). Likewise, cells purified from neuT-TLR2^{KO} tumors generated significantly fewer tumorspheres than those from neuT-TLR2^{WT} (Figure 1j), confirming that TLR2 promotes CSC survival and self-renewal, and plays a key role in HER2-driven mammary carcinogenesis.

TLR2 deletion alters Treg frequency without affecting other immune cell populations

Since TLR2 is expressed in many immune cells including neutrophils, myeloid-derived suppressor cells (MDSC), monocytes, DCs, macrophages, NK cells, T (including Treg), and B lymphocytes,[6] we assessed the percentage of the main immune cell types in the tumors, blood, and spleens from neuT-TLR2^{KO} and neuT-TLR2^{WT} mice at the experimental endpoint. The FACS gating strategy used is reported in Supplementary Fig 1b. While no significant differences were observed in most of the myeloid and lymphoid populations (Figure 2a-f) in tumors, blood, and spleens, and in intratumor macrophage polarization (Figure 2g), significantly lower Treg frequency was found in the tumors, blood, and spleens from neuT-TLR2^{KO} mice (Figure 2h-j). Since in the neuT mouse model the amount of Treg cells can positively correlate with tumor progression,[39] and we have observed an enhanced tumor progression in neuT-TLR2^{WT} mice as compared to neuT-TLR2^{KO} (Figure 1c-e), we analyzed the presence of Tregs in tumor-free TLR2^{WT} and TLR2^{KO} mice, to exclude that the observed difference in this cell population was due to variations in tumor burden and not to the expression of TLR2. Significantly lower levels of circulating Tregs were found in tumor-free TLR2^{KO} than in TLR2^{WT} mice (Figure 2k), suggesting that TLR2 can influence Treg expansion, regardless of the presence of cancer cells. Moreover, in TLR2^{WT} mice, about 50% of Tregs and only 10% of effector T cells were positive for TLR2 staining, with Tregs expressing higher TLR2 levels (measured as MFI) than effector CD4$^+$ T cells (Figure 2l). Interestingly, when circulating T cells from tumor-bearing TLR2^{WT} mice were activated in the presence of TLR2 activators, PGN-SA or HMGB1, the percentage of Tregs significantly increased (Figure 2m), suggesting that TLR2 may directly promote Treg expansion.

TLR2^{KO} BC cells display impaired tumorigenic properties

To dissect the contribution of cancer and host cell TLR2 signaling to tumor progression, we generated cell lines from the primary tumors of neuT-TLR2^{WT} and neuT-TLR2^{KO} mice, named WT-874, WT-879, WT-880, and KO-M26, KO-E26, and KO-C26, respectively. WT-874, WT-879, WT-880 express TLR2, which as expected is absent in KO-M26, KO-E26, and KO-C26 cells (Supplementary Fig 2a). All these cells express HER2 and the luminal marker cytokeratin 19 (CK19) but are negative for the basal marker alpha smooth muscle actin (α-SMA) (Supplementary Fig 2a). *In vitro*, TLR2^{WT} cells displayed a slightly higher proliferation and lower basal apoptosis as compared to TLR2^{KO} cells (Supplementary Fig 2b, c).

We performed orthotopic cross transplantation of WT-874 and KO-M26 cells into TLR2^{WT} and TLR2^{KO} mice. Tumor onset and progression correlated to the presence of TLR2 in cancer cells. Indeed, WT-874 cells generated tumors in 100% of mice, regardless of the recipient mouse genotype, while KO-M26 cells generated tumors in only 20% and 30% of TLR2^{WT} and TLR2^{KO} mice, respectively (Figure 3a). Moreover, the tumors generated by KO-M26 cells remained very small (mean volumes at sacrifice <1.5 mm^3), regardless of the genotype of the receiving mice (Figure 3b). The tumors generated by WT-874 cells injected into TLR2^{KO} mice were significantly larger (mean volumes at sacrifice: 127 mm^3), and even significantly bigger tumors were generated by the WT-874 cells injected into TLR2^{WT} mice (mean volumes at sacrifice: 500 mm^3) (Figure 3b). Similar results were obtained using KO-E26 cells (Supplementary Fig 3).

To confirm the TLR2 tumor-cell-intrinsic effects, 4T1 cells were silenced for TLR2 and injected into syngeneic BALB/c mice. TLR2 silencing significantly impaired tumor growth compared to control cells (Figure 3c). Moreover, a transplantation experiment performed in NSG mice indicated that the decreased tumorigenic ability of TLR2^{KO} BC cells is maintained in immunodeficient mice. Indeed, KO-M26, KO-E26, and KO-C26 cells generated smaller tumors than WT-874, WT-879 and WT-880 cells (Figure 3d). These results, and the observations on Tregs, strongly suggest that TLR2 expressed in BC cells promotes BC growth, and that host TLR2-expressing cells provide a partial contribution to tumor progression.

TLR2 promotes CSC self-renewal and its inhibition impairs cell viability

We then exploited TLR2^{WT} and TLR2^{KO} cell lines to characterize the tumor-cell-intrinsic pro-carcinogenic effects of TLR2. When cultured in tumorsphere-forming conditions, WT-874 cells generated significantly more tumorspheres than KO-M26 and KO-E26 (Figure 4a). Moreover, the percentage of Aldefluor$^+$ cells was significantly higher in WT-874 than in KO-M26 and KO-E26 cells, both when cultured in 2D conditions and as CSC-enriched P1 tumorspheres (Figure 4b). Similarly, a higher frequency of cells expressing the CSC markers Musashi-1,[40] Oct4,[41] Sca1, and CD44$^+$CD24$^-$ was measured in WT-874, WT-879 and WT-880 cells than in KO-M26, KO-E26, and KO-C26 cells

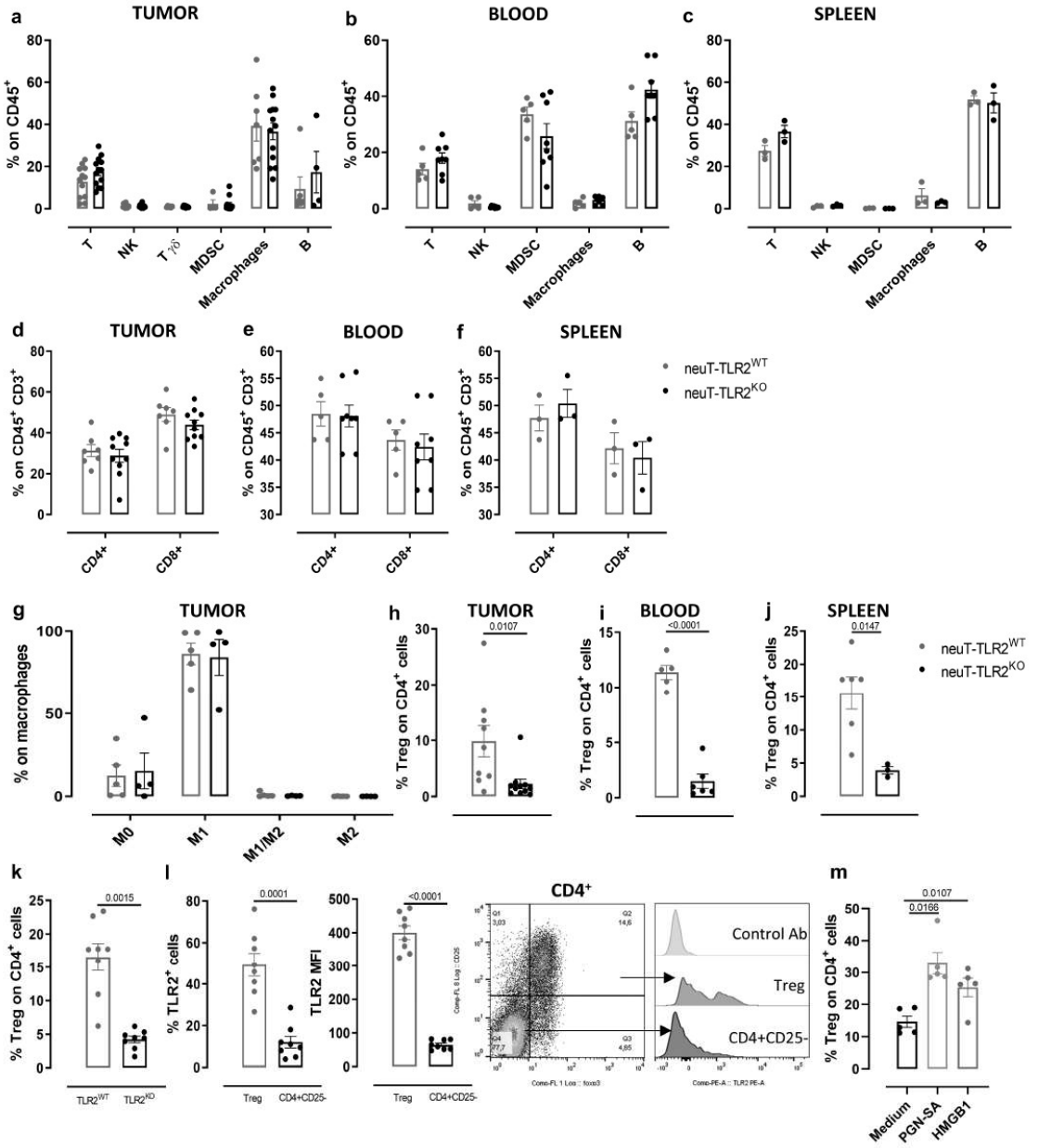


Figure 2. TLR2 deletion alters Treg cell frequency without affecting other immune populations. FACS analysis of immune cells in tumors (N ≥ 6 per group), blood (N = 5 neuT-TLR2^{KO} and 6 neuT-TLR2^{WT}) and spleens (N ≥ 3 per group) from neuT-TLR2^{KD} and neuT-TLR2^{WT} mice. Graphs show mean ± SEM of the percentage of (a-c) lymphocytes and myeloid cells from among CD45^{+} cells, (d-f) CD4^{+} and CD8^{+} from among CD3^{+} T cells, (g) M0, M1, M1/M2 and M2 from among total tumor macrophages, (h-j) Tregs from among CD4^{+} T cells. Each dot represents a mouse. (k) FACS analysis of peripheral Tregs in TLR2^{KO} and TLR2^{WT} mice. Graphs show mean ± SEM of the percentage of Tregs from among CD4^{+} T cells (N = 8 per group). (l) FACS analysis of TLR2 expression on Tregs and CD4^{+} CD25^{-} cells from TLR2^{WT} mice. Graphs show mean ± SEM of the percentage of TLR2^{+} cells and of TLR2 MFI (N = 8 per group). A representative density plot of Treg staining on CD4^{+} T cells and representative histograms of isotype control Ab or TLR2 staining on Treg and CD4^{+} CD25^{-} effector T cells are shown. (m) FACS analysis of Tregs from TLR2^{WT} mice upon *ex vivo* stimulation of blood T lymphocytes with TLR2 activating ligands. Graphs show mean ± SEM of the percentage of Tregs from among CD4^{+} cells. Each dot represents a mouse (N = 5 per group). Results come from at least 3 independent experiments. Unpaired Student's t test with Welch's correction.

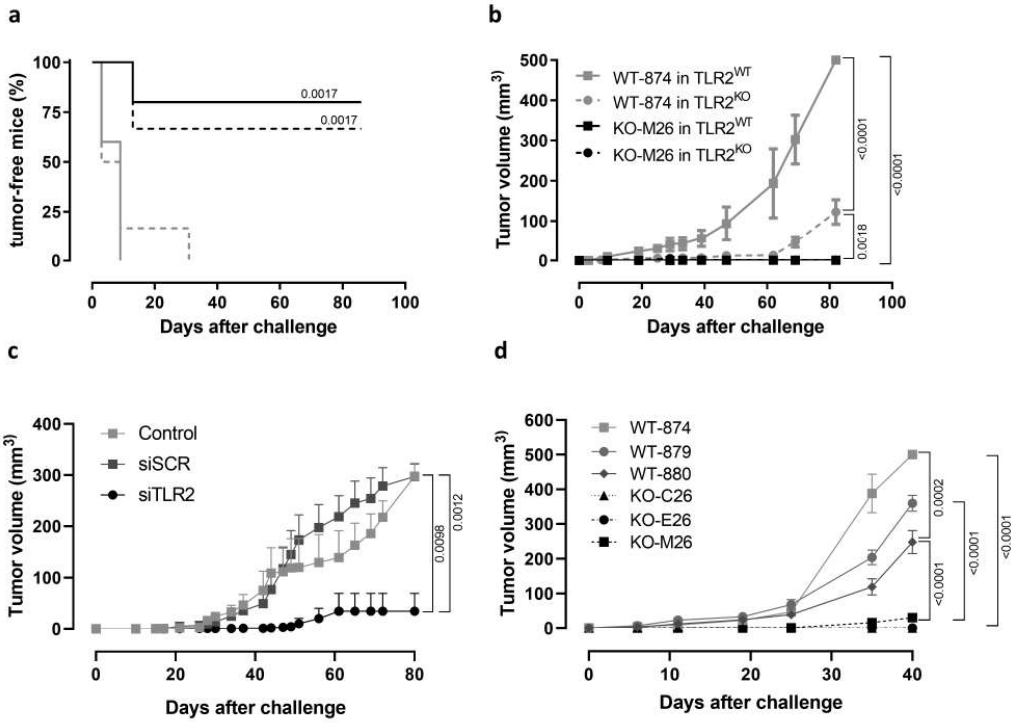


Figure 3. TLR2^{KO} BC cells display impaired tumorigenicity. (a) Tumor-free survival and (b) mean tumor volume of TLR2^{WT} and TLR2^{KO} mice (N = 6 per group, from 2 independent experiments) injected orthotopically with 1×10^6 WT-874 or KO-M26 cells. (c) Mean tumor volume of BALB/c mice orthotopically injected with 1×10^4 4T1 cells left untreated (N = 5), transfected with scrambled siRNAs (N = 7) or siRNAs to TLR2 (N = 7). (d) Mean tumor volume of NSG mice injected orthotopically with 1×10^6 WT-874, WT-879, WT-880, KO-C26, KO-M26 or KO-E26 cells (N = 6 per group from two independent experiments). (a) Log-rank (Mantel-Cox) of KO-M26 cells injected into TLR2^{WT} and TLR2^{KO} mice vs WT-874 cells injected into TLR2^{WT} mice. (b) two-way ANOVA test.

(Supplementary Fig 2d-g), indicating that TLR2 is involved in CSC self-renewal. Moreover, TLR2 induces the secretion of pro-tumoral cytokines, since, compared to KO-M26 or KO-E26 cells, WT-874 produced significantly higher amounts of TGF-β, IL-6, and VEGF (Figure 4c-e), which are responsible for triggering a pro-tumoral loop that promotes CSC self-renewal, proliferation, and invasion.[13]

Several mouse and human BC cell lines, including TUBO, 4T1, and MDA-MB-231, express TLR2 (figure 4f). We therefore assessed the effect of TLR2 activation on their tumorsphere-generation ability. Murine HER2$^+$ TUBO and TNBC 4T1 cells were stimulated with PGN-SA or HMGB1. Under these stimuli, TUBO and 4T1 cells generated significantly more spheres and expressed higher levels of the CSC marker Sca1 than control cells (Figure 4g, h and Supplementary Fig 4). This effect was TLR2-dependent, as was not observed in TLR2-silenced cells (Figure 4g, h). PGN-SA and HMGB1 also increased tumorsphere generation in human TNBC MDA-MB-231 cells (Figure 4i). Moreover, in both TUBO and 4T1 tumorspheres, TLR2 silencing with specific siRNAs decreased the mRNA level of the CSC markers Sca1, Nanog,[41] and Musashi-1[40] as compared to what observed in scrambled siRNA-transfected tumorspheres (Figure 4j), confirming that TLR2 promotes BC stemness, as we previously demonstrated.[13] As an independent indication of the relationship between TLR2 and CSC activity, we analyzed 33 BC transcriptomic datasets and reported that TLR2 expression positively correlates with a published breast CSC signature[16] in most of them (Figure 4k; Pearson correlation, Fisher's merged p-value across 33 datasets: 1.4×10^{-38}).

Finally, the effect of TLR2 pharmacological inhibition on BC cell viability was assessed. Indeed, the TLR2 inhibitor CU-CPT22 dose-dependently impaired WT-874, TUBO, 4T1, and MDA-MB-231 cell viability (Figure 4l), while it was ineffective on KO-M26 or KO-E26 cells (not shown). Overall, these results demonstrate that TLR2 signaling promotes breast CSC self-renewal and that its inhibition affects BC cell viability.

TLR2 mediates resistance to doxorubicin

High TLR2 expression in BC patients correlates with a significantly impaired response to chemotherapy, as chemotherapy-treated BC patients with TLR2^{high} tumors showed lower RFS than patients with TLR2^{low} tumors (Figure 5a), and TLR2 expression is significantly higher in non-responder than responder patients (Figure 5b). Accordingly, WT-874, WT-879 and WT-880 cells were more resistant to doxorubicin than KO-M26, KO-E26, and KO-C26 cells, which showed lower viability (Figure 5c) and significantly higher apoptosis (Figure 5d) in response to doxorubicin. Similar results in terms of viability

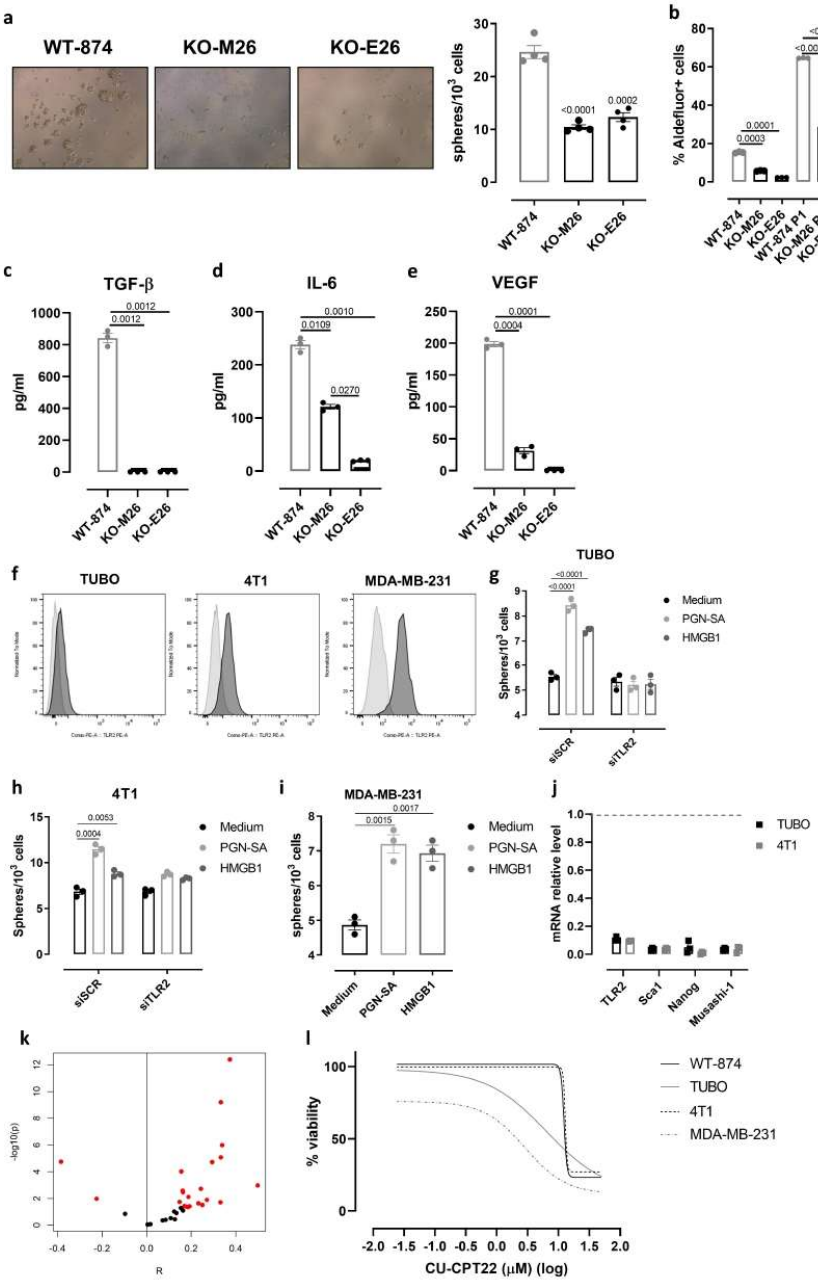


Figure 4. TLR2 promotes breast CSC self-renewal and its inhibition impairs cell viability. (a) Representative images of tumorspheres (Magnification 10X), and graph showing sphere-generating ability (number of tumorspheres generated every 10^3 plated cells) of WT-874, KO-M26, and KO-E26 cells cultured for 5 d in tumorsphere-forming conditions. (b) Means ± SEM of the percentage of Aldefluor$^+$ cells in WT-874, KO-M26, and KO-E26 cells cultured for 5 d in 2D or tumorsphere-forming conditions. (c-e) ELISA of TGF-β, IL-6 and VEGF released into the supernatant of WT-874, KO-M26, KO-E26 cultured for 48 hours in 2D conditions. (f) Representative FACS histograms of TLR2 (dark gray) and control (light gray) staining on TUBO, 4T1 and MDA-MB-231 cells. (g, h) Tumorsphere-generating ability of TUBO and 4T1 cells transfected with a pool of scrambled siRNAs (siSCR) or siRNAs to TLR2 (siTLR2) treated, 24 hours after transfection, with PGN-SA or HMGB1 for 4 d. (i) Tumorsphere-generating ability of MDA-MB-231 cells treated with PGN-SA or HMGB1 for 5 d. (j) Relative expression by qPCR of TLR2, Sca1, Nanog and Musashi-1 mRNA in TUBO and 4T1 tumorspheres transfected with siTLR2 as compared to those transfected with siSCR (gray dotted line). (k) Plot indicating the correlation between TLR2 expression, and a CSC signature computed with ssGSEA for each of the BC transcriptomic datasets comprised in MetaGxBreast. X axis shows the value of Pearson's correlation, y axis represents correlation's significance. Red dots label datasets with a p-value<0.05, showing that significant tests are skewed toward positive values. (l) Concentration-dependent cytotoxicity of CU-CPT22 (50 to 0.02 μM) on WT-874, TUBO, 4T1 and MDA-MB-231 cells, evaluated using MTT after 48 hours of treatment. The graph shows log(inhibitor) vs. response – variable slope (four parameters) non-linear regression of data from three independent experiments, calculated with GrapPad8 software. All graphs report data from 3 independent experiments. Student's t test.

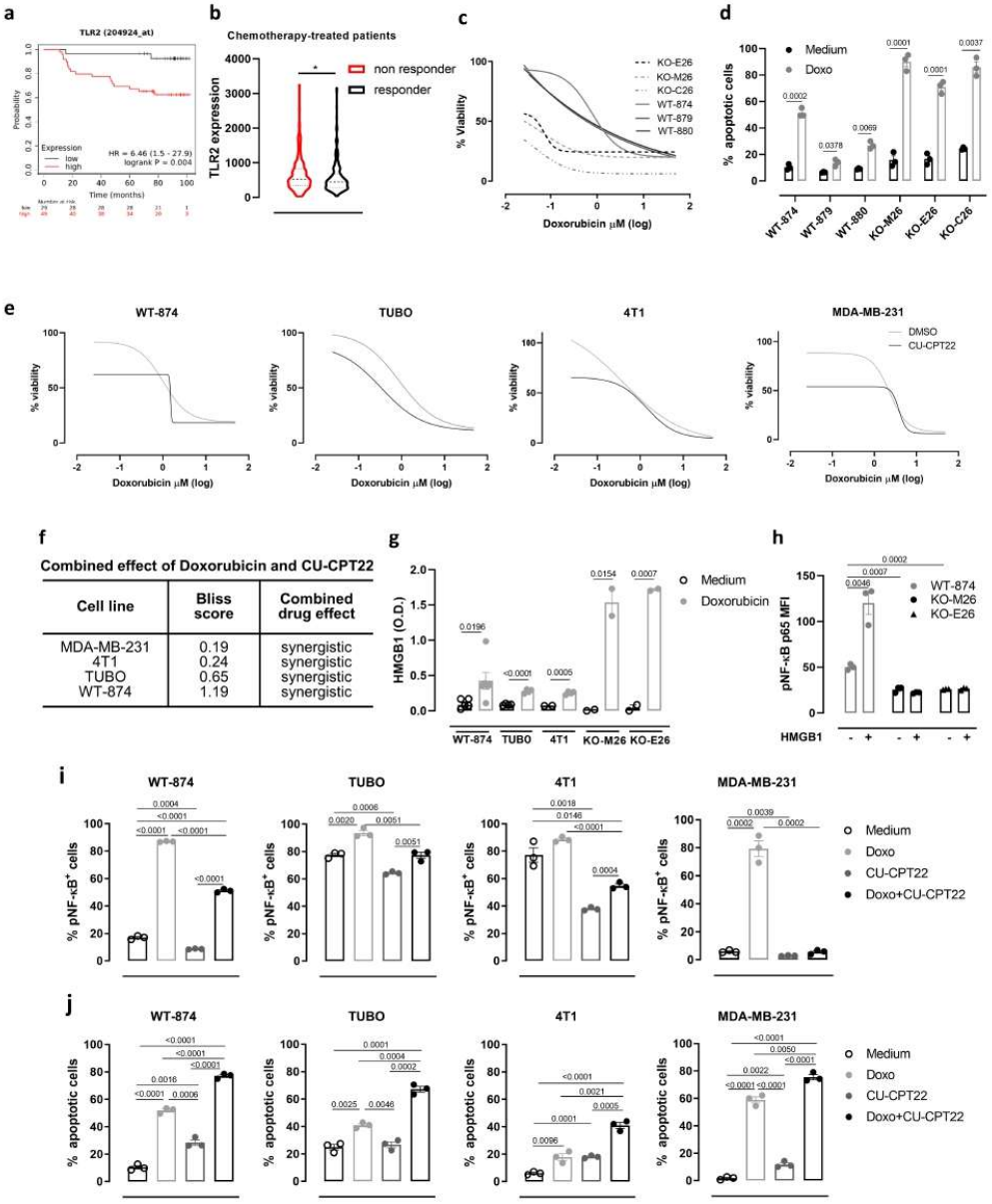


Figure 5. TLR2 promotes BC resistance to doxorubicin. (a) Kaplan–Meier plots displaying 5-y RFS of chemotherapy-treated BC patients stratified according to TLR2 mRNA expression (N = 78). (b) TLR2 mRNA expression levels in the tumors from BC patients that relapsed (non-responders; N = 221) or not (responders; N = 256) within 5 y of adjuvant chemotherapy. (c) Concentration-dependent cytotoxicity of doxorubicin (50 to 0.02 μM) on WT-874, WT-879, WT-880, KO-M26, KO-E26 and KO-C26 cells, evaluated by MTT after 48 hours of treatment. The graph shows log(inhibitor) vs. response – variable slope (four parameters) non-linear regression of data from three independent experiments, calculated using GrapPad8 software. (d) WT-874, WT-879, WT-880, KO-M26, KO-E26 and KO-C26 cells were treated with doxorubicin for 48 hours and analyzed using Annexin-V/propidium iodide FACS staining. The graph shows means ± SEM of the % of Annexin-V$^+$ from three independent experiments. (e) Concentration-dependent toxicity of doxorubicin (50 to 0.02 μM) alone or combined with 5 μM CU-CPT22 on WT-874, TUBO, 4T1 and MDA-MB-231 cells, evaluated via MTT after 48 hours of treatment in three independent experiments. (f) Analysis of the effect of the combination of doxorubicin and CU-CPT22 on BC cell lines. Bliss score > 0: synergistic effect; Bliss score = 0: additive effect; Bliss score < 0: antagonistic effect. (g) ELISA analysis of HMGB1 released into the supernatant by BC cells that were treated with doxorubicin for 48 hours or left untreated. The graph shows means ± SEM of HMGB1 concentration from ≥2 independent experiments. (h) FACS analysis of p65 NF-κB phosphorylation in WT-874, KO-M26 and KO-E26 cells treated with HMGB1 for 30 minutes or left untreated. The means ± SEM of mean fluorescence intensity (MFI) from three independent experiments are reported. (i, j) WT-874, TUBO, 4T1 and MDA-MB-231 cells were treated for 48 hours with or without doxorubicin, CU-CPT22 or a combination of both. (i) Graphs of FACS analysis of p65 NF-κB phosphorylation. (j) Annexin-V/propidium iodide analysis of cell apoptosis. All graphs report the means ± SEM of the percentage of positive cells from three independent experiments. Student's t tests.

and apoptosis were obtained using docetaxel, which – as doxorubicin – can induce ICD[42] (Supplementary Fig 5a, c). On the contrary, treatment with cisplatin, which is reported not to induce ICD,[42] impaired the viability and induced apoptosis of $TLR2^{WT}$ and $TLR2^{KO}$ cells to a similar extent (Supplementary Fig 5b, c). Interestingly, TLR2 inhibition with CU-CPT22 increased the sensitivity of $HER2^{+}$ (WT-874 and TUBO) and TN (4T1 and MDA-MB-231) BC cells to doxorubicin (Figure 5e). Significantly, the two drugs in combination exerted synergistic activity, as calculated using the Bliss independence model (figure 5f). To dissect the mechanisms involved in TLR2-dependent resistance to ICD-inducing drugs, we analyzed the supernatants of doxorubicin-treated cells and found that doxorubicin induced the release of HMGB1, which may activate TLR2, in all BC cells tested, with higher amounts released by KO-M26 and KO-E26 cells, which is in line with their higher sensitivity to doxorubicin (Figure 5g). Treatment with HMGB1 induced an increase in the phosphorylated form of the TLR2 downstream signal transducer p65 NF-κB in WT-874 cells but not in KO-M26 and KO-E26 cells (Figure 5h). As expected, doxorubicin increased phospho-NF-κB in WT-874, TUBO, 4T1, and MDA-MB-231 cells, while TLR2 inhibition with CU-CPT22 significantly reduced it. The addition of CU-CPT22 to doxorubicin-treated cells significantly reduced phosphorylated NF-κB in all cell lines (Figure 5i and Supplementary Fig 6a). Moreover, doxorubicin treatment induced the release of the NF-κB-regulated cytokine IL-6, which was abolished by adding CU-CPT22 (Supplementary Fig 7A). Since NF-κB inhibits apoptosis and promotes cell survival,[6] treatment with CU-CPT22 slightly induced apoptosis of WT-874, TUBO, 4T1, and MDA-MB-231 cells (Figure 5j and Supplementary Fig 6b). Of note, the level of apoptosis induced by CU-CPT22 was similar to the basal apoptosis observed in $TLR2^{KO}$ cells (Supplementary Fig 2c) and to that induced by siRNA-mediated TLR2 silencing in WT-874 cells (Supplementary Fig 6c). Most importantly, the addition of CU-CPT22 significantly improved doxorubicin apoptotic effect in WT-874, TUBO, 4T1, and MDA-MB-231 cells (Figure 5j and Supplementary Fig 6b). Of note, treatment of MDA-MB-231 cells with doxorubicin, alone or combined with CU-CPT22, increased the release of HMGB1 and other DAMPs that can potentially bind TLR2, such as HSP70, HSP90, Morgana (CHORDC1), HSP60, and Heat shock cognate 71 kDa protein (HSC70)[43] (Supplementary Fig 7b), confirming the potential capability of doxorubicin to induce TLR2 activation on cancer cells. The effects of CU-CPT22 were not due to off-target mechanisms, as CU-CPT22 treatment did not exert any activity on KO-M26 or KO-E26 cells (Supplementary Fig 8a, b). Interestingly, CU-CPT22 increased doxorubicin-induced apoptosis to a similar extent as treatment with the NF-κB inhibitor BAY 11–7082 (Supplementary Fig 8c) and HMGB1 antagonist BOX-A (Supplementary Fig 8d).

These results demonstrate that TLR2/NF-κB signaling, which is activated by doxorubicin-induced HMGB1 release, is involved in chemoresistance, and that TLR2 inhibition restores BC cell sensitivity to doxorubicin.

Treatment with a TLR2 inhibitor potentiates doxorubicin anti-cancer effects *in vivo*

To verify whether TLR2 inhibition exerts an antitumor effect *in vivo*, we treated 4T1 tumor-bearing BALB/c mice with two different doses of CU-CPT22 (10 or 50 μg) intratumorally, twice per week, starting when tumors reached 2 mm in mean diameter. Both CU-CPT22 doses significantly reduced tumor growth, and treatment at 50 μg significantly reduced the number of spontaneous lung metastases (Supplementary Fig 9). We then analyzed whether CU-CPT22 potentiates the activity of doxorubicin. 4T1 tumor-bearing mice were treated with doxorubicin, with and without CU-CPT22 (50 μg), twice per week. Both doxorubicin and CU-CPT22, administered as single treatments, significantly reduced tumor growth compared to control mice (Figure 6a). However, the combination of the two drugs induced a statistically significant reduction in tumor growth compared to the two single treatments (Figure 6a). Moreover, mice treated with CU-CPT22 + doxorubicin showed significantly fewer lung metastases than control or doxorubicin-treated mice (Figure 6b). Mice underwent MRI at the experimental end point to better characterize the effects of the combination treatment. T_{2w} morphological axial and coronal MR images were acquired at $B_0 = 7$ T. As shown in the representative T_{2w} axial images, a significant decrease in tumor volume occurred upon treatment with CU-CPT22 + doxorubicin (Figure 6c, upper). The MRI quantification of tumor volume showed decreases of 38 ± 2%, 47 ± 10%, and 75 ± 16% in mice treated with CU-CPT22, doxorubicin, or both, respectively, compared to control mice (Figure 6d). ADC-MRI maps, which report the degrees of freedom of water, were obtained using DWI-MRI. False color representative axial ADC maps of the tumor region (superimposed onto morphological T_{2w} MR images) are reported in Figure 6c (lower) for control mice and mice treated with doxorubicin and CU-CPT22 simultaneously. A significant higher ADC value, an indication of decreased cellularity, was observed in CU-CPT22 + doxorubicin-treated mice than in control mice, while no significant effect was detected in mice treated with doxorubicin or CU-CPT22 alone (Figure 6e). A cytofluorimetric analysis of tumors showed that the combination of CU-CPT22 and doxorubicin induced a statistically significant decrease in $Sca1^{+}$ and $CD44^{+}$ $CD24^{-}$ CSCs compared to tumors from mice treated with doxorubicin alone, demonstrating that CU-CPT22 impairs CSC survival also *in vivo* (figure 6f, g). Moreover, the combined therapy induced a significant increase in tumor-infiltrating $CD8^{+}$ T cells and a decrease in Tregs (Figure 6h, i), while no significant differences in $CD4^{+}$ T, NK cells, and $Ly6C^{+}$ monocytic MDSCs were observed (Figure 6j-l). Of note, CU-CPT22, alone or combined with doxorubicin, induced a significant reduction in $Ly6G^{+}$ granulocytic MDSCs (Figure 6m). Despite not inducing variations in the total macrophage population (Figure 6n), the combined treatment also significantly decreased M2 while increasing M1 macrophages (Figure 6o). Overall, these data indicate that treatment with TLR2 inhibitor enhances the efficacy of doxorubicin, reducing breast tumor growth and metastatic dissemination and restoring an immunocompetent TME.

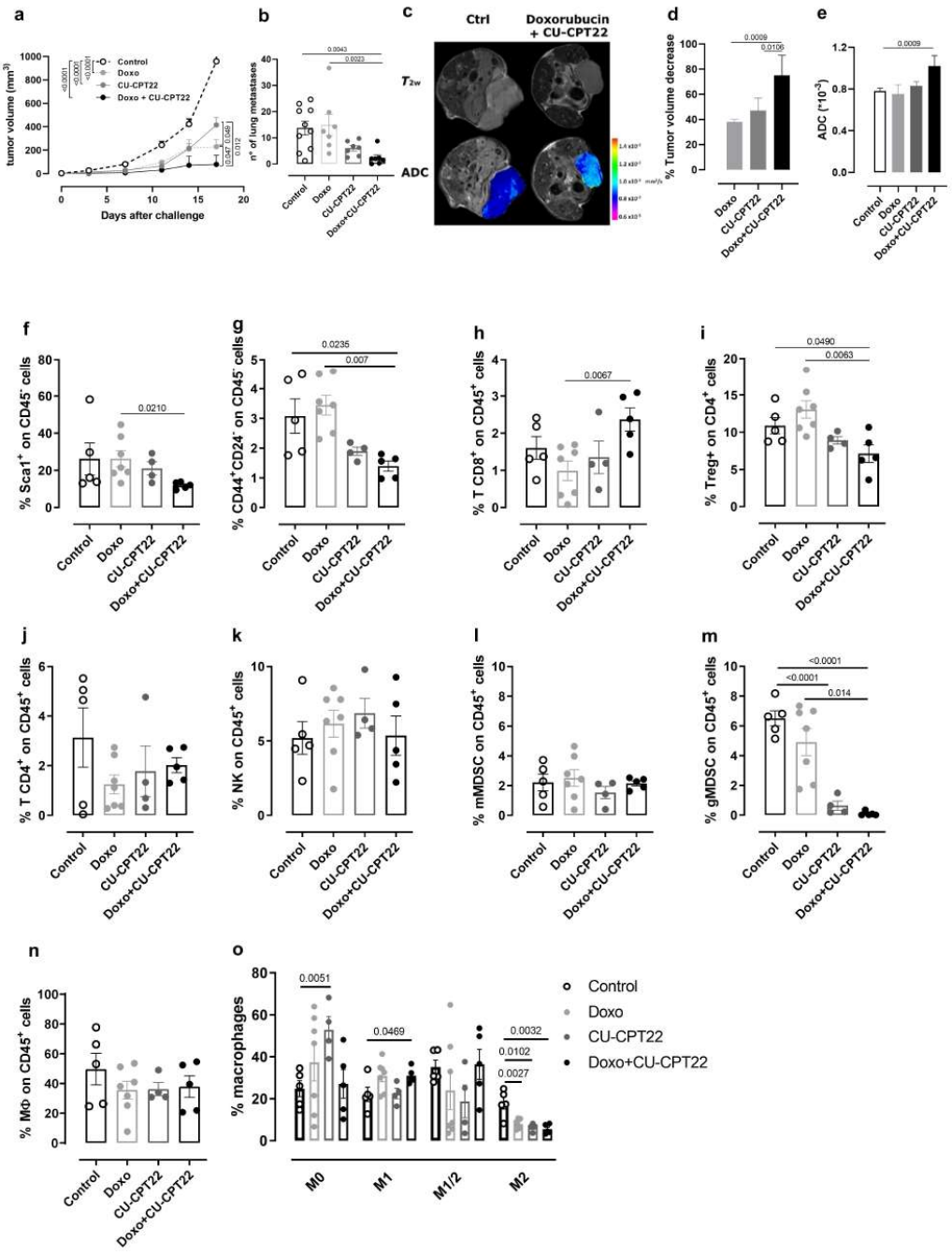


Figure 6. TLR2 inhibition increases doxorubicin anti-cancer activity *in vivo*. BALB/c mice were orthotopically challenged with 1×10^4 4T1 cells. When the tumors reached 2 mm in diameter, the mice were treated i.p. with 3 mg/kg doxorubicin and intratumorally with 50 µg CU-CPT22, or the vehicle alone as a control (N = 7 per treated groups and N = 10 per control group). The treatment was repeated twice per week. Graphs show (a) mean tumor volume, and (b) the number of spontaneous lung metastases per square mm measured in lungs. (c-e) T_{2w} and DWI axial MR images of mice were acquired at the end point of the treatment. (c) Representative T_{2w} axial images and false color representative axial ADC maps of the tumor region (superimposed on morphological T_{2w} MR images) of control and doxorubicin + CU-CPT22-treated mice. (d) Tumor volume was measured by manually drawing ROIs in the tumor for all axial slices covering the entire tumor (Fiji-ImageJ free software). Decrease of volume in the treated mice was reported as the percentage of the volume of control mice (mean ± SD). (e) Mean ± SD of ADC values from the tumors of treated mice. (f-o) FACS analysis of (f) $Sca1^+$ and (g) $CD44^+$ $CD24^-$ cells from among $CD45^-$, (h) $CD8^+$ T cells, (j) CD4 + T cells, (k) NK cells, (l) monocytic MDSCs, (m) granulocytic MDSCs, and (n) macrophages from among $CD45^+$ leucocytes and (i) Tregs from among $CD4^+$ T cells and (o) M1, M2, M1/M2 or M0 polarized macrophages among the macrophage population in the tumors. Graphs show means ± SEM of the percentage of positive cells (N ≥ 4). Each circle represents a mouse. Student's t test or Mann–Whitney test. In (a), two-way ANOVA analysis.

Discussion

Chemotherapy is still the main option for TNBC and metastatic BC patients, with neoadjuvant and adjuvant chemotherapy becoming mainstays for treating early BC. However, chemoresistance is common in both advanced and early BC, and about 30% of early-stage BC patients relapse despite treatment.[3,44] Therefore, the development of combined treatments to counteract chemoresistance and strengthen anticancer activity is an urgent medical need.

Since breast CSCs are chemotherapy-resistant and involved in tumor relapse,[15] we have previously sought genes that play a key role in breast CSC survival. We identified TLR2 as being overexpressed in breast CSCs and as playing a role in their self-renewal.[13] Herein, we have analyzed TLR2's role in mammary carcinogenesis by generating genetically modified mice that, to our knowledge, represent the only model of HER2-driven mammary carcinogenesis on a $TLR2^{KO}$ background. Although the carcinogenic process was not completely abolished, $TLR2^{KO}$ mice displayed delayed tumor onset and decreased tumor multiplicity, suggesting a contribution of TLR2 to BC development. The HER2 transgene acts as a potent tumor driver in neuT mice, not allowing to fully appreciate the contribution of TLR2 in affecting tumor growth. Moreover, we cannot exclude that the constitutive deletion of TLR2 may activate compensatory mechanisms that cannot be observed upon acute inhibition of TLR2. Indeed, while treatment of several BC cell lines with the TLR2 inhibitor CU-CPT22 dose-dependently decreased their viability, the cell lines generated from neuT-$TLR2^{KO}$ tumors displayed only a slight decrease in cell viability as compared to their $TLR2^{WT}$ counterpart. The generation of a conditional, tissue-specific $TLR2^{KO}$ mouse model might contribute to better elucidate the role of TLR2 in tumor progression.

However, data from BC patients, whose tumors express higher TLR2 levels than adjacent normal tissue and in which Wang et al. demonstrated that high tumor TLR2 expression, assessed by qPCR, is associated with poor OS and unresponsiveness to endocrine therapy in the luminal B subtype,[45] are in line with what was observed in our preclinical model. Significantly, several genetic alterations that result in increased TLR2-signaling-pathway activation, including mutations that generate constitutively active forms of TLR2 and amplifications in TLR2 downstream effector *IRAK1* (observed in 23.8% of patients), have been identified in BC patients.[46] In this study, we observed a significant association between high TLR2 expression and poor RFS in BC patients but not with OS. It should be noted that all the microarray datasets we analyzed are from the tumor bulk, where the expression of TLR2 in cancer and immune cells cannot be distinguished. The analysis of single-cell RNA sequencing datasets would allow to better correlate TLR2 expression on cancer cells and patients' outcome.

The role of TLR2 is, at least partly, mediated by its ability to promote breast-CSC self-renewal, as suggested by the higher frequency of cells that express typical breast CSC markers[38] and the enhanced CSC-enriched tumorsphere-generating ability of BC from TLR2-expressing mice compared to their neuT-$TLR2^{KO}$ counterparts. Indeed, we have previously demonstrated that TLR2 stimulation in breast CSCs leads to the activation of the MyD88/NF-κB and AKT pathways, which promote the secretion of several cytokines and growth factors, such as TGF-β and IL-6.[13] These cytokines promote CSC survival, self-renewal, and invasion via the autocrine activation of the STAT3 and Smad3 pathways,[6,13,47] in accordance with data that show increased TLR2 expression in BC cell lines endowed with metastatic potential.[48] However, CSC self-renewal and differentiation are controlled by a complex interplay among different signaling pathways, including those shared with normal stem cells, such as the Notch, Wnt, and Hedgehog pathways.[12] Therefore, TLR2 is one of the many players that support CSCs. Future experiments aimed at analyzing the tumorigenic potential of the putative CSC fraction isolated from neuT-$TLR2^{WT}$ or neuT-$TLR2^{KO}$ tumors could further demonstrate the impact of TLR2 deletion on cancer stemness. Nevertheless, our transplantation experiments confirmed that in cancer cells, TLR2 signaling mediates pro-tumorigenic effects as, unlike $TLR2^{WT}$ BC cells, $TLR2^{KO}$ BC cells have a poor ability to generate tumors when injected into both immunocompetent and NSG mice. Moreover, host-cell TLR2 also contributes to tumor progression, as $TLR2^{KO}$ mice represented a more hostile environment than $TLR2^{WT}$ mice for the growth of $TLR2^{+}$ BC. This suggests that TLR2 expression in immune cells may contribute to their immunosuppressive activity. In fact, several research groups have demonstrated that TLR2 stimulation in MDSCs induces their accumulation in the TME and lymphoid organs[49] and the production of IL-6 and IL-10, which polarize M2 macrophages and favor metastatic dissemination.[50,51] Moreover, TLR2 has been shown to promote Treg proliferation both directly, through the TLR2-MyD88-NF-κB axis,[52,53] and indirectly, via the activation of dysfunctional DCs that produce IL-6 and IL-10.[54] Fittingly, we observed a decrease in both tumor-infiltrating and peripheral Tregs in tumor-bearing neuT-$TLR2^{KO}$, compared to neuT-$TLR2^{WT}$ mice. This decrease was not due to the lower tumor burden characteristic of neuT-$TLR2^{KO}$ mice, since healthy, not neuT, $TLR2^{KO}$ mice showed a lower percentage of circulating Tregs than $TLR2^{WT}$ mice. We confirmed *in vitro* that TLR2 activation in T cells promotes the expansion of Tregs, which expresses higher TLR2 levels than effector $CD4^{+}$ T cells, suggesting that TLR2 plays an important role in Treg biology. However, TLR2 deficiency did not affect the percentages of other immune cell populations, whether in the tumor or periphery. Nevertheless, further studies are required to demonstrate their functional integrity.

Besides its role in breast carcinogenesis, TLR2 also plays a role in BC chemoresistance, as we observed that high TLR2 expression correlates with low RFS in chemotherapy-treated BC patients. Furthermore, the deletion or pharmacologic inhibition of TLR2 increases the sensitivity of several BC cell lines to doxorubicin. This mechanism of chemoresistance is mediated by the release of TLR2-activating DAMPs, such as HMGB1, following doxorubicin-induced ICD. Despite our study lacks the analysis of total NF-kB by WB due to technical issues, the increase of phospho-NF-κB in $TLR2^{WT}$ but not in $TLR2^{KO}$ cells treated with HMGB1 for 30 minutes, a time window insufficient to induce *de novo* NF-κB production, supports the role of NF-κB activation downstream to the

HMGB1/TLR2 axis. Although HMGB1 can also bind other receptors such as RAGE and TLR4,[6] we did not observe HMGB1-dependent NF-κB phosphorylation in $TLR2^{KO}$ BC cells, and TLR2 inhibition or silencing was sufficient to inhibit HMGB1 activity.[13] Thus, TLR2-activation induces the production of IL-6, a well-known promoter of survival, growth, and proliferation in both immunosuppressive and cancer cells,[55,56] thus protecting cells from apoptosis. Indeed, high HMGB1 levels correlate with poor response to neoadjuvant chemotherapy in TNBC patients,[18] and HMGB1 protects BC cells from chemotherapy and promotes metastasis formation.[57] Moreover, other DAMPs that can activate TLR2 may be released into the TME following ICD-inducing chemotherapy,[6,7,43] and indeed we observed the release of HSP70, HSP90, HSP60, and HSC70 from doxorubicin-treated MDA-MB-231 cells. Other chaperones, such as Morgana, are known to be constitutively released from MDA-MB-231 cells and to signal through TLR2.[43] Interestingly, TLR2 activation may also be induced by bacteria. Specific microbiota have recently been found in mammary glands, with normal and neoplastic samples showing alterations in amount and composition.[58] Neoadjuvant chemotherapy changes breast microbiota composition, inducing an increase in *Pseudomonas aeruginosa*, a potential TLR2 activator that stimulates BC cell proliferation.[59] Moreover, many chemotherapy-treated patients suffer from opportunistic infections from Gram-positive bacteria, with the commensal bacteria diffusing to the tumor, which could further activate TLR2.[60] Therefore, the administration of TLR2 inhibitors in combination with chemotherapy might not only impair the pro-inflammatory and pro-tumorigenic activity of HMGB1 and other DAMPs but may also counteract some of the detrimental effects of breast dysbiosis. Further experiments are needed to confirm this hypothesis.

Our *in vivo* therapeutic experiments have demonstrated that treatment with the TLR2 inhibitor CU-CPT22 enhances the capability of doxorubicin to hamper BC progression, potentiating its anti-cancer effects and decreasing metastatic dissemination. The combination of doxorubicin and TLR2 inhibition significantly decreased the frequency of $Sca1^+$ and $CD44^+$ $CD24^-$ cells in the tumors. Moreover, MRI analysis identified a significant reduction in tumor volume (about 75%) in mice treated with doxorubicin in combination with CU-CPT22 as compared to control mice. Further insights into tumor features have been gained by using DWI-MRI to obtain ADC maps that report the degree of freedom of water, which is a technique that is extensively applied to assess increases in cellularity during tumor growth.[36] Treatment with doxorubicin and CU-CPT22 caused an increase in water freedom, suggesting a lowering of cellularity because of tumor regression.

Significantly, although TLR2 is expressed in immune cells, no detrimental alterations in the immune system were observed in mice treated with CU-CPT22 and in $TLR2^{KO}$ mice, which supports the safety and feasibility of TLR2 targeting. Indeed, innate and acquired immune responses are well preserved in the absence of TLR2,[61] and phase I clinical trials with TLR2-targeted therapies showed initial promising results in hematological malignancies.[62,63] Importantly, anthracyclines, including doxorubicin, can induce ICD in cancer cells, leading to the promotion of an anti-tumor immune response.[64] Besides HMGB1, the main DAMPs that mediate this response are Annexin A1, ATP, and calreticulin, alongside several cytokines released by cancer cells that contribute to immune-stimulation.[65] Therefore, it should be emphasized that the determinants of immune stimulation in doxorubicin-induced ICD are diversified, and the inhibition of the HMGB1-TLR2 axis on immune cells could not be sufficient to halt the anti-tumor immune response. Moreover, it has been shown that the expression of TLR4, another HMGB1 receptor, on DCs is required for the induction of a tumor-specific T cell response, while lack of TLR2 did not affect it.[66] Conversely, TLR2 activation on MDSCs has been demonstrated to promote pro-tumoral inflammation, while TLR4 was not involved in this mechanism.[50] Moreover, activation of TLR2 can lead to the expansion of Tregs, thus suppressing anti-tumor immunity *in-vivo*.[52,53] Therefore, TLR2 and TLR4 appear to trigger opposite mechanisms in a cell-type-dependent manner, with TLR2 being dispensable for anti-tumor activity of DCs but required for pro-tumor activity of MDSCs and Tregs, and TLR4 being dispensable for pro-tumor activity of MDSCs but required for antitumor activity of DCs. Nevertheless, the anti-tumor vs pro-tumor effects resulting from TLR2 engagement are a complex matter of debate,[67] with TLR2 agonists having been reported as successful adjuvants for anti-cancer immunotherapy,[68] and TLR2 inhibitors (monoclonal antibodies or small-molecule inhibitors) successfully used in clinical trials for the treatment of acute myeloid leukemia and myelodysplastic syndrome.[62,63] In our 4T1-based mouse model, doxorubicin alone did not induce any significant changes in the proportion of immune cell populations infiltrating the tumor (except for a decrease in M2-polarized macrophages), while CU-CPT22 alone and even more when combined with doxorubicin significantly reduced Tregs, granulocytic MDSCs, and M2 macrophages while increasing $CD8^+$ cytotoxic T cells and M1 macrophages. These results suggest that the pro-tumor function exerted by TLR2 stimulation on cancer cells and immune-suppressive cells may hinder the capability of doxorubicin to generate an anti-tumor immune response. Conversely, the addition of CU-CPT22 unleashes the full immunogenic potential of doxorubicin-induced ICD, leading to a remodeling of the TME. Of note, similar results were observed when blocking the TLR2 ligand HMGB1 in a 4T1 tumor model, which improved the efficacy of immune checkpoint inhibitors.[69] The combined treatment with doxorubicin and CU-CPT22 was more effective than doxorubicin monotherapy in hindering 4T1 tumor progression *in vivo*, but tumor growth was not completely abolished. This could be due to the 4T1 intrinsic features that might lead to an underestimation of the potential effect of the combined protocol proposed. Indeed, the 4T1 model is quite resistant to several combined therapies and immunotherapies, and the combination of cyclophosphamide/doxorubicin with anti-PD-1 or anti-PD-L1 antibodies showed no, or very limited, increase in anti-tumor effect.[70,71]

The results so far obtained and described in this manuscript demonstrate that TLR2 plays a role in BC chemoresistance (Figure 7), although it cannot be considered a master regulator of BC onset and progression. Its targeting may enhance BC cell vulnerability to standard therapies, similarly to what is

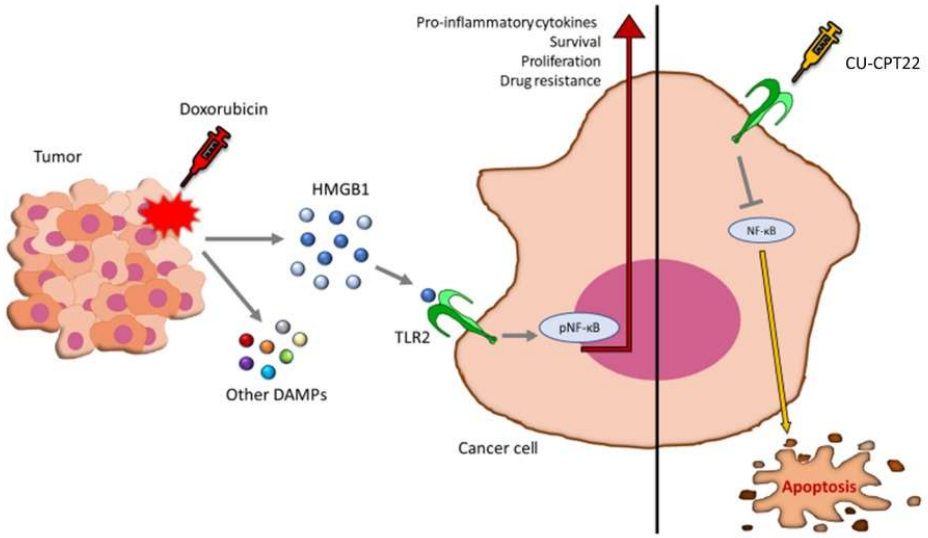


Figure 7. TLR2 inhibition promotes doxorubicin effects in impairing BC growth. Schematic representation of the mechanism of TLR2-dependent chemoresistance and of the effects of CU-CPT22 treatment in combination with doxorubicin.

observed in BC using immune checkpoint inhibitors.[70,71] In conclusion, our data add fresh knowledge on the complex role played by TLR2 in cancer and contribute with a slightly provocative view to the scientific debate on the opportunity of using either TLR2 agonists or inhibitors in cancer therapy.

Abbreviations

α-SMA: alpha smooth muscle actin; ADC: Apparent diffusion constant; BC: breast cancer; CK19: cytokeratin 19; CSC: cancer stem cells; DAMP: damage-associated molecular patterns; DC: dendritic cells; DWI-MRI: Diffusion Weighted Magnetic Resonance Imaging; ER: estrogen receptor; G-CSF: granulocyte-colony stimulating factor; HMGB1: high mobility group box 1; HSC70: heat shock cognate 71 kDa protein; HSP: heat shock protein; IL: interleukin; i.p.: intraperitoneal; MDSC: myeloid-derived suppressor cell; MRI: Magnetic Resonance Imaging; NSG: NOD SCID gamma; OS: overall survival; PGN-SA: peptidoglycan from S. aureus; PRR: pattern recognition receptors; RARE: Rapid Acquisition with Refocused Echoes; RFS: relapse-free survival; TGF-β: tumor growth factor; TLR2: Toll-like Receptor 2; TME: Tumor microenvironment; TNBC: triple negative breast cancer; Treg: T regulatory cell; VEGF: vascular endothelial growth factor.

Acknowledgments

We thank Dr. Dale Lawson for his revision and editing of the manuscript.

Author's contributions

L.C. and F.C. designed the project and the experiments. L.C., A.D.L., and E.B. wrote the paper, and F.C. and E.Q. reviewed it. E.B., A.D.L., I.M., F.R., L.A., E.Q., and R.R. performed experiments and analyzed the data. G.F. and E.D.G. performed and analyzed MRI. P. P. performed and M.B. supervised DAMP analysis. A.S. performed bioinformatics analysis. L.C. and F.C. coordinated and directed the study. All authors have read and approved the final version of the manuscript.

Data sharing statement

All data generated or analyzed during this study are included in this published article and its supplementary information files.

Ethics approval and consent to participate

Mice were bred and maintained under saprophytic and pathogen-free conditions at the animal facility of the Molecular Biotechnology Center, and treated in accordance with EU and institutional guidelines, with the approval of the Animal Care and Use Committee of University of Turin and of the Italian Ministry of Health (authorizations N° 107/2020-PR and 500/2017-PR).

Disclosure statement

The authors declare no potential conflicts of interest.

Financial support

The research leading to these results has received funding from AIRC under the IG 2021 – ID. 25766 project – principal investigator L. Conti, IG 2015 – ID. 16724 and IG 2018 – ID. 21468 projects – principal investigator F. Cavallo, IG 2020 – ID. 24930 project – principal investigator M. Brancaccio, from Fondazione Ricerca Molinette Onlus, from the University of Turin (Turin, Italy), and a liberal contribution from Banca d'Italia. The Italian Ministry for University and Research (MUR) is gratefully acknowledged for yearly FOE funding to the Euro-BioImaging Multi-Modal Molecular Imaging Italian Node (MMMI). Roberto Ruiu was supported by a fellowship from Fondazione Umberto Veronesi.

Funding

The research leading to these results has received funding from AIRC under the IG 2021 – ID. 25766 project – principal investigator L. Conti, IG 2015 – ID. 16724 and IG 2018 – ID. 21468 projects – principal investigator F. Cavallo, IG 2020 – ID. 24930 project – principal investigator M. Brancaccio, from Fondazione Ricerca Molinette Onlus, from the University of Turin (Turin, Italy), and a liberal contribution from Banca d'Italia. The Italian Ministry for University and Research (MUR) is gratefully acknowledged for yearly FOE funding to the Euro-BioImaging Multi-Modal Molecular Imaging Italian Node (MMMI). Roberto Ruiu was supported by a fellowship from Fondazione Umberto Veronesi.

ORCID

Antonino Di Lorenzo http://orcid.org/0000-0002-5037-3396
Elisabetta Bolli http://orcid.org/0000-0002-1550-2391
Roberto Ruiu http://orcid.org/0000-0002-0431-2656
Giuseppe Ferrauto http://orcid.org/0000-0003-4937-6140
Enza Di Gregorio http://orcid.org/0000-0002-1950-3957
Lidia Avalle http://orcid.org/0000-0002-5060-633X
Aurora Savino http://orcid.org/0000-0002-0783-7191
Irene Fiore Merighi http://orcid.org/0000-0003-1797-2829
Federica Riccardo http://orcid.org/0000-0002-9692-0172
Mara Brancaccio http://orcid.org/0000-0003-2327-6846
Elena Quaglino http://orcid.org/0000-0002-8151-9124
Federica Cavallo http://orcid.org/0000-0003-4571-1060
Laura Conti http://orcid.org/0000-0003-1780-098X

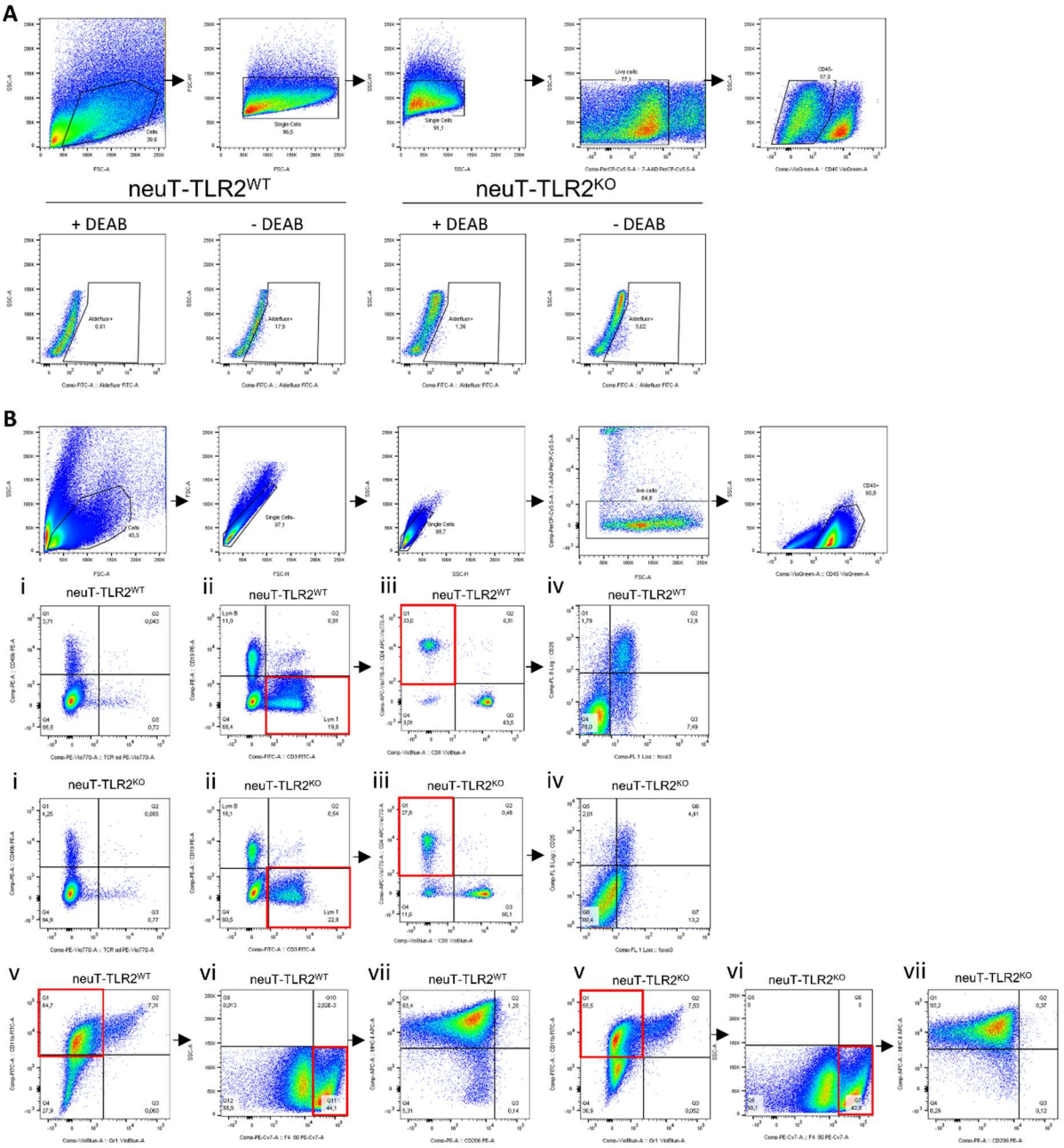
References

1. Sung H, Ferlay J, Siegel RL, Laversanne M, Soerjomataram I, Jemal A, Bray F. Global cancer statistics 2020: GLOBOCAN estimates of incidence and mortality worldwide for 36 cancers in 185 countries. CA Cancer J Clin. 2021;71:209–249. doi:10.3322/caac.21660
2. Ayala de la Pena F, Andres R, Garcia-Saenz JA, Manso L, Margeli M, Dalmau E, Pernas S, Prat A, Servitja S, Ciruelos E, et al. SEOM clinical guidelines in early stage breast cancer (2018). Clin Transl Oncol. 2019;21:18–30. doi:10.1007/s12094-018-1973-6
3. Nigdelis MP, Karamouzis MV, Kontos M, Alexandrou A, Goulis DG, Lambrinoudaki I. Updates on the treatment of invasive breast cancer: quo Vadimus? Maturitas. 2021;145:64–72. doi:10.1016/j.maturitas.2020.11.006
4. Ji X, Lu Y, Tian H, Meng X, Wei M, Cho WC. Chemoresistance mechanisms of breast cancer and their countermeasures. Biomed Pharmacother. 2019;114:108800. doi:10.1016/j.biopha.2019.108800
5. van Schaik TA, Chen KS, Shah K. Therapy-induced tumor cell death: friend or foe of immunotherapy? Front Oncol. 2021;11:678562. doi:10.3389/fonc.2021.678562
6. Di Lorenzo A, Bolli E, Tarone L, Cavallo F, Conti L. Toll-like receptor 2 at the crossroad between cancer cells, the immune system, and the microbiota. Int J Mol Sci. 2020;21:9418. doi:10.3390/ijms21249418
7. Galluzzi L, Humeau J, Buque A, Zitvogel L, Kroemer G. Immunostimulation with chemotherapy in the era of immune checkpoint inhibitors. Nat Rev Clin Oncol. 2020;17:725–741. doi:10.1038/s41571-020-0413-z
8. Jinushi M, Yagita H, Yoshiyama H, Tahara H. Putting the brakes on anticancer therapies: suppression of innate immune pathways by tumor-associated myeloid cells. Trends Mol Med. 2013;19:536–545. doi:10.1016/j.molmed.2013.06.001
9. Conti L, Ruiu R, Barutello G, Macagno M, Bandini S, Cavallo F, Lanzardo S. Microenvironment, oncoantigens, and antitumor vaccination: lessons learned from BALB-neuT mice. Biomed Res Int. 2014;2014:534969. doi:10.1155/2014/534969
10. Pandey S, Singh S, Anang V, Bhatt AN, Natarajan K, Dwarakanath BS. Pattern recognition receptors in cancer progression and metastasis. Cancer Growth Metastasis. 2015;8:25–34. doi:10.4137/CGM.S24314
11. Clarke MF. Clinical and Therapeutic Implications of Cancer Stem Cells. N Engl J Med. 2019;380:2237–2245. doi:10.1056/NEJMra1804280
12. Ruiu R, Tarone L, Rolih V, Barutello G, Bolli E, Riccardo F, Cavallo F, Conti L. Cancer stem cell immunology and immunotherapy: harnessing the immune system against cancer's source. Prog Mol Biol Transl Sci. 2019;164:119–188. doi:10.1016/bs.pmbts.2019.03.008
13. Conti L, Lanzardo S, Arigoni M, Antonazzo R, Radaelli E, Cantarella D, Calogero RA, Cavallo F. The noninflammatory role of high mobility group box 1/Toll-like receptor 2 axis in the self-renewal of mammary cancer stem cells. FASEB J. 2013;27:4731–4744. doi:10.1096/fj.13-230201
14. Brooks MD, Burness ML, Wicha MS. Therapeutic implications of cellular heterogeneity and plasticity in breast cancer. Cell Stem Cell. 2015;17:260–271. doi:10.1016/j.stem.2015.08.014
15. Quaglino E, Conti L, Cavallo F. Breast cancer stem cell antigens as targets for immunotherapy. Semin Immunol. 2020;47:101386. doi:10.1016/j.smim.2020.101386
16. Pece S, Disalvatore D, Tosoni D, Vecchi M, Confalonieri S, Bertalot G, Viale G, Colleoni M, Veronesi P, Galimberti V, et al. Identification and clinical validation of a multigene assay that interrogates the biology of cancer stem cells and predicts metastasis in breast cancer: a retrospective consecutive study. EBioMedicine. 2019;42:352–362. doi:10.1016/j.ebiom.2019.02.036
17. Bianchi ME, Crippa MP, Manfredi AA, Mezzapelle R, Rovere Querini P, Venereau E. High-mobility group box 1 protein orchestrates responses to tissue damage via inflammation, innate and adaptive immunity, and tissue repair. Immunol Rev. 2017;280:74–82. doi:10.1111/imr.12601
18. Tanabe Y, Tsuda H, Yoshida M, Yunokawa M, Yonemori K, Shimizu C, Yamamoto S, Kinoshita T, Fujiwara Y, Tamura K, et al. Pathological features of triple-negative breast cancers that showed progressive disease during neoadjuvant chemotherapy. Cancer Sci. 2017;108:1520–1529. doi:10.1111/cas.13274
19. Rovero S, Amici A, Di Carlo E, Bei R, Nanni P, Quaglino E, Porcedda P, Boggio K, Smorlesi A, Lollini P-L, et al. DNA vaccination against rat her-2/Neu p185 more effectively inhibits carcinogenesis than transplantable carcinomas in transgenic BALB/c mice. J Immunol. 2000;165:5133–5142. doi:10.4049/jimmunol.165.9.5133
20. Liu S, Chen H. Isolation of primary breast cancer cells from HER2 transgenic mice. Bio Protocol. 2016;6:e1956. doi:10.21769/BioProtoc.1956
21. Geninatti Crich S, Cadenazzi M, Lanzardo S, Conti L, Ruiu R, Alberti D, Cavallo F, Cutrin JC, Aime S. Targeting ferritin receptors for the selective delivery of imaging and therapeutic agents to breast cancer cells. Nanoscale. 2015;7:6527–6533. doi:10.1039/C5NR00352K
22. Gyorffy B. Survival analysis across the entire transcriptome identifies biomarkers with the highest prognostic power in breast cancer. Comput Struct Biotechnol J. 2021;19:4101–4109. doi:10.1016/j.csbj.2021.07.014
23. Michael D. Metap: meta-analysis of significance values. R package version 1.7., 2021.
24. Gendoo DMA, Zon M, Sandhu V, Manem VSK, Ratanasirigulchai N, Chen GM, Waldron L, Haibe-Kains B. MetaGxData: clinically annotated breast, ovarian and pancreatic cancer datasets and their use in generating a multi-cancer gene signature. Sci Rep. 2019;9:8770. doi:10.1038/s41598-019-45165-4
25. Deena MA, Ratanasirigulchai N, Schroeder MS, Pare L, Parker JS, Prat A, Haibe-Kains B. R package version 2.26.0; 2021. http://www.pmgenomics.ca/bhklab/software/genefu Accessed 13 March 2022.

26. Fekete JT, Gyorffy B. ROCplot.org: validating predictive biomarkers of chemotherapy/hormonal therapy/anti-HER2 therapy using transcriptomic data of 3,104 breast cancer patients. Int J Cancer. 2019;145:3140–3151. doi:10.1002/ijc.32369
27. Hanzelmann S, Castelo R, Guinney J. GSVA: gene set variation analysis for microarray and RNA-seq data. BMC Bioinform. 2013;14:7. doi:10.1186/1471-2105-14-7
28. Lanzardo S, Conti L, Rooke R, Ruiu R, Accart N, Bolli E, Arigoni M, Macagno M, Barrera G, Pizzimenti S, et al. Immunotargeting of antigen xCT attenuates stem-like cell behavior and metastatic progression in breast cancer. Cancer Res. 2016;76:62–72. doi:10.1158/0008-5472.CAN-15-1208
29. Conti L, De Palma R, Rolla S, Boselli D, Rodolico G, Kaur S, Silvennoinen O, Niccolai E, Amedei A, Ivaldi F, et al. Th17 cells in multiple sclerosis express higher levels of JAK2, which increases their surface expression of IFN-gammaR2. J Immunol. 2012;188:1011–1018. doi:10.4049/jimmunol.1004013
30. Conti L, Bolli E, Di Lorenzo A, Franceschi V, Macchi F, Riccardo F, Ruiu R, Russo L, Quaglino E, Donofrio G, et al. Immunotargeting of the xCT cystine/glutamate antiporter potentiates the efficacy of Her2-targeted immunotherapies in breast cancer. Cancer Immunol Res. 2020;8:1039–1053. doi:10.1158/2326-6066.CIR-20-0082
31. Bandini S, Macagno M, Hysi A, Lanzardo S, Conti L, Bello A, Riccardo F, Ruiu R, Merighi IF, Forni G, et al. The non-inflammatory role of C1q during Her2/neu-driven mammary carcinogenesis. Oncoimmunology. 2016;5:e1253653. doi:10.1080/2162402X.2016.1253653
32. Donofrio G, Tebaldi G, Lanzardo S, Ruiu R, Bolli E, Ballatore A, Rolih V, Macchi F, Conti L, Cavallo F, et al. Bovine herpesvirus 4-based vector delivering the full length xCT DNA efficiently protects mice from mammary cancer metastases by targeting cancer stem cells. Oncoimmunology. 2018;7:e1494108. doi:10.1080/2162402X.2018.1494108
33. Macagno M, Bandini S, Stramucci L, Quaglino E, Conti L, Balmas E, Smyth MJ, Lollini P-L, Musiani P, Forni G, et al. Multiple roles of perforin in hampering ERBB-2 (Her-2/neu) carcinogenesis in transgenic male mice. J Immunol. 2014;192:5434–5441. doi:10.4049/jimmunol.1301248
34. Conti L, Lanzardo S, Ruiu R, Cadenazzi M, Cavallo F, Aime S, Crich SG. L-Ferritin targets breast cancer stem cells and delivers therapeutic and imaging agents. Oncotarget. 2016;7:66713–66727. doi:10.18632/oncotarget.10920
35. She S, Zhao Y, Kang B, Chen C, Chen X, Zhang X, Chen W, Dan S, Wang H, Wang Y-J, et al. Combined inhibition of JAK1/2 and DNMT1 by newly identified small-molecule compounds synergistically suppresses the survival and proliferation of cervical cancer cells. Cell Death Dis. 2020;11:724. doi:10.1038/s41419-020-02934-8
36. Ferrauto G, Di Gregorio E, Lanzardo S, Ciolli L, Iezzi M, Aime S. Generation of multiparametric MRI maps by using Gd-labelled-RBCs reveals phenotypes and stages of murine prostate cancer. Sci Rep. 2018;8:10567. doi:10.1038/s41598-018-28926-5
37. Tallerico R, Conti L, Lanzardo S, Sottile R, Garofalo C, Wagner AK, Johansson MH, Cristiani CM, Kärre K, Carbone E, et al. NK cells control breast cancer and related cancer stem cell hematological spread. Oncoimmunology. 2017;6:e1284718. doi:10.1080/2162402X.2017.1284718
38. Grange C, Lanzardo S, Cavallo F, Camussi G, Bussolati B. Sca-1 identifies the tumor-initiating cells in mammary tumors of BALB-neuT transgenic mice. Neoplasia. 2008;10:1433–1443. doi:10.1593/neo.08902
39. Ambrosino E, Spadaro M, Iezzi M, Curcio C, Forni G, Musiani P, Wei W-Z, Cavallo F. Immunosurveillance of Erbb2 carcinogenesis in transgenic mice is concealed by a dominant regulatory T-cell self-tolerance. Cancer Res. 2006;66:7734–7740. doi:10.1158/0008-5472.CAN-06-1432
40. Troschel FM, Palenta H, Borrmann K, Heshe K, Hua SH, Yip GW, Kiesel L, Eich HT, Götte M, Greve B, et al. Knockdown of the prognostic cancer stem cell marker Musashi-1 decreases radio-resistance while enhancing apoptosis in hormone receptor-positive breast cancer cells via p21(WAF1/CIP1). J Cancer Res Clin Oncol. 2021;147:3299–3312. doi:10.1007/s00432-021-03743-y
41. Wang D, Lu P, Zhang H, Luo M, Zhang X, Wei X, Gao J, Zhao Z, Liu C. Oct-4 and Nanog promote the epithelial-mesenchymal transition of breast cancer stem cells and are associated with poor prognosis in breast cancer patients. Oncotarget. 2014;5:10803–10815. doi:10.18632/oncotarget.2506
42. Galluzzi L, Vitale I, Warren S, Adjemian S, Agostinis P, Martinez AB, Chan TA, Coukos G, Demaria S, Deutsch E, et al. Consensus guidelines for the definition, detection and interpretation of immunogenic cell death. J Immunother Cancer. 2020;8:e000337. doi:10.1136/jitc-2019-000337
43. Secli L, Avalle L, Poggio P, Fragale G, Cannata C, Conti L, Iannucci A, Carrà G, Rubinetto C, Miniscalco B, et al. Targeting the extracellular HSP90 co-chaperone morgana inhibits cancer cell migration and promotes anticancer immunity. Cancer Res. 2021;81:4794–4807. doi:10.1158/0008-5472.CAN-20-3150
44. Fisusi FA, Akala EO. Drug combinations in breast cancer therapy. Pharm Nanotechnol. 2019;7:3–23. doi:10.2174/2211738507666190122111224
45. Wang Y, Liu S, Zhang Y, Yang J. Dysregulation of TLR2 serves as a prognostic biomarker in breast cancer and predicts resistance to endocrine therapy in the luminal B subtype. Front Oncol. 2020;10:547. doi:10.3389/fonc.2020.00547
46. Scheeren FA, Kuo AH, van Weele LJ, Cai S, Glykofridis I, Sikandar SS, Zabala M, Qian D, Lam JS, Johnston D, et al. A cell-intrinsic role for TLR2-MYD88 in intestinal and breast epithelia and oncogenesis. Nat Cell Biol. 2014;16:1238–1248. doi:10.1038/ncb3058
47. Quaglino E, Cavallo F, Conti L. Cancer stem cell antigens as targets for new combined anti-cancer therapies. Int J Biochem Cell Biol. 2020;129:105861. doi:10.1016/j.biocel.2020.105861
48. Xie W, Huang Y, Xie W, Guo A, Wu W. Bacteria peptidoglycan promoted breast cancer cell invasiveness and adhesiveness by targeting toll-like receptor 2 in the cancer cells. PLoS One. 2010;5:e10850. doi:10.1371/journal.pone.0010850
49. Maruyama A, Shime H, Takeda Y, Azuma M, Matsumoto M, Seya T. Pam2 lipopeptides systemically increase myeloid-derived suppressor cells through TLR2 signaling. Biochem Biophys Res Commun. 2015;457:445–450. doi:10.1016/j.bbrc.2015.01.011
50. Kim S, Takahashi H, Lin WW, Descargues P, Grivennikov S, Kim Y, Luo J-L, Karin M. Carcinoma-produced factors activate myeloid cells through TLR2 to stimulate metastasis. Nature. 2009;457:102–106. doi:10.1038/nature07623
51. Sinha P, Clements VK, Bunt SK, Albelda SM, Ostrand-Rosenberg S. Cross-talk between myeloid-derived suppressor cells and macrophages subverts tumor immunity toward a type 2 response. J Immunol. 2007;179:977–983. doi:10.4049/jimmunol.179.2.977
52. Chen YQ, Li PC, Pan N, Gao R, Wen ZF, Zhang TY, Huang F, Wu F-Y, Ou X-L, Zhang J-P, et al. Tumor-released autophagosomes induces CD4(+) T cell-mediated immunosuppression via a TLR2-IL-6 cascade. J Immunother Cancer. 2019;7:178. doi:10.1186/s40425-019-0646-5
53. Yamazaki S, Okada K, Maruyama A, Matsumoto M, Yagita H, Seya T. TLR2-dependent induction of IL-10 and Foxp3+ CD25+ CD4+ regulatory T cells prevents effective anti-tumor immunity induced by Pam2 lipopeptides in vivo. PLoS One. 2011;6:e18833. doi:10.1371/journal.pone.0018833
54. Tang M, Diao J, Gu H, Khatri I, Zhao J, Cattral MS. Toll-like receptor 2 activation promotes tumor dendritic cell dysfunction by regulating IL-6 and IL-10 receptor signaling. Cell Rep. 2015;13:2851–2864. doi:10.1016/j.celrep.2015.11.053
55. Regis G, Icardi L, Conti L, Chiarle R, Piva R, Giovarelli M, Poli V, Novelli F. IL-6, but not IFN-gamma, triggers apoptosis and inhibits in vivo growth of human malignant T cells on STAT3 silencing. Leukemia. 2009;23:2102–2108. doi:10.1038/leu.2009.139

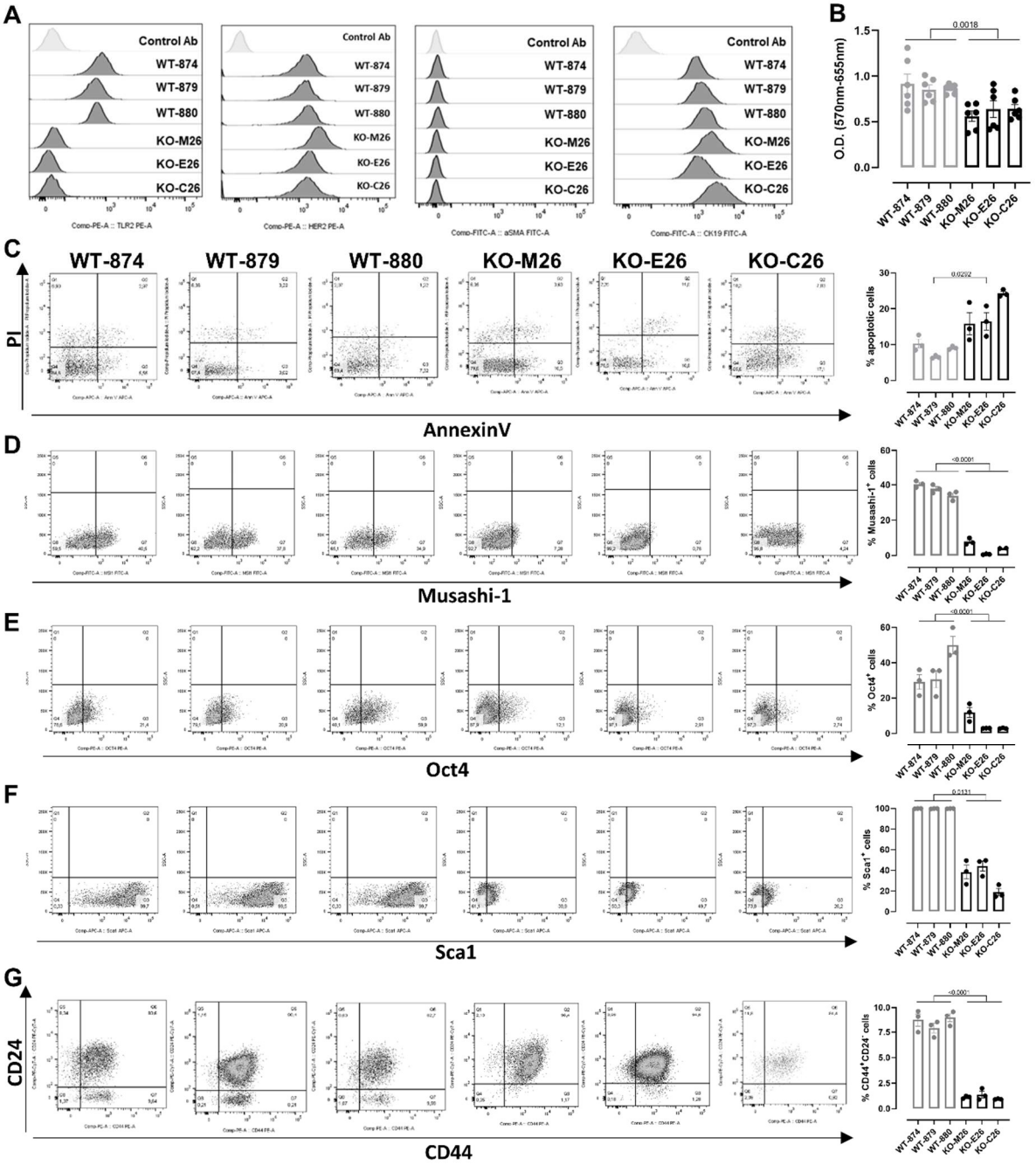
56. Masjedi A, Hashemi V, Hojjat-Farsangi M, Ghalamfarsa G, Azizi G, Yousefi M, Jadidi-Niaragh F. The significant role of interleukin-6 and its signaling pathway in the immunopathogenesis and treatment of breast cancer. Biomed Pharmacother. 2018;108:1415–1424. doi:10.1016/j.biopha.2018.09.177
57. Sohun M, Shen H. The implication and potential applications of high-mobility group box 1 protein in breast cancer. Ann Transl Med. 2016;4:217. doi:10.21037/atm.2016.05.36
58. Fernandez MF, Reina-Perez I, Astorga JM, Rodriguez-Carrillo A, Plaza-Diaz J, Fontana L. Breast cancer and its relationship with the microbiota. Int J Environ Res Public Health. 2018;15:1747. doi:10.3390/ijerph15081747
59. Chiba A, Bawaneh A, Velazquez C, Clear KYJ, Wilson AS, Howard-mcnatt M, Levine EA, Levi-Polyachenko N, Yates-Alston SA, Diggle SP, et al. Neoadjuvant chemotherapy shifts breast tumor microbiota populations to regulate drug responsiveness and the development of metastasis. Mol Cancer Res. 2020;18:130–139. doi:10.1158/1541-7786.MCR-19-0451
60. Montassier E, Gastinne T, Vangay P, Al-Ghalith GA, Bruley Des Varannes S, Massart S, Moreau P, Potel G, de La Cochetière MF, Batard E, et al. Chemotherapy-driven dysbiosis in the intestinal microbiome. Aliment Pharmacol Ther. 2015;42:515–528. doi:10.1111/apt.13302
61. Wooten RM, Ma Y, Yoder RA, Brown JP, Weis JH, Zachary JF, Kirschning CJ, Weis JJ. Toll-like receptor 2 is required for innate, but not acquired, host defense to Borrelia burgdorferi. J Immunol. 2002;168:348–355. doi:10.4049/jimmunol.168.1.348
62. Garcia-Manero G, Montalban-Bravo G, Yang H, Wei Y, Alvarado Y, Daver NG, DiNardo CD, et al. A clinical study of OPN-305, a Toll-like Receptor 2 (TLR-2) antibody, in patients with lower risk Myelodysplastic Syndromes (MDS) that have received prior Hypomethylating Agent (HMA). Ther Blood. 2016;128:227.
63. Kovacsovics TJ, Mims A, Salama ME, Pantin J, Rao N, Kosak KM, Ahorukomeye P, Glenn MJ, Deininger MWN, Boucher KM, et al. Combination of the low anticoagulant heparin CX-01 with chemotherapy for the treatment of acute myeloid leukemia. Blood Adv. 2018;2:381–389. doi:10.1182/bloodadvances.2017013391
64. Galluzzi L, Buqué A, Kepp O, Zitvogel L, Kroemer G. Immunogenic cell death in cancer and infectious disease. Nat Rev Immunol. 2016;17:97–111. doi:10.1038/nri.2016.107
65. Fucikova J, Kepp O, Kasikova L, Petroni G, Yamazaki T, Liu P, Zhao L, Spisek R, Kroemer G, Galluzzi L, et al. Detection of immunogenic cell death and its relevance for cancer therapy. Cell Death Dis. 2020;11:1013. doi:10.1038/s41419-020-03221-2
66. Apetoh L, Ghiringhelli F, Tesniere A, Criollo A, Ortiz C, Lidereau R, Mariette C, Chaput N, Mira J-P, Delaloge S, et al. The interaction between HMGB1 and TLR4 dictates the outcome of anticancer chemotherapy and radiotherapy. Immunol Rev. 2007;220:47–59. doi:10.1111/j.1600-065X.2007.00573.x
67. Kaczanowska S, Joseph AM, Davila E. TLR agonists: our best frenemy in cancer immunotherapy. J Leukoc Biol. 2013;93:847–863. doi:10.1189/jlb.1012501
68. Wang Y, Su L, Morin MD, Jones BT, Mifune Y, Shi H, et al. Adjuvant effect of the novel TLR1/TLR2 agonist Diprovocim synergizes with anti-PD-L1 to eliminate melanoma in mice. Proc Natl Acad Sci USA. 2018;115:E8698–E706.
69. Hubert P, Roncarati P, Demoulin S, Pilard C, Ancion M, Reynders C, Lerho T, Bruyere D, Lebeau A, Radermecker C, et al. Extracellular HMGB1 blockade inhibits tumor growth through profoundly remodeling immune microenvironment and enhances checkpoint inhibitor-based immunotherapy. J Immunother Cancer. 2021;9:e001966. doi:10.1136/jitc-2020-001966
70. Black M, Barsoum IB, Truesdell P, Cotechini T, Macdonald-Goodfellow SK, Petroff M, Siemens DR, Koti M, Craig AWB, Graham CH, et al. Activation of the PD-1/PD-L1 immune checkpoint confers tumor cell chemoresistance associated with increased metastasis. Oncotarget. 2016;7:10557–10567. doi:10.18632/oncotarget.7235
71. Grasselly C, Denis M, Bourguignon A, Talhi N, Mathe D, Tourette A, Serre L, Jordheim LP, Matera EL, Dumontet C, et al. The antitumor activity of combinations of cytotoxic chemotherapy and immune checkpoint inhibitors is model-dependent. Front Immunol. 2018;9:2100. doi:10.3389/fimmu.2018.02100

Supplementary Fig.1. FACS gating strategies



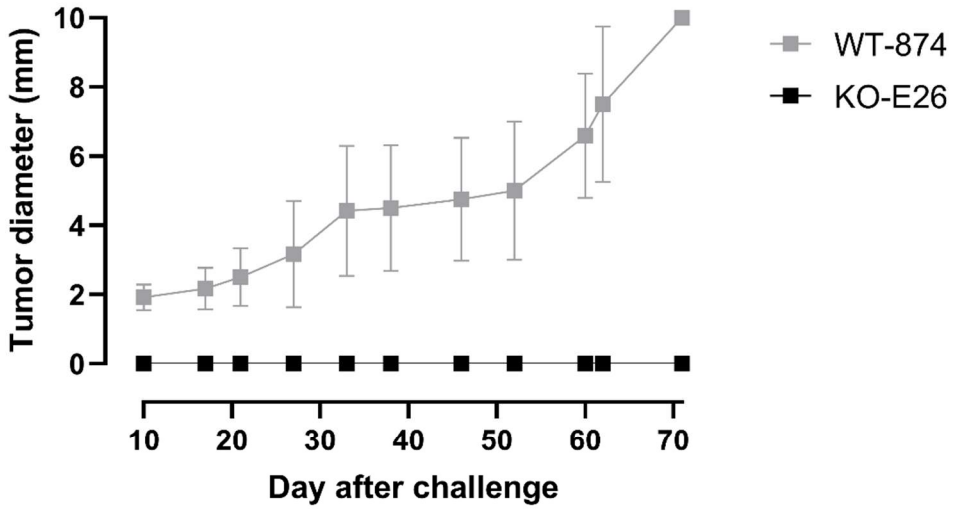
Supplementary Fig.1. FACS gating strategies. Density plots showing the gating strategies used for *ex vivo* staining of **(A)** CSC markers, with representative density plots showing the Aldefluor negative control (+DEAB) and the stained samples (-DEAB) and **(B)** for (i) NK and γδ T cells; (ii) B and T lymphocytes; (iii) $CD4^+$ and $CD8^+$ T lymphocytes; (iv) Treg cells; (v) MDSCs; (vi) macrophages; (vii) macrophage polarization, from tumors of neuT-$TLR2^{WT}$ or neuT-$TLR2^{KO}$ mice. Red squares and arrows show parent gates, where necessary.

Supplementary Fig.2. Characterization of cell lines derived from murine models



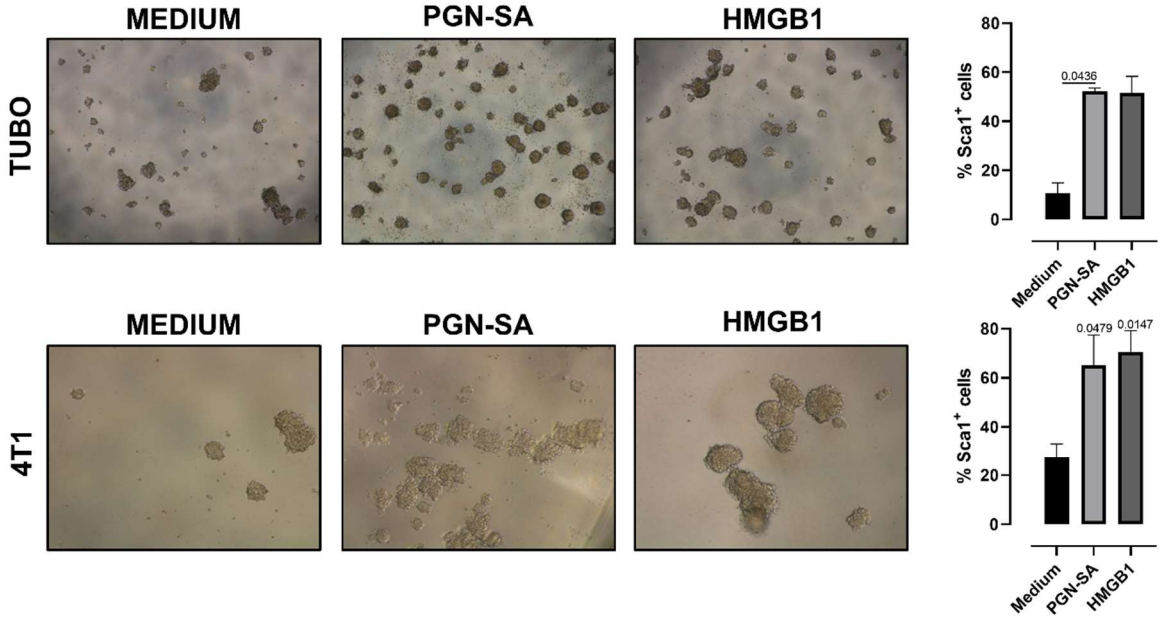
Supplementary Fig.2. Characterization of cell lines derived from murine models. (A) Representative FACS histograms of TLR2, HER2, αSMA, CK19, (all dark gray) or control (light gray) staining. **(B)** MTT assay of cells cultured in complete medium (N=6). FACS density plots of **(C)** PI and AnnexinV, (D) Musashi-1, **(E)** Oct4, **(F)** Sca1 and **(G)** CD44 and CD24 stainings on WT-874, WT-879, WT-880, KO-M26, KO-C26 and KO-E26 cells. Graphs show the mean values ± SEM from 3 independent experiments. Two-way ANOVA of grouped $TLR^{WT}2$ vs TLR^{KO} cells.

Supplementary Fig.3. TLR2 promotes breast cancer growth mainly through tumor-cell intrinsic mechanisms



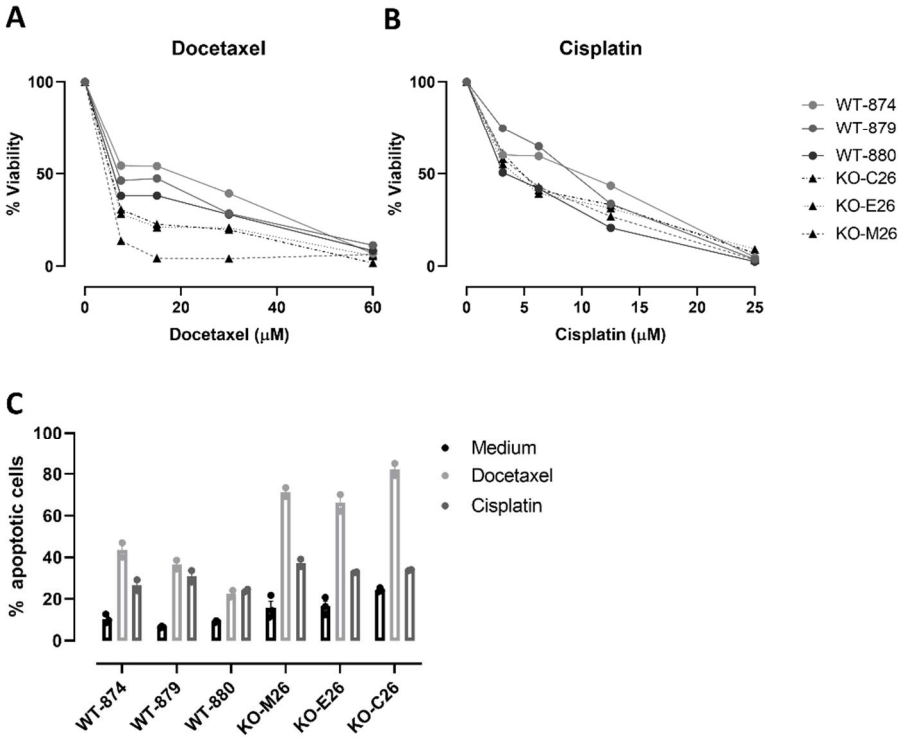
Supplementary Fig.3. TLR2 promotes breast cancer growth mainly through tumor-cell intrinsic mechanisms. Mean tumor diameter of $TLR2^{WT}$ mice (N = 6 per group, from 2 independent experiments) injected orthotopically with $1x10^6$ WT-874 or KO-E26 cells.

Supplementary Fig.4. TLR2 activation promotes CSC self-renewal



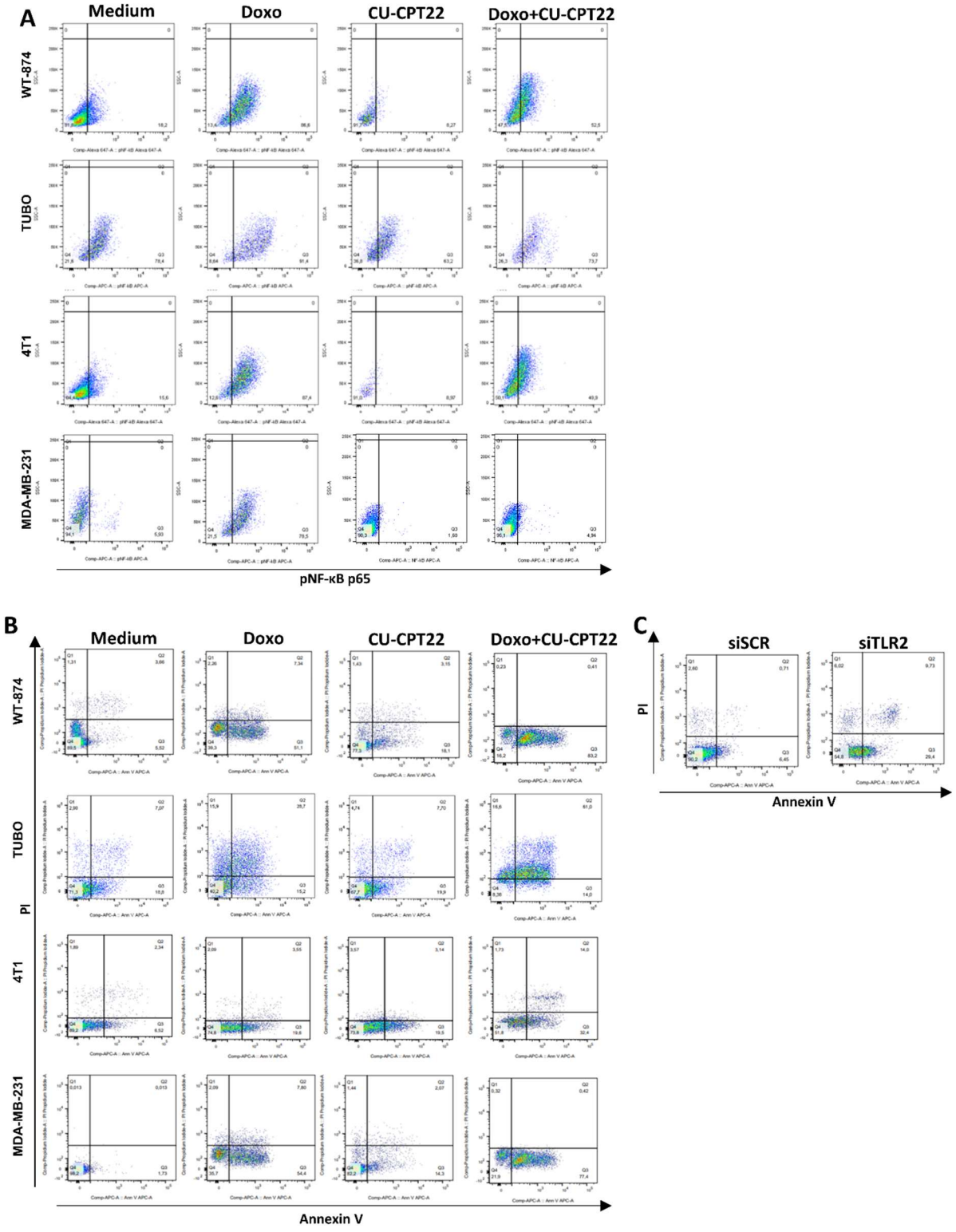
Supplementary Fig.4. TLR2 activation promotes CSC self-renewal. Representative images of tumorspheres (Magnification 10X), and means ± SEM of the percentage of Sca1^{+} TUBO and 4T1 cells cultured for 5 days in tumorsphere-forming conditions from 3 independent experiments. Student's *t*-test with Welch correction.

Supplementary Fig.5. TLR2 protects cells only from immunogenic cell death inducing chemotherapies.



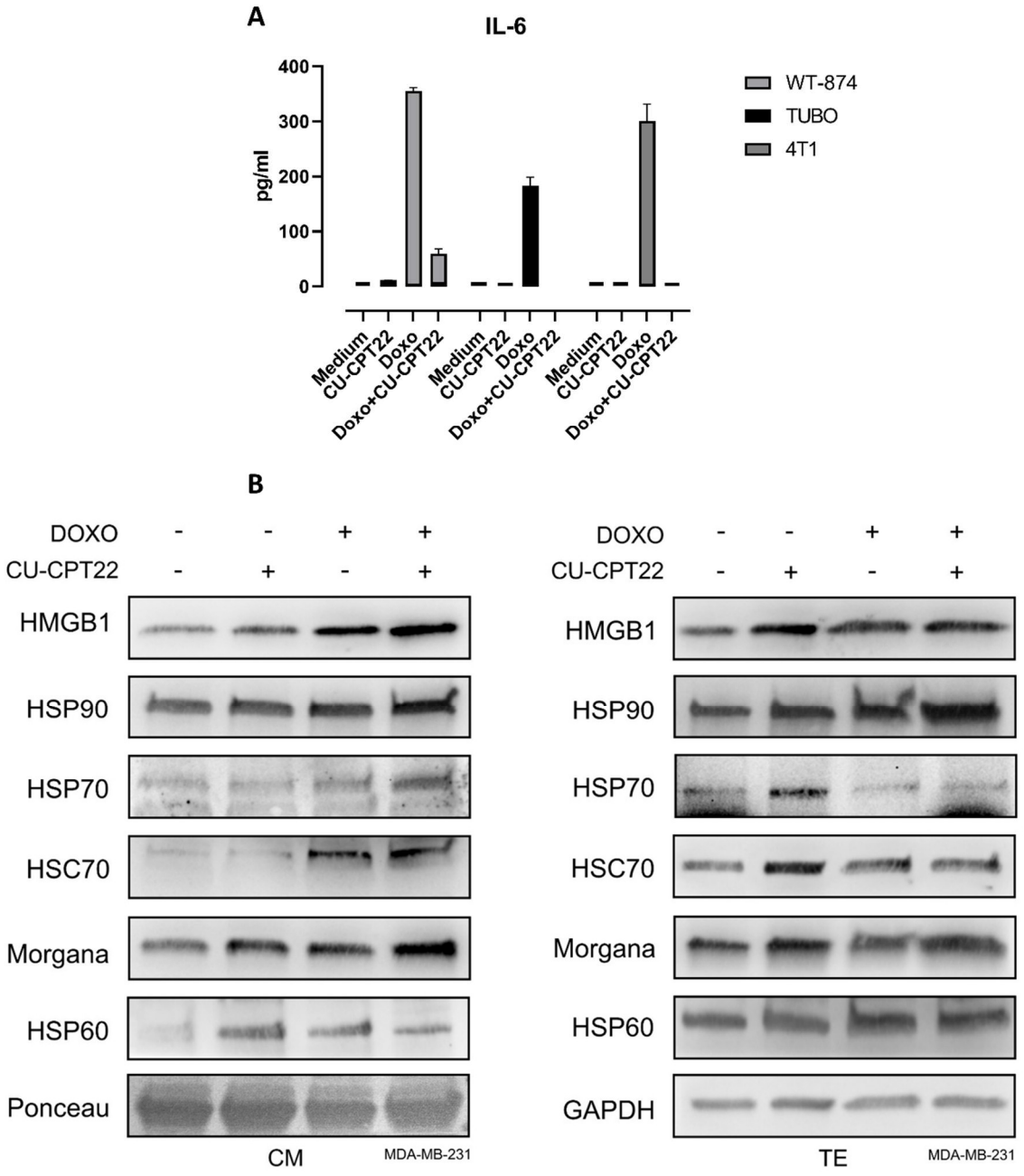
Supplementary Fig.5. TLR2 protects cells only from immunogenic cell death inducing chemotherapies. Concentration-dependent toxicity of **(A)** Docetaxel (60 to 7.5 μM) and **(B)** Cisplatin (25 to 3.125 μM) on WT-874, WT-879, WT-880, KO-M26, KO-E26 and KO-C26 cells evaluated using MTT after 48 hours of treatment and reported as % of viability as compared to untreated control cells. **(C)** FACS analysis of apoptosis in cells treated for 48 hours with or without docetaxel (15 μM) or cisplatin (15 μM). The graph reports means ± SEM of the percentage of Annexin-V^+ cells from 2 independent experiments.

Supplementary Fig.6. FACS analysis of NF-kB activation and apoptosis



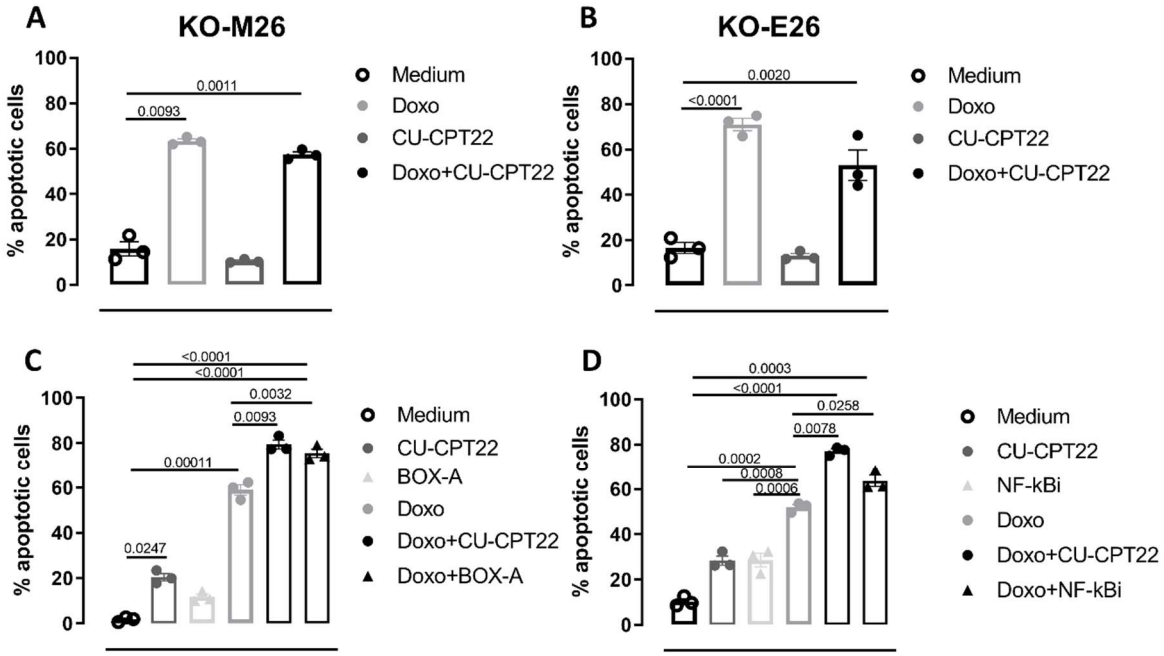
Supplementary Fig.6. FACS analysis of NF-kB activation and apoptosis. Representative density plots of (A) p65 NF-κB phosphorylation, (B) Annexin-V/propidium iodide analysis of WT-874, TUBO, 4T1 and MDA-MB-231 cells treated for 48 hours with doxorubicin alone or combined with 5 μM CU-CPT22 and (C) Annexin-V/propidium iodide analysis of WT-874 cells 48 hours after transfection with scrambled (siSCR) or TLR2 silencing (siTLR2) siRNAs.

Supplementary Fig.7. TLR2 inhibition impairs doxorubicin-induced IL-6 production and promotes DAMP release



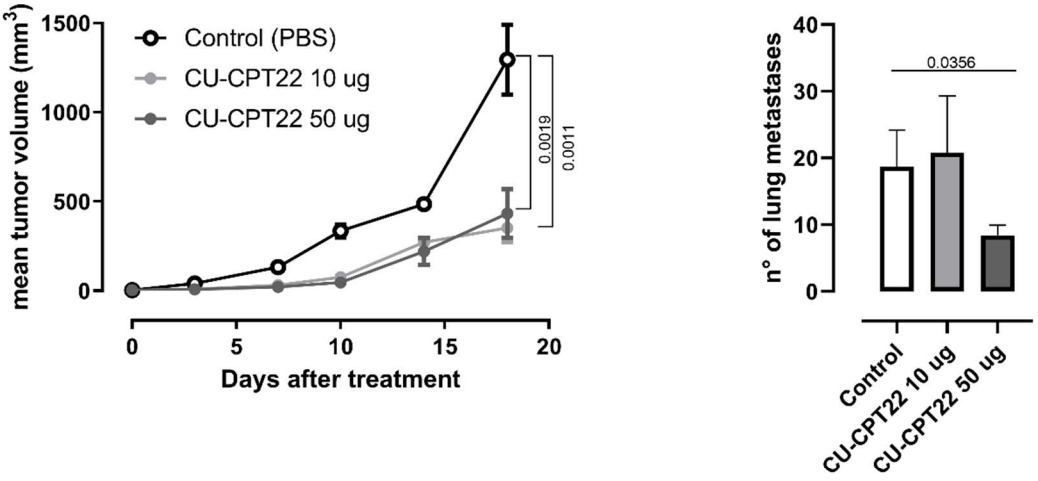
Supplementary Fig.7. TLR2 inhibition impairs doxorubicin-induced IL-6 production and promotes DAMP release. (A) ELISA analysis of IL-6 released in the supernatant by WT-874, TUBO, and 4T1 cells treated or not with doxorubicin for 48 hours. The graph shows means ± SEM of HMGB1 concentration from 3 independent experiments. (B) Western blot analysis of HMGB1, HSP90, HSP70, HSC70, Morgana (CHORDC1) and HSP60, in the conditioned medium (CM) and total cell protein extracts (TE) from MDA-MB-231 cells treated or not with doxorubicin and/or CU-CPT22 for 48 hours. Ponceau S and GAPDH were used as loading controls for CM and TE, respectively.

Supplementary Fig.8. TLR2, HMGB1 or NF-κB inhibition induce apoptosis in breast cancer cells



Supplementary Fig.8. TLR2, HMGB1 or NF-κB inhibition induce apoptosis in breast cancer cells. FACS analysis of apoptosis in **(A)** KO-M26 or **(B)** KO-E26 cells treated for 48 hours with or without doxorubicin, CU-CPT22 or a combination of both, **(C)** MDA-MB-231 cells treated for 48 hours with or without doxorubicin alone or combined with CU-CPT22 or BOX-A and **(D)** WT-874 cells treated for 48 hours with or without doxorubicin alone or combined with CU-CPT22 or BAY 11-7082 (8 μM). All the graphs report means ± SEM of the percentage of Annexin-V$^+$ cells from 3 independent experiments. Student's *t*-test

Supplementary Fig.9. CU-CPT22 hinders breast tumor growth and metastases



Supplementary Fig.9. CU-CPT22 hinders breast tumor growth and metastases. BALB/c mice were orthotopically challenged with $1x10^4$ 4T1 cells. When the tumors reached 2 mm diameter, mice were treated intratumorally with 10 or 50 µg CU-CPT22, or vehicle alone as a control (N = 5 per group). The treatment was repeated twice per week. Graphs show **(A)** mean tumor diameters and **(B)** the number of spontaneous lung metastases per square mm measured in lungs. Two-way ANOVA or Mann-Whitney test.

Supplementary methods.

Analysis of DAMPs secreted by doxorubicin-treated MDA-MB-231 cells.

Conditioned medium

A total of 4×10^6 cells were plated in DMEM 10% FBS into a 100-mm dish and allowed to settle for 24 hours. Cells were then washed twice with PBS and refed with 10 ml serum-free medium containing or not doxorubicin 2 μM and/or CU-CPT22 5 μM and incubated for 48 hours at 37°C. Conditioned medium (CM) was collected and concentrated at 2,000 × g by centrifugation with Vivaspin 20 centrifugal concentrator MWCO 10,000 Da (Sigma-Aldrich, Cat#Z614602) up to 1 ml.

Western blotting

For Western blot analysis, cells were lysed in TBS with 1% Triton X-100, plus phosphatase and protease inhibitors. Total protein extracts (30–50 μg) or concentrated CM (50 μl) were analyzed by Western blotting and detected by the chemiluminescent reagent LiteAblot (Euro-clone).

Western blotting was performed using the following primary antibodies: HMGB1 (Abcam, Cat#ab79823, 1:1000), HSP90 (BD, Cat#610418, 1:1000); HSP70 (Thermo Fisher Scientific, Cat#MA3-008, 1:1000), HSP60 (SantaCruz, Cat#sc-13115, 1:1000), HSC70 (SantaCruz, Cat#sc-7298,1:100), CHORDC1 (Sigma, Cat#HPA041040, 1:1000), GAPDH (Merck Millipore, Cat#Mab374, 1:5000). The secondary Ab used were anti-mouse IgG–peroxidase (Sigma-Aldrich, Cat#A4416, 1:6000) or anti-rabbit IgG–peroxidase (Sigma-Aldrich, Cat#A0545, 1:5000). Ponceau S (Sigma-Aldrich, Cat#P3504) staining was used as loading control for CM samples.

Supplementary Table I.

	RFS					RFS				
	p value					HR				
DATASET	total	basal	luminalA	luminalB	Her2+	total	basal	luminalA	luminalB	Her2+
E-MTAB-365	0.2619	0.0829	0.043	N.D.	0.0053	1.8	1.35	1.5	N.D.	1.3
GSE46184	0.0072	N.D.	0.0972	N.D.	N.D.	2.94	N.D.	3,33E+08	N.D.	N.D.
GSE2034	0.0677	0.1802	0.1258	0.0071	N.D.	0.69	0.57	2.14	0.5	N.D.
GSE16391	0.1438	N.D.	0.0056	N.D.	N.D.	0.4	N.D.	N.D.	N.D.	N.D.
GSE16446	0.1377	0.0911	N.D.	N.D.	0.0653	1.48	0.35	N.D.	N.D.	5.72
GSE42568	0.0333	0.3441	0.1236	0.3563	N.D.	1.86	0.62	4.55	0.6	N.D.
GSE20685	0.1914	0.4561	0.1572	0.1267	0.056	0.75	0.5	0.6	1.86	0.5
GSE21653	0.1188	0.1573	0.1	0.1091	N.D.	0.69	0.51	0.41	0.6	N.D.
GSE5327	0.1819	0.2942	N.D.	N.D.	N.D.	0.45	2.39	N.D.	N.D.	N.D.
GSE61304	0.338	N.D.	N.D.	N.D.	N.D.	1.7	N.D.	N.D.	N.D.	N.D.
GSE20711	0.0159	0.0051	N.D.	0.2049	N.D.	2.13	7.23	N.D.	2.21	N.D.
GSE17705	0.0497	N.D.	0.3581	0.0604	N.D.	0.58	N.D.	1.47	0.4	N.D.
GSE9195	0.2296	N.D.	0.0156	N.D.	N.D.	1.93	N.D.	9.25	N.D.	N.D.
GSE4611	0.0219	N.D.	0.0001	N.D.	0.1423	2.26	N.D.	8.6	N.D.	4.24
GSE31519	0.1755	0.4322	N.D.	N.D.	N.D.	0.48	0.64	N.D.	N.D.	N.D.
GSE25066	0.0002	0.3685	0.01449	0.3981	0.1739	2.05	0.8	2.16	1.46	2.7
GSE12093	0.1687	N.D.	0.1687	0.1789	N.D.	1.86	N.D.	2,8E+08	0.5	N.D.
GSE2990	0.0166	N.D.	0.0145	N.D.	N.D.	1.59	N.D.	2.16	N.D.	N.D.
GSE1456	0.0164	N.D.	0.0024	N.D.	N.D.	2.41	N.D.	6,8E+08	N.D.	N.D.
GSE48390	0.2427	N.D.	0.3699	N.D.	N.D.	1.42	N.D.	1	N.D.	N.D.
GSE2603	0.1968	0.2326	N.D.	0.16	N.D.	1.68	3.3	N.D.	3.1	N.D.
GSE45255	0.0453	N.D.	0.014	0.4207	N.D.	2.39	N.D.	3,9E+08	0.6	N.D.
GSE11121	0.068	0.4403	0.0485	0.181	N.D.	0.6	0.4	2.82	0.5	N.D.
GSE69031	0.1243	0.32	0.3699	N.D.	N.D.	1.6	2	1.99	N.D.	N.D.
GSE19615	0.0138	0.0274	N.D.	N.D.	N.D.	4.34	7.98	N.D.	8	N.D.
GSE12276	0.0051	0.1281	0.2698	N.D.	0.0541	1.49	0.65	1.55	N.D.	2.41
GSE26971	0.0302	N.D.	0.068	N.D.	N.D.	3.49	N.D.	2.93	N.D.	N.D.
GSE65194	0.054	0.1545	N.D.	N.D.	0.1176	3,62E+08	0	N.D.	N.D.	5.63
GSE7390	0.1511	0.0778	N.D.	N.D.	0.4943	1.45	2.96	N.D.	N.D.	1.7
GSE3494	0.108	0.2059	N.D.	N.D.	0.3307	1.71	3.66	N.D.	N.D.	1.6
GSE37946	0.1417	N.D.	N.D.	N.D.	0.1538	2.62	N.D.	N.D.	N.D.	4.37
GSE6532	0.2722	N.D.	N.D.	N.D.	N.D.	1.84	N.D.	N.D.	N.D.	N.D.

HR and p values of RFS in patients from the KMPlotter datasets, stratified according to TLR2 mRNA expression.

Chapter II

Development and characterization of RGD-functionalized nanoparticles for the delivery of chemotherapy and TLR2 inhibitors

Despite significant progress in developing effective anti-cancer treatments, traditional chemotherapy continues to face limitations in both efficacy and safety. These drugs often exhibit a narrow therapeutic window, as they are indiscriminately distributed throughout the body after systemic administration. This can lead to toxicity in healthy cells, resulting in severe side effects while striving to achieve adequate anti-cancer effects. Additionally, the non-specific toxicity of chemotherapeutic agents restricts the permissible dosage, thereby reducing their overall therapeutic potential. Other obstacles, such as enzymatic and hepatic degradation, elevated interstitial fluid pressure, cellular and nuclear membrane barriers, and drug efflux pumps, further hinder the effectiveness of systemically administered anti-cancer drugs. Indeed, chemotherapy drugs display a low accumulation and retention in cancer cells, which leads to treatment failure. To address these challenges, numerous nanomedicine formulations, including nanoparticles, have been developed and extensively studied over the years [118].

Nanomedicines are submicrometer-scale carrier systems designed to enhance the distribution of drugs within the body. By selectively targeting disease sites and sparing healthy tissues, these formulations aim to optimize the balance between the therapeutic benefits and toxicity of chemotherapeutic treatments. Nanomedicines include various formulations such as liposomes, nanoparticles, polymers, micelles, and antibodies. In particular, self-assembled nanoparticles loaded with drugs represent a promising strategy for chemotherapy delivery. These nanoparticles are generated by self-assembly, and can incorporate chemotherapeutic drugs, small molecule inhibitors, or nucleic acids [119]. They can target tumors either through passive accumulation or active targeting. Passive accumulation leverages the enhanced permeation and retention (EPR) effect, where the leaky vasculature and poor lymphatic drainage of tumors allow nanoparticles to accumulate at the tumor site. In contrast, active targeting involves the use of ligands like antibodies or peptides that bind specifically to receptors expressed on tumor cells. In addition to drug delivery, nanoparticles have been employed in imaging for disease detection and diagnosis. Advances in imaging technologies, including magnetic resonance imaging (MRI), computed tomography, ultrasound, optical imaging (OI), positron emission tomography (PET), and single-photon emission computed tomography (SPECT), have significantly improved disease detection capabilities. Recently, there has been considerable interest in integrating imaging probes with therapeutic agents into a single nanoparticle for simultaneous disease imaging and targeted therapy, referred to as nanotheranostics. These platforms combine diagnostic and therapeutic functions, enabling imaging-guided drug delivery. Nanotheranostics allow real-time

monitoring of drug distribution, release, and efficacy. Furthermore, theranostic nanomedicines facilitate tailored treatment strategies by predicting and monitoring therapeutic outcomes in real-time. Among the different platforms that can be used for the delivery of theranostic agents, lipid-based nanoparticles and liposomes are those that have been more extensively applied for drug delivery in solid cancer. Some of these formulations delivering chemotherapy are currently used in clinics. Doxil® is the first liposomal drug approved by the US Food and Drug Administration (FDA; 1995) and the European Medicine Agency (EMA; 1996). Initially, it was FDA-approved in 1995 for treating AIDS-related Kaposi's sarcoma and later for recurrent ovarian cancer and metastatic breast cancer. Doxil® is constituted by doxorubicin encapsulated in liposomes that are covered with polymers of poly-ethylene glycol (PEG) [120]. PEG coating of nanoparticles is a strategy to avoid their opsonization and rapid clearance, while improving accumulation in the tumor. The main advantage of Doxil® is the reduced cardiac toxicity compared to free doxorubicin [121]. Another form of encapsulated doxorubicin is Myocet, a non-pegylated liposome. Myocet is approved in Canada and Europe in combination with cyclophosphamide for the treatment of metastatic breast cancer. Similarly to Doxil®, Myocet increased cardiac protection compared to conventional doxorubicin [122]. Besides doxorubicin, there is also a liposomal formulation of cisplatin, named Lipoplatin, designed to reduce the systemic toxicity associated with cisplatin. It has undergone various clinical trials, showing promising potential in treating non-small cell lung cancer (NSCLC) and other malignancies [123]. Of note, lipid-based nanoparticles are not only used to deliver chemotherapy, but also other types of molecules. One largely exploited application is the delivery of nucleic acids. Furthermore, lipid-based nanoparticles for immunotherapy of cancer are under evaluation in pre-clinical and clinical trials. This strategy has been used for vaccines based on mRNAs coding for specific antigens. In this context, in February 2023, the FDA granted Moderna's mRNA cancer vaccine, known as mRNA-4157/V940, Breakthrough Therapy Designation for use in combination with pembrolizumab as an adjuvant treatment for patients with high-risk melanoma following complete resection. Soon after, In April 2023, it also received Prime Scheme Designation from EMA for the same application. Moreover, lipid-based nanosystems can be used to deliver ICI, cytokines or interfering RNAs to improve the anti-tumor immune response. For instance, short non-coding RNAs have been encapsulated in lipid nanoparticles and used as therapeutic agents to target endogenous mRNAs for cancer therapies [124]. Nanoparticle-based immunotherapies can be combined with other treatments, such as chemotherapy. Several of these combinations are currently being investigated for treatment of both solid and hematological cancers [125].

Overall, nanoparticle-based approaches represent promising tools with the potential to significantly improve cancer therapies. For these reasons, we chose to pursue this strategy in this thesis. The

methodologies employed and the results obtained are thoroughly described in the subsequent sections of this chapter.

The results shown in Chapter I suggested that the combined delivery of chemotherapy and TLR2 inhibitors may improve breast cancer treatment. However, the therapeutic approach proposed in Paper I was preliminary in some respects and required improvements to boost its translational potential. One key issue was the delivery of free chemotherapeutic drugs, which, as discussed above, results in poor tumor accumulation and high toxic effects. A second issue was related to the administration of the TLR2 inhibitor CU-CPT22, which had not been tested in vivo before. In Paper I, we opted for intra-tumor delivery of CU-CPT22, for two main reasons: its poor solubility in aqueous conditions and the need to minimize any potential systemic side effects. Notably, we did not observe any health issues in our $TLR2^{KO}$ mice or dysfunction in their immune systems, suggesting that TLR2 deficiency is well tolerated [108]. However, in clinical settings, systemic administration of TLR2 inhibitors might raise safety concerns. Despite this, intra-tumor injection is not an optimal translational strategy. To overcome these issues, we sought a system that would allow for tumor-targeted delivery of chemotherapy and systemic administration of CU-CPT22, with high tumor accumulation and minimal off-target effects. Additionally, improving CU-CPT22 solubility in physiological conditions was crucial. To achieve these goals, we continued our collaboration with Prof. Giuseppe Ferrauto's group, leveraging their expertise in chemistry. We hypothesized that nanoparticles capable of specifically delivering the drug to the tumor would offer a promising solution. This strategy could also be applied to the delivery of chemotherapy, potentially mitigating its well-known toxicity issues. Considering CU-CPT22's chemical characteristics and our objectives, we identified Poly lactic-co-glycolic acid (PLGA) nanoparticles as the most suitable system. PLGA is a biocompatible and biodegradable material approved by FDA and EMA for clinical use. The first part of this project is summarized in the attached Paper II, which describes an approach to improving PLGA nanoparticles for tumor drug delivery. Specifically, we developed PLGA nanoparticles functionalized with the cyclic Arg-Gly-Asp (RGD) tripeptide, which recognizes integrin $\alpha_v\beta_3$, a molecule overexpressed in many solid tumors, including breast cancer [109].

In a previous study by our group, Prof. Conti demonstrated that RGD effectively targets $\alpha_v\beta_3$ in murine models of spontaneous breast cancer. In that study, RGD was used as a diagnostic agent, and its sensitivity was sufficient to detect tumor presence in mice even before palpable lesions appeared [126].

To evaluate the benefits of RGD conjugation, testing PLGA loaded with well characterised anti-cancer drugs was a more reliable approach instead of directly using CU-CPT22, as no data about its

systemic use were available at the time. We considered to use doxorubicin since it is the other component of our combined therapy. However, due to its chemical properties, encapsulating doxorubicin into PLGAs was a highly inefficient process, leading us to explore alternative nanosystems for its delivery. Consequently, we opted to use docetaxel, a taxane commonly used in breast cancer chemotherapy. Docetaxel exhibits excellent solubility in PLGA, and the PLGA-docetaxel combination is well-studied, with largely available literature on its production and functional properties [127–129].

We produced theranostic PLGA nanoparticles, decorated or not with a cyclic RGD peptide and loaded with docetaxel, a fluorescent probe, and an MRI probe (Fig. II.1A). We evaluated their chemical and physical properties, biodistribution, and efficacy in treating breast cancer in preclinical models.

(For detailed results and Materials & Methods, please refer to Paper II).

In summary, the results demonstrated that PLGA nanoparticles functionalized or not with the RGD share similar chemical/physical properties and a good stability profile over time. Flow cytometry and confocal microscopy analyses performed on TN 4T1 and $HER2^+$ TUBO breast cancer cell lines incubated with the nanoparticles containing the FITC fluorescent molecule demonstrated that those functionalized with RGD were more efficient in accumulating in cells. In vitro, both targeted and untargeted nanoparticles led to increased cytotoxicity compared to free docetaxel.

To test the in vivo efficacy of RGD-targeted nanoparticles, orthotopic 4T1 TNBC murine models were generated and treated with docetaxel-containing nanoparticles. The biodistribution of the nanoparticles was followed by MRI, upon encapsulation of an amphipathic Gadolinium (Gd)-based MRI contrast agent. These *in vivo* studies revealed that RGD-functionalized PLGA nanoparticles exhibited significantly greater tumor accumulation than non-targeted nanoparticles, as confirmed by inductively coupled plasma mass spectrometry (ICP-MS) on explanted organs. Furthermore, treatment with RGD-functionalized PLGA nanoparticles resulted in a significant reduction in tumor growth as compared to untargeted nanoparticles or free docetaxel.

The study also evaluated the cardiac effects of docetaxel treatment, given its known adverse impact on cardiac function. The findings indicated that encapsulation of docetaxel within PLGA nanoparticles significantly reduced its cardiotoxicity, as evidenced by the preservation of ejection fraction and cardiac output in treated mice.

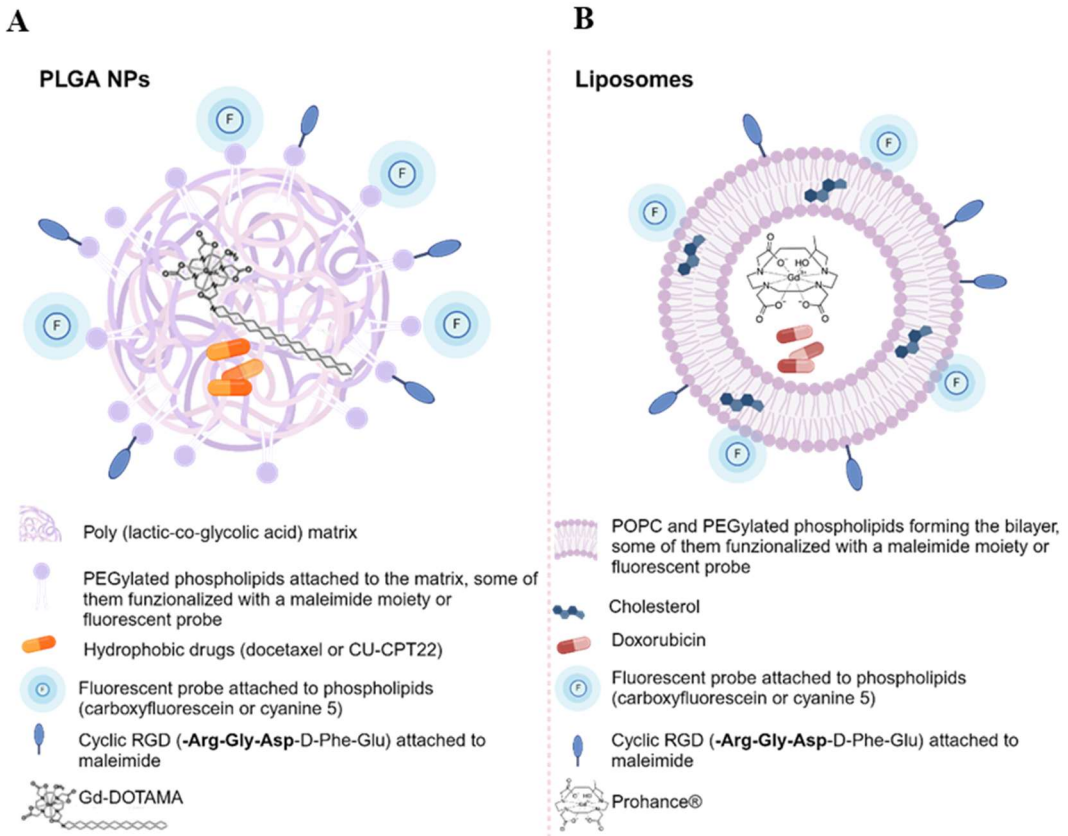


Figure II.1. Representation and description of the nanoparticles (NPs). Generation of PLGA NPs (A) and Liposomes (B). Structures of the NPs (B) Chemicals used for their preparation. Chemical reaction for cyclic RGD c(RGDfC) ligation. *(For detailed description of the chemicals and their employment, please refer to the Materials and Methods section).*

In conclusion, this study underscores the potential of RGD-functionalized PLGA nanoparticles as an effective drug delivery system for breast cancer treatment. Their ability to specifically target tumor cells while minimizing systemic side effects positions these nanoparticles as a promising therapeutic approach to enhance treatment efficacy and improve patient quality of life.

Overall, this work lays the foundation for further investigation into the use of RGD-functionalised nanoparticles to efficiently deliver CU-CPT22 or other therapeutic agents systemically, with specific targeting of tumors.

Paper II

cancers

MDPI

Article

RGD_PLGA Nanoparticles with Docetaxel: A Route for Improving Drug Efficiency and Reducing Toxicity in Breast Cancer Treatment

Enza Di Gregorio *,†, Chiara Romiti †, Antonino Di Lorenzo *, Federica Cavallo, Giuseppe Ferrauto ‡ and Laura Conti ‡

Department of Molecular Biotechnology and Health Sciences, University of Turin, Via Nizza 52, 10126 Turin, Italy
* Correspondence: enza.digregorio@unito.it (E.D.G.); antonino.dilorenzo@unito.it (A.D.L.); Tel.: +39-011-6708459 (E.D.G.); +39-011-6706458 (A.D.L.)
† These authors contributed equally to this work.
‡ These authors contributed equally to this work.

Simple Summary: Breast cancer is the most prevalent cancer in women and the leading cause of cancer-associated deaths. Although several therapeutic approaches are available, systemic chemotherapy remains the primary choice, especially for the treatment of advanced breast cancers. Unfortunately, systemic chemotherapy causes numerous side effects and damage to distal organs and requires high doses of drugs to achieve a therapeutic concentration in the tumor region. The use of nanosystems for drug delivery is a promising strategy to overcome these drawbacks. In this study, we developed Poly (lactic-co-glycolic acid) nanoparticles (PLGA-NPs) containing the chemotherapeutic drug Docetaxel, functionalized with a cyclic RGD tripeptide to allow the active targeting of $\alpha_v\beta_3$ integrins, which are overexpressed in breast cancer. We demonstrated that PLGAs effectively deliver the drug to breast cancer cells in preclinical models, and are more effective than free Docetaxel in hampering tumor progression, while reducing side effects.

check for updates

Citation: Di Gregorio, E.; Romiti, C.; Di Lorenzo, A.; Cavallo, F.; Ferrauto, G.; Conti, L. RGD_PLGA Nanoparticles with Docetaxel: A Route for Improving Drug Efficiency and Reducing Toxicity in Breast Cancer Treatment. *Cancers* **2023**, *15*, 8. https://doi.org/10.3390/cancers15010008

Academic Editors: Stefania Biffi and Matteo Calvaresi

Received: 11 November 2022
Revised: 13 December 2022
Accepted: 14 December 2022
Published: 20 December 2022

Copyright: © 2022 by the authors. Licensee MDPI, Basel, Switzerland. This article is an open access article distributed under the terms and conditions of the Creative Commons Attribution (CC BY) license (https://creativecommons.org/licenses/by/4.0/).

Abstract: Breast cancer is the leading cause of cancer-related death in women. Although many therapeutic approaches are available, systemic chemotherapy remains the primary choice, especially for triple-negative and advanced breast cancers. Unfortunately, systemic chemotherapy causes serious side effects and requires high doses to achieve an effective concentration in the tumor. Thus, the use of nanosystems for drug delivery may overcome these limitations. Herein, we formulated Poly (lactic-co-glycolic acid) nanoparticles (PLGA-NPs) containing Docetaxel, a fluorescent probe, and a magnetic resonance imaging (MRI) probe. The cyclic RGD tripeptide was linked to the PLGA surface to actively target $\alpha_v\beta_3$ integrins, which are overexpressed in breast cancer. PLGA-NPs were characterized using dynamic light scattering, fast field-cycling ^{1}H-relaxometry, and ^{1}H-nuclear magnetic resonance. Their therapeutic effects were assessed both in vitro in triple-negative and HER2+ breast cancer cells, and in vivo in murine models. In vivo MRI and inductively coupled plasma mass spectrometry of excised tumors revealed a stronger accumulation of PLGA-NPs in the RGD_PLGA group. Targeted PLGAs have improved therapeutic efficacy and strongly reduced cardiac side effects compared to free Docetaxel. In conclusion, RGD-PLGA is a promising system for breast cancer treatment, with positive outcome in terms of therapeutic efficiency and reduction in side effects.

Keywords: breast cancer; Docetaxel; PLGA nanoparticles; magnetic resonance imaging; RGD; theranostic

1. Introduction

Breast cancer (BC) is the most common cancer in women, and its incidence is increasingly high [1]. Although noteworthy advances in diagnosis and therapy have improved

patient prognosis in recent years, BC is still the primary cause of cancer-associated death in women in many countries [1]. Despite therapy, many patients progress to metastatic BC, a disease that is very difficult to treat [2].

Surgery, chemotherapy, radiotherapy, and hormone therapy represent the pillars of BC treatment, and several targeted therapies and immunotherapies are entering clinical practice [3]. Systemic chemotherapy based on anthracyclines or cyclophosphamide remains the main treatment for triple-negative (TN) BC, advanced BC, and high-risk luminal cancers [2]. Moreover, doxorubicin-based neoadjuvant chemotherapy is frequently used for operable tumors [4].

The onset of side effects and damage to distal organs are important issues related to the use of systemic chemotherapy [5]. The most common side effects, generally shared by all chemotherapeutic drugs, include gastrointestinal and skin disorders, neuropathies, nephropathies, suppression of bone marrow, fatigue, and hair loss [6]. Additionally, some other drug-specific side effects can occur [7]. Indeed, many chemotherapeutic drugs, including anthracyclines, taxanes, alkylating agents, antimicrotubule agents, and antimetabolites, are known to strongly affect cardiac output (CO) and ejection fraction (EF%), with severe consequences on patient health and life expectancy [8–10].

Therefore, important goals in cancer treatment are to reduce the dose of administered drugs, enhance their specific accumulation in the tumor site, and reduce the overall side effects. A challenge is presented by the transition from traditional to targeted chemotherapy, where the drug is specifically delivered at high doses to cancer cells [11,12].

Thus, approaches using biocompatible nanoparticles (NPs) targeting epitopes specifically overexpressed by tumor cells can be the best choice. Several drug-filled nanotherapeutic systems have already been tested at the preclinical level, and some have already entered clinical stages with hope for success [13–16]. Nanomedicine for cancer treatment has shown strong benefits in terms of efficacy, reduction in side effects and drug resistance, and good pharmacokinetics and biocompatibility.

Different classes of natural and/or synthetic chemicals can be employed to generate self-assembling and highly stable NPs, such as phospholipids (e.g., liposomes and micelles), lipids (e.g., nucleolipids), polysaccharides (e.g., cyclodextrins), nucleic acids, polypeptides (e.g., peptide-based nanoparticles) and polymers (e.g., PLGA and polymersomes) [17–21].

Among the available polymers, Poly (lactic-co-glycolic acid) (PLGA) is one of the most frequently used biodegradable and biocompatible synthetic polymers capable of generating very stable nanometric and spherical nanoparticles (PLGA-NPs) [22]. It is a Poly (lactic acid) (PLA) and Poly (glycolic acid) (PGA) block copolymer that is commercially available with different copolymer compositions (generally 50:50 PLA-PGA) and molecular weights. Owing to its biological and chemical properties (low toxicity, controlled and persistent release, and biocompatibility with cells and tissues), it has been approved by the US Food and Drug Administration and European Medicines Agency for human use in drug delivery systems [23]. The hydrolysis of PLGA leads to glycolic and lactic acids, which are non-immunogenic endogenous molecules that are easily metabolized by enzymes [22]. As generally adopted for all nanoparticles, including PLGA-NPs, the loading of polyethyleneglycol (PEG) moiety can be efficient in improving the pharmacokinetic properties of nanoparticles. In particular, PEG can: (i) improve NPs' suspensibility and reduce aggregation, (ii) reduce uptake by macrophages, thus enhancing the blood half-life, and (iii) prevent nonspecific interactions with cell surfaces [24,25]. Indeed, it is well known that PEG chains create a hydrophilic protective layer around NPs, which reduces serum-dependent phagocytosis, by inhibiting the adsorption of opsonin proteins such as IgG and complement factors on NP surfaces [24,25].

PLGA-NPs can be very efficient in entrapping hydrophobic anticancer drugs, among which are molecules belonging to the taxane family (e.g., Docetaxel and Paclitaxel) or anthracycline family (e.g., Doxorubicin) that normally display low blood solubility [26–29].

Taxanes are considered one of the conventional treatments for BC and can significantly ameliorate patients' progression-free and overall survival [26,27]. Their mechanism of

action implies that they bind to tubulin and stabilize its polymerization. This blocks cell division, leading to cell cycle arrest and apoptosis. Despite their good therapeutic efficiency (either as single agentsor when administered in combination with other drugs), their pharmaceutical formulation remains a challenge. Taxanes contain lipophilic substituents that cause very poor aqueous solubility and stability [26,27]. The administration of taxane-containing NPs can overcome this drawback. Docetaxel (Taxotere®; Rhone-Poulenc Rorer, Inc., Paris, France) is one of the most commonly used drugs. It is a semisynthetic analog of Paclitaxel, originally synthesized starting from Baccatin III, a precursor molecule extracted from the needles of the European yew tree *Taxus baccata* [30]. The presence of two minor chemical structural modifications with respect to Paclitaxel makes it more favorable for preclinical and clinical applications [26,27]. Docetaxel has already been encapsulated inside PLGA-NPs with a good encapsulation rate [28,31].

NPs can passively deliver the drug to tumor cells through an enhanced permeability and retention (EPR) mechanism, which is typical of nanosized systems and leaky tumor endothelium [32].

However, in view of further enhancing proper delivery to the tumor region and limiting side effects to distal organs, active NPs targeting can be exploited [33–35].

The surface of PLGA-NPs can be chemically modified to host a targeting molecule capable of recognizing epitopes expressed on the tumor. A widely exploited possibility relies on the use of the cyclic Arg-Gly-Asp tripeptide (RGD), which targets integrin $\alpha_v\beta_3$, commonly upregulated in inflammatory diseases and many solid cancers such as BC [36,37]. Integrin $\alpha_v\beta_3$ interacts with the RGD sequence present in several extracellular matrix proteins and increases the invasiveness and metastasis of many solid cancers. Integrin $\alpha_v\beta_3$ is considered a marker of tumor development, metastasis and neo-angiogenesis, because it is expressed at low levels in normal blood vessels and is overexpressed in tumor vessels and in many cancer cells [38]. The possibility of targeting integrin $\alpha_v\beta_3$ using synthetic cyclic RGD makes this molecule an interesting target for tumor delivery systems.

Starting from the above-reported considerations, herein we exploited the feasibility of using RGD-PLGA-NPs filled with Docetaxel in BC models.

RGD-PLGA-NPs were prepared and extensively characterized from a chemo-physical point of view; then, their potentiality as a chemotherapeutic system was tested in vitro on murine BC cell lines. To this aim, cell lines belonging to two different tumor subtypes, the $HER2^+$ TUBO cells [39] and the TN 4T1 cells, were used. Finally, orthotopic 4T1 TNBC murine models were generated and treated with Docetaxel-containing RGD-PLGA-NPs. The delivery of RGD-PLGA-NPs was followed by magnetic resonance imaging (MRI), upon encapsulation of an amphipathic Gadolinium (Gd)-based MRI contrast agent in the PLGA-NPs.

RGD-PLGA-NPs were compared with untargeted PLGA-NPs to check the effect of the targeting moiety on the in vitro and in vivo biodistribution of the NPs and on their efficiency.

2. Materials and Methods

2.1. Chemicals

1,2-distearoyl-sn-glycero-3-phosphoethanolamine-N-[maleimide(polyethylene glycol)-2000] (ammonium salt) (DSPE-PEG2000-maleimide), 1,2-distearoyl-sn-glycero-3-phosphoethanolamine-N-[methoxy(polyethylene glycol)-2000] (ammonium salt) (DPPE-PEG2000-methoxy), and 1,2-dioleoyl-sn-glycero-3-pshosphoethanolamine-N-(carboxyfluorescein) (ammonium salt) (DOPE-CF) were purchased from Avanti Polar Lipids Inc. (Birmingham, AL, USA) (Figure 1B).

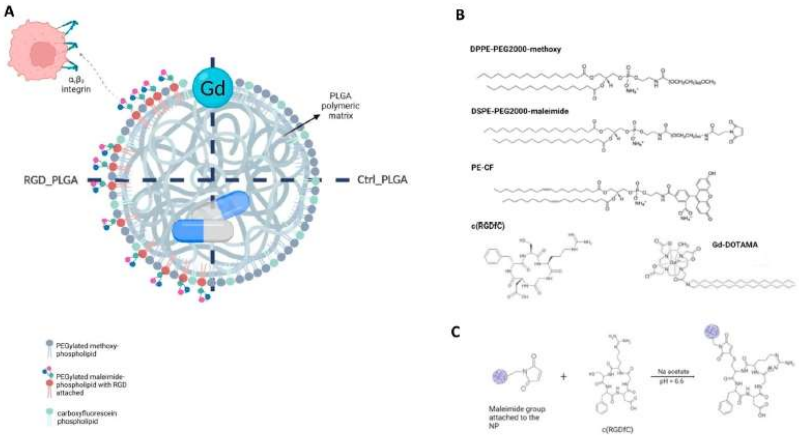


Figure 1. Generation of PLGA-NPs. (**A**) Structures of RGD_PLGA and Ctrl_PLGA-NPs. (**B**) Chemicals used for PLGA preparation. (**C**) Chemical reaction for c(RGDfC) ligation.

Poly(D,L-lactide-co-glycolide) (50:50, mol wt 30,000–60,000) (PLGA), poly vinyl alcohol (mol wt 31,000–50,000) (PVA), Trimethylsilylpropanoic acid (TSP, NMR standard) sodium chloride, sodium acetate, HEPES (4-(2-hydroxyethyl)-1-piperazineethanesulfonic acid), sodium hydroxide, hydrochloric acid, nitric acid, chloroform, methanol, 3-(4,5-Dimethylthiazol-2-yl)-2,5-Diphenyltetrazolium Bromide, and all the other chemicals were acquired from Sigma-Aldrich Co. LLC (Burlington, NJ, USA) and used without further purification.

Cyclo(-Arg-Gly-Asp-D-Phe-Cys) acetate salt (c(RGDfC) was purchased from Bachem AG (Bubendorf, Switzerland).

Gd-amphiphilic complex, Gd(III)-DOTAMA (C18)2 (Gd-DOTAMA) was synthesized as previously reported [40]. Gd-ions were checked to be lower than 0.3% mol/mol by applying the orange xylenol procedure [41]. The exact concentration of Gd-complex was measured using a relaxometric approach, as previously reported [42]. Docetaxel (DTX) was purchased from Tocris Bioscience (Bristol, UK).

2.2. PLGA-NP Preparation

The method of the oil/water emulsion solvent extraction was used to prepare PLGA-NPs.

Briefly, the organic phase was prepared by dissolving Poly(D,L-lactide-co-glycolide) (50:50, mol/mol; *MW* = 30,000–60,000) (PLGA), pegylated phospholipid (DPPE-PEG(2000)-methoxy) and all the other components in a chloroform/methanol 2:1 *v/v* mixture. For this purpose, 25 mg PLGA and 2.2 mg DPPE-PEG2000 methoxy—or, alternatively, for RGD-functionalized NPs, 1.0 mg DPPE -PEG2000 methoxy and 1.2 mg DSPE-PEG2000-Maleimide—were dissolved in 450 µL chloroform (purity ≥ 99.9%). 6.0 mg DTX (Docetaxel, drug) or 3.2 mg Gd-DOTAMA (MRI probe) were also added for Docetaxel- and Gd-loaded NP preparations, respectively [43,44]. Then, 50 µL of a solution containing DPPE-N-carboxyfluorescein (fluorescent probe) 1 mg/mL in pure chloroform was added for fluorescence microscopy exploitation.

The water phase was a poly vinyl alcohol (PVA) aqueous solution. PVA was chosen because it is a good emulsifier, able to produce NPs with a relatively uniform and small size, and is easily suspensible in water buffers [43,44]. The organic phase (0.5 mL) was gently dropped into 3 mL of aqueous phase containing 3% Poly (vinyl alcohol) (PVA), in ice. Sonication was performed with an immersion-tip instrument (SONOPULS HD 2070.2 Bandelin ultrasonic homogenizer, 20 KHz; Bandelin Electronic, Berlin, Germany) in 2 cycles of 1.5 min each, power 80–90%.

Evaporation of the organic solvent from the oil/water emulsion was carried out for 2 h under vacuum-rotation, and NPs were purified with centrifugation through filters and dialysis against fresh buffer [43,44].

Polymers and Gd-DOTAMA residuals were removed through dialysis at 6 °C against HEPES/NaCl buffer (1 L), under mild stirring (membrane with a 14 kDa MW cutoff). Centrifugation at 4 °C, 5500 rpm in Vivaspin® tubes (300K MWCO) was used to wash the remaining PVA and concentrate the PLGA to the wanted volume (ca.3.5 mL). This was performed in HEPES/NaCl for Ctrl_RGD NPs and in Na^+/acetate buffer 0.15 M (pH 6.6) for RGD NPs (diluting to 20 mL). Ctrl_RGD NPs were stored at 4 °C. pH of NPs for RGD ligation was checked after the concentration step, upon a 3-point calibration of the pHmeter (FiveEasyTM by Mettler Toledo), and pH was assessed to be around 6.6.

For RGD_PLGA, maleimide-pegylated phospholipid (DPPE-PEG (2000) maleimide) was added to the formulation and used to conjugate the cyclic RGD tripeptide (hereinafter indicated as c(RGDfC)) to the external surface of NPs, with the previously reported procedure [33] (Figure 1B, chemicals used for PLGA-NP preparation; Figure 1C, scheme of RGD binding). Ligation with c(RGDfC) was carried out by adding c(RGDfC) to the PLGA emulsion (5 folds stoichiometric excess of c(RGDfC) with respect to externally exposed maleimide moieties, in Na+/acetate buffer, pH 6.6) in a three-neck balloon, for 2 h, RT, under nitrogen flow and stirring [36]. Then, NPs were purified through dialysis (4 h in HEPES/NaCl). RG-functionalized NPs were also stored at 4 °C.

2.3. PLGA-NP Characterization, Quantification of Docetaxel Encapsulation and Release by NMR

The size of the formed nanoparticles was checked by using dynamic light scattering (DLS) with a Malvern Zetasizer Nano Series DLS (Malvern Panalytical, Malvern, UK) instrument, upon diluting NPs 1:100 in HEPES/NaCl buffer.

The amount of Docetaxel encapsulated in PLGA-NPs was measured by using high-resolution ^{1}H-NMR, using a Bruker Avance 600 MHz (B0 = 14.09 T) spectrometer equipped with 5 mm probes and using CDCl3 as an internal lock spectrometer (Bruker, Billerica, USA). The temperature was controlled with Bruker thermostating units and fixed at 298 K. The experimental settings were the following: spectral width 30 ppm, 1024 scans, 4 dummy scans, water signal suppression, automatic RG, and recycle delay.

Preliminarily, a Docetaxel calibration curve was obtained by acquiring NMR spectra of Docetaxel at variable concentration (1.03–9.1 mg/mL) in CDCl3/MetOD (2:1 vol/vol) in the presence of 0.33 mg/mL of TSP (Trimethylsilylpropanoic acid) as a quantitative standard ($\Delta\delta$ of TSP = 0).

Three ^{1}H signals of Docetaxel were considered for the preparation of the calibration curve and following calculation of Docetaxel in PLGA specimens, i.e., 5.68, 6.19, and 8.1 ppm (see Figures S2 and S3).

For analysis of PLGA and quantification of Docetaxel, 50 mL of Ctrl_PLGA or RGD_PLGA or Ctrl_PLGA were placed in glass tube and exsiccated under vacuum (using a rotavapor). Then, they were resuspended in 0.5 mL of CDCl3/MetOD (2:1 vol/vol) containing 0.33 mg/mL of TSP (Trimethylsilylpropanoic acid) as quantitative standard. ^{1}H-NMR spectra of specimens were acquired as reported above and the intensity of peaks at 5.68, 6.19, and 8.1 ppm were measured, taking as reference the intensity of TSP ($\Delta\delta$ of TSP = 0).

Based on the calibration curve, the amount of encapsulated Docetaxel was calculated.

The encapsulation efficiency (EE%) of Docetaxel was calculated as follows:

$$EE_{Docetaxel}\% = \frac{Docetaxel_{encap}}{Docetaxel_{tot}} \times 100 \quad (1)$$

where $Docetaxel_{encap}$ was the amount of encapsulated Docetaxel (quantified as reported above) and $Docetaxel_{tot}$ was the amount used for PLGA preparation.

2.4. Quantification of Gd-DOTAMA in PLGA-NPs and Assessment of PLGA-NPs' Stability by 1H-Relaxometry

The encapsulation efficiency (EE%) of Gd-DOTAMA was calculated as follows:

$$EE_{Gd-DOTAMA}\% = \frac{Gd - DOTAMA_{encap}}{Gd - DOTAMA_{tot}} \times 100 \quad (2)$$

where Gd-DOTAMA$_{encap}$ was the amount of encapsulated Gd-DOTAMA and Gd-DOTAMA$_{tot}$ was the amount used for PLGA preparation.

The amount of encapsulated Gd-DOTAMA was calculated by quantifying the concentration of Gd through ^{1}H-relaxometry. Briefly, Ctrl_PLGA or RGD_PLGA were mixed in equal volumes with 37% HCl and incubated overnight at 120 °C in sealed vials to solubilize the free Gd^{3+} aqua ion. The R_1 values were measured using a Stelar SpinMaster relaxometer (Stelar, Mede, Italy) operating at 21.5 MHz. The inversion recovery method was used (16 experiments, two scans, recovery time $\geq 5 \times$ T1). The reproducibility of the R_1 data was $\pm$ 0.1%. Temperature (T = 25 °C) was regulated by a Stelar VTC-91 airflow heater, and the temperature inside the probe was measured using a calibrated digital thermometer (RS PRO RS55-11 RS, Sesto San Giovanni, Italy).

The concentration of Gd was determined using the following equation:

$$R_1 = R_{1d} + r_{1p} \times [Gd^{3+}] \quad (3)$$

where R_{1d} is the diamagnetic contribution (0.5 s^{-1}) and r_{1p} is the relaxivity of the free Gd^{3+} aqua ion (13.7 mM^{-1} s^{-1}) under the same experimental conditions.

The stability of PLGA-NPs was assessed by monitoring over time the water proton longitudinal relaxation rates (R_1) of Ctrl_PLGA or RGD_PLGA placed in HEPES/NaCl buffer or in human serum, at T = 37 °C.

2.5. ^{1}H-Nuclear Magnetic Resonance Dispersion (NMRD) Profiles

Ctrl_PLGA and RGD_PLGA water proton longitudinal relaxation rates (R_1) were measured as a function of the magnetic field strength in aqueous solutions using a fast field-cycling Stelar SmarTracer relaxometer (Stelar s.r.l., Mede, Italy), over a continuum of magnetic field strengths from 0.00024 to 0.25 T (0.01−10 MHz proton Larmor frequencies). This relaxometer works under computer control with an absolute uncertainty in $1/T_1$ of 1%. Additional longitudinal relaxation data in the range of 20−70 MHz were obtained using a Stelar relaxometer connected to a Bruker WP80 NMR electromagnet. The ^{1}H T_1 relaxation times were acquired using the standard inversion recovery method (with a 90° pulse width of 3.5 µs, 16 experiments, and 4 scans). The temperature was controlled by a Stelar VTC-91 airflow heater (Stelar, Mede, Italy) equipped with a calibrated copper−constantan thermocouple (uncertainty of $\pm$ 0.1 °C).

Data were reported as normalized millimolar relaxivity (r_{1p}):

$$r_{1p} = \frac{R_1 - R_{1d}}{[Gd^{3+}]} \quad (4)$$

2.6. Cell Cultures

4T1 cells were obtained in 2018 from the American Type Culture Collection (ATCC), stocked as frozen aliquots, then thawed and used for maximum 10 passages in RPMI 1640 (ThermoFisher Scientific Inc., Waltham, MA, USA) supplemented with 10% FBS (Sigma-Aldrich, Burlington, MA, USA). The TUBO cell line was derived from a mammary tumor arisen in a BALB-neuT female mouse and cultured in DMEM 20% FBS [45]. All cells tested negative for Mycoplasma using the MycoAlert kit (Lonza, Basilea, Switzerland), following the manufacturer's instructions [46].

2.7. 3-(4,5-Dimethylthiazol-2-yl)-2,5-diphenyltetrazolium Bromide (MTT) Assay

5×10^3 TUBO or 4T1 cells were cultured overnight in 96-well plates, and scalar doses of either Docetaxel, Ctrl_PLGA, or RGD_PLGA were then added. Viability was analyzed after 48 h using MTT. Briefly, MTT (0.5 mg/mL; Sigma Aldrich, Burlington, VT, USA) was added for 4 h at 37 °C, then supernatants removed and 150 µl/well dimethyl sulfoxide added to dissolve formazan crystals. Absorbance was measured on a 680XR microplate reader (BioRad Laboratories Inc., Hercules, CA, USA) at 570 and 650 nm (background subtraction) [47].

2.8. Flow Cytometric Analysis

To analyze integrin $\alpha_v\beta_3$ expression, exponentially growing 4T1 or TUBO cells were detached, washed with washing buffer (PBS 0,2% BSA), and stained for 30 min at 4 °C with an anti-$\alpha_v\beta_3$ integrin monoclonal antibody (cloneLM609, Millipore, Burlington, VT, USA), or with an isotype-matched negative control Ig. After washing, cells were stained with a carboxyfluorescein (FITC)-labelled rabbit anti-mouse Ig (Agilent Dako, Santa Clara, CA, USA) for 30 min at 4 °C [38]. To analyze the uptake of PLGA-NPs by BC cells, TUBO and 4T1 cells were incubated for 4 h at 37 °C with 12 µM Ctrl_PLGA and RGD_PLGA containing the FITC fluorochrome. At different time points, an aliquot of cells was harvested, washed, and analyzed using FACS for the FITC signal. To evaluate whether RGD_PLGA-NPs are internalized by the cells or remain bound to their surface, cells were incubated for 1 h with RGD_PLGA at 37 °C to allow internalization, or at 4 °C, a condition in which the internalization is impaired [48–50]. In parallel experiments, after washing, some samples were treated with acid pH (PBS 0.2% bovine serum albumin, 100 mM glycine, and 2 M urea (pH 2.5)) for 5 min at 4 °C to remove cell-surface-associated PLGA [48,51]. Cells were then washed and analyzed using FACS for the FITC signal [51]. In all samples, propidium iodide was added before acquisition in order to exclude dead cells from the analysis [52]. Cells were acquired on a BD FACSVerse (BD Bioscience, Franklin Lakes, NJ, USA) and analyzed using FlowJO10.5.3.

2.9. Confocal Microscopy Analysis of Cells

A total of 1.5×10^4 4T1 cells were seeded into 8-well µ-slides in fresh medium. 24 h later, cells were incubated with either Ctrl_PLGA or RGD_PLGA containing DOPE-CarboxyFluorescein for 30 min. Cells were then gently washed several times to remove any unbound PLGA-NPs. Z-stack images were acquired using laser scanning confocal microscopy (Leica TCS SP5, Leica Microsystems, Wetzlar, Germany) to obtain a series of parallel images along the Z-axis that could be used to reconstruct tridimensional images of the PLGA-labeled cells. The following wavelength was considered for microscopy: λ^{ex} = 495 nm, λ^{em} = 520 nm for DOPE-CF. Fluorescent images were processed using ImageJ Fiji freeware software.

2.10. Mice

Mice were bred and maintained under pathogen- and saprophytic-free conditions in the animal facility of the Molecular Biotechnology Center "Guido Tarone", and treated in accordance with institutional and EU guidelines. The project was approved by the Animal Care and Use Committee of the University of Turin and by the Italian Ministry of Health (authorizations No. 107/2020-PR and 500/2017-PR).

1×10^4 4T1 cells were orthotopically injected into the third mammary gland of N = 40 8-week-old female BALB/c mice. For the pharmacokinetics experiments, mice were analyzed 20 days after cell injection, when bearing 200 mm^3 mean volume tumors. For the therapeutic experiments, when the tumors reached 2 mm mean diameter, mice were blindly randomized into four groups, which received intraperitoneal (i.p.) injections of: the vehicle, i.e., 0.25 mL NaCl/HEPES solution (control); 5 mg/kg free Docetaxel; 5 mg/kg Ctrl_PLGA; 5 mg/kg RGD_PLGA. Mice were treated twice a week, for a total of 5 treatments. Mice were checked daily for any signs of suffering and weighed twice per week to assess pharmacotoxicity. Tumor diameters were measured twice per week with a

caliper. One day after the last treatment, mice were sacrificed and tumors removed. Tumors were weighed, fixed in 4% formaldehyde, and processed for histology.

2.11. Magnetic Resonance Imaging of Phantom and Mice

MRI scans were acquired at 7 T using a Bruker Avance 300 spectrometer (Bruker, Billerica, MA, USA), equipped with the Micro 2.5 microimaging probe. MRI was carried out both on an in vitro phantom and on animals.

For in vitro analysis, a phantom was composed of glass capillaries filled with RGD_PLGA, Ctrl_PLGA or Gd-HPDO3A at variable concentrations.

T_{2W} images were acquired by using a standard RARE (rapid acquisition with refocused echoes) sequence with the following parameters: TR = 4000 ms, TE = 5.5 s, FOV = 10 mm × 10 mm, slice thickness = 1 mm, RARE factor = 32, matrix size = 128 × 128, in plane spatial resolution = 0.078 × 0.078 mm^2/pixel, number of averages = 4.

T_{1W} images were acquired by using a standard MSME (multislice multiecho) sequence with the following parameters: TR = 250 ms, TE = 3.3 s, FOV = 10 mm × 10 mm, slice thickness = 1 mm, matrix size 128 × 128, in plane spatial resolution 0.078 × 0.078 mm^2/pixel, number of averages = 6. ROIs were manually drawn.

The T_1 contrast enhancement (T_{1enh}%) was calculated as follows:

$$T_{1enh}\% = \frac{SI_{sample} - SI_{ref}}{SI_{sample}} \times 100 \quad (5)$$

where SI_{sample} and SI_{ref} are signal intensities of the analyzed NP-sample and of the reference water-filled tube, respectively.

For in vivo analysis, tumor-bearing mice were anesthetized with 20 mg/kg tiletamine/zolazepam (Zoletil 100; Virbac SA, Carros, France) and 5 mg/kg xylazine (Rompun; Bayer, Leverkusen, Germany) by intramuscular injection using a 27-G syringe. MRI acquisitions were carried out before and after the i.v. injection of RGD_PLGA or Ctrl_PLGA (dose = 0.033 mmol/kg of Gd, 0.1 mL). A glass tube containing water was placed in proximity to the mouse, as MRI reference.

T_{1W} images were acquired by using a standard multislice multiecho (MSME) sequence, characterized by the following parameters: TR = 250 ms, TE = 3.3 s, FOV = 1 cm × 1 cm, slice thickness = 1 mm, matrix size = 128 × 128. T_{2W} images were acquired by using a standard rapid acquisition with refocused echoes (RARE) sequence with the following parameters: TR = 4000 ms, TE = 5.5 s, FOV = 30 mm × 30 mm, slice thickness = 1 mm, RARE factor = 32, matrix size = 128 × 128, in plane spatial resolution = 0.234 × 0.234 mm^2/pixel, number of parallel slices = 9, number of averages = 4. ROIs were drawn manually.

The T_1 contrast enhancement (T_{1enh}%) was calculated as follows:

$$T_{1enh}\% = \frac{SI_{post} - SI_{pre}}{SI_{pre}} \times 100 \quad (6)$$

where SI_{post} and SI_{pre} are signal intensities post- and pre-administration of the PLGA-NPs, normalized for signal in a reference water-filled tube.

Cardiac function was assessed by acquiring cardio-MR images with the same MRI scanner. A small animal ECG device (1025-MR, SA Instruments Inc., Stony Brook, NY, USA) was used for reliable electrocardiographic (ECG) synchronization and high-resolution heart imaging. Heart rate was monitored by electrocardiogram.

Many T_{2w} scout images were acquired in the transverse plane and the long axis plane of the left ventricle to determine the orientation of the short axis. The localization of the central short-axis slice was planned halfway between the apex and the base. The whole heart was covered by acquiring 5–7 short-axis parallel slices (slice thickness = 1 mm, number of slices was chosen to cover the entire heart). CINE MRI was carried out by using an ECG-triggered FLASH CINE gradient-spoiled gradient echo sequence with the following parameters: FA = 15°, TR = 8 ms, TE = 2.5 ms, FOV = 35 mm × 35 mm, matrix size = 192 × 192,

in plane spatial resolution = 0.182 × 0.182 mm^2/pixel, slice thickness = 1 mm, number of averages = 6, heart cycle sampled with 20 images. After the acquisition, morphological parameters of interest for cardiac function were measured in diastole and systole. Left end diastolic volume (EDV) and left end systolic volume (ESV) were manually measured. Then, left stroke volume (SV), cardiac output (CO) and ejection fraction (EF%) were calculated by applying the following formulae:

$$SV = EDV - ESV \quad (7)$$

$$EF\% = \frac{SV}{EDV} \times 100 \quad (8)$$

$$CO = HR \times SV \quad (9)$$

2.12. ICP-MS

At the end of the MRI experiments, the animals were sacrificed by cervical dislocation, in agreement with ethical rules. Cancer tissues, kidneys, liver, spleen, and muscles were explanted, weighed, and processed for ICP-MS analysis [53]. The tissues were added to 1 mL of concentrated HNO_3 (70%). Upon dissolution of the tissues, samples were further digested through microwave heating (MicroSYNTH, Microwave labstation, Microsynth, Balgach, Switzerland, equipped with an optical fiber temperature control and HPR-1000/6M high-pressure reactor, Milestone, Bergamo, Italy). After digestion, ultrapure water was added to each sample up to a 2 mL total volume, then samples were filtered with 0.45 µm filter and analyzed using ICP-MS for quantification of Gd^{3+}, using a Thermo Scientific ELEMENT 2 ICP-MS-Finnigan, Rodano, Italy. A calibration curve obtained by using four gadolinium absorption standard solutions (Sigma-Aldrich, Burlington, MA, USA) in the range 0.005–0.1 µg/mL was used for the quantification. The total mass of Gd^{3+} retained in each specimen was calculated with respect to the weight of the tumor tissue (as µg of Gd^{3+}/g of tissue).

2.13. Histology

After MRI acquisition, mice were sacrificed. Cancer tissues, kidneys, liver, spleen, muscles, heart, and lungs were excised, washed twice in PBS, fixed in 5 in 4% formaldehyde and paraffin embedded. Sections of 5 µm thickness were cut with a microtome along the entire organ. Tumors were cut into 4 sections spaced by 50 µm. Sections were deparaffined with xylol and ethanol solutions, rinsed twice in PBS, and stained with hematoxylin/eosin (H/E stain) (BioOptic S.p.a., Milano, Italy). Samples were imaged under an Olympus BX41 microscope (Olympus, Tokio, Japan) equipped with a Leica photographic system (Leica Microsystems, Wetzlar, Germany).

2.14. Statistical Analysis

Statistical analyses were performed using the GraphPad8 software. All values are reported as means ± standard deviation or standard error. Data were analyzed using a two-tailed unpaired Student's *t*-test, non-parametric Mann–Whitney or Kruskal–Wallis test, when the distribution calculated using a Shapiro–Wilk or Kolmogorov–Smirnov test was not normal. Differences in tumor growth were analyzed using two-way ANOVA with a Bonferroni post-test. $p < 0.05$ was considered significant.

3. Results

3.1. Preparation and Chemo-Physical Characterization of PLGA Nanoparticles

In this study, two types of PLGA-NPs were prepared and compared both in vitro and in vivo: (i) RGD-containing PLGA-NPs (hereinafter named RGD_PLGA) and (ii) control untargeted PLGA-NPs (hereinafter named Ctrl_PLGA).

The first batch of RGD_PLGA and Ctrl_PLGA contained an amphipathic Gd-complex (as an MRI probe), while the second batch contained Docetaxel (as a chemotherapeutic

agent). All the nanoparticles also contained a fluorescent amphipathic probe (for optical microscopy) and a PEGylated phospholipid.

The general scheme of the NP formulation and chemical structures of the molecules used are shown in Figure 1A. The proposed NPs act as a stealth theranostic system, detectable by both optical imaging and MRI.

PLGA-NPs were prepared using the classic oil/water emulsion solvent extraction method [41]. Figure 1B reports chemicals used for PLGA-NP preparation, whereas Figure 1C reports the scheme of RGD binding.

All data regarding the PLGA-NPs' formulations and their characterization are summarized in Table 1. RGD_PLGA and Ctrl_PLGA displayed a very high degree of analogy, from a chemo-physical perspective. The average hydrodynamic diameters, obtained by dynamic light scattering (DLS) measurements, corresponded to 146 ± 16 nm and 149 ± 12 nm for RGD_PLGA and Ctrl_PLGA, respectively (PDI < 0.1 for all preparations), with a negligible change in size upon RGD binding (Table 1). Analogously, only a slight difference in ζ-potential was recorded (−2.96 ± 0.3 mV vs. −3.69 ± 0.5 mV for RGD_PLGA and Ctrl_PLGA, respectively) (Table 1).

Table 1. PLGA-NPs employed in this work.

	RGD_PLGA			Ctrl_PLGA	
Name	**RGD_PLGA**	**RGD_PLGA**	**Empty_PLGA**	**Ctrl_PLGA**	**Ctrl_PLGA**
Formulation	PLGA, DOPE-CF, DSPE-PEG2000 maleimide, DPPE-PEG2000-methoxy, Gd-DOTAMA, c(RGDfC).	PLGA, DOPE-CF, DSPE-PEG2000-maleimide, DPPE-PEG2000-methoxy, DTX, c(RGDfC).	PLGA, DOPE-CF, DPPE-PEG2000-methoxy, c(RGDfC).	PLGA, DOPE-CF, DPPE-PEG2000-methoxy, Gd-DOTAMA, c(RGDfC).	PLGA, DOPE-CF, DPPE-PEG2000-methoxy, DTX, c(RGDfC).
Hydrodynamic diameter (nm) + PDI measured by DLS at 25 °C in HEPES/NaCl buffer	135 PDI = 0.10	158 PDI = 0.07	149 PDI = 0.08	161 PDI = 0.09	136 PDI = 0.07
ζ-potential (mV) measured by DLS at 25 °C in HEPES/NaCl buffer	−2.59	−3.32	/	−2.52	−4.85
Relaxivity (mM^{-1} s^{-1}) at 21.5 MHz and 25 °C	24.10	/	/	24.76	/
Gd-DOTAMA (%)	77 ± 5%	/	/	85 ± 8%	/
Number of Gd/NP	$1.2 \pm 0.1 \times 10^5$	/	/	$1.3 \pm 0.1 \times 10^5$	/
Docetaxel encapsulation efficiency (EE%)	/	18.2 ± 5	/	/	27.3 ± 7

The amount of encapsulated Docetaxel was assessed using quantitative NMR. In fact, even though Docetaxel has a characteristic UV-vis absorption profile, the presence of the PLGA polymer (and other components) makes the background signal too intense and it is difficult to correctly extract the drug for its quantification. For this reason, Docetaxel quantification was carried out in NPs, without the Gd-complex, using high-resolution quantitative NMR, as reported in the Materials and Methods section. Data on NMR quantification have been added as Supplementary Materials (Figures S1–S3). The encapsulation efficiency (EE%) of Docetaxel was quantified as 18.2 ± 5 and 27.3 ± 7 for RGD_PLGA and Ctrl_PLGA, respectively. The lower EE% for RGD_PLGA is reasonably a consequence of the c(RGDfC) binding procedure and subsequent additional washing steps (Table 1).

The retention of the drug inside the NPs was assessed after multiple cycles of dialysis by NMR analysis of the external buffer (containing the eliminated Docetaxel). The results reported in Figure 2A indicate the analog kinetics of Docetaxel release from the two NPs, with no effect of c(RGDfC) on drug retention.

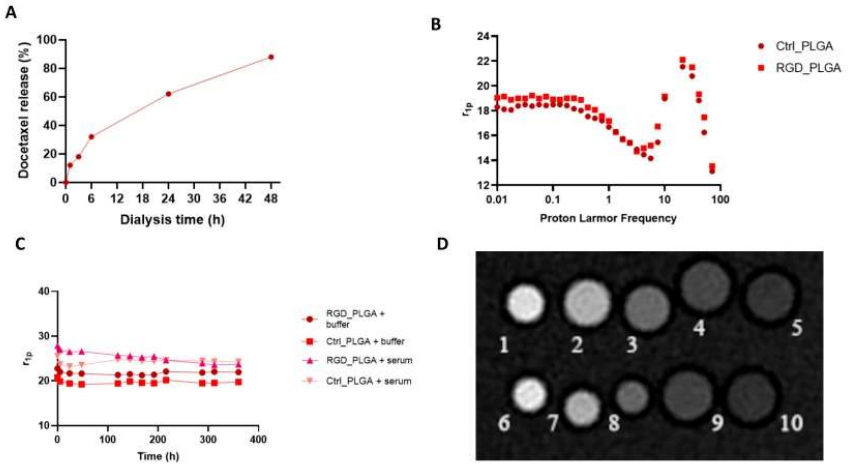


Figure 2. Chemo-physical characterization of PLGA nanoparticles. (**A**) In vitro release of Docetaxel. (**B**) NMRD profiles of Gd_PLGA-NPs. (**C**) Gd_PLGA-NPs' molar relaxivities over time in HEPES/NaCl buffer and human serum for assessing PLGA stability over time. (**D**) Representative T_{1w} MR image of a phantom containing glass capillaries filled with variable concentrations of RGD_PLGA or Ctrl_PLGA (Legend: capillaries number 1–5 RGD_PLGA in PBS at variable concentrations, i.e., 1, 0.5, 0.2, 0.1, 0.05 mM; capillaries number 6–10 Ctrl_PLGA in PBS at variable concentrations, i.e., 1, 0.5, 0.2, 0.1, 0.05 mM).

Subsequently, contrastographic and structural characterization of Gd-containing NPs was carried out using ^{1}H-relaxometry (at fixed and variable magnetic field) and MRI at 7.1T. First, the Gd-DOTAMA encapsulation yield in PLGA was assessed by relaxometry (mineralization of the sample and relaxometric measurements, see Materials and Methods), demonstrating that it corresponded to 77% and 85% for RGD_PLGA and Ctrl_PLGA, respectively (Table 1). Hence, the number of Gd-DOTAMA molecules loaded in one nanoparticle (*ca.* 1×10^5) is of the same order as that previously reported for other PLGA, liposomes or other NPs containing Gd-complexes (Table 1) [54,55].

The ^{1}H-nuclear magnetic relaxation dispersion (NMRD) profiles of RGD_PLGA and Ctrl_PLGA were recorded at variable magnetic fields (0.01–80 MHz) and T = 25 °C (Figure 2B).

Relaxivities of the two PLGA-NP preparations were quite similar, with no significant contribution of c(RGDfC) addition. In the NPs' NMRD profiles, a relaxivity hump at approximately 20–30 MHz was observed, typical of slowly moving systems (r_{1p} = 21–22 $s^{-1}mM^{-1}$ at B_0 = 0.5 T, corresponding to a proton Larmor frequency of ca. 21 MHz). R.N. Mariano and co-workers reported an analog hump for Gd-DOTAMA-PLGA-NPs with a size of 140 nm [56]. They reported a strong reduction in the overall NMRD profile and of the hump when the NPs' size increased up to the near disappearance of the contribution to relaxivity for micrometric PLGA particles [56]. Moreover, the relaxation enhancement has been suggested to be due to the strong interaction between the hydrophobic PLGA polymer and lipophilic chains of the Gd-complexes, which induces a reduction in the reorientational time (τ_R) of the paramagnetic complex [56].

A relaxometric approach was also used to assess NP stability (Figure 2C). For this purpose, RGD_PLGA and Ctrl_PLGA were placed in isotonic HEPES/NaCl buffer or in the presence of human serum (Seronorm^{TM}, Sero AS, Billingstad, Norway) at 37 °C for

several days. Stability was checked by measuring the relaxation rates of NP suspensions at T = 37 °C and B_0 = 0.5 T (corresponding to a proton Larmor frequency of 21 MHz). No significant change in the r_{1p} value was detected, indicating overall good stability of the NPs for at least 10 days. After this time, a small increase in the relaxation rate was observed for both NPs in buffer but not in serum. This suggests an overall small destabilization of PLGA-NPs due to hydrolysis of the polymer ester bonds. In the serum, stability was enhanced.

These data were corroborated by the assessment of no significant change in DLS size and ζ-potential in NPs on days after preparation. Moreover, these data indicate that serum albumin is not able to extract Gd-DOTAMA complexes from the PLGA-NP core, thus ensuring good stability in the blood for in vivo experiments.

Finally, the proof of concept of the feasibility of using such NPs as MRI contrast agents was carried out by acquiring MR images of a phantom composed of RGD_PLGA and Ctrl_PLGA at variable concentrations and comparing them with the standard clinically employed Gadoteridol (ProHance®, Bracco Imaging S.p.A., based on the Gd-HPDO3A complex). MRI showed a comparable enhancement of signal intensity for the two PLGA preparations, with or without RGD (Figure 2D). The good sensitivity of the Gd-DOTAMA incorporated into the PLGA-NPs is very promising for in vivo molecular imaging applications, where the accumulation of NPs in the tumor region is limited, and also in presence of a targeting system.

Altogether, the relaxometric measurements, DLS size, ζ-potential, and EE% clearly indicated that RGD_PLGA and Ctrl_PLGA share similar chemical/physical properties and a good stability profile over time, indicating possible applications for in vitro and in vivo experiments. Furthermore, MRI proof of concept indicated the feasibility of following NP biodistribution in vivo by MRI (see In vivo application of PLGA-NPs).

3.2. In Vitro Characterization of PLGA-NPs' Binding to BC Cells

To assess the capability of RGD_PLGA and Ctrl_PLGA to deliver Docetaxel to BC cells in vitro, we first verified the expression of integrin $\alpha_v\beta_3$ in BC cells. Triple negative 4T1 and HER2$^+$ TUBO murine BC cell lines were stained with an anti-integrin $\alpha_v\beta_3$ monoclonal antibody. Flow cytometric analysis showed that integrin $\alpha_v\beta_3$ was expressed at high levels on the cell surface of both cell lines (Figure 3A), confirming our previous data obtained from TUBO cells [38].

4T1 and TUBO cells were then incubated with RGD_PLGA or Ctrl_PLGA ([Docetaxel] = 12 μM), which contained the FITC fluorochrome, and the fluorescent signal was analyzed using flow cytometry on aliquots of cells harvested after 1, 2 or 4 h. Incubation was performed at 37 °C to allow PLGA internalization in cells, since the PLGA-NP cell internalization mechanism was found to be mainly dependent on caveolae-mediated endocytosis [49], and RGD can induce integrin receptor-mediated endocytosis, which are both active at 37 °C but impaired at 4 °C [50]. As shown in Figure 3B, the fluorescent signal progressively increased in 4T1 and TUBO cells treated with both compounds. However, at 4 h, TUBO cells displayed a lower uptake of Ctrl_PLGA than 4T1 cells, likely reflecting different degrees of endocytosis in the two cell lines. Notably, in both cell lines, cells incubated with RGD_PLGA showed a higher signal than those treated with Ctrl_PLGA, and the levels measured at 4 h were similar in 4T1 and TUBO cells, indicating that RGD increases the delivery of the PLGA to BC cells and may overcome a cell's intrinsic low endocytosis of untargeted PLGA-NPs.

To verify whether RGD_PLGA-NPs were internalized by the cells or remained bound to their surface, cells were incubated for 1 h with RGD_PLGA at 4 or 37 °C, then PLGA bound to the cell membrane were stripped by incubation with an acidic solution, and cells were analyzed using flow cytometry. As shown in Figure 3C, cells incubated with RGD_PLGA at 37 °C showed a significantly higher FITC signal than cells incubated with RGD_PLGA at 4 °C, suggesting that RGD_PLGA was internalized in cells. Indeed, when cells incubated at 37 °C were treated with an acidic solution to remove all the PLGA bound

to the cell surface, only a mild reduction in the signal was observed, confirming that the majority of RGD_PLGA was internalized by BC cells.

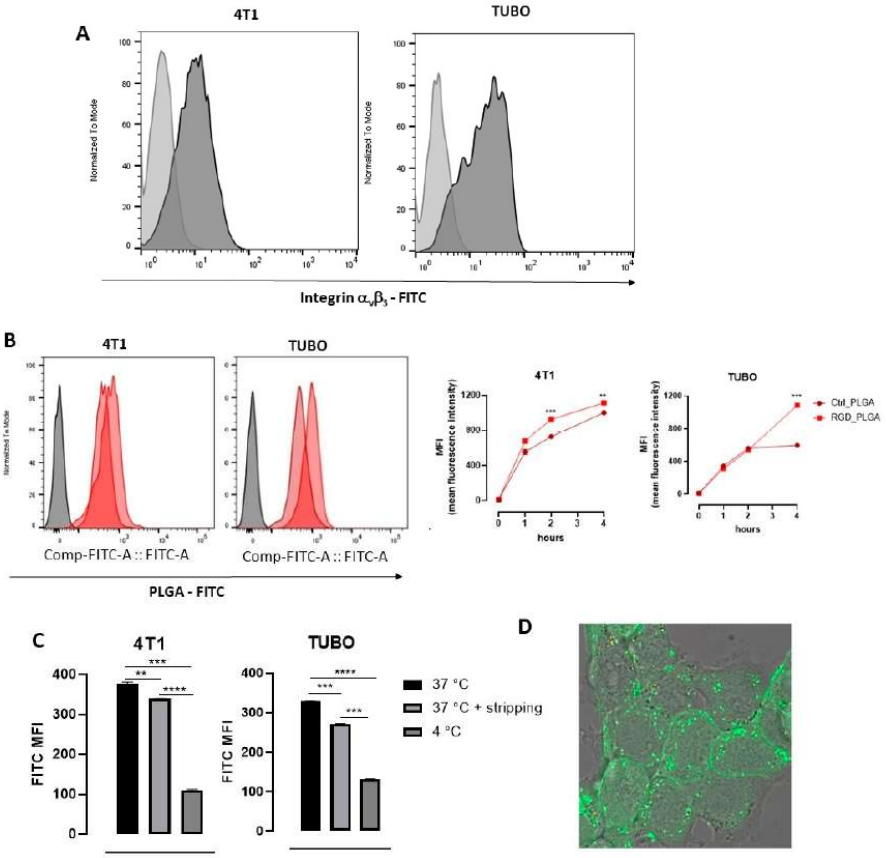


Figure 3. In vitro characterization of PLGA-NPs' binding to BC cells. (**A**) Expression of $\alpha_v\beta_3$ integrin on 4T1 and TUBO cell lines, measured by using a specific anti-$\alpha_v\beta_3$ integrin monoclonal antibody. Representative FACS histograms are shown. Light gray histograms show the background signal obtained by staining cells with an isotype control antibody; dark gray histograms show the signal obtained by staining with the anti-$\alpha_v\beta_3$ antibody. (**B**) FACS analysis of the kinetics of the uptake of PLGA-NPs in BC cells. 4T1 and TUBO cells were incubated at 37 °C with 12 μM FITC-containing Ctrl_PLGA or RGD_PLGA. Aliquots of cells were analyzed using FACS after 1, 2, and 4 h. Representative FACS histograms are shown, showing in gray the background signal of untreated cells, in light red the signal of cells incubated for 4 h with Ctrl_PLGA, and in dark red the histogram obtained in cells incubated for 4 h with RGD_PLGA. The graphs report the means ± SEM of the mean fluorescence intensity (MFI) measured in 2 independent experiments. (**C**) FACS analysis of RGD_PLGA-NP internalization into BC cells. 4T1 and TUBO cells were incubated for 1 h at 37 °C or 4 °C with 12 μM FITC-containing RGD_PLGA. An aliquot of cells was subjected to acidic stripping to remove membrane-bound PLGA-NPs before analysis. The graphs report the means ± SEM of the FITC MFI measured in two independent experiments. (**D**) Confocal fluorescence images of 4T1 cells upon 30 min incubation at 37 °C in presence of FITC-labelled RGD_PLGA-NPs. **, $p < 0.01$; ***, $p < 0.001$; ****, $p < 0.0001$, Student's t test.

The internalization of RGD_PLGA inside the cells was further confirmed by confocal fluorescence microscopy of 4T1 cells incubated for 30 min at 37 °C in presence of FITC-labelled RGD_PLGA-NPs (Figure 3D). The fluorescence signal localized in discrete spots clearly indicated the internalization of PLGA-NPs and compartmentalization in endosome-like vesicles.

3.3. Assessment of BC Cells Viability upon Treatment with Docetaxel Loaded PLGA Nanoparticles

To analyze whether RGD_PLGA and Ctrl_PLGA-NPs loaded with Docetaxel could affect the viability of BC cells and improve the efficacy of Docetaxel, 4T1 and TUBO cells were treated for 48 h with scalar doses of free Docetaxel, RGD_PLGA or Ctrl_PLGA containing Docetaxel, or with empty PLGA as a control. Cell viability was measured using an MTT assay. As shown in Figure 4A, empty PLGA did not exert a toxic effect on 4T1 or TUBO cells, and only the highest dose of PLGA slightly impaired their viability. In contrast, both RGD_PLGA and Ctrl_PLGA significantly impaired the viability of 4T1 and TUBO cells, and their effects were greater than those exerted by free Docetaxel. Statistical analysis of the results obtained with 12 µM Docetaxel demonstrated that RGD_PLGA and Ctrl_PLGA induced a significantly higher reduction in cell viability than Docetaxel alone (Figure 4B).

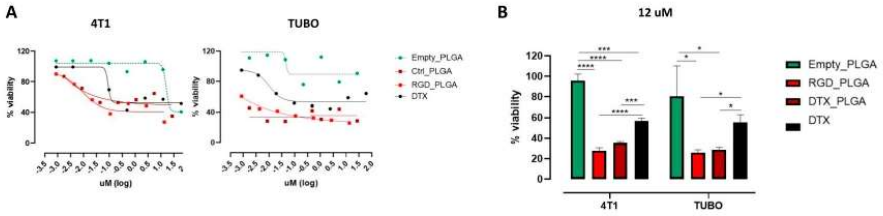


Figure 4. Effect of DTX_PLGA on BC cell viability. (**A**) MTT assays on TUBO and 4T1 cell lines performed with PLGA-NPs with and without Docetaxel, and Docetaxel alone at various concentrations. (**B**) Cell viability of the same cells treated with 12 µM Docetaxel (free or encapsulated in PLGA-NPs), or with empty PLGA. *, $p < 0.05$; ***, $p < 0.001$; ****, $p < 0.0001$, Student's *t*-test.

3.4. In Vivo Application of PLGA-NPs and Biodistribution

Based on the in vitro results, experiments using mouse models of BC were performed. For this purpose, 1×10^4 4T1 TNBC cells were injected into the adipose tissue of the third mammary gland of syngeneic BALB/c female mice. After 20 days, the tumors reached a mean volume of ca. 200 mm^3, which was considered suitable for clinical applications. First, the in vivo biodistribution of RGD_PLGA and Ctrl_PLGA was assessed by MRI. Mice bearing 4T1 were treated with Gd-DOTAMA-containing RGD_PLGA or Ctrl_PLGA, administered intravenously at a dose of 0.033 mmol/kg of Gd. This dose of Gd is ca. twenty-fold lower than the minimum dose normally used for clinical application (in clinical MRI 0.05–0.4 mmol Gd/kg are used for humans, corresponding to 0.6–4.8 mmol/kg in mice) [57].

Mice were subjected to MRI (Bruker 7.1 T spectrometer) before the administration of RGD_PLGA or Ctrl_PLGA and at t = 15 min, t = 4 h and t = 24 h post injection. Anatomical T_{2w} and Gd-contrasted T_{1w} scans were acquired. Signal enhancement in T_{1w} images after the injection of NPs was calculated with reference to pre-injection images for the tumor region, muscles, spleen, liver, and kidneys.

T_{1w} MR images of the tumor area were analyzed at different time points, and data are shown in Figure 5. In the tumor region, T_{1enh} was ca. 12% for both applications of RGD_PLGA or Ctrl_PLGA because of the passive accumulation of PLGA-NPs in the tumor region through the enhanced and permeability retention (EPR) effect. This value decreased to less than 5% at t = 4 h and t = 24 h for Ctrl_PLGA, owing to the natural *wash-out* effect. Conversely, in mice treated with RGD_PLGA, $T_1{}^{enh}$ increased to ~22% at t = 4 h and was maintained to ~18% at t = 24 h (Figure 5A). This is a consequence of active targeting and accumulation in the integrin-rich tumor region. These data are in line

with data from the literature, showing that RGD-targeting normally has an accumulation peak at approximately 3–6 h post injection [36,37]. MRI analysis of other organs showed that the elimination of PLGA-NPs occurs through the liver route, as generally occurs for nanosystems [25]. In fact, T_{1enh} in the liver was ~21% for both RGD_PLGA and Ctrl_PLGA at t = 15 min, then it increased up to 38% and 55% for RGD_PLGA at t = 4 h and 24 h and up to 29% and 37% for Ctrl_PLGA at t = 4 h and 24 h, respectively (Figure S4). Analysis of the muscle and kidney revealed only a small signal enhancement (lower than 10%) for both NPs at all tested time points (Figure S4). Finally, in the spleen, there was a higher accumulation of RGD_PLGA at t = 15 min and t = 4 h than in Ctrl_PLGA. At t = 24 h, no significant difference in signal enhancement in the spleen was revealed by comparing RGD_PLGA and Ctrl_PLGA.

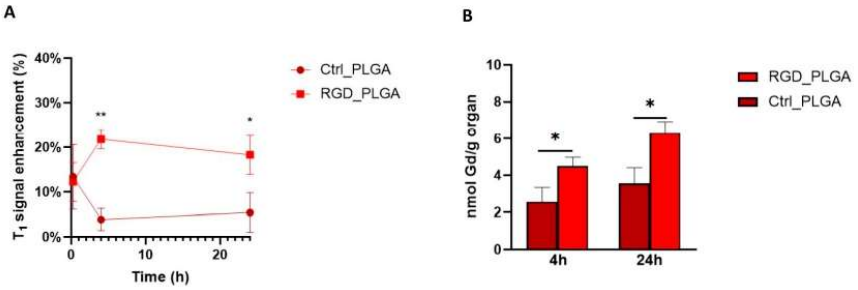


Figure 5. In vivo biodistribution of RGD_PLGA and Ctrl_PLGA. (**A**) T_1^{enh} in the tumor region at different time points upon administration of RGD_PLGA or Ctrl_PLGA. (**B**) Quantification of Gd retained in the tumor by inductively coupled plasma mass spectrometry (ICP-MS), at t = 4 h and t = 24 h. *, $p < 0.05$; **, $p < 0.01$, Student's *t*-test.

The higher accumulation of targeted PLGA-NPs in the liver and spleen may be due to the expression of integrins in macrophages, which are abundant in these organs [40].

After MRI analysis, tumors and other organs were excised for analytical quantification of Gd retained in the organs by ICP-MS, at t = 4 h and t = 24 h. Figure 5B and Figure S5 report the quantification of Gd in the tumor and liver, respectively. Analytical data confirmed the MRI biodistribution. At both t = 4 h and t = 24 h, the accumulation of Gd was more intense in both the tumors and liver of mice treated with RGD_PLGA than in mice treated with Ctrl_PLGA (approximately 44% and 48% higher in the two organs, respectively). Similar to what was demonstrated by MRI, the accumulation in the liver was much higher than that in the tumors, as expected for all drugs, and especially for nanosystems. Quantification of the muscles, kidneys and spleen is shown in Figure S5. As for MRI, a low Gd concentration was reported in the muscles and kidneys.

MRI experiments and ICP analysis reported a good effect of using PLGA-NPs, which were able to accumulate in the tumor region. This effect was more pronounced in the presence of RGD.

Using quantitative ICP-MS analysis, it was estimated that ca. 2.0×10^{16} and 3.1×10^{16} RGD_PLGA-NPs per gram of tumor tissue can be accumulated at t = 4 h and t = 24 h, respectively.

Hence, the use of RGD_PLGA can increase the effective dose in the tumor, minimizing side effects on distal organs.

3.5. In Vivo Application for Anticancer Therapy

To analyze the therapeutic efficacy of the NPs, mice were treated with RGD_PLGA or Ctrl_PLGA. 4T1 cells were injected into the third mammary gland of female BALB/c mice. When the tumors reached a mean diameter of 2 mm, a dimension that we know to be suitable for therapeutic studies [45,46,58–60], tumor-bearing mice were randomly assigned to four different experimental groups, treated i.p. as follows: (i) RGD_PLGA;

(ii) Ctrl_PLGA; (iii) free docetaxel, as a control; (iv) physiological saline solution. Figure 6A shows the treatment protocol used. The mice were treated twice per week for a total of five treatments. A total dose of 25 mg/Kg of docetaxel was administered to each mouse. At this dose, docetaxel, either free or encapsulated into PLGA-NPs, did not induce systemic toxicity, as demonstrated by the lack of reduction in body weight in treated mice compared to the controls (Figure 6B).

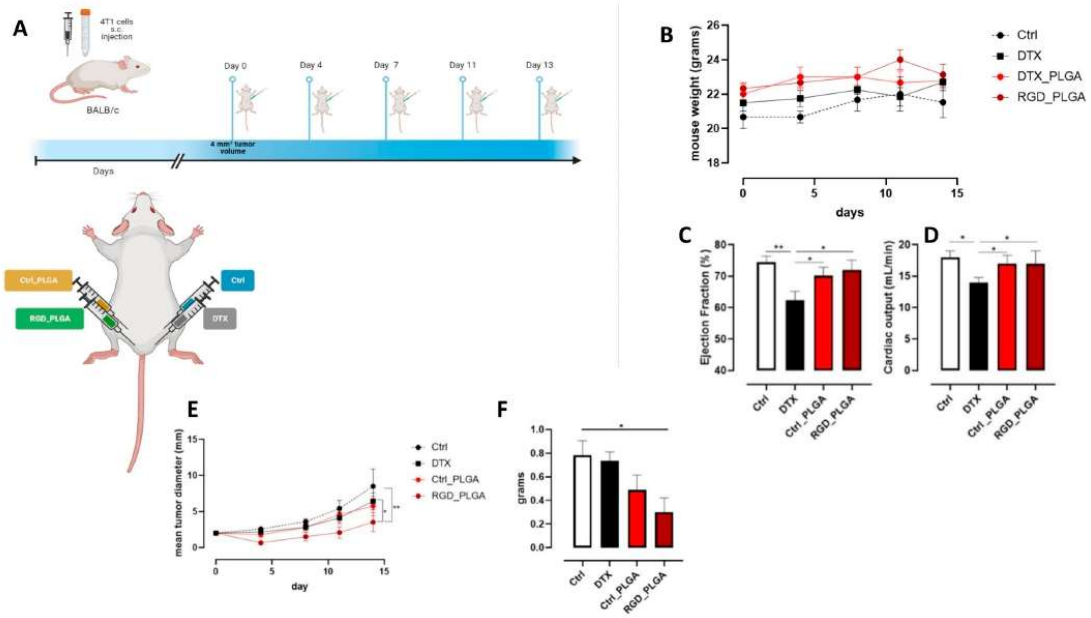


Figure 6. In vivo effect of PLGA-NPs. (**A**) BALB/c mice were orthotopically challenged with 1×10^4 4T1 cells. When the tumors reached 2 mm in diameter, the mice were treated with RGD_PLGA, Ctrl_PLGA, free docetaxel, or physiological saline solution as a control (N = 6 per group). The treatment was repeated twice per week for a total of 5 administrations. Graphs show (**B**) mouse weight, (**C**) heart ejection fraction (EF%) as assessed by cardioMRI, (**D**) heart cardiac output (CO) as assessed by flash cine cardioMRI, (**E**) mean tumor diameter, and (**F**) tumor weight at the end of the experiment. *, $p < 0.05$; **, $p < 0.01$; two-way ANOVA (**F**), unpaired Student's t test (**C**,**D**) or Mann–Whitney test (**E**). Panel A was created with Biorender.com.

Since docetaxel is known to have negative side effects on heart function [7,8], cardio MR images were acquired for the four groups of mice. For this purpose, cine FLASH cardio MRI was recorded and EF% and CO were measured as previously reported [8].

In Figure S6, systolic and diastolic MR images of the heart regions for representative mice of the four groups are shown. Quantitative data for EF% and CO are shown in Figure 6C,D, respectively. In mice treated with free docetaxel, a significant decrease in the two cardiac parameters was observed compared to that in control mice (EF% = 62% vs. 75%; CO = 14 mL/min vs. 18 mL/min for mice treated with docetaxel and control mice, respectively). Treatment with NPs (both RGD_PLGA and Ctrl_PLGA) preserved the cardiac function (EF% = 72% and CO = 17 mL/min in RGD_PLGA-treated mice; EF% = 70% and CO = 17 mL/min in Ctrl_PLGA-treated mice). This effect was present for both PLGA formulations because it was not due to the presence of the active targeting moiety but to the caging of docetaxel inside PLGA and the active/passive accumulation in the tumor region.

Treatment with free docetaxel did not hinder tumor growth, as reported in previous studies using similar amounts of docetaxel in 4T1-tumor-bearing mice [61,62], while Ctrl_PLGA induced a mild, not significant, effect. In contrast, treatment with RGD_PLGA significantly slowed tumor growth compared to that in control mice (Figure 6E). Thus, tumors explanted from RGD_PLGA-treated mice displayed a significantly lower weight than those explanted from control or free docetaxel-treated mice (Figure 6F), indicating that RGD_PLGA increased the efficacy of docetaxel in vivo.

Finally, MRI was carried out at the treatment end point. Representative axial T_{2w}-MR images of tumors at the endpoint are reported in Figure 7A. MRI confirmed data obtained by caliper measurements. MR images showed that tumors are heterogeneous, with the onset of necrotic area, especially in mice treated with free docetaxel. Both RGD_PLGA and Ctrl_PLGA provided a significant decrease in tumor growth, with a more intense effect of targeted PLGA. Figure 7B reports representative hematoxylin/eosin staining of tumors, confirming the lower size of tumors in mice treated with RGD_PLGA with respect to the other groups. Furthermore, mice treated with RGD_PLGA show reduced areas of necrosis with respect to control mice and mice treated with free docetaxel or with Ctrl_PLGA.

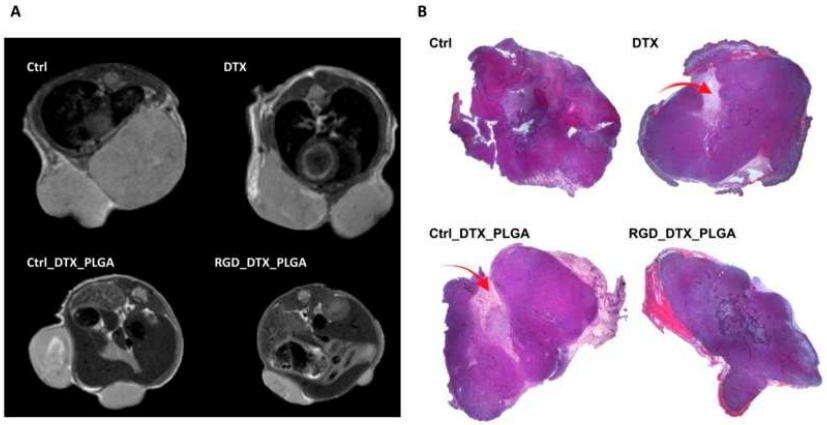


Figure 7. MRI and histological analyses of 4T1 tumors from mice treated with free docetaxel or with PLGA-NPs containing docetaxel. (**A**) Representative axial T_{2w}-MR images of tumor region in mice treated with physiological saline solution as a control, free docetaxel (DTX), Ctrl_PLGA or RGD_PLGA (N = 6 per group). (**B**) Representative hematoxylin/eosin histological staining of 4T1 tumors of mice belonging to the four groups of treatment. The red arrows highlight the necrotic areas.

4. Discussion

The treatment of BC remains a challenging task. Indeed, targeted therapies are available only for a small proportion of patients affected by specific BC subtypes, such as $HER2^+$. Generally, most BC patients still rely on surgery, chemo- and radiotherapy [1]. In particular, taxane-based chemotherapy is widely used for advanced BC treatment.

Taxanes display poor aqueous solubility, which is currently improved by adding large amounts of nonionic surfactants to the formulations used in the clinic. However, these surfactants may have considerable side effects [63]. In this scenario, we decided to design a nanosystem for the delivery of antitumor drugs that could improve their therapeutic efficacy and reduce their side effects.

Several nanosystems, including virus-like particles, liposomes, and silica-based NPs, have been developed to deliver chemotherapy. However, these systems are immunogenic and display slow degradation in vivo [64]. To avoid these drawbacks, PLGA-NPs were selected in this study because they are one of the most attractive biocompatible and biodegradable nanocarriers in current clinical and preclinical practices [11]. More than

twenty PLGA-based drug products have been approved by the FDA, in which the PLGA provides sustained drug release in long-acting formulations such as NPs and solid or gel implants [65]. PLGA-NPs are characterized by a hydrophobic core, allowing the entrapping of hydrophobic molecules which are water-insoluble, such as docetaxel, a cornerstone in BC treatment. Docetaxel is a microtubule inhibitor, capable of interfering with cancer cell division and eventually causing cell death via apoptosis [30]. Encapsulation of docetaxel in PLGA has already been performed and tested in different preclinical models of cancer, with different NP formulation or functionalizations, reporting generally positive results [28,66–69]. However, to improve tumor targeting, we decided to functionalize PLGA with the RGD peptide for active targeting of $\alpha_v\beta_3$ integrins, which are overexpressed in BC cells [38]. Recently, RGD was successfully exploited to deliver PLGA–poloxamer NPs containing an inhibitory neuropeptide to HeLa cells [70]. Similarly, RGD_PLGA has been used to target HUVEC and transplantable liver cancer cells [35].

To assess whether RGD could improve PLGA targeting to BC and ameliorate docetaxel-based therapy, two different classes of PLGA-NPs, untargeted (Ctrl_PLGA) and RGD-functionalized (RGD_PLGA), were prepared using oil-in-water emulsion and compared in both in vitro and in vivo BC models. In parallel experiments, both targeted and untargeted NPs were formulated to load docetaxel or an amphipathic Gd-complex, exploited for NP characterization and to follow their in vivo biodistribution and accumulation. Indeed, the above-described PLGA-NPs are versatile systems, since they can work either as MRI probes or as optical probes, depending on the formulation, including Gd-complexes or FITC. All NPs also held at least one PEGylated phospholipid, used for multiple reasons, e.g., to improve NPs' suspensibility and reduce their aggregation, to limit their uptake by macrophages, enhance their blood half-life, and prevent nonspecific interactions with cellular surfaces. It is well known that PEG chains create a protective hydrophilic layer around the NPs, thus reducing serum-dependent phagocytosis by inhibiting opsonin protein adsorption on NP surfaces [25]. The prepared PLGA-NPs had a diameter of approximately 150 nm and a small negative charge on the surface, with no significant inhomogeneity resulting from the RGD ligation. The amount of encapsulated docetaxel, measured through NMR to circumvent PLGA-related background signals in UV/vis spectrometry, corresponds to ca. 18% and 27% of the total for RGD_PLGA and Ctrl_PLGA, respectively. The lower EE% value for RGD_PLGA is reasonably because of the cyclic RGD ligation and subsequent additional washing steps. The water proton longitudinal relaxation rate (R_1) values indicate that the NPs are highly stable under physiological conditions over a 10-day period. Experiments carried out on TN 4T1 and $HER2^+$ TUBO cells demonstrated that PLGA-NPs successfully reached the BC cell surface, especially with the RGD-targeting moiety. RGD_PLGAs could also penetrate the cells, as assessed through flow cytometry and confocal microscopy. It is important to note that the addition of the RGD moiety was able to restore the lower level of PLGA endocytosis shown by TUBO cells than 4T1 cells, which suggests that RGD_PLGA may be successfully used for drug delivery in tumors that show a low endocytic capacity. The mechanisms underlying the intracellular differences affecting NP cell uptake remain to be elucidated, although endocytic profiling of different cancer cell lines has recently identified differences in the organization of both the endolysosomal and the Golgi systems that influence membrane trafficking between the plasma membrane and endosomes, determining the rate of untargeted PLGA internalization [71].

In vitro analysis showed that treatment with DTX_PLGA was more effective in inducing TUBO and 4T1 cytotoxicity than docetaxel alone, whereas the empty PLGA exhibited no toxic effects. This result shows that the observed pharmacological effect is not related to the NPs' structure, confirming the biocompatibility and nontoxicity of this polymer. Similar results were obtained in human MCF-7 and MDA-MB-231 BC cells using docetaxel-loaded PLGA containing d-α-tocopherol polyethylene glycol 1000 succinate (TPGS) as a surfactant [66], while other studies did not show significant differences in the viability of MDA-MB-231 cells treated with either free docetaxel or rod-shaped docetaxel-loaded PLGA-NPs, suggesting that PLGA efficacy can vary according to the NP formulation [28].

Altogether, the nice docetaxel entrapment and the successful delivery achieved by the NPs persuaded us to proceed with their in vivo administration. For this purpose, we used BALB/c female mice that received orthotopic 4T1 injections to induce the development of TNBC. MR images revealed good accumulation of PLGA-NPs at the lesion site, owing to the EPR effect. As expected, the presence of the RGD moiety enhanced tumor accumulation of the PLGA nanocarriers, especially in the first hours after injection. Interestingly, data in the literature indicate that RGD-mediated targeting leads to a peak in NP accumulation approximately 3–6 h after injection, as we previously demonstrated using an RGD-based optical imaging probe [34]. Accumulation was also confirmed by ICP-MS, strengthening our assumption of using PLGA-NPs to help the drug selectively localize at the tumor site, with the aim of reducing drug doses and, hence, unwanted effects on distal organs. Indeed, $\alpha_v\beta_3$ integrin is not only overexpressed in BC cells but also in the tumor endothelium [72]. RGD_PLGA-NPs may, thus, extravasate more effectively than untargeted PLGA-NPs, and enter the tumor owing to the enhanced permeability and retention effect. This increased accumulation in the tumor allows the RGD peptide to bind to $\alpha_v\beta_3$ integrins expressed in BC cells, inducing their cellular uptake and drug delivery.

Through therapeutic experiments in this BC murine model, carried out by administering Ctrl_PLGA or RGD_PLGA five times over a 2-week period, for a total dose of 25 mg/kg of docetaxel per mouse, we demonstrated an increased therapeutic efficacy of Ctrl_PLGA with respect to free docetaxel, and even higher improvements were obtained with RGD_PLGA. Indeed, tumors from mice treated with RGD_PLGA underwent enhanced growth reduction and appeared shrunken and less necrotized. Notably, free docetaxel did not significantly impair tumor growth, in accordance with previous studies reporting no effects of treatment of 4T1-tumor-bearing mice with similar doses of docetaxel [61,62]. To obtain an anticancer effect in this tumor model, higher doses of free docetaxel should be used, which increases the probability of developing side effects [73,74]. Finally, we monitored cardiac parameters (EF% and CO) to check heart-related side effects of the treatment, demonstrating that the entrapment of Docetaxel in the PLGA was significantly less harmful to cardiac function.

Summing up, the obtained results demonstrated that RGD_PLGA-NPs are stable and nontoxic nanocarriers, endowed with higher efficiency in hindering cancer cell viability compared to untargeted PLGA and to free Docetaxel. Thus, exploitation of the RGD-targeting system was a winning choice throughout the entire set of experiments, significantly improving drug delivery. Notably, the administration of Docetaxel encapsulated into NPs reduced its deposition in distal organs (e.g., heart), consequently lowering the side effects. These promising data suggest that PLGA-NPs have great potential for use in BC therapies.

5. Conclusions

In this study, we developed a Docetaxel-loaded PLGA-NP system functionalized with an RGD tripeptide to improve BC targeting. In vitro functional experiments showed that the use of these NPs induced higher antitumor activity than free Docetaxel or untargeted PLGA-NPs. In vivo studies demonstrated that RGD_PLGA-NPs enhanced drug accumulation in the tumor, significantly impairing tumor growth. Thus, this study demonstrated the possibility of improving the efficacy of PLGA-NPs as a nanosystem for specific drug delivery in BC by the addition of the RGD peptide. RGD_PLGA-NP-based drug delivery may provide a strategy for overcoming resistance and increasing drug concentrations in tumor cells and the tumor microenvironment in patients with drug-resistant BC. Thus, we have very recently started to put efforts into exploiting these nanosystems for combined therapy, involving both a chemotherapeutic agent and small molecules targeting tumor antigens that play important roles in tumor progression. These PLGA-NP-based therapies are valuable means for the development of novel strategies for BC treatment, and further investigation can provide groundbreaking advances in the next few years, possibly leading to their clinical application.

Supplementary Materials: The following supporting information can be downloaded at: https://www.mdpi.com/article/10.3390/cancers15010008/s1. Figure S1. NMR spectra of Docetaxel; Figure S2. Docetaxel calibration curve; Figure S3. NMR spectra of PLGA-NPs; Figure S4. MRI biodistribution of Ctrl_PLGA or RGD_PLGA-NPs; Figure S5. ICP-MS quantification of Gd in organs upon administration of Ctrl_PLGA or RGD_PLGA-NPs; Figure S6. Cardio-MR images.

Author Contributions: L.C., G.F., E.D.G. and F.C. designed the project and the experiments. G.F. and E.D.G. conceived the nanoparticles and, together with C.R., prepared and characterized them. A.D.L. and L.C. performed in vitro and in vivo experiments and analyzed the data. E.D.G., C.R. and G.F. performed and analyzed MRI, ICP-MS, histology, and confocal microscopy. The manuscript was written through contributions of all authors. All authors have read and agreed to the published version of the manuscript.

Funding: The research leading to these results has received funding from AIRC under the IG 2021 ID. 25766 project (principal investigator L.C.) and the IG 2018 ID.21468 project (principal investigator F. Cavallo), from Fondazione Ricerca Molinette Onlus, and from the University of Turin (principal investigator G.F. and L.C.). The authors acknowledge the Italian Ministry of Research for FOE contribution to the Euro-BioImaging MultiModal Molecular Imaging Italian Node (www.mmmi.unito.it (accessed on 10 October 2022)). This research was performed in the framework of COST Action AC15209 (EURELAX).

Institutional Review Board Statement: Experiments involving mice were approved by the Animal Care and Use Committee of the University of Turin and by the Italian Ministry of Health (authorizations No. 107/2020-PR and 500/2017-PR).

Informed Consent Statement: Not applicable.

Data Availability Statement: The data presented in this study are available in the article and Supplementary Materials.

Conflicts of Interest: The authors declare no conflict of interest.

References

1. Sung, H.; Ferlay, J.; Siegel, R.L.; Laversanne, M.; Soerjomataram, I.; Jemal, A.; Bray, F. Global Cancer Statistics 2020: GLOBOCAN Estimates of Incidence and Mortality Worldwide for 36 Cancers in 185 Countries. *CA Cancer J. Clin.* **2021**, *71*, 209–249. [CrossRef]
2. Nigdelis, M.P.; Karamouzis, M.V.; Kontos, M.; Alexandrou, A.; Goulis, D.G.; Lambrinoudaki, I. Updates on the treatment of invasive breast cancer: Quo Vadimus? *Maturitas* **2020**, *145*, 64–72. [CrossRef] [PubMed]
3. Waks, A.G.; Winer, E.P. Breast Cancer Treatment: A Review. *JAMA* **2019**, *321*, 288–300. [CrossRef] [PubMed]
4. de la Peña, F.A.; Andrés, R.; Garcia-Sáenz, J.A.; Manso, L.; Margelí, M.; Dalmau, E.; Pernas, S.; Prat, A.; Servitja, S.; Ciruelos, E. SEOM clinical guidelines in early stage breast cancer (2018). *Clin. Transl. Oncol.* **2018**, *21*, 18–30. [CrossRef] [PubMed]
5. Schirrmacher, V. From chemotherapy to biological therapy: A review of novel concepts to reduce the side effects of systemic cancer treatment (Review). *Int. J. Oncol.* **2019**, *54*, 407–419. [CrossRef]
6. Banach, M.; Juranek, J.K.; Zygulska, A.L. Chemotherapy-induced neuropathies-a growing problem for patients and health care providers. *Brain Behav.* **2016**, *7*, e00558. [CrossRef] [PubMed]
7. Bhagat, A.; Kleinerman, E.S. Anthracycline-Induced Cardiotoxicity: Causes, Mechanisms, and Prevention. *Curr. Adv. Osteosarcoma* **2020**, *1257*, 181–192. [CrossRef]
8. Gallo, S.; Spilinga, M.; Albano, R.; Ferrauto, G.; Di Gregorio, E.; Casanova, E.; Balmativola, D.; Bonzano, A.; Boccaccio, C.; Sapino, A.; et al. Activation of the MET receptor attenuates doxorubicin-induced cardiotoxicity in vivo and in vitro. *Br. J. Pharmacol.* **2020**, *177*, 3107–3122. [CrossRef]
9. Jeyaprakash, P.; Sangha, S.; Ellenberger, K.; Sivapathan, S.; Pathan, F.; Negishi, K. Cardiotoxic Effect of Modern Anthracycline Dosing on Left Ventricular Ejection Fraction: A Systematic Review and Meta-Analysis of Placebo Arms from Randomized Controlled Trials. *J. Am. Heart Assoc.* **2021**, *10*, e018802. [CrossRef]
10. Yeh, E.T.; Bickford, C.L. Cardiovascular Complications of Cancer Therapy: Incidence, Pathogenesis, Diagnosis, and Management. *J. Am. Coll. Cardiol.* **2009**, *53*, 2231–2247. [CrossRef]
11. Gavas, S.; Quazi, S.; Karpiński, T.M. Nanoparticles for Cancer Therapy: Current Progress and Challenges. *Nanoscale Res. Lett.* **2021**, *16*, 173. [CrossRef] [PubMed]
12. Wang, Y.; Sun, S.; Zhang, Z.; Shi, D. Nanomaterials for Cancer Precision Medicine. *Adv. Mater.* **2018**, *30*, e1705660. [CrossRef] [PubMed]
13. Liu, F.; Wang, X.; Liu, Q.; Zhang, H.; Xie, L.; Wang, Q.; Li, L.; Li, R. Biocompatible Nanoparticles as a Platform for Enhancing Antitumor Efficacy of Cisplatin–Tetradrine Combination. *Nanoscale Res. Lett.* **2021**, *16*, 61. [CrossRef] [PubMed]

14. Yu, Z.; Gao, L.; Chen, K.; Zhang, W.; Zhang, Q.; Li, Q.; Hu, K. Nanoparticles: A New Approach to Upgrade Cancer Diagnosis and Treatment. *Nanoscale Res. Lett.* **2021**, *16*, 88. [CrossRef]
15. Gigliotti, C.L.; Minelli, R.; Cavalli, R.; Occhipinti, S.; Barrera, G.; Pizzimenti, S.; Cappellano, G.; Boggio, E.; Conti, L.; Fantozzi, R.; et al. In Vitro and In Vivo Therapeutic Evaluation of Camptothecin-Encapsulated β-Cyclodextrin Nanosponges in Prostate Cancer. *J. Biomed. Nanotechnol.* **2016**, *12*, 114–127. [CrossRef]
16. Minelli, R.; Occhipinti, S.; Gigliotti, C.L.; Barrera, G.; Gasco, P.; Conti, L.; Chiocchetti, A.; Zara, G.P.; Fantozzi, R.; Giovarelli, M.; et al. Solid lipid nanoparticles of cholesteryl butyrate inhibit the proliferation of cancer cells in vitro and in vivo models. *Br. J. Pharmacol.* **2013**, *170*, 233–244. [CrossRef]
17. Mokhtarzadeh, A.; Vahidnezhad, H.; Youssefian, L.; Mosafer, J.; Baradaran, B.; Uitto, J. Applications of Spherical Nucleic Acid Nanoparticles as Delivery Systems. *Trends Mol. Med.* **2019**, *25*, 1066–1079. [CrossRef]
18. Nakhaei, P.; Margiana, R.; Bokov, D.O.; Abdelbasset, W.K.; Kouhbanani, M.A.J.; Varma, R.S.; Marofi, F.; Jarahian, M.; Beheshtkhoo, N. Liposomes: Structure, Biomedical Applications, and Stability Parameters with Emphasis on Cholesterol. *Front. Bioeng. Biotechnol.* **2021**, *9*, 705886. [CrossRef]
19. Doll, T.A.P.F.; Dey, R.; Burkhard, P. Design and optimization of peptide nanoparticles. *J. Nanobiotechnol.* **2015**, *13*, 73. [CrossRef]
20. Conti, L.; Lanzardo, S.; Ruiu, R.; Cadenazzi, M.; Cavallo, F.; Aime, S.; Crich, S.G. L-Ferritin targets breast cancer stem cells and delivers therapeutic and imaging agents. *Oncotarget* **2016**, *7*, 66713–66727. [CrossRef]
21. Piccolo, M.; Ferraro, M.G.; Raucci, F.; Riccardi, C.; Saviano, A.; Krauss, I.R.; Trifuoggi, M.; Caraglia, M.; Paduano, L.; Montesarchio, D.; et al. Safety and Efficacy Evaluation In Vivo of a Cationic Nucleolipid Nanosystem for the Nanodelivery of a Ruthenium(III) Complex with Superior Anticancer Bioactivity. *Cancers* **2021**, *13*, 5164. [CrossRef] [PubMed]
22. Danhier, F.; Ansorena, E.; Silva, J.M.; Coco, R.; Le Breton, A.; Préat, V. PLGA-based nanoparticles: An overview of biomedical applications. *J. Control. Release* **2012**, *161*, 505–522. [CrossRef] [PubMed]
23. Ding, D.; Zhu, Q. Recent advances of PLGA micro/nanoparticles for the delivery of biomacromolecular therapeutics. *Mater. Sci. Eng. C* **2018**, *92*, 1041–1060. [CrossRef] [PubMed]
24. Ferrauto, G.; Carniato, F.; Di Gregorio, E.; Tei, L.; Botta, M.; Aime, S. Large photoacoustic effect enhancement for ICG confined inside MCM-41 mesoporous silica nanoparticles. *Nanoscale* **2016**, *9*, 99–103. [CrossRef] [PubMed]
25. Rafiei, P.; Haddadi, A. Docetaxel-loaded PLGA and PLGA-PEG nanoparticles for intravenous application: Pharmacokinetics and biodistribution profile. *Int. J. Nanomed.* **2017**, *12*, 935–947. [CrossRef]
26. Gligorov, J.; Lotz, J.P. Preclinical Pharmacology of the Taxanes: Implications of the Differences. *Oncologist* **2004**, *9*, 3–8. [CrossRef] [PubMed]
27. Zhang, Z.; Zhang, X.; Chen, S.; Jiang, J.; Qi, R.; Zhang, X.; Xi, Y.; Li, M.; Zheng, H.; Hua, B. Taxane-based chemotherapy and risk of breast cancer-related lymphedema: Protocol for a systematic review and meta-analysis. *Medicine* **2019**, *98*, e16563. [CrossRef]
28. Bowerman, C.J.; Byrne, J.D.; Chu, K.S.; Schorzman, A.N.; Keeler, A.W.; Sherwood, C.A.; Perry, J.L.; Luft, J.C.; Darr, D.B.; Deal, A.M.; et al. Docetaxel-Loaded PLGA Nanoparticles Improve Efficacy in Taxane-Resistant Triple-Negative Breast Cancer. *Nano Lett.* **2016**, *17*, 242–248. [CrossRef]
29. Choi, Y.; Yoon, H.Y.; Kim, J.; Yang, S.; Lee, J.; Choi, J.W.; Moon, Y.; Kim, J.; Lim, S.; Shim, M.K.; et al. Doxorubicin-Loaded PLGA Nanoparticles for Cancer Therapy: Molecular Weight Effect of PLGA in Doxorubicin Release for Controlling Immunogenic Cell Death. *Pharmaceutics* **2020**, *12*, 1165. [CrossRef]
30. Kelly, C.; Alken, S. Benefit risk assessment and update on the use of docetaxel in the management of breast cancer. *Cancer Manag. Res.* **2013**, *5*, 357–365. [CrossRef]
31. Martins, C.; Sarmento, B. Microfluidic Manufacturing of Multitargeted PLGA/PEG Nanoparticles for Delivery of Taxane Chemotherapeutics. *Methods Mol. Biol.* **2019**, *2059*, 213–224. [CrossRef]
32. Greish, K. Enhanced permeability and retention (EPR) effect for anticancer nanomedicine drug targeting. In *Cancer Nanotechnology*; Humana Press: New York, NY, USA, 2010; Volume 624, pp. 25–37. [CrossRef]
33. Lee, S.-J.; Kim, H.-J.; Huh, Y.-M.; Kim, I.W.; Jeong, J.H.; Kim, J.-C.; Kim, J.-D. Functionalized Magnetic PLGA Nanospheres for Targeting and Bioimaging of Breast Cancer. *J. Nanosci. Nanotechnol.* **2018**, *18*, 1542–1547. [CrossRef] [PubMed]
34. Shipunova, V.O.; Kovalenko, V.L.; Kotelnikova, P.A.; Sogomonyan, A.S.; Shilova, O.N.; Komedchikova, E.N.; Zvyagin, A.V.; Nikitin, M.P.; Deyev, S.M. Targeting Cancer Cell Tight Junctions Enhances PLGA-Based Photothermal Sensitizers' Performance In Vitro and In Vivo. *Pharmaceutics* **2021**, *14*, 43. [CrossRef] [PubMed]
35. Danhier, F.; Vroman, B.; Lecouturier, N.; Crokart, N.; Pourcelle, V.; Freichels, H.; Jérôme, C.; Marchand-Brynaert, J.; Feron, O.; Préat, V. Targeting of tumor endothelium by RGD-grafted PLGA-nanoparticles loaded with Paclitaxel. *J. Control. Release* **2009**, *140*, 166–173. [CrossRef]
36. Ferrauto, G.; Tripepi, M.; Di Gregorio, E.; Bitonto, V.; Aime, S.; Castelli, D.D. Detection of U-87 Tumor Cells by RGD-Functionalized/Gd-Containing Giant Unilamellar Vesicles in Magnetization Transfer Contrast Magnetic Resonance Images. *Investig. Radiol.* **2020**, *56*, 301–312. [CrossRef]
37. Lanzardo, S.; Conti, L.; Brioschi, C.; Bartolomeo, M.P.; Arosio, D.; Belvisi, L.; Manzoni, L.; Maiocchi, A.; Maisano, F.; Forni, G. A new optical imaging probe targeting αVβ3 integrin in glioblastoma xenografts. *Contrast Media Mol. Imaging* **2011**, *6*, 449–458. [CrossRef]

38. Conti, L.; Lanzardo, S.; Iezzi, M.; Montone, M.; Bolli, E.; Brioschi, C.; Maiocchi, A.; Forni, G.; Cavallo, F. Optical imaging detection of microscopic mammary cancer in ErbB-2 transgenic mice through the DA364 probe binding$\alpha v\beta 3$integrins. *Contrast Media Mol. Imaging* **2013**, *8*, 350–360. [CrossRef]
39. Rovero, S.; Amici, A.; Di Carlo, E.; Bei, R.; Nanni, P.; Quaglino, E.; Porcedda, P.; Boggio, K.; Smorlesi, A.; Lollini, P.L.; et al. DNA vaccination against rat her-2/Neu p185 more effectively inhibits carcinogenesis than transplantable carcinomas in transgenic BALB/c mice. *J. Immunol.* **2000**, *165*, 5133–5142. [CrossRef]
40. Di Gregorio, E.; Lattuada, L.; Maiocchi, A.; Aime, S.; Ferrauto, G.; Gianolio, E. Supramolecular adducts between macrocyclic Gd(iii) complexes and polyaromatic systems: A route to enhance the relaxivity through the formation of hydrophobic interactions. *Chem. Sci.* **2020**, *12*, 1368–1377. [CrossRef]
41. Anelli, P.L.; Lattuada, L.; Lorusso, V.; Schneider, M.; Tournier, H.; Uggeri, F. Mixed micelles containing lipophilic gadolinium complexes as MRA contrast agents. *Magn. Reson. Mater. Phys. Biol. Med.* **2001**, *12*, 114–120. [CrossRef]
42. Barge, A.; Cravotto, G.; Gianolio, E.; Fedeli, F. How to determine free Gd and free ligand in solution of Gd chelates. A technical note. *Contrast Media Mol. Imaging* **2006**, *1*, 184–188. [CrossRef] [PubMed]
43. Alberti, D.; Protti, N.; Franck, M.; Stefania, R.; Bortolussi, S.; Altieri, S.; Deagostino, A.; Aime, S.; Geninatti Crich, S. Theranostic Nanoparticles Loaded with Imaging Probes and Rubrocurcumin for Combined Cancer Therapy by Folate Receptor Targeting. *ChemMedChem* **2017**, *12*, 502–509. [CrossRef] [PubMed]
44. Ruggiero, M.R.; Crich, S.G.; Sieni, E.; Sgarbossa, P.; Forzan, M.; Cavallari, E.; Stefania, R.; Dughiero, F.; Aime, S. Magnetic hyperthermia efficiency and1H-NMR relaxation properties of iron oxide/paclitaxel-loaded PLGA nanoparticles. *Nanotechnology* **2016**, *27*, 285104. [CrossRef] [PubMed]
45. Donofrio, G.; Tebaldi, G.; Lanzardo, S.; Ruiu, R.; Bolli, E.; Ballatore, A.; Rolih, V.; Macchi, F.; Conti, L.; Cavallo, F. Bovine herpesvirus 4-based vector delivering the full length xCT DNA efficiently protects mice from mammary cancer metastases by targeting cancer stem cells. *OncoImmunology* **2018**, *7*, e1494108. [CrossRef]
46. Rolih, V.; Caldeira, J.; Bolli, E.; Salameh, A.; Conti, L.; Barutello, G.; Riccardo, F.; Magri, J.; Lamolinara, A.; Parra, K.; et al. Development of a VLP-Based Vaccine Displaying an xCT Extracellular Domain for the Treatment of Metastatic Breast Cancer. *Cancers* **2020**, *12*, 1492. [CrossRef] [PubMed]
47. Conti, L.; Bolli, E.; Di Lorenzo, A.; Franceschi, V.; Macchi, F.; Riccardo, F.; Ruiu, R.; Russo, L.; Quaglino, E.; Donofrio, G.; et al. Immunotargeting of the xCT Cystine/Glutamate Antiporter Potentiates the Efficacy of HER2-Targeted Immunotherapies in Breast Cancer. *Cancer Immunol. Res.* **2020**, *8*, 1039–1053. [CrossRef]
48. Conti, L.; Regis, G.; Longo, A.; Bernabei, P.; Chiarle, R.; Giovarelli, M.; Novelli, F. In the absence of IGF-1 signaling, IFN-γ suppresses human malignant T-cell growth. *Blood* **2006**, *109*, 2496–2504. [CrossRef]
49. de Oliveira, T.D.; Travassos, L.R.; Arruda, D.C.; Tada, D.B. Intracellular Targeting of Poly Lactic-Co-Glycolic Acid Nanoparticles by Surface Functionalization with Peptides. *J. Biomed. Nanotechnol.* **2021**, *17*, 1320–1329. [CrossRef]
50. Rigo, A.; Vinante, F. Flow cytometry analysis of receptor internalization/shedding. *Cytom. Part B Clin. Cytom.* **2016**, *92*, 291–298. [CrossRef]
51. Conti, L.; De Palma, R.; Rolla, S.; Boselli, D.; Rodolico, G.; Kaur, S.; Silvennoinen, O.; Niccolai, E.; Amedei, A.; Ivaldi, F.; et al. Th17 Cells in Multiple Sclerosis Express Higher Levels of JAK2, Which Increases Their Surface Expression of IFN-γR2. *J. Immunol.* **2012**, *188*, 1011–1018. [CrossRef]
52. Proserpio, V.; Conti, L.; Oliviero, S. Flow Cytometry for Beginners: Hints and Tips for Approaching the Very First Single-Cell Technique. *Methods Mol. Biol.* **2021**, *2386*, 27–41. [CrossRef]
53. DI Gregorio, E.; Ferrauto, G.; Furlan, C.; Lanzardo, S.; Nuzzi, R.; Gianolio, E.; Aime, S. The Issue of Gadolinium Retained in Tissues: Insights on the Role of Metal Complex Stability by Comparing Metal Uptake in Murine Tissues Upon the Concomitant Administration of Lanthanum- and Gadolinium-Diethylentriamminopentaacetate. *Investig. Radiol.* **2018**, *53*, 167–172. [CrossRef]
54. Esposito, G.; Crich, S.G.; Aime, S. Efficient Cellular Labeling by CD44 Receptor-Mediated Uptake of Cationic Liposomes Functionalized with Hyaluronic Acid and Loaded with MRI Contrast Agents. *ChemMedChem* **2008**, *3*, 1858–1862. [CrossRef] [PubMed]
55. Huang, C.-H.; Tsourkas, A. Gd-based Macromolecules and Nanoparticles as Magnetic Resonance Contrast Agents for Molecular Imaging. *Curr. Top. Med. Chem.* **2013**, *13*, 411–421. [CrossRef] [PubMed]
56. Mariano, R.N.; Alberti, D.; Cutrin, J.C.; Crich, S.G.; Aime, S. Design of PLGA Based Nanoparticles for Imaging Guided Applications. *Mol. Pharm.* **2014**, *11*, 4100–4106. [CrossRef]
57. Di Gregorio, E.; Furlan, C.; Atlante, S.; Stefania, R.; Gianolio, E.; Aime, S. Gadolinium Retention in Erythrocytes and Leukocytes From Human and Murine Blood Upon Treatment With Gadolinium-Based Contrast Agents for Magnetic Resonance Imaging. *Investig. Radiol.* **2020**, *55*, 30–37. [CrossRef]
58. Di Lorenzo, A.; Bolli, E.; Ruiu, R.; Ferrauto, G.; Di Gregorio, E.; Avalle, L.; Savino, A.; Poggio, P.; Merighi, I.F.; Riccardo, F.; et al. Toll-like receptor 2 promotes breast cancer progression and resistance to chemotherapy. *OncoImmunology* **2022**, *11*, 2086752. [CrossRef]
59. Lanzardo, S.; Conti, L.; Rooke, R.; Ruiu, R.; Accart, N.; Bolli, E.; Arigoni, M.; Macagno, M.; Barrera, G.; Pizzimenti, S.; et al. Immunotargeting of Antigen xCT Attenuates Stem-like Cell Behavior and Metastatic Progression in Breast Cancer. *Cancer Res.* **2016**, *76*, 62–72. [CrossRef]

60. Bolli, E.; O'Rourke, J.P.; Conti, L.; Lanzardo, S.; Rolih, V.; Christen, J.M.; Barutello, G.; Forni, M.; Pericle, F.; Cavallo, F. A Virus-Like-Particle immunotherapy targeting Epitope-Specific anti-xCT expressed on cancer stem cell inhibits the progression of metastatic cancer in vivo. *Oncoimmunology* **2017**, *7*, e1408746. [CrossRef]
61. Harris, A.R.; Perez, M.J.; Munson, J.M. Docetaxel facilitates lymphatic-tumor crosstalk to promote lymphangiogenesis and cancer progression. *BMC Cancer* **2018**, *18*, 718. [CrossRef]
62. Hu, Y.; Liu, J.; Cui, P.; Liu, T.; Piao, C.; Xu, X.; Zhang, Q.; Xiao, M.; Lu, Y.; Liu, X.; et al. Synergistic effect of adoptive immunotherapy and docetaxel inhibits tumor growth in a mouse model. *Cell. Immunol.* **2019**, *348*, 104036. [CrossRef]
63. Luo, Z.; Jiang, L.; Ding, C.; Hu, B.; Loh, X.J.; Li, Z.; Wu, Y. Surfactant Free Delivery of Docetaxel by Poly[(*R*)-3-hydroxybutyrate-(*R*)-3-hydroxyhexanoate]-Based Polymeric Micelles for Effective Melanoma Treatments. *Adv. Health Mater.* **2018**, *7*, e1801221. [CrossRef] [PubMed]
64. Abu Lila, A.S.; Ishida, T. Liposomal Delivery Systems: Design Optimization and Current Applications. *Biol. Pharm. Bull.* **2017**, *40*, 1–10. [CrossRef] [PubMed]
65. Wang, Y.; Qin, B.; Xia, G.; Choi, S.H. FDA's Poly (Lactic-Co-Glycolic Acid) Research Program and Regulatory Outcomes. *AAPS J.* **2021**, *23*, 92. [CrossRef] [PubMed]
66. Tran, P.; Nguyen, T.N.; Lee, Y.; Tran, P.N.; Park, A.J.-S. Docetaxel-loaded PLGA nanoparticles to increase pharmacological sensitivity in MDA-MB-231 and MCF-7 breast cancer cells. *Korean J. Physiol. Pharmacol.* **2021**, *25*, 479–488. [CrossRef]
67. Badran, M.M.; Alomrani, A.H.; Harisa, G.I.; Ashour, A.; Kumar, A.; Yassin, A.E. Novel docetaxel chitosan-coated PLGA/PCL nanoparticles with magnified cytotoxicity and bioavailability. *Biomed. Pharmacother.* **2018**, *106*, 1461–1468. [CrossRef]
68. Cai, J.; Qian, K.; Zuo, X.; Yue, W.; Bian, Y.; Yang, J.; Wei, J.; Zhao, W.; Qian, H.; Liu, B. PLGA nanoparticle-based docetaxel/LY294002 drug delivery system enhances antitumor activities against gastric cancer. *J. Biomater. Appl.* **2019**, *33*, 1394–1406. [CrossRef]
69. Al-Nemrawi, N.K.; Altawabeyeh, R.M.; Darweesh, R.S. Preparation and Characterization of Docetaxel-PLGA Nanoparticles Coated with Folic Acid-chitosan Conjugate for Cancer Treatment. *J. Pharm. Sci.* **2021**, *111*, 485–494. [CrossRef]
70. Kaur, S.; Pandey, S.K.; Sharma, D.; Sharma, R.K.; Wangoo, N. Enkephalin loaded and RGD decorated PLGA–poloxamer nanoparticles for effective targeting in cancer cells. *J. Mater. Sci.* **2022**, *57*, 17416–17432. [CrossRef]
71. Sayers, E.J.; Peel, S.E.; Schantz, A.; England, R.M.; Beano, M.; Bates, S.M.; Desai, A.S.; Puri, S.; Ashford, M.B.; Jones, A.T. Endocytic Profiling of Cancer Cell Models Reveals Critical Factors Influencing LNP-Mediated mRNA Delivery and Protein Expression. *Mol. Ther.* **2019**, *27*, 1950–1962. [CrossRef]
72. Liu, Z.; Wang, F.; Chen, X. Integrin $\alpha_v\beta_3$-targeted cancer therapy. *Drug Dev. Res.* **2008**, *69*, 329–339. [CrossRef] [PubMed]
73. Da Rocha, M.C.O.; Da Silva, P.B.; Radicchi, M.A.; Andrade, B.Y.G.; De Oliveira, J.V.; Venus, T.; Merker, C.; Estrela-Lopis, I.; Longo, J.P.F.; Báo, S.N. Docetaxel-loaded solid lipid nanoparticles prevent tumor growth and lung metastasis of 4T1 murine mammary carcinoma cells. *J. Nanobiotechnol.* **2020**, *18*, 43. [CrossRef] [PubMed]
74. Li, Y.; Jin, M.; Shao, S.; Huang, W.; Yang, F.; Chen, W.; Zhang, S.; Xia, G.; Gao, Z. Small-sized polymeric micelles incorporating docetaxel suppress distant metastases in the clinically-relevant 4T1 mouse breast cancer model. *BMC Cancer* **2014**, *14*, 329. [CrossRef] [PubMed]

Disclaimer/Publisher's Note: The statements, opinions and data contained in all publications are solely those of the individual author(s) and contributor(s) and not of MDPI and/or the editor(s). MDPI and/or the editor(s) disclaim responsibility for any injury to people or property resulting from any ideas, methods, instructions or products referred to in the content.

Supplementary material

RGD_PLGA Nanoparticles with Docetaxel: A Route for Improving Drug Efficiency and Reducing Toxicity in Breast Cancer Treatment

Enza Di Gregorio *,†, Chiara Romiti †, Antonino Di Lorenzo *, Federica Cavallo, Giuseppe Ferrauto ‡ and Laura Conti ‡

Department of Molecular Biotechnology and Health Sciences, University of Turin, Via Nizza 52, 10126 Turin, Italy

* Correspondence: enza.digregorio@unito.it (E.D.G.); antonino.dilorenzo@unito.it (A.D.L.); Tel.: +39 011-6708459 (E.D.G.); +39 011-6706458 (A.D.L.)

† These authors contributed equally to this work.

‡ These authors contributed equally to this work.

Keywords: breast cancer; Docetaxel; PLGA nanoparticles; magnetic resonance imaging; RGD; theranostic

Supplementary figures

Figure S1. NMR spectra of Docetaxel

Figure S2. Docetaxel calibration curve

Figure S3. NMR spectra of PLGA NPs.

Figure S4. MRI biodistribution of Ctrl_PLGA or RGD_PLGA NPs

Figure S5. ICP-MS quantification of Gd in organs upon administration of Ctrl_PLGA or RGD_PLGA NPs

Figure S6. Cardio-MR images

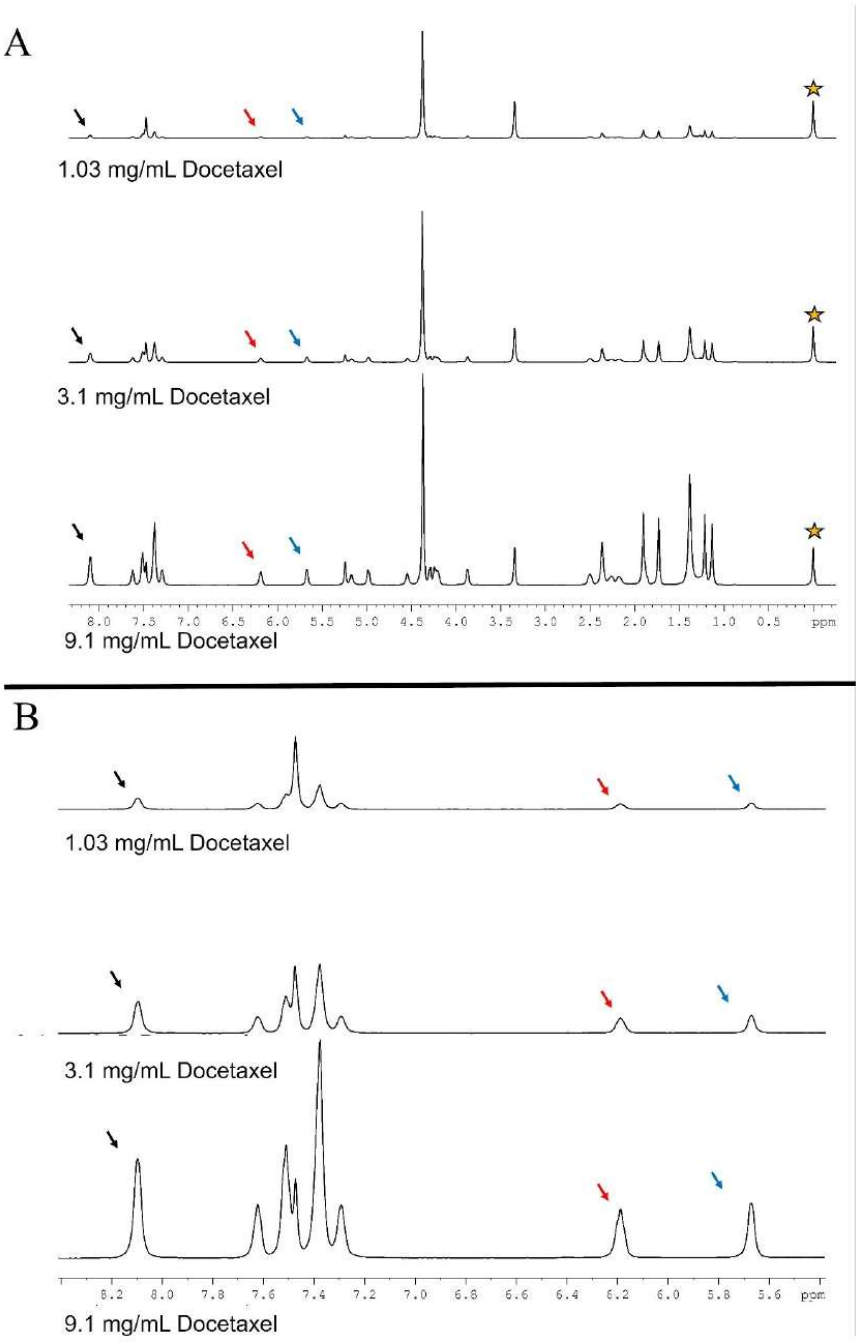


Figure S1. (A) NMR spectra of Docetaxel at variable concentration in CDCl3/MetOD (2:1 vol/vol) in presence of 0.33 mg/mL standard TSP) (B_0==14 T, T=298K). (B) magnification of spectra reported in (A). Yellow stars indicate NMR resonance of TSP (3-Trimethylsilylpropanoic acid) standard; black, red and blue arrows indicate characteristic resonances of Docetaxel used for calibration curves reported in Figure S3 (8.1, 6.19, 5.68 ppm, respectively).

	Int. 8.1	Int. 6.19	Int. 5.68
Best-fit values			
Slope	0.06576	0.06656	0.06760
Y-intercept	-0.004045	-0.002897	-0.005842
X-intercept	0.06152	0.04353	0.08643
1/slope	15.21	15.03	14.79
Std. Error			
Slope	0.0009047	0.001185	0.001560
Y-intercept	0.004459	0.005842	0.007688
95% Confidence Intervals			
Slope	0.06187 to 0.06965	0.06145 to 0.07166	0.06089 to 0.07431
Y-intercept	-0.02323 to 0.01514	-0.02803 to 0.02224	-0.03892 to 0.02724
X-intercept	-0.2401 to 0.3399	-0.3531 to 0.4010	-0.4332 to 0.5409
Goodness of Fit			
R square	0.9996	0.9994	0.9989
Sy.x	0.005628	0.008563	0.01126
Is slope significantly non-zero?			
F	5284	3152	1878
DFn, DFd	1, 2	1, 2	1, 2
P value	0.0002	0.0003	0.0005
Deviation from zero?	Significant	Significant	Significant
Equation	Y = 0.06576*X - 0.004045	Y = 0.06656*X - 0.002897	Y = 0.06760*X - 0.005842

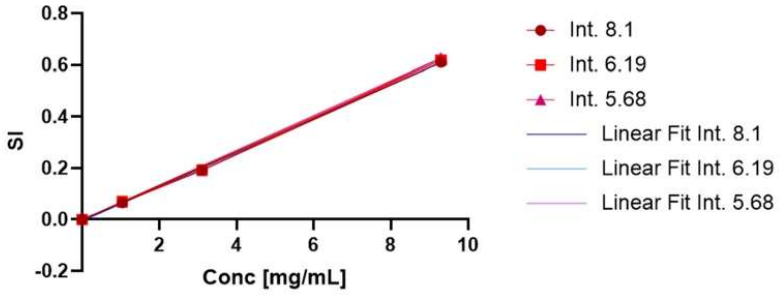


Figure S2. Docetaxel calibration curve obtained through NMR spectroscopy (spectra in Fig.S2)

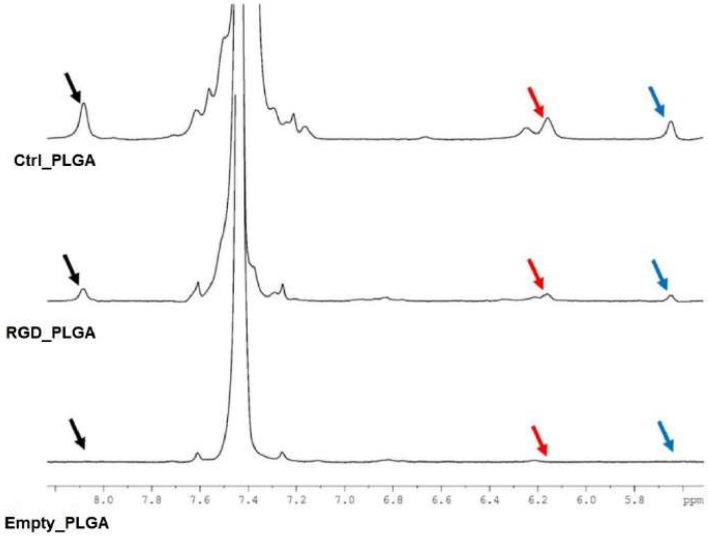


Figure S3. NMR spectra of PLGA NPs in CDCl3/MetOD (2:1 vol/vol) in presence of 0.33 mg/mL standard TSP) (B0==14 T, T=298K) normalised respect to the signal of standard TSP reference. Black, red and blue arrows indicate characteristic resonances of Docetaxel (8.1, 6.19, 5.68 ppm, respectively), used for the quantification of the drug content using the calibration curves reported in Figure S3.

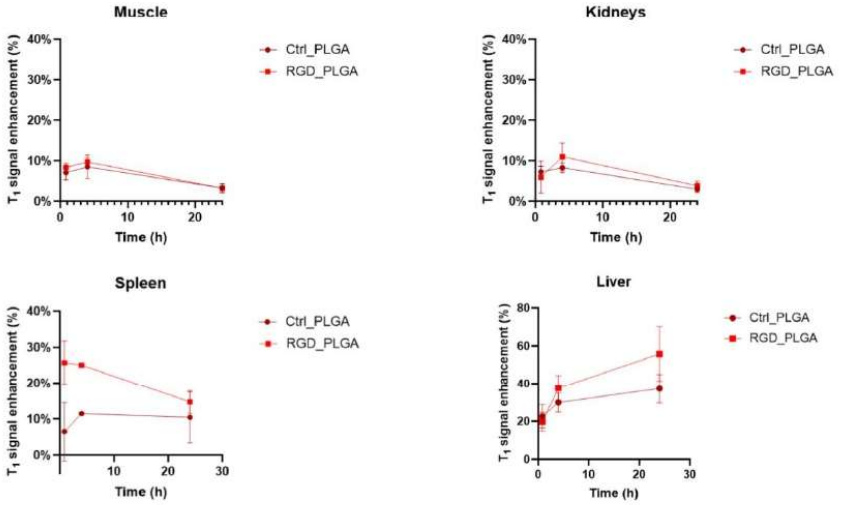


Figure S4. T_1 MRI signal enhancement (%) in muscles, kidneys, spleen, and liver upon i.p. administration of RGD_PLGA or Ctrl_PLGA at t= 5min, 4h or 24h.

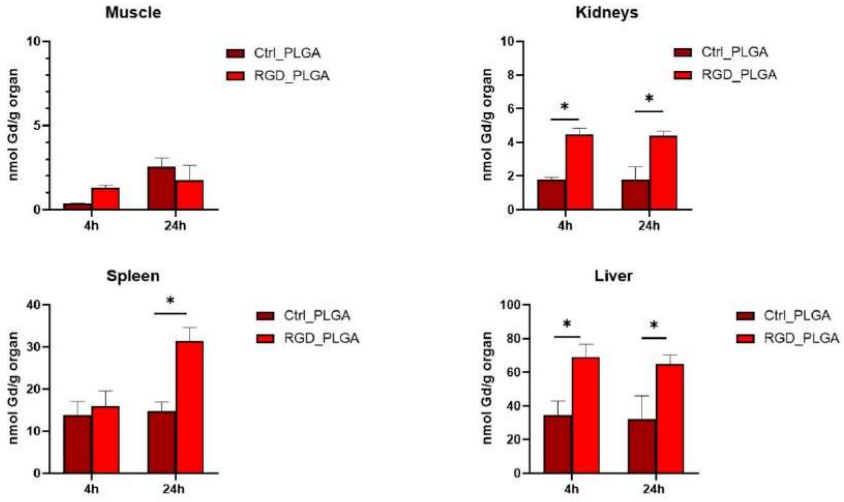


Figure S5. Quantification of Gd by ICP-MS in muscles, kidneys, spleen, and liver upon i.v. administration of RGD_PLGA or Ctrl _PLGA at t=4h or 24h.

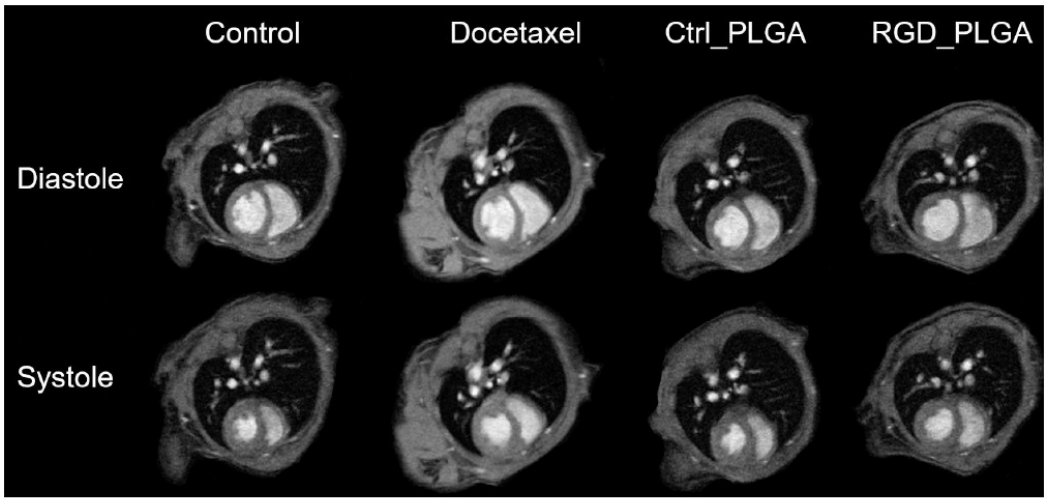


Figure S6. Representative diastolic or systolic axial MRI images of heart of BALB/c mice orthotopically challenged with $1x10^4$ 4T1 cells and treated with physiological saline solution as a control, free Docetaxel, Ctrl_PLGA or RGD_PLGA, C (N = 6 per group) (Flash cine cardioMR images).

The second part of this chapter reports unpublished data describing the development and evaluation of RGD-targeted nanoparticles for the delivery of CU-CPT22 and doxorubicin. To this end, we produced RGD-PLGA loaded with CU-CPT22 and started their characterization. Regarding doxorubicin, according to its chemical properties, liposomes were the most appropriate system for its delivery (Fig. II.1B). Doxorubicin-loaded liposomes, including RGD-modified variants, have already been extensively studied [130], reducing the need for deep characterization in this case. Consequently, we concentrated on the development and characterization of RGD-PLGA nanoparticles loaded with CU-CPT22 (PLGA-CU), evaluating their performance both independently and in combination with RGD-liposomes containing doxorubicin.

Once PLGA-CU were prepared and chemically characterized, the following steps involved evaluating their functional properties and efficacy both *in vitro* and *in vivo*.

To this end, we first assessed whether PLGA-CU was as specific as free CU-CPT22 in inhibiting TLR2 signaling. Since we have previously demonstrated that the TLR2 downstream pathway in breast cancer cells converges on NF-kB activation and that CU-CPT22 inhibits this signal [108], we incubated WT-874 mammary cancer cells with 7 µM PLGA-CU or CU-CPT22 and subsequently analysed NF-kB phosphorylation (p-NF-kB) by flow cytometry. As positive control, cells were incubated with *Staphylococcus aureus* peptidoglycan (PGN-SA; 20 µg/ml), a bacterial molecule known to activate TLR2 signaling, alone or in combination with the nanoparticles or the free drug. As expected, PGN-SA increased p-NF-kB levels compared to untreated cells; however, this effect was completely abolished when PLGA-CU or 7 µM CU-CPT22 was added to the culture medium (Fig. II.2A-B). These findings demonstrate that PLGA-CU specifically inhibits TLR2 signaling to the same extent as free CU-CPT22 *in vitro*.

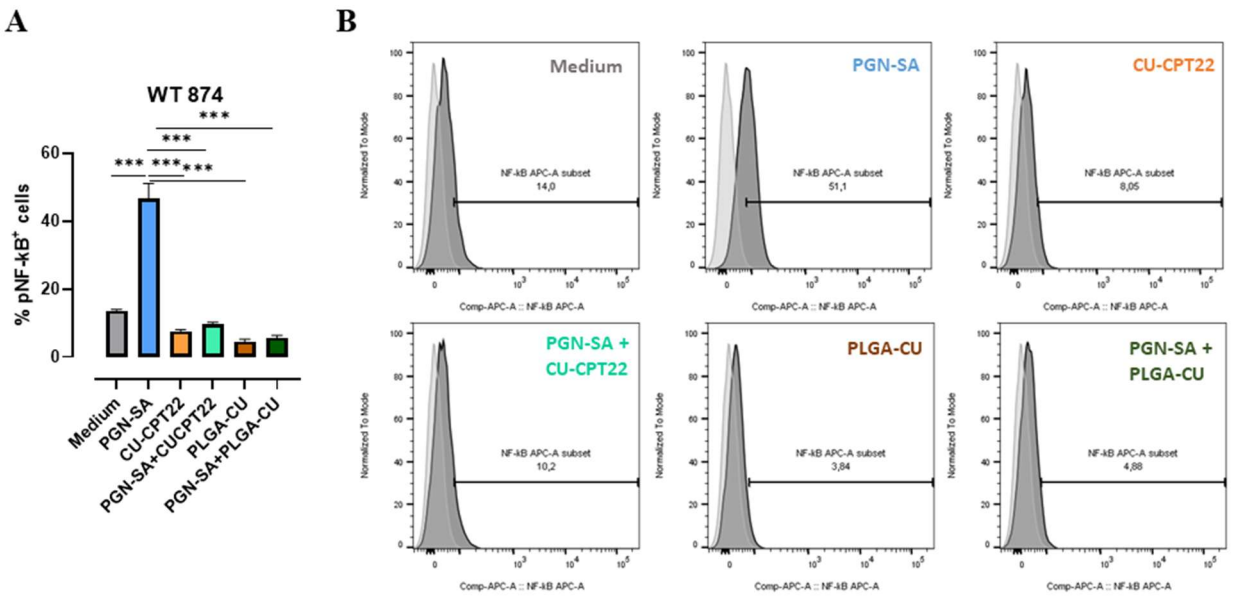


Figure II.2. CU-CPT22-loaded PLGA specifically inhibits TLR2 signaling. WT 874 cells were treated for 48h with or without PGN-SA (200 μg/ml) and CU-CPT22 or PLGA-CU (7 μM), alone or in combination. (A) Graph showing FACS analysis of p65 NF-κB phosphorylation (pNF-kB). Two-way ANOVA. (B) Representative FACS histograms of pNF-κB (dark gray) and control (light gray) staining. *, $p < 0.05$; **, $p < 0.01$; ***, $p < 0.001$; ****, $p < 0.0001$.

To determine whether PLGA-CU retains the same inhibitory activity on breast cancer cell viability as the free CU-CPT22, we assessed the effect of PLGA-CU, CU-CPT22 and empty PLGA on cell viability. To this end, three different murine breast cancer cell lines (WT-874, 4T1 and TUBO) were incubated with scalar doses of the three compounds, and cell viability was analysed by MTT assay after 48 hours. The empty PLGA nanoparticles showed no effect except on cell viability, except at the highest dose. This was likely due to the excessive dilution of the cell culture medium by the physiological solution in which the nanoparticles were prepared, causing a slight inhibition of cell viability (Fig. II.3A-C). As expected, CU-CPT22 exhibited an inhibitory effect on cancer cell viability. Notably, this effect was even more pronounced with PLGA-CU (Fig. II.3A-C), although the difference between the effect of CU-CPT22 and PLGA-CU was not substantial. This limited difference is expected *in vitro* because the direct addition of free drugs to the cell culture medium ensures high bioavailability, allowing the drug to easily reach its target and exert its effects. As a result, the advantages of nanoparticles for drug delivery are less pronounced *in vitro*, although they offer improved drug solubility and controlled release, particularly for poorly soluble compounds like CU-CPT22. *In vivo*, however, the scenario is markedly different. Nanoparticles, especially when conjugated with the RGD peptide, enable more efficient drug distribution, resulting in significantly higher tumor accumulation and reduced side effects compared to the free compound. These benefits were clearly demonstrated in the first part of this study (see Paper II, [109]) and are further supported by the *in vivo* experiments presented later in this chapter.

Differently from CU-CPT22, doxorubicin (Doxo) is not a specific drug, thus we directly evaluated the anti-cancer efficacy of the Doxo-loaded liposome (Lipo-Doxo) preparation by MTT assay. 4T1 cells were incubated with scalar doses of Lipo-Doxo, free Doxo or the empty liposome (Lipo) as a control for 48 hours. Both Lipo-Doxo and Doxo impaired cancer cell viability. At lower doses, Lipo-Doxo was more effective than free Doxo, suggesting that the liposome favours drug uptake by cancer cells. Lipo did not affect cancer cell viability (Fig. II.3D).

To better evaluate the effect induced by PLGA-CU and Lipo-Doxo on breast cancer cells, and to verify whether their combination could improve the efficacy of the single treatments, we measured apoptosis in cells treated for 48 hours with the two nanoparticles alone or in combination. These results were compared to apoptosis induced by the free drugs. Treatment of WT-874 and 4T1 cells

with 7 µM PLGA-CU or 1 µM Lipo-Doxo induced more apoptosis than the respective free drugs, and their combination had a significantly higher effect compared to the free drug combination (Fig II.3E-F).

Overall, these data gave the first indication about the efficacy of the nanoparticles for *in vitro* treatment of breast cancer cells.

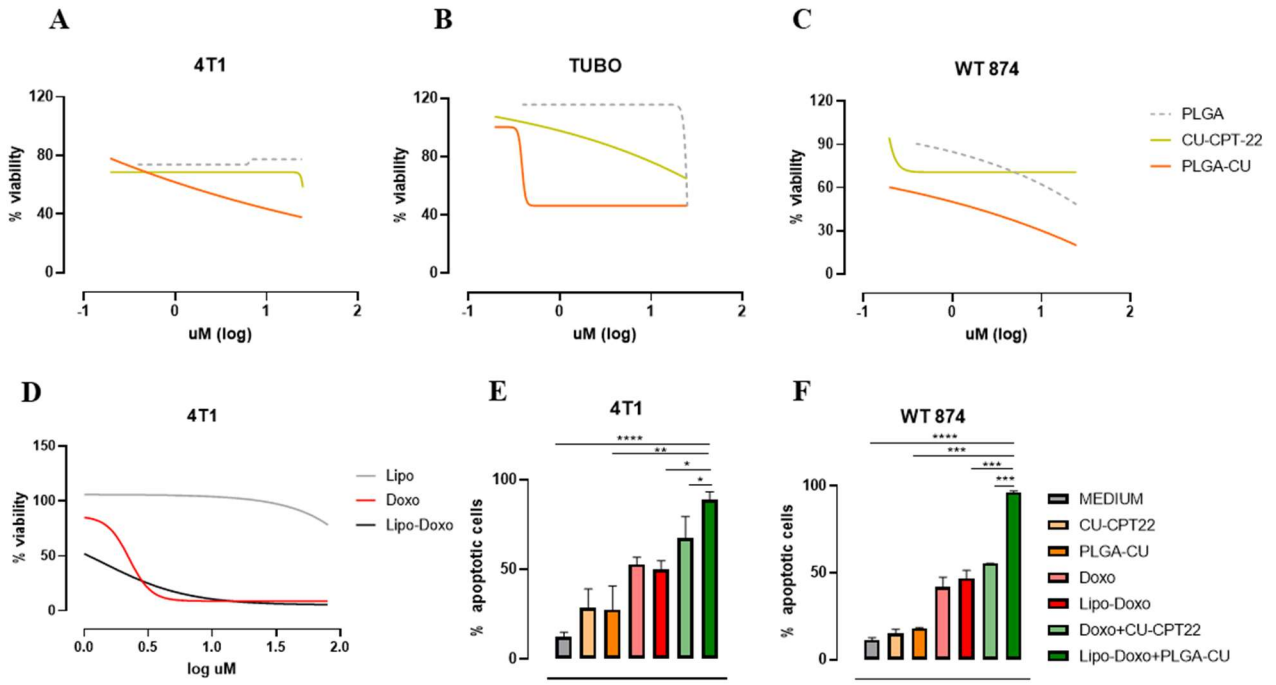


Figure II.3. PLGA-CU and Lipo-Doxo impair breast cancer cell viability, and their combination is more effective. (A-C) Dose-dependent toxicity of CU-CPT22, PLGA-CU and empty PLGA at different concentrations (25 to 0.098 µM, dilution 1:2) on 4T1, TUBO and WT 874 cells. Cell viability evaluated by MTT assay after 48h of treatment. (D) Dose-dependent toxicity of doxorubicin (Doxo), Lipo-Doxo and empty liposome (Lipo) at different concentrations (80 to 0.312 µM, dilution 1:2) on 4T1 cells. Cell viability evaluated by MTT assay after 48h of treatment. (E, F) Annexin-V/propidium iodide analysis of cell apoptosis by FACS. 4T1 and WT 874 cells were treated with or without CU-CPT22 (7 µM), Doxo (1 µM) and their combination, both as free and encapsulated drugs. All graphs report the means ± SEM of the percentage of positive cells from three independent experiments. Student's t tests. *, $p < 0.05$; **, $p < 0.01$; ***, $p < 0.001$; ****, $p < 0.0001$.

In Paper I, we described a mechanism of chemoresistance mediated by TLR2. Specifically, we demonstrated that ICD-inducing chemotherapies, such as doxorubicin, activate TLR2 signaling in cancer cells by producing the release of DAMPs. This signaling pathway converges on NF-kB, leading to several pro-tumoral effects. Conversely, treatment with CU-CPT22 inhibits doxorubicin-induced NF-kB activation [108]. To confirm that this effect is also observable using nanoparticles, we treated 4T1 cells for 48 hours with Lipo-Doxo (1 µM) and PLGA-CU (7 µM), either alone or in combination, and then measured p-NF-kB levels by flow cytometry. As expected, nanoparticles modulated NF-kB activation in the same manner as the free drugs used as controls. Specifically, Lipo-Doxo induced NF-kB phosphorylation, while PLGA-CU inhibited it. Notably, when the two nanoparticles were combined, PLGA-CU completely prevented NF-kB activation. These results confirm that the drugs encapsulated within the nanoparticles function similarly to their free forms and suggest that PLGA-CU can restore cell sensitivity to chemotherapy (Fig. II.4A-B).

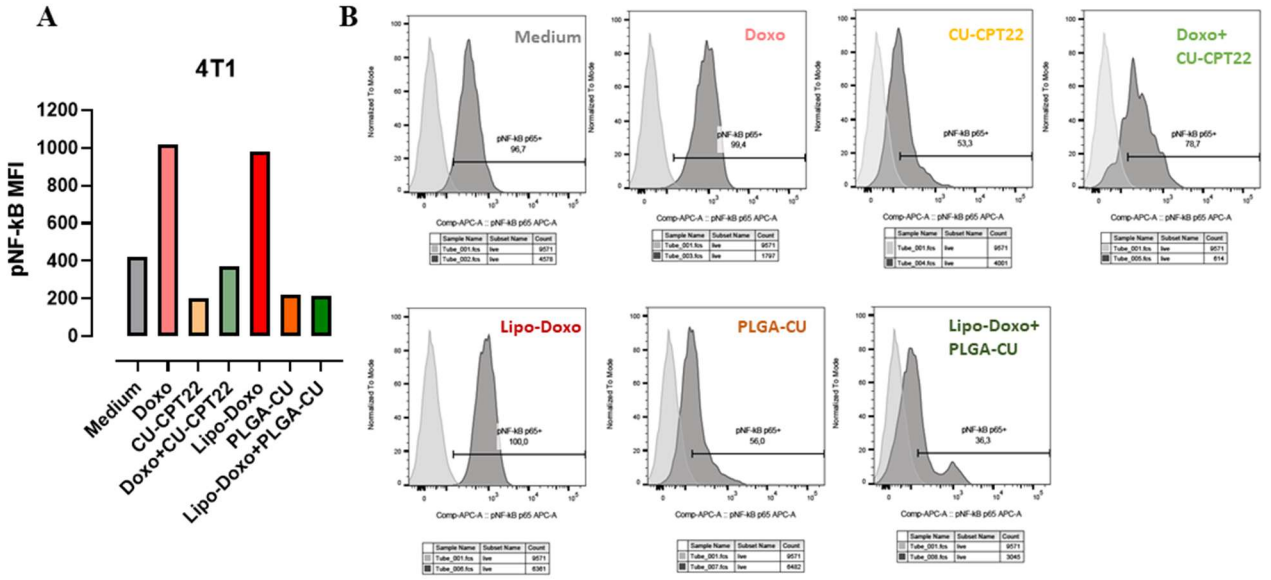


Figure II.4. Mechanism of action: PLGA-CU prevents doxorubicin-induced NF-kB activation. 4T1 cells were treated for 48h with or without Doxo (1 µM), CU-CPT22 (7 µM) and their combination, both as free or encapsulated drugs (A) Graph showing FACS analysis of p65 NF-κB phosphorylation. (B) Representative FACS histograms of pNF-κB (dark gray) and control (light gray) staining.

As mentioned above, a critical advantage of using nanoparticles for the delivery of anti-cancer drugs is their ability to improve drug accumulation in tumors. Simultaneously, reducing drug availability in other organs, thereby minimizing side effects, is another key goal. To address these objectives, we developed nanoparticles conjugated with the RGD tag, which specifically recognizes the $\alpha_v\beta_3$ integrin expressed by cancer cells and endothelial cells within tumors [126]. As previously discussed, in Paper II we demonstrated that decorating nanoparticles with RGD peptide significantly increases intra-

tumor accumulation of docetaxel-loaded PLGA compared to non- RGD-modified nanoparticles. In parallel, we showed that one of the most common adverse effects of docetaxel, cardiac toxicity, is mitigated when using nanoparticles instead of the free drug [109]. Building on that research, we developed RGD-targeted PLGA-CU and Lipo-Doxo nanoparticles for the combined therapy proposed in this chapter.

To confirm that these new nanoparticles retained the same advantages as PLGA-docetaxel, we performed biodistribution experiments. Specifically, we prepared nanoparticles containing the fluorescent probe cyanin 5 (Cy5) to analyse their biodistribution by OI. Cy5-labeled PLGA-CU or Lipo-Doxo were injected i.p. in tumor-bearing mice, and biodistribution was monitored at 0, 4 and 24 hours post-injection using the IVIS Spectrum instrument from Perkinelmer. The analysis revealed that, by 4 hours post-injection, Lipo-Doxo was already present in significant amounts in the tumor, and the signal remained stable at 24 hours. In contrast, PLGA-CU exhibited slower kinetics, but by 24 hours post-injection, its tumor accumulation was comparable to that of Lipo-Doxo. Importantly, neither nanoparticle formulations showed significant accumulation in muscle tissue, confirming their tumor-selective targeting (Fig. II.5A-B).

These findings are consistent with the results of Paper II regarding docetaxel-loaded RGD-PLGA nanoparticles and further support the reduced toxicity previously observed with nanoparticle-based delivery systems.

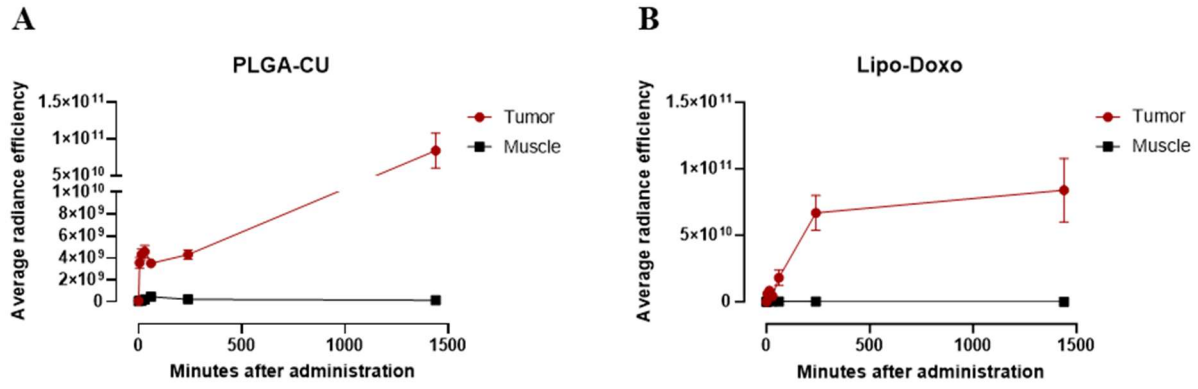


Figure II.5. RGD-targeted nanoparticles have a high accumulation in the tumor but not in other tissues. *In vivo* biodistribution of (A) PLGA-CU and (B) Lipo-Doxo. Analysis performed by in vivo optical imaging (IVIS) of mice systemically injected with Cy5-labeled nanoparticles at 0, 4 and 24h post-administration. Comparison between tumor and control muscle.

The positive results regarding the *in vitro* activity of the nanoparticles and their biodistribution represented fundamental steps toward establishing the proof-of-concept for the therapeutic efficacy of the nanoparticles *in vivo*. In this context, our first objective was to identify the appropriate dose of

PLGA-CU for *in vivo* use. While extensive information is available about systemic administration of doxorubicin in mice, including data from our findings shown in Paper I [108], no data exists regarding the *in vivo* application of CU-CPT22. Moreover, although Paper I established a protocol for the *in vivo* use of CU-CPT22 for the first time, that study employed intra-tumoral administration rather than and systemic administration. To address this gap, we tested two different doses of PLGA-CU in tumor-bearing mice. Specifically, we orthotopically injected 4T1 cells into BALB/c mice. Once the tumors became palpable, treatment with PLGA-CU (corresponding to 50 or 100 μg CU-CPT22) or the control vehicle was initiated. Treatments were administered i.p twice a week for 2 weeks. Interestingly, both doses of PLGA-CU significantly hindered tumor progression compared to the control, with the higher proving most effective (Fig. II.6A). Based on these results, we selected 100 μg of PLGA-CU for subsequent experiments.

To evaluate the combined efficacy of the two nanoparticles, we injected BALB/c mice with 4T1 cells. Once the tumors were palpable, treatment was initiated with PLGA-CU (100 μg) and Lipo-Doxo (a dose corresponding to 3 mg/kg of doxorubicin), either alone or in combination, or with vehicle as control. Mice were treated twice a week until sacrifice (Fig. II.6B). As expected, both nanoparticles significantly impaired tumor progression compared to the control, but their combination exhibited an even more potent effect (Fig. II.6C-D). A cytofluorimetric analysis of tumor masses explanted at the end of the experiment showed that PLGA-CU significantly reduced the percentages of $CD44^+CD24^-$ and $Sca1^+$ CSC populations in the tumor. A similar trend was observed when PLGA-CU was combined with Lipo-Doxo (Fig. II.6E-F). This finding is in line with the role of TLR2 in promoting CSC self-renewal, as described in Chapter I. Furthermore, the combined therapy induced a significant increase in $CD8^+$ T cell infiltration in tumors (Fig. II.6G). These results closely recapitulate our previous findings on the use of free doxorubicin and CU-CPT22 in pre-clinical models of breast cancer [108] and confirm that TLR2 inhibition contributes to reversing the immunosuppressive tumor microenvironment typical of breast cancer.

In addition, Chemical Exchange Saturation Transfer Magnetic Resonance Imaging (CEST MRI) analysis was performed prior to mice sacrifice. CEST MRI technique detects proton exchange between chemical groups of specific metabolites and the surrounding water at a certain resonance frequence [131]. In this experimental model, the purpose of CEST MRI was to identify alterations in tumor biochemistry, providing additional information about the therapies effect on the tumor that might be difficult to detect using other techniques. Interestingly, CEST MRI revealed intratumor variations in the CEST peak at 2 ppm among the treatment groups. The CEST 2ppm signal has been demonstrated to correlate with creatin levels [132]. Notably, the combined therapy significantly decreased creatin levels compared to both the control and the Lipo-Doxo group (Fig. II.6H).

Historically, creatin was considered a tumor-suppressive molecule. However, recent studies suggest that creatin may have a pro-tumoral and pro-metastatic role depending on the context [132,133]. In addition to tumor type and creatin levels, factors such as the expression of enzymes, kinases, and transporters involved in the creatine synthesis, modification, and trafficking should also be considered. For instance, while both creatin and its analogue cyclocreatin can be easily phosphorylated by creatin kinase, phosphocyclocreatin is less efficiently catalysed to produce ATP. As a result, phosphocyclocreatin can act as an energy deprivation source that inhibits cancer progression. Creatin also serves as a primary source of energy for $CD8^+$ T cells which depend on ATP for activation and proliferation. Consequently, creatin may suppress tumor growth by promoting a cytotoxic immune response against cancer cells. Conversely, recent studies propose that creatin can promote cancer cell proliferation and metastasis. For example, in breast cancer, adipocytes can enhance creatin synthesis and supply it to nearby cancer cells to support their growth. Similarly, in colorectal and pancreatic cancer metastatic models, cancer cells upregulate creatin phosphorylation, exploiting it to activate ECM remodeling pathways and facilitate metastasis [133]. These new findings may partially explain our observations, suggesting a correlation between slower tumor growth and reduced creatin levels in the group treated with the combined therapy. However, it remains unclear whether the therapy directly impacted cancer metabolism, leading to reduced creatin levels and subsequent impairment of tumor progression, or if the reduction in creatine is a secondary effect of effective tumor targeting, which in turn alters cancer metabolism.

Nevertheless, this result provides valuable insight into the relationship between cancer metabolism, tumor aggressiveness, and the efficacy of anti-cancer therapies. Further investigation into these mechanisms is warranted in future studies.

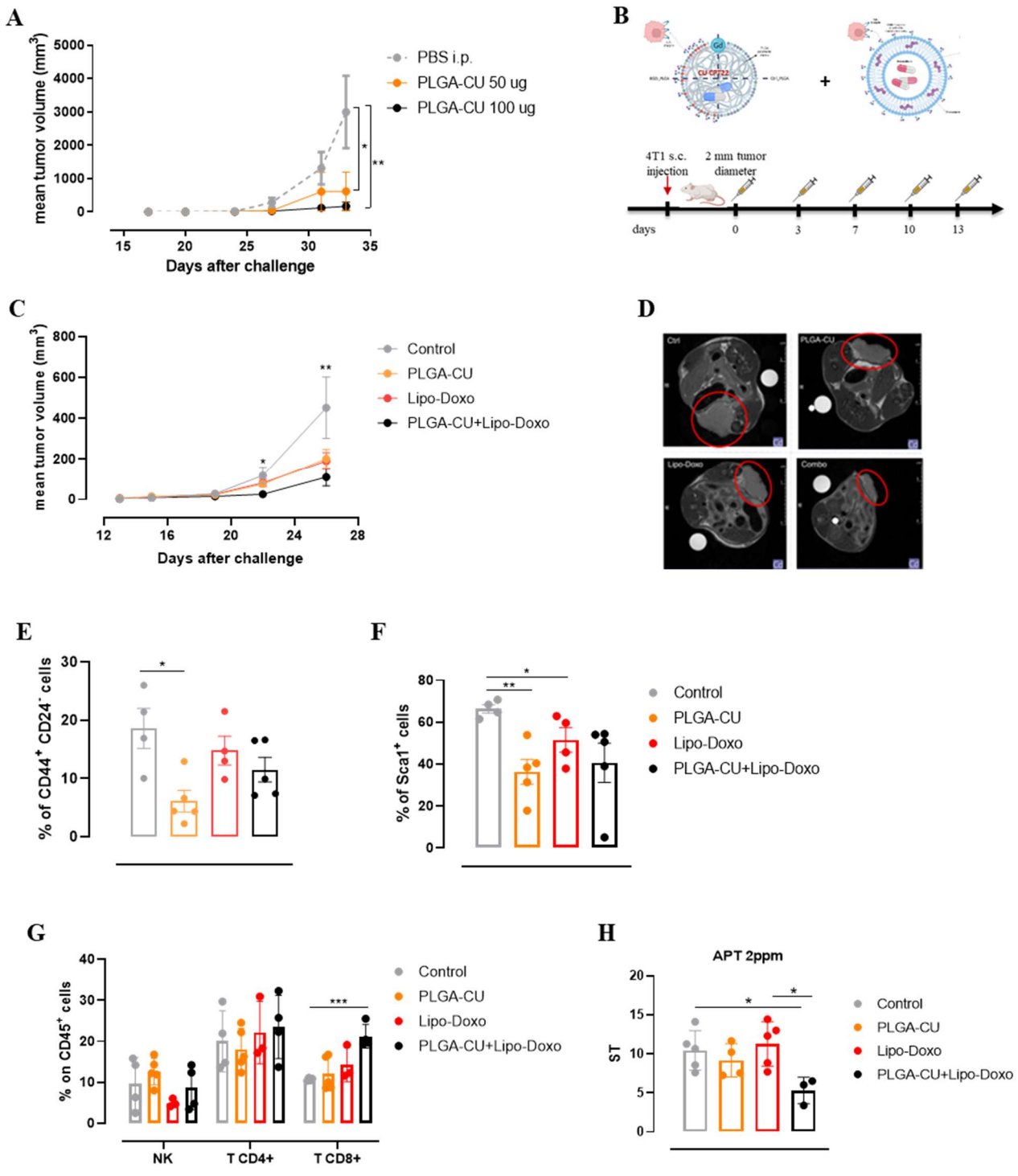


Figure II.6. Nanoparticles hinder breast cancer progression in mice. (A) BALB/c mice were orthotopically challenged with 1 × 10^4 4T1 cells. When the tumors reached 2 mm in mean diameter, mice were treated i.p. with 50 or 100 µg of PLGA-CU, or the control vehicle. The treatment was repeated twice per week. Graph shows mean tumor volume. Two-way ANOVA. (B) Timeline of the in vivo experiment reported in C, combining PLGA-CU and Lipo-Doxo. (C) BALB/c mice were orthotopically challenged with 1 × 10^4 4T1 cells. When the tumors reached 2 mm in mean diameter, the mice were treated i.p. with 3 mg/kg Lipo-Doxo and 100 µg PLGA-CU, or the control vehicle. The treatment was repeated twice per week. Graphs show: (C) mean tumor volume, (D) MRI scan of tumors from one mouse per group. FACS analysis of

tumor cells and tumor immune infiltrate were performed at the endpoint. Graphs show percentages of (E) $CD44^{+}CD24^{-}$ CSCs, (F) $Sca1^{+}$ CSCs, (G) NK and T lymphocytes. (H) CEST MRI analysis of the intratumor 2ppm peak associated with creatin levels. (C, E, F, G, H) Student's t test. *, $p < 0.05$; **, $p < 0.01$; ***, $p < 0.001$.

Recent literature suggests that the role of TLR2 in cancer extends beyond its involvement in cancer cells and the immune system. Notably, other components of the TME also express TLR2, which, upon activation, exerts diverse functions. Among these components, blood vessels are particularly relevant. Angiogenesis is crucial for supporting tumor growth, and cancer cells employ several strategies to drive this process. TLR2 is expressed by endothelial cells, and its signaling can be activated by ligands in the TME, similarly to what occurs in cancer and immune cells. This activation of TLR2 promotes angiogenesis, thereby contributing to tumor progression [134].

In addition to endothelial cell-intrinsic effect of TLR2, it also exhibits a pro-angiogenic role when expressed on cancer cells. As described in Paper I, TLR2 activation enhances the release of pro-tumoral cytokines, including VEGF [108]. Based on this evidence and findings from the literature, we investigated tumor vascularization in response to PLGA-CU and Lipo-Doxo. Using FFPE tumor samples from the *in vivo* experiment previously described, we performed IHC analysis of CD31, a widely used endothelial marker. Our results revealed that tumors in the untreated group had the highest vascularization, followed by the Lipo-Doxo group. In contrast, treatment with PLGA-CU, either alone or in combination with the Lipo-Doxo, significantly reduced vascularization compared to both the untreated and Lipo-Doxo groups (Fig. II.7A). This finding suggests that the TLR2 inhibitor CU-CPT22 impairs angiogenesis, contributing to decreased tumor progression. To further elucidate the mechanism, we conducted additional *in vitro* experiments. First, we analysed VEGF secretion from breast cancer and tumor endothelial cells following 48 hours of treatment with PLGA-CU and Lipo-Doxo, either alone or in combination. For comparison, cells were also treated with the free drugs. In 4T1 cancer cells, both Lipo-Doxo and free doxorubicin significantly increased VEGF secretion compared to the control (Fig. II.7B-C). This observation aligns with the fact that doxorubicin induces the release of DAMPs that activate TLR2, leading to the production of pro-tumoral cytokines such as VEGF. However, this effect was significantly reduced or completely abolished by CU-CPT22 and PLGA-CU, even when combined with doxorubicin and Lipo-Doxo, respectively (Fig. II.7B). Interestingly, similar results were obtained in human breast cancer cells (MDA-MB-231) and in the BEND3 murine endothelioma cell line (Fig. II.7C, D), indicating that the mechanism is TLR2-dependent in both cancer and tumor endothelial cells.

Beyond promoting angiogenesis via VEGF production, TLR2 may also protect tumor endothelial cells from doxorubicin-dependent apoptosis, as previously shown for breast cancer cells (see Chapter I). To test this hypothesis, we analysed apoptosis in BEND3 cells after treatment with free drugs or

nanoparticles. Treatment with 1 µM doxorubicin or Lipo-Doxo only induced of apoptosis in BEND3 cells, suggesting their resistance to chemotherapy. Similarly, treatment with CU-CPT22 at 7 µM did not induce apoptosis. However, PLGA-CU at the same concentration increased apoptosis compared to untreated cells. Notably, the combination of doxorubicin and CU-CPT22, as well as Lipo-Doxo and PLGA-CU, significantly enhanced apoptosis compared to single treatments, demonstrating that TLR2 inhibition sensitizes tumor endothelial cells to chemotherapy (Fig. II.7E).

Taken together, these results highlight the pro-angiogenic role of TLR2 in breast cancer and demonstrate that combining chemotherapy with TLR2 inhibition hinders cancer progression through multiple mechanisms, including the disruption of tumor angiogenesis.

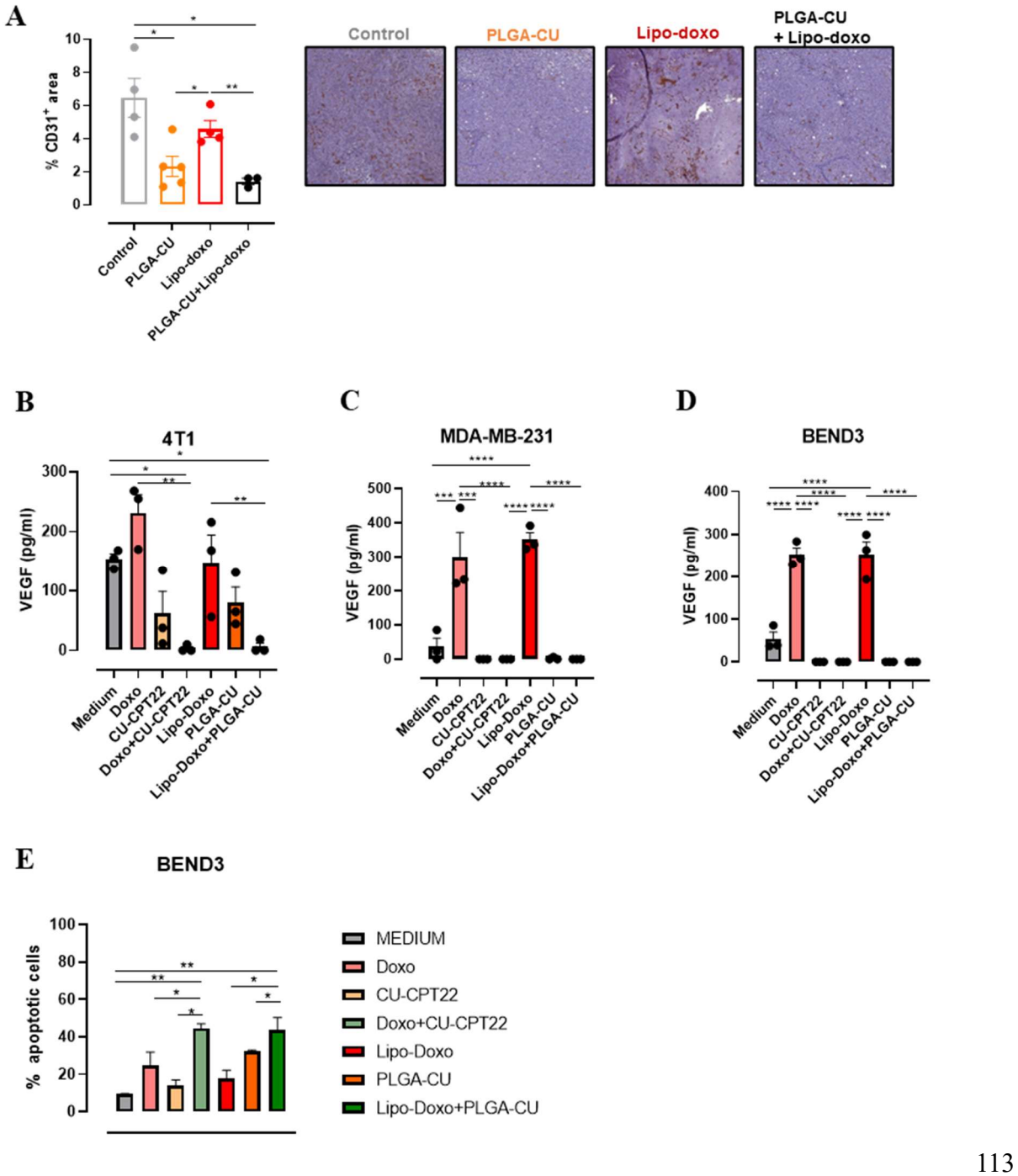


Figure II.7. TLR2 inhibition decreases tumor angiogenesis. BALB/c mice were orthotopically challenged with 1×10^4 4T1 cells. When the tumors reached 2 mm in mean diameter, mice were treated i.p. with 3 mg/kg Lipo-Doxo and 100 µg PLGA-CU, or the control vehicle. The treatment was repeated twice per week. (A) Graph shows percentages of CD31+ cells in tumors of the different groups; images show representative IHC stainings. (B-D) ELISA of VEGF released into the supernatant of 4T1, MDA-MB-231, and BEND3 cells treated for 48 hours with or without doxorubicin (1 µM), CU-CPT22 (7 µM) and their combination, either as free or encapsulated drugs. (E) Annexin-V/propidium iodide analysis of cell apoptosis by FACS. BEND3 cells were treated with or without CU-CPT22 (7 µM), doxorubicin (1 µM) and their combination, either as free or encapsulated drugs. All graphs report the means ± SEM of the percentage of positive cells from three independent experiments. Student's t tests. *, $p < 0.05$; **, $p < 0.01$; ***, $p < 0.001$; ****, $p < 0.0001$.

In summary, the results presented in this chapter demonstrate that RGD decoration significantly enhances the efficacy of PLGA nanoparticles loaded with anti-cancer drugs in preclinical models of breast cancer. Notably, the toxic effects of aggressive therapies, such as chemotherapies, are consistently reduced when using RGD-modified PLGA nanoparticles. These findings lay the groundwork for advancing the therapeutic approach proposed in Chapter I.

Importantly, we have demonstrated for the first time that the TLR2 inhibitor CU-CPT22 can be effectively administered systemically in mice using a relatively simple strategy. This breakthrough is significant for two key reasons. First, PLGA nanoparticles enable the efficient solubilization of CU-CPT22 under physiological conditions, overcoming its poor solubility and making it suitable for therapeutic applications. Second, RGD-conjugated PLGA nanoparticles limit the diffusion of the TLR2 inhibitor into healthy tissues while promoting its accumulation in the tumor. This selective targeting is critical for potential clinical applications, as it allows precise modulation of TLR2 signaling in the tumor microenvironment, reducing its pro-tumoral activity.

Additionally, experiments combining PLGA-CU with LIPO-DOXO confirmed that TLR2 inhibition enhances the efficacy of doxorubicin, providing a highly promising strategy for breast cancer treatment.

Overall, the use of RGD-coated nanoparticles to deliver TLR2 inhibitors and chemotherapy agents improves the efficacy of free drugs, reduces toxic side effects, and enhances tumor-specific targeting. These studies provide valuable tools for the development of more effective breast cancer therapies.

Chapter III

Exploiting TLR2 inhibition to improve pharmacological and immunological breast cancer treatment

In this Chapter, I propose a combinatorial approach to breast cancer treatment based on targeting multiple antigens and employing various therapeutic strategies. The ideas presented in this section stem partly from the data reported in the previous Chapters of this thesis and in part from my prior laboratory experience as a Master's Degree student. Specifically, during my time in the laboratory of Prof. Federica Cavallo for my Master's thesis, under the supervision of Prof. Laura Conti, I contributed to a project focused on developing viral vector-based vaccines for breast cancer immunotherapy. In this project, we tested the efficacy of a combined vaccination targeting the tumor antigens HER2 and xCT in pre-clinical models of breast cancer.

In previous studies, the research group of Prof. Cavallo demonstrated that the multipass transmembrane protein xCT, encoded by the gene *SLC7A11*, is overexpressed in breast CSCs and plays a key role in their self-renewal and resistance to therapy [45]. xCT is the light chain of the antiporter system x_c^-, which mediates the cell uptake of cystine in exchange for glutamate. The activity of xCT significantly impacts both intra-cellular and extra-cellular processes. Glutamate released in the TME by xCT stimulates the proliferation and activation of Tregs through the Metabotropic Glutamate Receptor 1 (MGR1), promoting their immunosuppressive activity. Moreover, by binding to MGR8 expressed on breast cancer cells, glutamate promotes invasion [135,136]. Concurrently, the imported cystine is reduced to cysteine, the rate-limiting precursor in the synthesis of glutathione (GSH). GSH is the primary intracellular antioxidant that protects cells from ferroptosis, differentiation, autophagy, senescence, and toxicity induced by xenobiotics such as chemotherapeutic drugs [44].

xCT is expressed by only a few normal cell types (astrocytes, microglia, some myeloid cells and activated T lymphocytes), but it is highly expressed in various tumor types. In breast tissue, xCT is absent in healthy mammary glands but is expressed in atypical hyperplasia and invasive ductal carcinoma of different histological subtypes, where it is particularly overexpressed in CSCs [44,45]. Notably, the stem cell markers CD44v and Mucin-1 interact with xCT and stabilize it at the cell membrane [137]. Importantly, xCT overexpression is associated with poor prognosis in TNBC patients [138]. Based on these findings, xCT represented a promising target candidate for the development of breast cancer therapies.

The pharmacological inhibition of xCT as a therapeutic strategy has been extensively studied, and several compounds have been investigated. Among them, the most commonly used are erastin, the FDA-approved drugs sulfasalazine (SAS) and sorafenib [139,140]. However, erastin and SAS are

insoluble under physiological conditions, have poor metabolic stability, and exhibit unfavorable pharmacokinetics, precluding their reliable use *in vivo*. Additionally, SAS and sorafenib show low specificity for xCT, and their ability to inhibit NF-kB and various kinases, respectively, leads to significant side effects [44,139,141]. Therefore, in order to specifically target xCT for clinical applications, alternative strategies need to be developed.

Immunotherapy represents an emerging strategy for cancer treatment. Our group has previously developed various vaccine platforms to specifically target xCT, utilizing plasmidic DNA, virus-like particles decorated with xCT extracellular loops, or DNA viral vectors. Using these vaccines, we demonstrated that xCT vaccination impairs breast CSC self-renewal and survival, while effectively inhibits cancer metastatic dissemination in syngeneic transplantable mouse models of breast cancer. However, while xCT vaccination shows good efficacy in preventing metastasis, its effect on primary tumor growth is limited [43,45,46]. This limitation led the group to consider potential combinations with other therapies.

During my thesis internship, I contributed to the study of a combination therapy involving a viral vector-based vaccination using Bovine Herpes Virus-4 (BoHV-4) as a scaffold to deliver the DNA sequence of xCT or HER2. These vaccines were produced and provided by the group of Prof. Gaetano Donofrio at the University of Parma. BoHV-4 is a double stranded DNA γ-herpesvirus isolated from cattle that has been successfully used for vaccine therapy. It can be easily manipulated as a Bacterial Artificial Chromosome (BAC) and leveraged for sustained transgene expression, thereby eliciting a strong host immune response. The safety and efficacy of these vaccines as single therapies were previously demonstrated during several years of collaboration between the groups of Prof. Donofrio and Prof. Cavallo [43,142].

BoHV-4 vectors encoding for the full-length mouse xCT protein (BoHV4-xCT) have proven superior to other anti-xCT vaccines developed by Prof. Cavallo's group in inducing a specific immune response, as it is the only vaccine capable of breaking $CD8^+$ T cell tolerance and inducing xCT-specific cytotoxic T lymphocytes [43,45]. Based on this evidence, during my Master's thesis, we tested BoHV4-HER2 and BoHV-4-xCT vaccines both individually and in combination in BALB-NeuT mice [110]. The results were highly promising, as the combination of xCT and HER2 vaccination elicited a potentiated immune response that significantly hindered tumor progression in these mice, where most treatments are poorly effective [42]. This work demonstrated the high therapeutic potential of xCT vaccination when combined with other therapies.

As discussed in the previous Chapters, targeting TLR2 can enhance the efficacy of chemotherapy and revert tumor-induced immunosuppression. Since both TLR2 and xCT are involved in CSC self-renewal, I hypothesized that their combined targeting could produce a stronger inhibitory effect on

CSCs than single treatments. Therefore, I hypothesized that a combination of TLR2 inhibition, chemotherapy, and xCT immunotargeting could represent an even more powerful strategy for breast cancer treatment.

To assess whether the combined inhibition of xCT and TLR2 is more effective than single treatments in impairing CSC self-renewal, I evaluated the ability of breast cancer cell lines to generate tumorspheres upon inhibition of TLR2 and xCT, either alone or in combination. As detailed in paragraph 2.5 of the Introduction, tumorspheres are enriched in CSCs [74], thus the number of spheres formed after treatment can be considered a read-out of the modulatory effect exerted on CSCs. We treated TUBO and 4T1 tumorspheres with the xCT inhibitor SAS (500 μM) and a neutralizing anti-TLR2 monoclonal antibody (clone T2.5, Invivogen, 10 μg/ml), either alone or in combination. In both cell lines, both SAS and the anti-TLR2 significantly reduced the number of tumorspheres compared to those formed by untreated cells. However, when combined, the effect was significantly stronger than the effects of the single treatments (Fig. III.1A-B). This result suggested that combining TLR2 and xCT targeting can impair CSC self-renewal and produce a more potent anti-tumor effect. Interestingly, both TLR2 and xCT are involved in resistance to chemotherapy. Since we have already demonstrated that TLR2 inhibition restores and even potentiates the efficacy of chemotherapy, we hypothesized that combining TLR2 and xCT targeting could enhance this effect. To test this hypothesis, we analysed the viability of four different breast cancer cell lines after 48 hours of treatment with escalating doses of doxorubicin in combination with fixed doses of CU-CPT22 (5 μM) and SAS (100 μM). In all the cell lines, the combination of doxorubicin with both inhibitors had a stronger effect than the combination with either single drug (Fig. III.1C-F). Moreover, specific doses of the three drugs (Doxo 3 μM, CU-CPT22 5 μM, SAS 100 μM) were tested alone or in combination in the same cell lines. The sensitivities to individual drugs varied among the cell lines. Overall, CU-CPT22 and SAS alone exhibited minimal inhibitory effects on cancer cell viability. TUBO cells were more sensitive to SAS compared to the other cell lines, whereas MDA-MB-231 cells showed the greatest sensitivity to CU-CPT22, where the efficacy was comparable to Doxo. WT-874 cells were the most resistant to doxorubicin, while other cell lines experienced approximately 50% viability inhibition with this chemotherapy. The addition of SAS or CU-CPT22 to Doxo moderately enhanced its efficacy across all cell lines, albeit to varying degrees. Notably, in all cell lines, the triple therapy significantly increased cancer cell viability inhibition compared to individual treatments (Fig. III.1G-J). Apoptosis levels were assessed by flow cytometry to evaluate the impact of single and combined therapies. SAS and CU-CPT22 alone, or in combination, induced low apoptosis in 4T1 and MDA-MB-231 cells, but higher levels in TUBO and WT-874 cells. Doxo induced apoptosis in the range of 40-50% across all cell lines, with slight increases observed when SAS or CU-CPT22 were added.

However, the combination of all three drugs led to a significantly higher induction of apoptosis in all cell lines (Fig. III.1K-N).

Taken together, these data demonstrated that combining TLR2 and xCT inhibition significantly increase breast cancer cell sensitivity to Doxo. These results suggest that the combination of TLR2 inhibition and xCT targeting may also improve the efficacy of chemotherapy *in vivo*.

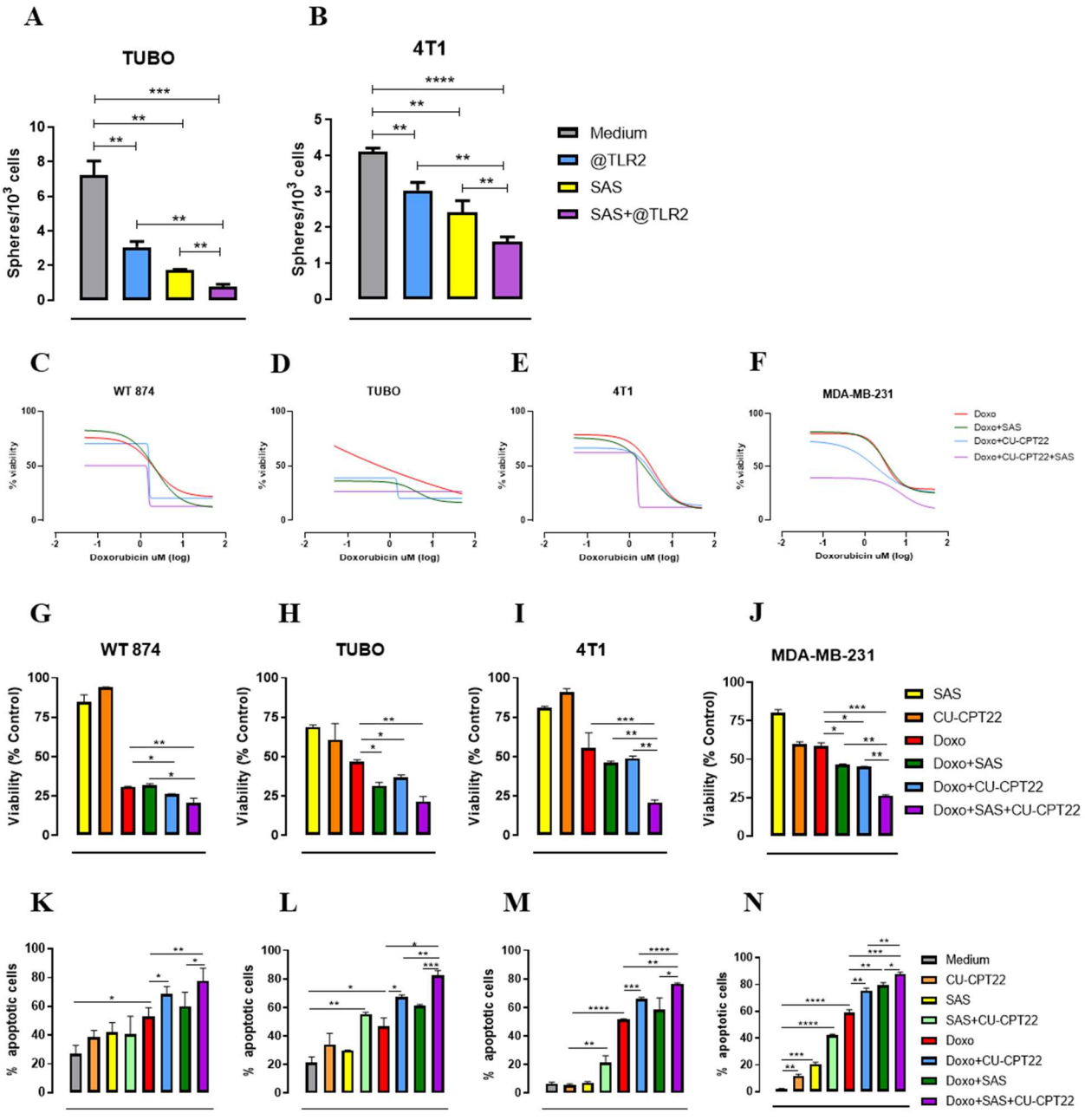


Figure III.1. The combination of chemotherapy with TLR2 and xCT inhibition has anti-tumor efficacy *in vitro*. TUBO and 4T1 cells were cultured under non-adherent conditions, in serum-free medium supplemented with growth factors to generate tumorspheres. After 5 days, completely formed tumorspheres were enzymatically dissociated to obtain a single cell-suspension. $1x10^4$ cells per well were plated in a 96-well plate and treated with or without anti-TLR2 (clone

T2.5, Invivogen, 10 μg/ml), SAS (500 μM) or their combination. After 5 days, the number of newly formed spheres per each well was counted. (A,B) Graphs show the means ± SEM of the number of spheres per thousand of cells from three independent experiments. (C-F) Dose-dependent toxicity of scalar doses of Doxo (80 to 0.312 μM, dilution 1:2) combined with fixed doses of SAS (100 μM), CU-CPT22 (5 μM) or both on WT 874, TUBO, 4T1 and MDA-MB-231 cells. Cell viability evaluated by MTT assay after 48h of treatment. (G-J) Toxicity of SAS (100 μM), CU-CPT22 (5 μM), Doxo (3 μM) and their combinations on WT 874, TUBO, 4T1 and MDA-MB-231 cells. Cell viability evaluated by MTT assay after 48h of treatment. Graphs show the means ± SEM of the percentage of viability from three independent experiments. (E, F) Annexin-V/propidium iodide analysis of cell apoptosis by FACS. WT 874, TUBO, 4T1 and MDA-MB-231 cells were treated with or without SAS (100 μM), CU-CPT22 (5 μM), Doxo (3 μM) and their combination. All graphs report the means ± SEM of the percentage of positive cells from three independent experiments. (A,B,G,H,I,J,K,L,M,N) Student's t test. *, $p < 0.05$; **, $p < 0.01$; ***, $p < 0.001$; ****, $p < 0.0001$.

As mentioned at the beginning of this chapter, vaccination against xCT is high effective in preventing metastasis in mice, but its effect on primary tumors is limited. Therefore, additional therapies more effective at hindering tumor progression are required to enhance the potential of xCT immunotherapy. Considering the promising results obtained from *in vitro* experiments, we decided to evaluate whether the combination of TLR2 inhibition and chemotherapy could improve the efficacy of xCT immunotargeting in pre-clinical models of breast cancer. To this end, we orthotopically injected 4T1 cells in the fourth left mammary gland of BALB/c mice. One week after the injection, we divided the mice into four groups. Two groups were vaccinated with BoHV4-xCT vaccine, and the other two with a control empty vaccine (called A29) [43]. Mice received two total vaccinations with either the xCT or control vaccine, administered one and two weeks after cancer cell challenge. Two weeks after cell challenge, when tumors became palpable, we started treating one group vaccinated with the A29 and one group vaccinated with BoHV4-xCT with Doxo i.p. (3 mg/kg) and CU-CPT22 i.t. (100 μg) twice a week for two weeks. The other two groups received only the control vehicle (PBS) i.p. and i.t.. Tumor growth was measured using an electronic caliper until the mice were sacrificed, one month after cancer cell challenge. As demonstrated in Paper I, the combination of Doxo + CU-CPT22 significantly reduced tumor growth compared to control mice. As expected, the BoHV4-xCT vaccine alone did not induce a significant reduction in tumor growth, although a trend was observed. However, the combination of xCT immunotherapy with TLR2 inhibition and Doxo significantly hampered tumor progression more than vaccination alone and compared to the untreated mice (Fig. III.2A). Additionally, we performed a survival analysis, considering the time of death as when tumors reached mean diameter of 10 mm. This analysis showed that the combination of Doxo and CU-CPT22 significantly increased overall survival compared to control mice. These results were further enhanced when this pharmacological therapy was combined with xCT vaccination (Fig. III.2B). As we previously demonstrated, Doxo and CU-CPT22, as well as and BoHV4-xCT, decreased the

number of spontaneous lung metastases compared to the control. The inhibition of metastasis formation was even greater in mice treated with the combined triple therapy (Fig. III.2C). FACS analysis of tumors after sacrifice revealed several relevant effects of the therapies. In particular, both Doxo + CU-CPT22 and BoHV-4-xCT vaccination significantly decreased the frequency of CSCs, identified by the $Sca1^+$ and $CD44^+CD24^-$ populations. This reduction was further significantly enhanced by the triple therapy, underscoring the role of TLR2 and xCT in this population of cancer cells (Fig. III.2D-E).

To investigate the mechanisms underlying the improved efficacy of the triple therapy, we analysed the immune infiltrate in tumors. Interestingly, the addition of Doxo and TLR2 inhibitors potentiated the immune response induced by the vaccination, increasing infiltration and activation of both $CD4^+$ and CD8 T^+ cells in the tumor (Fig. III.2F-I). This finding suggests that TLR2 inhibition enhances the immune response induced by xCT-targeted immunotherapy.

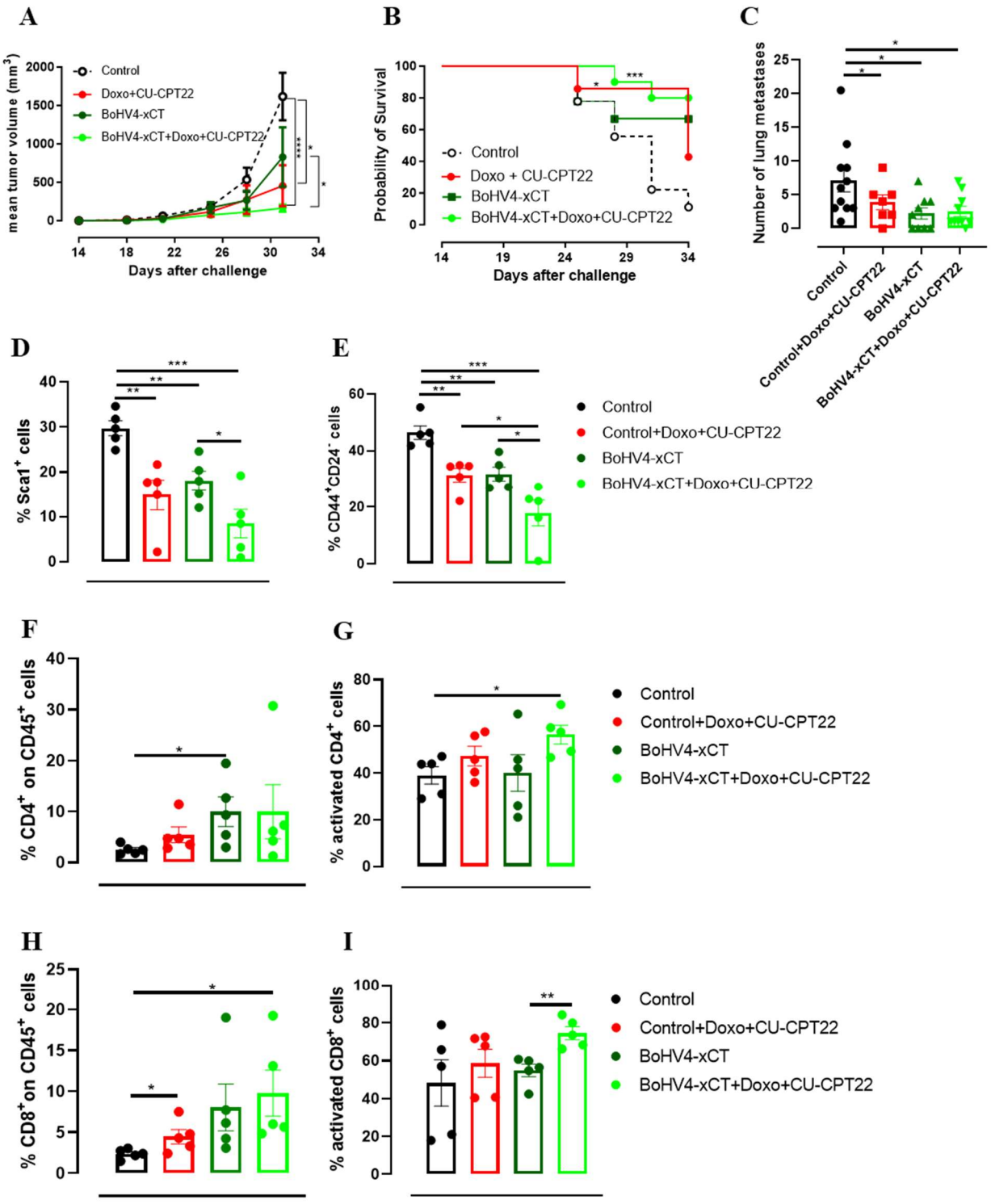


Figure III.2. The combination of TLR2 inhibition and chemotherapy improves the efficacy of anti-xCT immunotherapy. BALB/c mice were orthotopically challenged with 1 × 10^4 4T1 cells and then randomly distributed into four groups. One and two weeks after cancer cell injection, two groups of mice received xCT vaccine (BoHV4-xCT) and the other two the control vaccine (A29). When the tumors reached 2 mm in mean diameter, mice were treated with Doxo and CU-CPT22 according to the following experimental setting: i) A29, ii) A29 + Doxo + CU-CPT22, iii) BoHV4-xCT, iiii) BoHV4-xCT + Doxo + CU-CPT22. (Doxo i.p. 3 mg/kg and CU-CPT22 i.t. 100 µg). Doxo and CU-CPT22 treatments were repeated twice per week until endpoint. Graphs show: (A) mean tumor volume, (B) survivals, (C) number of lung

metastases. FACS analysis of tumor cells and immune infiltrate. Graphs show percentages of (D) $Sca1^+$ CSCs, (E) $CD44^+CD24^-$ CSCs, (F) $CD4^+$ T cells, (G) activated $CD4^+$ T cells, (H) $CD8^+$ T cells, (I) activated $CD8^+$ T cells (A) Two-way ANOVA, (C-I) Student's T tests. *, $p < 0.05$; **, $p < 0.01$; ***, $p < 0.001$; ****, $p < 0.0001$.

We have previously demonstrated that the humoral response plays a pivotal role in the anti-tumor effects induced by xCT vaccination [43,45]. We therefore assessed the production of xCT-specific antibodies in the different groups of mice. As shown in Fig. III.3A, BoHV-4-xCT induced the production of high levels of xCT-specific antibodies, which were not altered by the combination with Doxo and CU-CPT22. When incubated with syngeneic splenocytes, these antibodies were able to induce antibody-dependent cellular cytotoxicity (ADCC) of 4T1 cells. Notably, ADCC was even more pronounced in the case of triple therapy, suggesting that this combination increased the efficacy of the antibody-mediated immune response (Fig. III.3B). In addition to their indirect activity, these antibodies also exerted a direct inhibitory effect on breast cancer cells. To investigate this, we used the sera from vaccinated mice as a substitute for SAS to replicate the tumorsphere generation experiment described earlier in this chapter. TUBO and 4T1 cells were treated with the anti-TLR2 monoclonal antibody alone and in combination with the sera of mice vaccinated with BoHV4-xCT or the control A29 vaccine. The sera from vaccinated mice, combined with anti-TLR2, inhibited tumorsphere formation significantly more than the control sera or single treatments, perfectly recapitulating the results obtained with SAS (Fig. III.3C-D). This experiment further demonstrated that combining TLR2 and xCT targeting affects CSC self-renewal and produces a stronger anti-tumor effect.

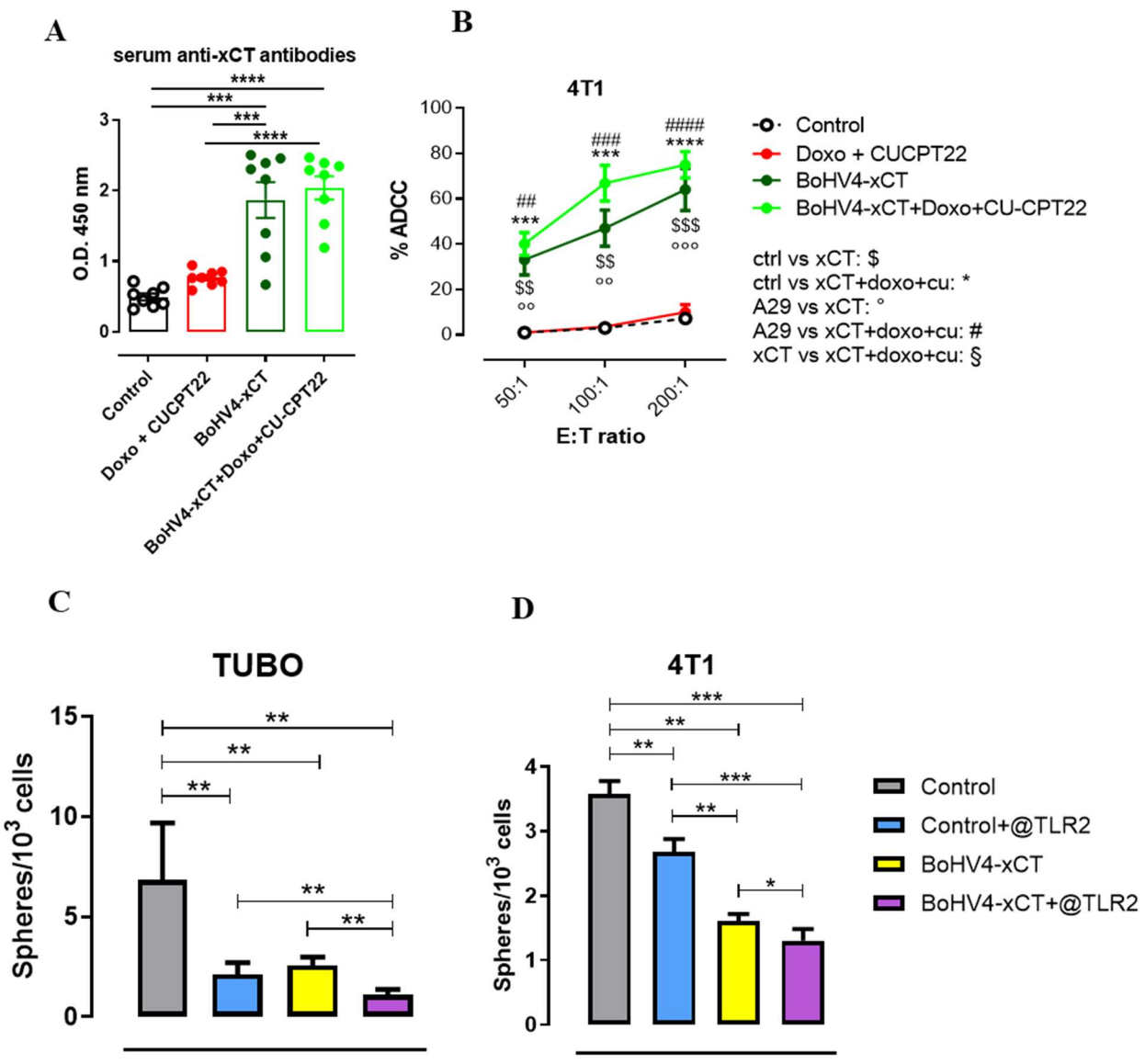


Figure III.3. Vaccination produces xCT-specific antibodies with anti-tumor activity. At the endpoint of the *in vivo* experiment described in Fig. III.2, sera were collected from mice all the mice and used for further experiments. (A) ELISA of pooled sera from the four groups on xCT full-length protein. Graph shows means of three pools analysed in three independent experiments. (B) Means ± SEM of the percentage of ADCC of $CFSE^+$ 4T1 cells incubated with pooled sera (1:50) and SPC from naive mice at 200, 100, and 50:1 effector:target (E:T) ratios. TUBO and 4T1 cells were cultured under non-adherent conditions, in serum-free medium supplemented with growth factors to generate tumorspheres. After 5 days, completely formed tumorspheres were enzymatically dissociated to obtain a single cell-suspension. $1x10^4$ per well were plated in a 96-well plate and treated with or without anti-TLR2 (clone T2.5, Invivogen, 10 µg/ml), pooled sera from control or xCT-vaccinated mice, or their combinations. After 5 days, the number of newly formed spheres per each well was counted. (A,B) Graphs show the means ± SEM of the number of spheres per thousand of cells from three independent experiments. (A-D) Student's t tests. *, $p < 0.05$; **, $p < 0.01$; ***, $p < 0.001$; ****, $p < 0.0001$.

In summary, the results reported in this chapter show that TLR2 targeting can be combined with different types of therapies to enhance their efficacy. In particular, the combination with xCT targeting appears to be a promising strategy for breast cancer treatment. Both antigens play a role in the self-renewal of CSCs, which are responsible for therapy resistance, immune evasion, and metastasis. *In vitro*, the combination of chemotherapy, TLR2 and xCT inhibitors shows strong anti-tumor efficacy in $HER2^+$ and triple negative breast cancer cells. However, the most significant evidence emerged from the *in vivo* setting. In this context, TLR2 targeting revealed its potential not only in synergy with chemotherapy but also with immunotherapy. Remarkably, TLR2 targeting contributed to the potentiation of the anti-tumor immune response and the reduction of CSC frequency elicited by xCT vaccination. Taken together, these results suggest that this combinatorial approach could be applied in various breast cancer therapies, especially as adjuvant and neoadjuvant treatments.

Currently, we are focusing our efforts on characterising any potential crosstalk between TLR2 and xCT to gain a deeper understanding of their roles in breast cancer and to provide valuable insights for their therapeutic targeting. Preliminary data suggest that the inflammatory pathways activated downstream of TLR2 might regulate xCT expression. However, this mechanism still requires further investigation. Moreover, TLR2 and xCT are expressed in a variety of cancer types, where they exert pro-tumoral functions. Accordingly, the possibility of targeting TLR2 and xCT could be explored not only in breast cancer but also for applications in other tumor therapies. All these aspects require further research, and this is likely something that I will pursue after completing my PhD.

Conclusions

In recent years, significant progress has been achieved in the diagnosis and treatment of breast cancer. Particularly in Western countries, advancements in routine screening techniques and their widespread adoption have improved early detection, which remains crucial for preventing adverse prognosis in breast cancer patients. Additionally, substantial efforts to deepen our understanding of the molecular characteristics of breast cancer subtypes have driven the development of more effective therapeutic interventions. Together, these advancements have significantly improved survival rates among breast cancer patients.

However, breast cancer remains the leading cause of cancer-related death in women underscoring that it is still far from being a fully manageable or curable disease. The latest report by the American Cancer Society estimates that, in 2025, breast cancer will continue to be the first cause of cancer in women (32% of total cancers). The projections predict 319,750 new cases of breast cancer and 42,680 deaths only in the US [143]. This highlights the pressing need to continue advancing scientific research to improve patient outcomes.

Building on this premise, my PhD research sought to address a critical question: how can breast cancer treatments be further improved?

To tackle this question, we focused on the key issues contributing to therapy failure and poor outcomes. As outlined in the Introduction, numerous mechanisms underlie therapy resistance. Notably, breast CSCs have been widely implicated in resistance to conventional therapies. CSCs exhibit phenotypic plasticity, including epithelial-to-mesenchymal transitions, metabolic reprogramming, and dynamic changes in gene expression. These characteristics enable CSCs to evade treatment and drive metastasis.

For several years, our research group has concentrated on identifying potential therapeutic targets to eliminate CSCs, which are among the most resistant cancer cell populations within tumors. This led to several publications reporting studies about the promising results obtained by targeting xCT and other antigens in breast cancer or other tumors [42,43,45,46,144,145]. This thesis focuses on investigating one such target, TLR2, and its role in breast cancer.

TLR2 is known to play an important role in activating immune responses against pathogens and cancer. However, emerging evidence reveals that its role in cancer is ambivalent and context dependent. While some studies suggest that TLR2 ligands can serve as effective adjuvants in cancer therapies, particularly vaccination, others indicate that TLR2 can mediate pro-tumoral mechanisms and propose its inhibition as a potential therapeutic approach.

Our group previously demonstrated that TLR2 is expressed by breast cancer cells and is upregulated by CSCs. TLR2 promotes the expression of several stem cell markers and activates pro-tumorigenic pathways such as NF-κB, whose downstream signaling contributes to breast CSC self-renewal [74].

Importantly, our analysis of public datasets revealed that high TLR2 expression correlates with poor prognosis and chemoresistance in breast cancer patients. Based on this discovery, we hypothesized that TLR2 could serve as a novel therapeutic target.

This thesis establishes that TLR2 and its ligands play a significant role in breast cancer progression. Specifically, in Chapter I, we identified a novel non-immunological role for TLR2 in breast cancer cells, where it is activated by DAMPs, such as HMGB1, present in the TME. TLR2 activation triggers NF-κB signaling, leading to the production of pro-tumoral cytokines, including IL-6, TGF-β, and VEGF. These cytokines establish cancer cell-intrinsic pro-tumoral loops, induce resistance to apoptosis, and drive tumor neoangiogenesis. Furthermore, we demonstrated that TLR2 activation is necessary for the recruitment and activation of immunosuppressive cells, such as Tregs. Thus, TLR2 mediates both cancer cell-intrinsic and extrinsic mechanisms that promote tumor progression.

We also uncovered a key role for TLR2 in chemoresistance. Chemotherapeutic agents such as doxorubicin induce the release of DAMPs by cancer cells, leading to hyperactivation of TLR2 signaling, which exacerbates tumor progression and therapy resistance. Notably, we showed that inhibiting TLR2 using the small molecule CU-CPT22 exerts anti-tumor effects. TLR2 inhibition not only reverses resistance to doxorubicin but also enhances its therapeutic efficacy. Remarkably, the combination of CU-CPT22 and doxorubicin exhibits synergistic anti-tumor effects *in vivo*, significantly reducing tumor progression, decreasing CSC frequency, and enhancing anti-tumor immune responses in murine models of mammary cancer.

Building on these promising results, in Chapter II, we sought to further refine this therapeutic approach to enhance its translational potential. In collaboration with Prof. Giuseppe Ferrauto's group, we developed targeted nanoparticles for the delivery of CU-CPT22 and doxorubicin. Based on the chemical properties of these drugs, PLGA nanoparticles were employed to encapsulate CU-CPT22, while liposomes were used for doxorubicin delivery. These nanoparticles were coated with the RGD peptide, a targeting moiety that binds integrin $\alpha_v\beta_3$, which is overexpressed in many tumors, including breast cancer. These targeted nanoparticles enhance drug accumulation in tumors while minimizing off-target distribution, significantly reducing chemotherapy-associated side effects such as cardiotoxicity. Furthermore, they localize TLR2 inhibition within the TME, avoiding systemic inhibition that could lead to undesirable effects.

The use of nanomedicine in cancer treatment has expanded rapidly in recent years, and we believe that this approach has strong clinical potential. Additionally, while immunotherapies have become a cornerstone of cancer treatment, they remain vulnerable to resistance. In Chapter III of this Thesis, we proposed combining TLR2 inhibition and chemotherapy to enhance the efficacy of a vaccination-based immunotherapy targeting xCT, a protein involved in oxidative stress prevention, CSC self-

renewal, drug resistance, and metastases. Our *in vitro* and *in vivo* experiments demonstrated that this combined therapy has high therapeutic efficacy. This strategy aligns with emerging trends in cancer treatment, which emphasize multi-targeted approaches and the integration of diverse pharmacological strategies to improve therapeutic outcomes.

In conclusion, while the findings presented in this thesis are at the pre-clinical stage and require further development to meet the standards of clinical translation, their potential is substantial. The multi-disciplinary and multi-targeted approach underlying this therapeutic strategy offers a promising avenue for advancing breast cancer treatment and holds the potential to deliver meaningful improvements in patient outcomes.

In the near future, this project will advance in several key areas. One of the most promising directions involves extending TLR2 and xCT targeting to a broader range of tumor types. These antigens are already known to be expressed in various tumors, where they frequently play pro-tumoral roles, as observed in breast cancer [58,146]. Recently, we discovered that both xCT and TLR2 are expressed in multiple myeloma. Preliminary experiments involving the combined targeting of these antigens in multiple myeloma models demonstrated remarkable therapeutic efficacy. These findings open new avenues for investigating TLR2 and xCT targeting across different types of tumors.

This research holds great potential for clinical translation. Of note, the safety and efficacy of TLR2 targeting by small molecule inhibitors or neutralizing monoclonal antibodies has been demonstrated in several clinical trials performed in patients suffering from Myelodysplastic Syndrome and Acute Myeloid Leukemia [147]. Similarly, xCT inhibitors such as sulfasalazine, which is approved by FDA for the treatment of ulcerative colitis and rheumatoid arthritis, are under clinical evaluation for the treatment of several cancer types [148–150]. Thus, the combination of TLR2 and xCT targeting could significantly improve the lives of many cancer patients.

The prospect of achieving such impactful outcomes is one of the strongest motivations driving me to continue the work initiated during my PhD and reported in this thesis.

Materials and Methods

This section contains materials and methods employed for the experiments reported in the unpublished parts of this Thesis (second part of Chapter II, and Chapter III). For information regarding the published parts, please refer to materials and methods of the attached papers (Chapter I and Chapter II).

Cell cultures

MDA-MB-231 and 4T1 cell lines were purchased from American Type Culture Collection (ATCC) in 2018. BEND3 cells were provided by Dr. Federica Pericle (Immunogenesis Inc.). Aliquots were frozen and used up to 10 passages. Cells were cultured in DMEM or RPMI 1640 (Sigma-Aldrich) 10% FBS (Sigma-Aldrich), respectively. TUBO cell line was derived from a BALB-neuT primary tumor and cultured in DMEM 20% FBS [151]. WT-874 cell line was derived, as described in the study of Liu and Chen [152], from mammary tumors isolated from C57Bl6-neuT mice either TLR2 wild-type (neuT-TLR2^{WT}) and cultured in DMEM-F12 (ThermoFisher Scientific) with 20% FBS. All cells were tested negative for mycoplasma [153]. Tumorspheres were generated as in Conti et al. 2013 [74] and cultured in tumorsphere medium, i.e. serum-free DMEM-F12 medium (ThermoFisher Scientific) supplemented with 20 ng/ml basic fibroblast growth factor (bFGF), 20 ng/ml epidermal growth factor (EGF), 5 µg/ml insulin, and 0.4% bovine serum albumin (all from Sigma-Aldrich).

Nanoparticles

(Chapter II) PLGA NPs were prepared using the water-in-oil emulsion method, as described in Di Gregorio et al. 2022 [109], and CU-CPT22 encapsulation occurred during the self-assembly of the polymeric matrix. Briefly, the organic phase was prepared by dissolving Poly(D,L-lactide-co-glycolide) (PLGA) (Sigma-Aldrich Co.), pegylated phospholipids (DPPE-PEG(2000)methoxy) and all the other components in a chloroform/methanol mixture. For this purpose, 25 mg PLGA, 1.0 mg 1,2-distearoyl-sn-glycero-3-phosphoethanolamine-N-[methoxy(polyethylene glycol)-2000] (ammonium salt) (18:0 PEG2000 PE) and 1.2 mg 1,2-distearoyl-sn-glycero-3-phosphoethanolamine-N-[maleimide(polyethyleneglycol)-2000] (ammonium salt) (DSPE-PEG2000-Maleimide) (Avanti Polar Lipids Inc.) were dissolved in chloroform (purity ≥ 99.9%). 2 mg of CU-CPT22 were also dissolved in chloroform for drug-loaded PLGA-NPs. The water phase was a 3% poly vinyl alcohol (PVA) aqueous solution. The organic phase was gently dropped into the aqueous phase containing 3% Poly (vinyl alcohol) (PVA), in ice. Sonication was performed with an immersion-tip instrument in 2 cycles of 1.5 min each, 70% power amplitude. Evaporation of the organic solvent from the

oil/water emulsion was carried out for 2 h under vacuum-rotation, RT. NPs were purified with centrifugation through filters and dialysis against fresh buffer. Centrifugation at 4 °C, 5500 rpm in Vivaspin® tubes was used to wash the remaining PVA and concentrate the PLGA to the wanted volume. Cyclic RGD tripeptide (Bachem) was added to the formulation and conjugated to the surface of NPs through the procedures previously reported [109,154,155].

Liposomes were obtained through lipidic thin-film hydration and solvent evaporation. Briefly, each formulation contained 72% 2-Oleoyl-1-palmitoyl-sn-glycero-3-phosphocholine (POPC) (Avanti Polar Co.), 25% cholesterol (Sigma-Aldrich), 1.5% 18:0 PEG2000 PE, and 1.5% DSPE-PEG2000-Maleimide, for a total lipid concentration of 30 mg/mL. Cholesterol and phospholipids were dissolved in chloroform and transferred to a round-bottom flask for solvent evaporation under vacuum-rotation (10 min 37°C, 2h RT) in order to create a monolayered lipidic film. This is subsequently hydrated with ammonium sulphate 0.12 M, pH 5.5 at 55°C to create spontaneous multilamellar vesicles, then extruded through 400 nm and 200 nm-cutoff membrane pores to form a monodispersed suspension with liposome-NPs under 200 nm. Doxorubicin (hydrochloric salt) incorporation in the internal liposome aqueous phase was done by incubating 0.04 mol of drug per 1 mol of phospholipids, for 1 h at 55°C as described [156,157]. Unbound drug was washed out through an o.n. dialysis cycle in acetate buffer 0.15 M, pH 6.5-6.8. RGD surface ligation was carried out as previously described for PLGA NPs.

Physicochemical properties (size, surface ζ potential) were determined by Dynamic Light Scattering (DLS). The amount of encapsulated drug was measured through UV/vis for Doxorubicin and NMR spectroscopy for CU-CPT22. ^{1}H-NMR relaxometry measurements indicated NPs stability in a physiological environment over time.

For fluorescent liposomes and PLGA-NPs, 0.17 mg of 1,2-distearoyl-sn-glycero-3-phosphoethanolamine-N-[amino(polyethylene glycol)-2000]-N-(Cyanine 5) (DSPE PEG(2000)-N-Cy5) was added to the organic phase during the synthesis. Gd-DOTAMA or Prohance®, two gadolinium-based probes, were embedded in the PLGAs matrix or liposomes core, respectively, to facilitate their physicochemical characterization and to follow up their in vivo biodistribution via MRI.

In vivo experiments

Mice were bred and maintained under saprophytic and pathogen-free conditions at the animal facility of the Molecular Biotechnology Center and treated in accordance with EU and institutional

guidelines, with the approval of the Animal Care and Use Committee of the University of Turin and the Italian Ministry of Health (authorizations N° 10/2023-PR; CC652.191). To test the *in vivo* efficacy of PLGA-CU *(Chapter II)*, 1×10^4 4T1 cells were injected orthotopically into female BALB/c mice (N = 15). When the tumors reached 2 mm mean diameter, mice were blindly randomized into three groups, which received intraperitoneal (i.p.) injections of control vehicle (PBS), 50 µg PLGA-CU or 100 µg PLGA-CU twice per week. Tumor growth was monitored twice per week using an electronic caliper. When tumors in control mice reached 10 mm mean diameter, mice were culled. For the therapeutic experiments combining Lipo-Doxo and PLGA-CU *(Chapter II)*, BALB/c mice were orthotopically challenged with 1×10^4 4T1 cells. When the tumors reached 2 mm in mean diameter, mice were treated i.p. with 3 mg/kg Lipo-Doxo, 100 µg PLGA-CU, their combination or the control vehicle. The treatment was repeated twice per week. Tumor growth was monitored twice per week using a caliper. MRI and MRI CEST analysis of the tumors were performed before endpoint. When tumors in control mice reached 10 mm mean diameter, mice were culled. Tumors were removed and a part was processed for FACS analysis, while another part fixed in 4% formaldehyde, paraffin embedded, sectioned into four sections spaced by 50 µm and prepared for IHC. To test the combination of anti-xCT vaccination, chemotherapy and TLR2 targeting *(Chapter III)*, BALB/c mice were orthotopically challenged with 1×10^4 4T1 cells. The BoHV-4-xCT vaccine and the control vector BoHV-4-A29 (called A29) were generated and $TCID_{50}$ quantified by Prof. G. Donofrio, University of Parma, as previously described [43]. When the tumors reached 2 mm in mean diameter, mice were treated with control vaccine A29, A29 + doxorubicin + CU-CPT22, BoHV4-xCT, BoHV4-xCT + doxorubicin + CU-CPT22. (doxorubicin was given i.p. 3 mg/kg, and CU-CPT22 i.t. 100 µg). Control and xCT vaccination were performed once a week per two weeks. Mice were vaccinated by i.p. injections of 100 µl of DMEM containing 10^6 $TCID_{50}$ of A29 or BoHV4-xCT [42]. Doxorubicin and CU-CPT22 treatments were repeated twice per week until endpoint. Tumor growth was monitored twice per week using a caliper. When control tumors reached 10 mm mean diameter, mice were culled. Tumors were removed and processed for FACS. Lungs were fixed in 4% formaldehyde, paraffin embedded, sectioned into four sections spaced by 50 µm and stained with hematoxylin and eosin. Pictures were acquired using a Nikon SMZ1000 stereomicroscope (Mager Scientific) and metastases counted with ImageJ.28. Immune sera were collected from post-vaccinations blood sampling as reported in Conti et al. 2020 [42] and stored at -20° C for further experiments.

Magnetic resonance imaging (MRI)

At the end of the *in vivo* experiment testing the combination of Lipo-Doxo and PLGA-CU *(Chapter II)*, mice were subjected to MR imaging at 7.1T on a Bruker Avance300 spectrometer equipped with the Micro2.5 microimaging probe. T_{2W} morphological images were acquired at room temperature using a standard RARE (Rapid Acquisition with Refocused Echoes) sequence with the following parameters: TR=4000 ms, TE=40.57 ms, RARE factor=24, flip angle=180°, number of averages=4, FOV=30 mm x 30 mm, matrix size 256x256, and spatial resolution=0.117x0.117 mm/pixel, slice thickness 1 mm.

For Chemical Exchange Saturation Transfer (CEST) Amide Proton Transfer (APT)-MRI analysis, a typical RARE sequence was used (TE=3 ms, TR=5 s) with isotropic 64 x 64 acquisition matrix, FOV= 1 cm, slice thickness =1 mm (NEX=2, RARE Factor= 16). The whole sequence was preceded by a saturation scheme consisting of a continuous rectangular wave pulse 1.5s long with a RF intensity typically corresponding to B1=3 μT (other B1 powers were tested). A frequency offset range of ±20 ppm was investigated.

The Z-spectra were interpolated by smoothing splines to identify the zero-offset on a pixel-by-pixel basis of the bulk water and then, to assess the correct ST % value over the entire range of frequency offsets investigated. Custom-made software, compiled in the Matlab platform (Mathworks Inc., Natick, MA), was used. The extent of CEST effect is calculated as follows:

$$ST\% = (1 - (Ms/M0)) \times 100$$

where Ms is the intensity of the bulk water NMR signal after irradiation on resonance ($\Delta\omega$= 3.4 ppm) of the mobile proton pool and M0 is the intensity of the bulk water NMR signal after irradiation at -$\Delta\omega$ (i.e. -3.4 ppm).

The analysis was carried out at two different chemical shifts, i.e. 2 ppm and 3.47 ppm. The first resonance is related to the CEST@2ppm signal, typical of creatine and other amine-containing metabolites. The second resonance is related to amide protons of polypeptides (i.e. Amide Proton Transfer, APT, MRI).

Optical imaging (OI)

Optical imaging was performed with the IVIS Spectrum small animal imaging system (PerkinElmer, Waltham, MA, USA) *(Chapter II)*. Images were acquired and analysed with Living Image Software 4.7 (PerkinElmer). Data were acquired using a customized filter set, exciting at both 480 and 620 nm and acquiring at 670 nm. Excitation at 480 was used to evaluate the background, and at 620 nm to

assess the probe-specific signal. Identical illumination settings (f-stop/field of views/binning/acquisition time, 2/12.5/medium/0.5 s) were used to acquire all the images. Mice bearing 4T1 tumors in both 4th mammary glands were injected i.p. with PLGA-CU or LIPO-DOXO containing 1 nmol Cy5, anesthetized with 2.5% isoflurane (Abbott Laboratories), and analysed by optical imaging after 5-15-30-60 minutes, 4 and 24 hours (n = 6 for each time point). Regions of interest (ROI) were designed on tumors and quadriceps muscles, and fluorescence emission was normalized to average radiant efficiency (p/s/cm 2 /sr)/(µW/cm 2).

3-(4,5-Dimethylthiazol-2-yl)-2,5-Diphenyltetrazolium Bromide (MTT) Assay

(Chapter II) 4T1, WT 874 (5×10^3) or TUBO (7×10^3) cells were seeded in 96-well plates and cultured overnight. Scalar doses of CU-CPT22, doxorubicin, PLGA-CU, LIPO-DOXO or of the empty nanoparticles were then added. *(Chapter III)* 4T1, WT 874, MDA-MB-231 (5×10^3) or TUBO (7×10^3) cells were seeded in 96-well plates and cultured overnight. Scalar doses of doxorubicin with or without fixed doses of SAS (100 µM) and CU-CPT22 (5 µM) were then added. After 48 hours, cell viability was assessed using the MTT assay. MTT solution (0.5 mg/ml; Sigma-Aldrich, Burlington, USA) was added to each well and incubated for 4 hours at 37°C. Following incubation, supernatants were removed, and 150 µl of dimethyl sulfoxide (DMSO) was added to dissolve the formazan crystals. Absorbance was measured at 570 nm with background subtraction at 650 nm using a 680XR microplate reader (BioRad Laboratories Inc., Hercules, USA).

FACS analysis

To analyse NF-κB activation *(Chapter II)*, WT 874 or 4T1 (1×10^5) cells were seeded in 6-well plates and cultured overnight. Then, WT 874 cells were treated with 20 µg/ml peptidoglycan from *S. aureus* (PGN-SA; InvivoGen, Cat#tlrl-pgns2), 7 µM CU-CPT22 or PLGA-CU, and their combinations. 4T1 cells were treated with 1 µM doxorubicin or Lipo-Doxo, 7 µM CU-CPT22 or PLGA-CU, and their combinations. After 48 hours, cells were fixed with 4% formaldehyde for 15 minutes at 4° C, washed in PBS 0,05% bovine serum albumin (BSA), and fixed with 90% methanol (Sigma-Aldrich) for 10 minutes at 4° C. After washing, cells were permeabilized with PBS 0,5% saponin and then stained for 30 minutes at 4°C with Alexa Fluor 647-conjugated anti-pNF-κB p65-S536 (Cell Signaling Technology, Cat#4887). To analyse apoptosis, *(Chapter II)* WT 874, 4T1 or BEND3 cells were seeded and treated as for the NF-κB staining. *(Chapter III)* WT 874, 4T1, MDA-MB-231 (1×10^5) and TUBO ($1{,}5 \times 10^5$) cells were seeded in 6-well plates and cultured overnight. Then, cells were treated with 1

μM doxorubicin, 100 μM SAS, 5 μM CU-CPT22 or their combinations. After 48 hours, cells were stained with AnnexinV-Apoptosis Kit-APC (eBioscience, Cat#88-8007-72).

(Chapter II and III) Single-cell suspensions were obtained from fresh primary tumors as in Conti et al. 2020 [42]. 1×10^6 cells were treated with Fc-receptor blocker (BD Bioscience, Cat#01245B) and stained for 30 minutes at 4° C with anti-mouse CD45-VioGreen (Cat#130-110-803), CD3-FITC (Cat#130-119-135), CD4-APC/Vio770 (Cat#130-119-134), CD8-VioBlue (Cat#130-123-865), CD49b-PE (Cat#130-123-702) (all from Miltenyi), CD69-PE/Cy7 (Cat#104512), CD44-PE (Cat#103007), CD24-PE/Cy7 (Cat#101822), Sca1-AlexaFluor647 (Cat#122518), all from Biolegend. At least 50,000 $CD45^+$ events per sample were acquired on a BD-FACSVerse and analysed with FlowJO10.5.3. Cells were gated according to their physical parameters, and dead cells were excluded following propidium iodide (Sigma-Aldrich, Cat#P4864) staining. The $CD45^+$ leucocytes and $CD45^-$ cells were gated, and cell populations analysed as follows: NK: $CD3^-$ $CD49b^+$; activated $CD4^+$ T cells: $CD3^+$ $CD49b^-$ $CD4^+$ $CD69^+$; activated $CD8^+$ T cells: $CD3^+$ $CD49b^-$ $CD8^+$ $CD69^+$; CSCs: $CD45^-$ $Sca1^+$, $CD45^-$ $CD44^+$ $CD24^-$.

Immunohistochemistry (IHC) analysis

The tumors of mice were formalin-fixed and paraffin-embedded, and 4 μm-thick slices were obtained. For immunohistochemistry staining, peroxidase activity was inhibited by a 3% hydrogen peroxide aqueous solution for 10 min. Samples were pre-treated by microwave antigen retrieval using EDTA buffer, citrate pH 6 (Dako, Milan, Italy) or protease (Ventana, Segrate, Italy), and incubated with anti-CD31 antibody (Abcam, Cat#ab182981, 1:2000) for 30 to 48 min at room temperature. The rabbit EnVision system (Dako), anti-mouse-HRP (GE Healthcare) or biotinylated goat anti-rat (Bio-Rad, Hercules, CA, USA) followed by HRP-conjugated streptavidin (Millipore, Milan, Italy), were used before diaminobenzidine tetrahydrochloride (Dako) incubation. Negative and positive controls were performed to set up the staining protocol. All slides were stained for the same antigen, together with the same antigen-retrieval buffer and antibody dilution. Tissues were examined in a double-blind fashion and digital images of representative areas were taken. The presence of positive cells was defined as absent (score 0.2), scarce (score 0.4), moderate (score 0.6), strong (score 0.8), or huge (score 1) on sections stained with the different antibodies.

Antibody-dependent cell-mediated cytotoxicity (ADCC) assay

(Chapter III) Fresh splenocytes from healthy donor mice were collected and isolated as described in Conti et al. 2020 [42]. 1×10^4 4T1 target cells were incubated with 2 µmol/L CFSE (Molecular Probes, cod. C34554) for 20 minutes at 37° C, washed with RPMI1640 supplemented with 10% FBS, and then cultured for 48 hours with fresh splenocytes at different effector:target (E:T) ratios and with a 1:50 dilution of immune sera, collected as described in the "In vivo experiments" paragraph. Cells were then stained with 1 µg/mL 7-Amino-ActinomycinD (7-AAD, BD Biosciences), acquired using a BD FACSVerse (BD Biosciences) and analysed using FlowJO10.5.3. Percent killing was obtained by back-gating on the $CFSE^+$ targets and measuring the percentage of 7-AAD^+ dead cells. Percent-specific lysis was calculated with the formula [(dead targets in sample (%) – spontaneously dead targets (%))/(dead target maximum − spontaneously dead targets (%))] × 100. Spontaneous death was obtained by culturing target cells without splenocytes, whereas maximal death was obtained after treatment with PBS supplemented with 1% saponin.

Enzyme-linked immunosorbent assay (ELISA)

(Chapter II) Supernatants of 4T1, MDA-MB-231 and BEND3 cells treated with or without 5 µM CU-CPT22 or PLGA-CU and with or without 2 µM doxorubicin or LIPO-DOXO, or their combinations, were harvested after 48 hours, and VEGF was quantified using ELISA (R&D Systems). *(Chapter II)* Thawed immune sera (1:50) were incubated on plates coated with recombinant mouse xCT (Cloud-Clone-Corp., 40 ng/well), and binding was detected with horseradish peroxidase–conjugated anti-mouse-IgG using a 680XR Microplate Reader (BioRad Laboratories Inc., Hercules, USA), as described in Conti et al. 2020 [42].

Sphere generation assays

(Chapter III) To test the effect of xCT and TLR2 targeting on CSC self-renewal, TUBO and 4T1 tumorspheres were dissociated and cultured 5 days in tumorsphere medium supplemented or not with sulfasalazine (100 µM) or a 1:50 dilution of immune sera, in the absence or presence of the TLR2-blocking monoclonal antibody T2.5 (Invivogen, Cat#mab2-mtlr2) (10 µg/mL). Spheres were then aliquoted in 96 well plates (20 µl/well) and the number of spheres was manually counted under Leica DMi1 inverted microscope (4x magnification).

Statistical analysis

Statistical significance was evaluated using GraphPad8 software. Differences in survival were analysed using Mantel-Cox log-rank test. Differences in sphere formation, FACS and ELISA data, cell viability, and IHC data were analysed using two-tailed unpaired Student's t test (with Welch's correction for samples with different variance) and non-parametric Mann–Whitney or Kruskal–Wallis test when the distribution calculated using Shapiro-Wilk or Kolmogorov Smirnov test was not normal. Differences in cell viability and tumor growth were analysed using two-way ANOVA with Bonferroni posttest. $P < 0.05$ was considered significant.

References

1. Simon, A.; Robb, K. Breast Cancer. *Cambridge Handbook of Psychology, Health and Medicine, Second Edition* **2024**, 577–580, doi:10.1017/CBO9780511543579.131.

2. Alex, A.; Bhandary, E.; McGuire, K.P. Anatomy and Physiology of the Breast during Pregnancy and Lactation. *Adv Exp Med Biol* **2020**, *1252*, 3–7, doi:10.1007/978-3-030-41596-9_1.

3. Obeagu, E.I.; Obeagu, G.U. Breast Cancer: A Review of Risk Factors and Diagnosis. *Medicine* **2024**, *103*, E36905, doi:10.1097/MD.0000000000036905.

4. Li, M.R.; Liu, M.Z.; Ge, Y.Q.; Zhou, Y.; Wei, W. Assistance by Routine CT Features Combined With 3D Texture Analysis in the Diagnosis of BRCA Gene Mutation Status in Advanced Epithelial Ovarian Cancer. *Front Oncol* **2021**, *11*, 696780, doi:10.3389/FONC.2021.696780/BIBTEX.

5. Buist, D.S.M.; Abraham, L.; Lee, C.I.; Lee, J.M.; Lehman, C.; O'Meara, E.S.; Stout, N.K.; Henderson, L.M.; Hill, D.; Wernli, K.J.; et al. Breast Biopsy Intensity and Findings Following Breast Cancer Screening in Women With and Without a Personal History of Breast Cancer. *JAMA Intern Med* **2018**, *178*, 458–468, doi:10.1001/JAMAINTERNMED.2017.8549.

6. Hu, X.; Zhang, Q.; Xing, W.; Wang, W. Role of MicroRNA/LncRNA Intertwined With the Wnt/β-Catenin Axis in Regulating the Pathogenesis of Triple-Negative Breast Cancer. *Front Pharmacol* **2022**, *13*, 814971, doi:10.3389/FPHAR.2022.814971/BIBTEX.

7. Thigpen, D.; Kappler, A.; Brem, R. Response to Comment on Thigpen D. et al. The Role of Ultrasound in Screening Dense Breasts—A Review of the Literature and Practical Solutions for Implementation. Diagnostics 2018, 8, 20. *Diagnostics 2018, Vol. 8, Page 38* **2018**, *8*, 38, doi:10.3390/DIAGNOSTICS8020038.

8. Vatankhah, H.; Khalili, P.; Vatanparast, M.; Ayoobi, F.; Esmaeili-Nadimi, A.; Jamali, Z. Prevalence of Early and Late Menopause and Its Determinants in Rafsanjan Cohort Study. *Sci Rep* **2023**, *13*, doi:10.1038/S41598-023-28526-Y.

9. Garnæs, K.K.; Elvebakk, T.; Salvesen, Ø.; Stafne, S.N.; Mørkved, S.; Salvesen, K.Å.; Moholdt, T. Dietary Intake in Early Pregnancy and Glycemia in Late Pregnancy among Women with Obesity. *Nutrients* **2022**, *14*, doi:10.3390/NU14010105.

10. Kunyahamu, M.S.; Daud, A.; Jusoh, N. Obesity among Health-care Workers: Which Occupations Are at Higher Risk of Being Obese? *Int J Environ Res Public Health* **2021**, *18*, doi:10.3390/IJERPH18084381.

11. Belachew, E.B.; Sewasew, D.T. Molecular Mechanisms of Endocrine Resistance in Estrogen-Positive Breast Cancer. *Front Endocrinol (Lausanne)* **2021**, *12*, doi:10.3389/FENDO.2021.599586/XML/NLM.

12. Mills, Z.B.; Faull, R.L.M.; Kwakowsky, A. Is Hormone Replacement Therapy a Risk Factor or a Therapeutic Option for Alzheimer's Disease? *Int J Mol Sci* **2023**, *24*, doi:10.3390/IJMS24043205.

13. Wang, Y.; Chen, H.; Li, N.; Ren, J.; Zhang, K.; Dai, M.; He, J. Ultrasound for Breast Cancer Screening in High-Risk Women: Results from a Population-Based Cancer Screening Program in China. *Front Oncol* **2019**, *9*, doi:10.3389/FONC.2019.00286/XML/NLM.

14. Yersal, O.; Barutca, S. Biological Subtypes of Breast Cancer: Prognostic and Therapeutic Implications. *World J Clin Oncol* **2014**, *5*, 412–424, doi:10.5306/WJCO.V5.I3.412.

15. Shaath, H.; Elango, R.; Alajez, N.M. Molecular Classification of Breast Cancer Utilizing Long Non-Coding Rna (Lncrna) Transcriptomes Identifies Novel Diagnostic Lncrna Panel for Triple-Negative Breast Cancer. *Cancers (Basel)* **2021**, *13*, 5350, doi:10.3390/CANCERS13215350/S1.

16. Orrantia-Borunda, E.; Anchondo-Nuñez, P.; Acuña-Aguilar, L.E.; Gómez-Valles, F.O.; Ramírez-Valdespino, C.A. Subtypes of Breast Cancer. *Breast Cancer* **2022**, 31–42, doi:10.36255/EXON-PUBLICATIONS-BREAST-CANCER-SUBTYPES.

17. Zhou, G.Q.; Lv, J.W.; Tang, L.L.; Mao, Y.P.; Guo, R.; Ma, J.; Sun, Y. Evaluation of the National Comprehensive Cancer Network and European Society for Medical Oncology Nasopharyngeal Carcinoma Surveillance Guidelines. *Front Oncol* **2020**, *10*, doi:10.3389/FONC.2020.00119/PDF.

18. Paluch-Shimon, S.; Cherny, N.I.; de Vries, E.G.E.; Dafni, U.; Piccart, M.J.; Latino, N.J.; Cardoso, F. Application of the ESMO-Magnitude of Clinical Benefit Scale (V.1.1) to the Field of Early Breast Cancer Therapies. *ESMO Open* **2020**, *5*, e000743, doi:10.1136/ESMOOPEN-2020-000743/ATTACHMENT/6F35702A-1C14-4D11-8134-C4A10E27C047/MMC2.PDF.

19. Inic, Z.; Zegarac, M.; Inic, M.; Markovic, I.; Kozomara, Z.; Djurisic, I.; Inic, I.; Pupic, G.; Jancic, S. Difference between Luminal A and Luminal B Subtypes According to Ki-67, Tumor Size, and Progesterone Receptor Negativity Providing Prognostic Information. *Clin Med Insights Oncol* **2014**, *8*, 107–111, doi:10.4137/CMO.S18006/ASSET/IMAGES/LARGE/10.4137_CMO.S18006-FIG2.JPEG.

20. Krishnamurti, U.; Silverman, J.F. HER2 in Breast Cancer: A Review and Update. *Adv Anat Pathol* **2014**, *21*, 100–107, doi:10.1097/PAP.0000000000000015.

21. Figueroa-Magalhães, M.C.; Jelovac, D.; Connolly, R.M.; Wolff, A.C. Treatment of HER2-Positive Breast Cancer. *The Breast* **2014**, *23*, 128–136, doi:10.1016/J.BREAST.2013.11.011.

22. Kumar, P.; Aggarwal, R. An Overview of Triple-Negative Breast Cancer. *Archives of Gynecology and Obstetrics 2015 293:2* **2015**, *293*, 247–269, doi:10.1007/S00404-015-3859-Y.

23. Kerr, A.J.; Dodwell, D.; McGale, P.; Holt, F.; Duane, F.; Mannu, G.; Darby, S.C.; Taylor, C.W. Adjuvant and Neoadjuvant Breast Cancer Treatments: A Systematic Review of Their Effects on Mortality. *Cancer Treat Rev* **2022**, *105*, doi:10.1016/j.ctrv.2022.102375.

24. Shien, T.; Iwata, H. Adjuvant and Neoadjuvant Therapy for Breast Cancer. *Jpn J Clin Oncol* **2020**, *50*, 225–229, doi:10.1093/JJCO/HYZ213.

25. Waks, A.G.; Winer, E.P. Breast Cancer Treatment: A Review. *JAMA* **2019**, *321*, 288–300, doi:10.1001/JAMA.2018.19323.

26. Burguin, A.; Diorio, C.; Durocher, F. Breast Cancer Treatments: Updates and New Challenges. *J Pers Med* **2021**, *11*, doi:10.3390/jpm11080808.

27. Syed, Y.Y. Oncotype DX Breast Recurrence Score®: A Review of Its Use in Early-Stage Breast Cancer. *Mol Diagn Ther* **2020**, *24*, 621–632, doi:10.1007/S40291-020-00482-7.

28. Andre, F.; Ismaila, N.; Allison, K.H.; Barlow, W.E.; Collyar, D.E.; Damodaran, S.; Henry, N.L.; Jhaveri, K.; Kalinsky, K.; Kuderer, N.M.; et al. Biomarkers for Adjuvant Endocrine and Chemotherapy in Early-Stage Breast Cancer: ASCO Guideline Update. *Journal of Clinical Oncology* **2022**, *34*, doi:10.1200/JCO.22.00069.

29. Korde, L.A.; Somerfield, M.R.; Carey, L.A.; Crews, J.R.; Denduluri, N.; Shelley Hwang, E.; Khan, S.A.; Loibl, S.; Morris, E.A.; Perez, A.; et al. Neoadjuvant Chemotherapy, Endocrine Therapy, and Targeted Therapy for Breast Cancer: ASCO Guideline. *Journal of Clinical Oncology* **2021**, *39*, 1485–1505, doi:10.1200/JCO.20.03399.

30. Wu, Y.T.; Xu, Z.; Zhang, K.; Wu, J.S.; Li, X.; Arshad, B.; Li, Y.C.; Wang, Z.L.; Li, H.Y.; Wu, K.N.; et al. Efficacy and Cardiac Safety of the Concurrent Use of Trastuzumab and Anthracycline-Based Neoadjuvant Chemotherapy for HER2-Positive Breast Cancer: A Systematic Review and Meta-Analysis. *Ther Clin Risk Manag* **2018**, *14*, 1789–1797, doi:10.2147/TCRM.S176214.

31. Dieci, M.V.; Vernaci, G.; Guarneri, V. Escalation and De-Escalation in HER2 Positive Early Breast Cancer. *Curr Opin Oncol* **2019**, *31*, 35–42, doi:10.1097/CCO.0000000000000492.

32. Ye, F.; Dewanjee, S.; Li, Y.; Jha, N.K.; Chen, Z.S.; Kumar, A.; Vishakha; Behl, T.; Jha, S.K.; Tang, H. Advancements in Clinical Aspects of Targeted Therapy and Immunotherapy in Breast Cancer. *Mol Cancer* **2023**, *22*, doi:10.1186/S12943-023-01805-Y.

33. Husinka, L.; Koerner, P.H.; Miller, R.T.; Trombatt, W. Review of Cyclin-Dependent Kinase 4/6 Inhibitors in the Treatment of Advanced or Metastatic Breast Cancer. *J Drug Assess* **2021**, *10*, 27–34, doi:10.1080/21556660.2020.1857103.

34. Salemme, V.; Centonze, G.; Cavallo, F.; Defilippi, P.; Conti, L. The Crosstalk Between Tumor Cells and the Immune Microenvironment in Breast Cancer: Implications for Immunotherapy. *Front Oncol* **2021**, *11*, doi:10.3389/FONC.2021.610303/FULL.

35. Mittal, D.; Gubin, M.M.; Schreiber, R.D.; Smyth, M.J. New Insights into Cancer Immunoediting and Its Three Component Phases-Elimination, Equilibrium and Escape. *Curr Opin Immunol* **2014**, *27*, 16–25, doi:10.1016/j.coi.2014.01.004.

36. Schreiber, R.D.; Old, L.J.; Smyth, M.J. Cancer Immunoediting: Integrating Immunity's Roles in Cancer Suppression and Promotion. *Science (1979)* **2011**, *331*, 1565–1570, doi:10.1126/SCIENCE.1203486.

37. Wu, B.; Zhang, B.; Li, B.; Wu, H.; Jiang, M. Cold and Hot Tumors: From Molecular Mechanisms to Targeted Therapy., doi:10.1038/s41392-024-01979-x.

38. Debien, V.; De Caluwé, A.; Wang, X.; Piccart-Gebhart, M.; Tuohy, V.K.; Romano, E.; Buisseret, L. Immunotherapy in Breast Cancer: An Overview of Current Strategies and Perspectives. *NPJ Breast Cancer* **2023**, *9*, doi:10.1038/S41523-023-00508-3.

39. Villacampa, G.; Navarro, V.; Matikas, A.; Ribeiro, J.M.; Schettini, F.; Tolosa, P.; Martínez-Sáez, O.; Sánchez-Bayona, R.; Ferrero-Cafiero, J.M.; Salvador, F.; et al. Neoadjuvant Immune Checkpoint Inhibitors Plus Chemotherapy in Early Breast Cancer A Systematic Review and Meta-Analysis. *JAMA Oncol* **2024**, doi:10.1001/JAMAONCOL.2024.3456.

40. Zhu, S.Y.; Yu, K. Da Breast Cancer Vaccines: Disappointing or Promising? *Front Immunol* **2022**, *13*, doi:10.3389/FIMMU.2022.828386/XML/NLM.

41. Ruiu, R.; Di Lorenzo, A.; Cavallo, F.; Conti, L. Are Cancer Stem Cells a Suitable Target for Breast Cancer Immunotherapy? *Front Oncol* **2022**, *12*, doi:10.3389/FONC.2022.877384/XML/NLM.

42. Conti, L.; Bolli, E.; Di Lorenzo, A.; Franceschi, V.; MacChi, F.; Riccardo, F.; Ruiu, R.; Russo, L.; Quaglino, E.; Donofrio, G.; et al. Immunotargeting of the XCT Cystine/Glutamate Antiporter

Potentiates the Efficacy of HER2-Targeted Immunotherapies in Breast Cancer. *Cancer Immunol Res* **2020**, *8*, 1039–1053, doi:10.1158/2326-6066.CIR-20-0082.

43. Donofrio, G.; Tebaldi, G.; Lanzardo, S.; Ruiu, R.; Bolli, E.; Ballatore, A.; Rolih, V.; Macchi, F.; Conti, L.; Cavallo, F. Bovine Herpesvirus 4-Based Vector Delivering the Full Length XCT DNA Efficiently Protects Mice from Mammary Cancer Metastases by Targeting Cancer Stem Cells. *Oncoimmunology* **2018**, *7*, doi:10.1080/2162402X.2018.1494108.

44. Ruiu, R.; Rolih, V.; Bolli, E.; Barutello, G.; Riccardo, F.; Quaglino, E.; Merighi, I.F.; Pericle, F.; Donofrio, G.; Cavallo, F.; et al. Fighting Breast Cancer Stem Cells through the Immune-Targeting of the XCT Cystine–Glutamate Antiporter. *Cancer Immunology, Immunotherapy* **2019**, *68*, 131–141, doi:10.1007/S00262-018-2185-1.

45. Lanzardo, S.; Conti, L.; Rooke, R.; Ruiu, R.; Accart, N.; Bolli, E.; Arigoni, M.; Macagno, M.; Barrera, G.; Pizzimenti, S.; et al. Immunotargeting of Antigen XCT Attenuates Stem-like Cell Behavior and Metastatic Progression in Breast Cancer. *Cancer Res* **2016**, *76*, 62–72, doi:10.1158/0008-5472.CAN-15-1208/652029/AM/IMMUNOTARGETING-OF-ANTIGEN-XCT-ATTENUATES-STEM.

46. Bolli, E.; O'Rourke, J.P.; Conti, L.; Lanzardo, S.; Rolih, V.; Christen, J.M.; Barutello, G.; Forni, M.; Pericle, F.; Cavallo, F. A Virus-Like-Particle Immunotherapy Targeting Epitope-Specific Anti-XCT Expressed on Cancer Stem Cell Inhibits the Progression of Metastatic Cancer in Vivo. *Oncoimmunology* **2018**, *7*, doi:10.1080/2162402X.2017.1408746.

47. Rafiq, S.; Hackett, C.S.; Brentjens, R.J. Engineering Strategies to Overcome the Current Roadblocks in CAR T Cell Therapy. *Nat Rev Clin Oncol* **2020**, *17*, 147–167, doi:10.1038/S41571-019-0297-Y.

48. Łukasiewicz, S.; Czeczelewski, M.; Forma, A.; Baj, J.; Sitarz, R.; Stanisławek, A. Breast Cancer—Epidemiology, Risk Factors, Classification, Prognostic Markers, and Current Treatment Strategies—An Updated Review. *Cancers (Basel)* **2021**, *13*, doi:10.3390/CANCERS13174287.

49. Kinnel, B.; Singh, S.K.; Oprea-Ilies, G.; Singh, R. Targeted Therapy and Mechanisms of Drug Resistance in Breast Cancer. *Cancers (Basel)* **2023**, *15*, doi:10.3390/CANCERS15041320.

50. Vadlapatla, R.; Vadlapudi, A.; Pal, D.; Mitra, A. Mechanisms of Drug Resistance in Cancer Chemotherapy: Coordinated Role and Regulation of Efflux Transporters and Metabolizing Enzymes. *Curr Pharm Des* **2013**, *19*, 7126–7140, doi:10.2174/13816128113199990493.

51. He, J.; Fortunati, E.; Liu, D.X.; Li, Y. Pleiotropic Roles of Abc Transporters in Breast Cancer. *Int J Mol Sci* **2021**, *22*, 1–24, doi:10.3390/IJMS22063199.

52. Woods, D.; Turchi, J.J. Chemotherapy Induced DNA Damage Response Convergence of Drugs and Pathways. *Cancer Biol Ther* **2013**, *14*, 379–389, doi:10.4161/CBT.23761.

53. Bukowski, K.; Kciuk, M.; Kontek, R. Mechanisms of Multidrug Resistance in Cancer Chemotherapy. *Int J Mol Sci* **2020**, *21*, doi:10.3390/IJMS21093233.

54. Henneman, L.; Van Miltenburg, M.H.; Michalak, E.M.; Braumuller, T.M.; Jaspers, J.E.; Drenth, A.P.; De Korte-Grimmerink, R.; Gogola, E.; Szuhai, K.; Schlicker, A.; et al. Selective Resistance to the PARP Inhibitor Olaparib in a Mouse Model for BRCA1-Deficient Metaplastic Breast Cancer. *Proc Natl Acad Sci U S A* **2015**, *112*, 8409–8414, doi:10.1073/PNAS.1500223112/ASSET/FA105AAF-D16F-4483-A2F0-0A39D1F13890/ASSETS/GRAPHIC/PNAS.1500223112SFIG02.JPEG.

55. Zhu, J.; Zou, Z.; Nie, P.; Kou, X.; Wu, B.; Wang, S.; Song, Z.; He, J. Downregulation of MicroRNA-27b-3p Enhances Tamoxifen Resistance in Breast Cancer by Increasing NR5A2 and CREB1 Expression. *Cell Death Dis* **2016**, *7*, doi:10.1038/CDDIS.2016.361.

56. Wang, X.; Zhang, H.; Chen, X. Drug Resistance and Combating Drug Resistance in Cancer. *Cancer Drug Resistance* **2019**, *2*, 141–160, doi:10.20517/CDR.2019.10.

57. Lima, J.F.; Nofech-Mozes, S.; Bayani, J.; Bartlett, J.M.S. EMT in Breast Carcinoma—A Review. *J Clin Med* **2016**, *5*, doi:10.3390/JCM5070065.

58. Di Lorenzo, A.; Bolli, E.; Tarone, L.; Cavallo, F.; Conti, L. Toll-like Receptor 2 at the Crossroad between Cancer Cells, the Immune System, and the Microbiota. *Int J Mol Sci* 2020, *21*, 1–26.

59. Pernas, S.; Tolaney, S.M. HER2-Positive Breast Cancer: New Therapeutic Frontiers and Overcoming Resistance. *Ther Adv Med Oncol* **2019**, *11*, doi:10.1177/1758835919833519.

60. Goel, S.; Wang, Q.; Watt, A.C.; Tolaney, S.M.; Dillon, D.A.; Li, W.; Ramm, S.; Palmer, A.C.; Yuzugullu, H.; Varadan, V.; et al. Overcoming Therapeutic Resistance in HER2-Positive Breast Cancers with CDK4/6 Inhibitors. *Cancer Cell* **2016**, *29*, 255–269, doi:10.1016/j.ccell.2016.02.006.

61. Zhang, Y. The Root Cause of Drug Resistance in HER2-Positive Breast Cancer and the Therapeutic Approaches to Overcoming the Resistance. *Pharmacol Ther* **2021**, *218*, doi:10.1016/j.pharmthera.2020.107677.

62. Nedeljković, M.; Damjanović, A. Mechanisms of Chemotherapy Resistance in Triple-Negative Breast Cancer-How We Can Rise to the Challenge. *Cells* **2019**, *8*, doi:10.3390/CELLS8090957.

63. Ruiu, R.; Tarone, L.; Rolih, V.; Barutello, G.; Bolli, E.; Riccardo, F.; Cavallo, F.; Conti, L. Cancer Stem Cell Immunology and Immunotherapy: Harnessing the Immune System against Cancer's Source. *Prog Mol Biol Transl Sci* **2019**, *164*, 119–188, doi:10.1016/bs.pmbts.2019.03.008.

64. Kleffel, S.; Schatton, T. Tumor Dormancy and Cancer Stem Cells: Two Sides of the Same Coin? *Adv Exp Med Biol* **2013**, *734*, 145–179, doi:10.1007/978-1-4614-1445-2_8.

65. Gordon, R.R.; Nelson, P.S. Cellular Senescence and Cancer Chemotherapy Resistance. *Drug Resistance Updates* **2012**, *15*, 123–131, doi:10.1016/j.drup.2012.01.002.

66. Gordon, R.R.; Nelson, P.S. Cellular Senescence and Cancer Chemotherapy Resistance. *Drug Resistance Updates* **2012**, *15*, 123–131, doi:10.1016/j.drup.2012.01.002.

67. Zhong, Z.; Virshup, D.M. Wnt Signaling and Drug Resistance in Cancer. *Mol Pharmacol* **2020**, *97*, 72–89, doi:10.1124/MOL.119.117978.

68. Takebe, N.; Warren, R.Q.; Ivy, S.P. Breast Cancer Growth and Metastasis: Interplay between Cancer Stem Cells, Embryonic Signaling Pathways and Epithelial-to-Mesenchymal Transition. *Breast Cancer Research* **2011**, *13*, doi:10.1186/BCR2876.

69. Mani, S.A.; Guo, W.; Liao, M.J.; Eaton, E.N.; Ayyanan, A.; Zhou, A.Y.; Brooks, M.; Reinhard, F.; Zhang, C.C.; Shipitsin, M.; et al. The Epithelial-Mesenchymal Transition Generates Cells with Properties of Stem Cells. *Cell* **2008**, *133*, 704–715, doi:10.1016/j.cell.2008.03.027.

70. Martin-Orozco, E.; Sanchez-Fernandez, A.; Ortiz-Parra, I.; Ayala-San Nicolas, M. WNT Signaling in Tumors: The Way to Evade Drugs and Immunity. *Front Immunol* **2019**, *10*, doi:10.3389/FIMMU.2019.02854/FULL.

71. Wang, H.; Gong, P.; Li, J.; Fu, Y.; Zhou, Z.; Liu, L. Role of CD133 in Human Embryonic Stem Cell Proliferation and Teratoma Formation. *Stem Cell Res Ther* **2020**, *11*, doi:10.1186/S13287-020-01729-0.

72. Kahn, M.; Kim, Y. The Role of the Wnt Signaling Pathway in Cancer Stem Cells: Prospects for Drug Development. *Res Rep Biochem* **2014**, 1, doi:10.2147/RRBC.S53823.

73. Feng, Y.; Spezia, M.; Huang, S.; Yuan, C.; Zeng, Z.; Zhang, L.; Ji, X.; Liu, W.; Huang, B.; Luo, W.; et al. Breast Cancer Development and Progression: Risk Factors, Cancer Stem Cells, Signaling Pathways, Genomics, and Molecular Pathogenesis. *Genes Dis* **2018**, *5*, 77–106, doi:10.1016/j.gendis.2018.05.001.

74. Conti, L.; Lanzardo, S.; Arigoni, M.; Antonazzo, R.; Radaelli, E.; Cantarella, D.; Calogero, R.A.; Cavallo, F. The Noninflammatory Role of High Mobility Group Box 1/Toll-like Receptor 2 Axis in the Self-Renewal of Mammary Cancer Stem Cells. *The FASEB Journal • Research Communication*, doi:10.1096/fj.13-230201.

75. Quaglino, E.; Conti, L.; Cavallo, F. Breast Cancer Stem Cell Antigens as Targets for Immunotherapy. *Semin Immunol* **2020**, *47*, doi:10.1016/j.smim.2020.101386.

76. Rock, F.L.; Hardiman, G.; Timans, J.C.; Kastelein, R.A.; Bazan, J.F. A Family of Human Receptors Structurally Related to Drosophila Toll. *Proc Natl Acad Sci U S A* **1998**, *95*, 588–593, doi:10.1073/PNAS.95.2.588.

77. Valanne, S.; Wang, J.-H.; Rämet, M. The Drosophila Toll Signaling Pathway . *The Journal of Immunology* **2011**, *186*, 649–656, doi:10.4049/JIMMUNOL.1002302.

78. Roh, J.S.; Sohn, D.H. Damage-Associated Molecular Patterns in Inflammatory Diseases. *Immune Netw* **2018**, *18*, doi:10.4110/IN.2018.18.E27.

79. Amarante-Mendes, G.P.; Adjemian, S.; Branco, L.M.; Zanetti, L.C.; Weinlich, R.; Bortoluci, K.R. Pattern Recognition Receptors and the Host Cell Death Molecular Machinery. *Front Immunol* **2018**, *9*, doi:10.3389/FIMMU.2018.02379/TEXT.

80. Matzinger, P. Tolerance, Danger, and the Extended Family. *Annu Rev Immunol* **1994**, *12*, 991–1045, doi:10.1146/ANNUREV.IY.12.040194.005015.

81. Liston, A.; Masters, S.L. Homeostasis-Altering Molecular Processes as Mechanisms of Inflammasome Activation. *Nat Rev Immunol* **2017**, *17*, 208–214, doi:10.1038/NRI.2016.151.

82. van Bergenhenegouwen, J.; Plantinga, T.S.; Joosten, L.A.B.; Netea, M.G.; Folkerts, G.; Kraneveld, A.D.; Garssen, J.; Vos, A.P. TLR2 & Co: A Critical Analysis of the Complex Interactions between TLR2 and Coreceptors. *J Leukoc Biol* **2013**, *94*, 885–902, doi:10.1189/JLB.0113003.

83. Oliveira-Nascimento, L.; Massari, P.; Wetzler, L.M. The Role of TLR2 Ininfection and Immunity. *Front Immunol* **2012**, *3*, doi:10.3389/FIMMU.2012.00079/PDF.

84. Conti, L.; Ruiu, R.; Barutello, G.; Macagno, M.; Bandini, S.; Cavallo, F.; Lanzardo, S. Microenvironment, Oncoantigens, and Antitumor Vaccination: Lessons Learned from BALB-NeuT Mice. *Biomed Res Int* **2014**, *2014*, doi:10.1155/2014/534969.

85. Kono, H.; Rock, K.L. How Dying Cells Alert the Immune System to Danger. *Nat Rev Immunol* **2008**, *8*, 279–289, doi:10.1038/NRI2215.

86. Kang, R.; Zhang, Q.; Zeh, H.J.; Lotze, M.T.; Tang, D. HMGB1 in Cancer: Good, Bad, or Both? *Clinical Cancer Research* **2013**, *19*, 4046–4057, doi:10.1158/1078-0432.CCR-13-0495.

87. Joffre, O.; Nolte, M.A.; Spörri, R.; Sousa, C.R.E. Inflammatory Signals in Dendritic Cell Activation and the Induction of Adaptive Immunity. *Immunol Rev* **2009**, *227*, 234–247, doi:10.1111/J.1600-065X.2008.00718.X.

88. Cossu, C.; Di Lorenzo, A.; Fiorilla, I.; Todesco, A.M.; Audrito, V.; Conti, L. The Role of the Toll-like Receptor 2 and the CGAS-STING Pathways in Breast Cancer: Friends or Foes? *International Journal of Molecular Sciences 2024, Vol. 25, Page 456* **2023**, *25*, 456, doi:10.3390/IJMS25010456.

89. Sutmuller, R.P.M.; Den Brok, M.H.M.G.M.; Kramer, M.; Bennink, E.J.; Toonen, L.W.J.; Kullberg, B.J.; Joosten, L.A.; Akira, S.; Netea, M.G.; Adema, G.J. Toll-like Receptor 2 Controls Expansion and Function of Regulatory T Cells. *Journal of Clinical Investigation* **2006**, *116*, 485–494, doi:10.1172/JCI25439.

90. McBride, A.; Konowich, J.; Salgame, P. Host Defense and Recruitment of Foxp3+ T Regulatory Cells to the Lungs in Chronic Mycobacterium Tuberculosis Infection Requires Toll-like Receptor 2. *PLoS Pathog* **2013**, *9*, doi:10.1371/JOURNAL.PPAT.1003397.

91. Ye, L.; Zhang, Q.; Cheng, Y.; Chen, X.; Wang, G.; Shi, M.; Zhang, T.; Cao, Y.; Pan, H.; Zhang, L.; et al. Tumor-Derived Exosomal HMGB1 Fosters Hepatocellular Carcinoma Immune Evasion by Promoting TIM-1+ Regulatory B Cell Expansion. *J Immunother Cancer* **2018**, *6*, doi:10.1186/S40425-018-0451-6.

92. Chen, Y.Q.; Li, P.C.; Pan, N.; Gao, R.; Wen, Z.F.; Zhang, T.Y.; Huang, F.; Wu, F.Y.; Ou, X.L.; Zhang, J.P.; et al. Tumor-Released Autophagosomes Induces CD4+ T Cell-Mediated Immunosuppression via a TLR2-IL-6 Cascade. *J Immunother Cancer* **2019**, *7*, doi:10.1186/S40425-019-0646-5.

93. Wang, Z.; Yang, C.; Li, L.; Jin, X.; Zhang, Z.; Zheng, H.; Pan, J.; Shi, L.; Jiang, Z.; Su, K.; et al. Tumor-Derived HMGB1 Induces CD62Ldim Neutrophil Polarization and Promotes Lung Metastasis in Triple-Negative Breast Cancer. *Oncogenesis* **2020**, *9*, doi:10.1038/S41389-020-00267-X.

94. Niu, X.; Yin, L.; Yang, X.; Yang, Y.; Gu, Y.; Sun, Y.; Yang, M.; Wang, Y.; Zhang, Q.; Ji, H. Serum Amyloid A 1 Induces Suppressive Neutrophils through the Toll-like Receptor 2–Mediated Signaling Pathway to Promote Progression of Breast Cancer. *Cancer Sci* **2022**, *113*, 1140–1153, doi:10.1111/CAS.15287.

95. Xie, W.; Wang, Y.; Huang, Y.; Yang, H.; Wang, J.; Hu, Z. Toll-like Receptor 2 Mediates Invasion via Activating NF-KB in MDA-MB-231 Breast Cancer Cells. *Biochem Biophys Res Commun* **2009**, *379*, 1027–1032, doi:10.1016/j.bbrc.2009.01.009.

96. Scheeren, F.A.; Kuo, A.H.; Van Weele, L.J.; Cai, S.; Glykofridis, I.; Sikandar, S.S.; Zabala, M.; Qian, D.; Lam, J.S.; Johnston, D.; et al. A Cell-Intrinsic Role for TLR2–MYD88 in Intestinal and Breast Epithelia and Oncogenesis. *Nature Cell Biology 2014 16:12* **2014**, *16*, 1238–1248, doi:10.1038/ncb3058.

97. Schwitalla, S.; Fingerle, A.A.; Cammareri, P.; Nebelsiek, T.; Göktuna, S.I.; Ziegler, P.K.; Canli, O.; Heijmans, J.; Huels, D.J.; Moreaux, G.; et al. Intestinal Tumorigenesis Initiated by Dedifferentiation and Acquisition of Stem-Cell-like Properties. *Cell* **2013**, *152*, 25–38,

doi:10.1016/J.CELL.2012.12.012/ATTACHMENT/5A15D896-DAD3-47C7-B744-983D9739CAD9/MMC2.PDF.

98. Parida, S.; Sharma, D. The Power of Small Changes: Comprehensive Analyses of Microbial Dysbiosis in Breast Cancer. *Biochim Biophys Acta Rev Cancer* **2019**, *1871*, 392, doi:10.1016/J.BBCAN.2019.04.001.

99. Huang, B.; Zhao, J.; Shen, S.; Li, H.; He, K.L.; Shen, G.X.; Mayer, L.; Unkeless, J.; Li, D.; Yuan, Y.; et al. Listeria Monocytogenes Promotes Tumor Growth via Tumor Cell Toll-like Receptor 2 Signaling. *Cancer Res* **2007**, *67*, 4346–4352, doi:10.1158/0008-5472.CAN-06-4067.

100. Krzysiek-Maczka, G.; Targosz, A.; Szczyrk, U.; Strzalka, M.; Brzozowski, T.; Ptak-Belowska, A. Involvement of Epithelial-Mesenchymal Transition-Inducing Transcription Factors in the Mechanism of Helicobacter Pylori-Induced Fibroblasts Activation. *Journal of Physiology and Pharmacology* **2019**, *70*, doi:10.26402/JPP.2019.5.08.

101. Parida, S.; Wu, S.; Siddharth, S.; Wang, G.; Muniraj, N.; Nagalingam, A.; Hum, C.; Mistriotis, P.; Hao, H.; Conover, C.; et al. A Procarcinogenic Colon Microbe Promotes Breast Tumorigenesis and Metastatic Progression and Concomitantly Activates Notch and B-Catenin Axes. *Cancer Discov* **2021**, *11*, 1138–1157, doi:10.1158/2159-8290.CD-20-0537.

102. Kahraman Gürsoy, U.; Kantarci, A.; Enersen, M.; Guncu, G.N.; Bachrach, G.; Abed, J.; Maalouf, N.; Parhi, L.; Chaushu, S.; Mandelboim, O. Tumor Targeting by Fusobacterium Nucleatum: A Pilot Study and Future Perspectives. *Frontiers in Cellular and Infection Microbiology | www.frontiersin.org* **2017**, *1*, 295, doi:10.3389/fcimb.2017.00295.

103. Jia, Y.P.; Wang, K.; Zhang, Z.J.; Tong, Y.N.; Han, D.; Hu, C.Y.; Li, Q.; Xiang, Y.; Mao, X.H.; Tang, B. TLR2/TLR4 Activation Induces Tregs and Suppresses Intestinal Inflammation Caused by Fusobacterium Nucleatum in Vivo. *PLoS One* **2017**, *12*, e0186179, doi:10.1371/JOURNAL.PONE.0186179.

104. Bernardo, G.; Le Noci, V.; Ottaviano, E.; De Cecco, L.; Camisaschi, C.; Guglielmetti, S.; Di Modica, M.; Gargari, G.; Bianchi, F.; Indino, S.; et al. Reduction of Staphylococcus Epidermidis in the Mammary Tumor Microbiota Induces Antitumor Immunity and Decreases Breast Cancer Aggressiveness. *Cancer Lett* **2023**, *555*, 216041, doi:10.1016/j.canlet.2022.216041.

105. Chiba, A.; Bawaneh, A.; Velazquez, C.; Clear, K.Y.J.; Wilson, A.S.; Howard-McNatt, M.; Levine, E.A.; Levi-Polyachenko, N.; Yates-Alston, S.A.; Diggle, S.P.; et al. Neoadjuvant Chemotherapy Shifts Breast Tumor Microbiota Populations to Regulate Drug Responsiveness and the Development of Metastasis. *Molecular Cancer Research* **2020**, *18*, 130–139, doi:10.1158/1541-7786.MCR-19-0451/82259/AM/NEOADJUVANT-CHEMOTHERAPY-SHIFTS-BREAST-TUMOR.

106. Montassier, E.; Gastinne, T.; Vangay, P.; Al-Ghalith, G.A.; Bruley Des Varannes, S.; Massart, S.; Moreau, P.; Potel, G.; De La Cochetière, M.F.; Batard, E.; et al. Chemotherapy-Driven Dysbiosis in the Intestinal Microbiome. *Aliment Pharmacol Ther* **2015**, *42*, 515–528, doi:10.1111/APT.13302.

107. Dong, H.; Zhang, L.; Liu, S. Targeting HMGB1: An Available Therapeutic Strategy for Breast Cancer Therapy. *Int J Biol Sci* **2022**, *18*, 3421–3434, doi:10.7150/IJBS.73504.

108. Di Lorenzo, A.; Bolli, E.; Ruiu, R.; Ferrauto, G.; Di Gregorio, E.; Avalle, L.; Savino, A.; Poggio, P.; Merighi, I.F.; Riccardo, F.; et al. Toll-like Receptor 2 Promotes Breast Cancer Progression and

Resistance to Chemotherapy. *Oncoimmunology* **2022**, *11*, doi:10.1080/2162402X.2022.2086752.

109. Di Gregorio, E.; Romiti, C.; Di Lorenzo, A.; Cavallo, F.; Ferrauto, G.; Conti, L. RGD_PLGA Nanoparticles with Docetaxel: A Route for Improving Drug Efficiency and Reducing Toxicity in Breast Cancer Treatment. *Cancers (Basel)* **2023**, *15*, 8, doi:10.3390/CANCERS15010008/S1.

110. Iezzi, M.; Calogero, R.A.; Spadaro, M.; Musiani, P.; Forni, G.; Cavallo, F. BALB-NeuT Female Mice as a Dynamic Model of Mammary Cancer. *Translational Animal Models in Drug Discovery and Development* **2012**, 139–166, doi:10.2174/978160805469511201010139.

111. Wooten, R.M.; Ma, Y.; Yoder, R.A.; Brown, J.P.; Weis, J.H.; Zachary, J.F.; Kirschning, C.J.; Weis, J.J. Toll-Like Receptor 2 Is Required for Innate, But Not Acquired, Host Defense to Borrelia Burgdorferi. *The Journal of Immunology* **2002**, *168*, 348–355, doi:10.4049/JIMMUNOL.168.1.348.

112. Reilly, M.; Miller, R.M.; Thomson, M.H.; Patris, V.; Ryle, P.; Mcloughlin, L.; Mutch, P.; Gilboy, P.; Miller, C.; Broekema, M.; et al. Randomized, Double-Blind, Placebo-Controlled, Dose-Escalating Phase I, Healthy Subjects Study of Intravenous OPN-305, a Humanized Anti-TLR2 Antibody. *Clin Pharmacol Ther* **2013**, *94*, 593–600, doi:10.1038/CLPT.2013.150.

113. Garcia-Manero, G.; Montalban-Bravo, G.; Yang, H.; Wei, Y.; Alvarado, Y.; DiNardo, C.D.; Daver, N.G.; Konopleva, M.; Hearn, K.P.; Miller, R.; et al. A Clinical Study of OPN-305, a Toll-like Receptor 2 (TLR-2) Antibody, in Patients with Lower Risk Myelodysplastic Syndromes (MDS) That Have Received Prior Hypomethylating Agent (HMA) Therapy. *Blood* **2016**, *128*, 227–227, doi:10.1182/BLOOD.V128.22.227.227.

114. Kovacsovics, T.J.; Mims, A.; Salama, M.E.; Pantin, J.; Rao, N.; Kosak, K.M.; Ahorukomeye, P.; Glenn, M.J.; Deininger, M.W.N.; Boucher, K.M.; et al. Combination of the Low Anticoagulant Heparin CX-01 with Chemotherapy for the Treatment of Acute Myeloid Leukemia. *Blood Adv* **2018**, *2*, 381–389, doi:10.1182/BLOODADVANCES.2017013391.

115. Tye, H.; Kennedy, C.L.; Najdovska, M.; McLeod, L.; McCormack, W.; Hughes, N.; Dev, A.; Sievert, W.; Ooi, C.H.; Ishikawa, T.O.; et al. STAT3-Driven Upregulation of TLR2 Promotes Gastric Tumorigenesis Independent of Tumor Inflammation. *Cancer Cell* **2012**, *22*, 466–478, doi:10.1016/j.ccr.2012.08.010.

116. Zhang, W.; Liu, W.; Hu, X. Robinin Inhibits Pancreatic Cancer Cell Proliferation, EMT and Inflammation via Regulating TLR2-PI3k-AKT Signaling Pathway. *Cancer Cell Int* **2023**, *23*, 1–13, doi:10.1186/S12935-023-03167-3/FIGURES/8.

117. Farnebo, L.; Shahangian, A.; Lee, Y.; Shin, J.H.; Scheeren, F.A.; Sunwoo, J.B.; Farnebo, L.; Shahangian, A.; Lee, Y.; Shin, J.H.; et al. Targeting Toll-like Receptor 2 Inhibits Growth of Head and Neck Squamous Cell Carcinoma. *Oncotarget* **2015**, *6*, 9897–9907, doi:10.18632/ONCOTARGET.3393.

118. Wei, G.; Wang, Y.; Yang, G.; Wang, Y.; Ju, R. Recent Progress in Nanomedicine for Enhanced Cancer Chemotherapy. *Theranostics* **2021**, *11*, 6370–6392, doi:10.7150/THNO.57828.

119. Liu, S. Self-Assembled Lipid-Based Nanoparticles for Chemotherapy against Breast Cancer. *Front Bioeng Biotechnol* **2024**, *12*, doi:10.3389/FBIOE.2024.1482637/TEXT.

120. Barenholz, Y. Doxil® - The First FDA-Approved Nano-Drug: Lessons Learned. *Journal of Controlled Release* **2012**, *160*, 117–134, doi:10.1016/J.JCONREL.2012.03.020.

121. Gabizon, A.; Shmeeda, H.; Barenholz, Y. Pharmacokinetics of Pegylated Liposomal Doxorubicin: Review of Animal and Human Studies. *Clin Pharmacokinet* **2003**, *42*, 419–436, doi:10.2165/00003088-200342050-00002.

122. Batist, G.; Barton, J.; Chaikin, P.; Swenson, C.; Welles, L. Myocet (Liposome-Encapsulated Doxorubicin Citrate): A New Approach in Breast Cancer Therapy. *Expert Opin Pharmacother* **2002**, *3*, 1739–1751, doi:10.1517/14656566.3.12.1739.

123. Stathopoulos, G.P.; Antoniou, D.; Dimitroulis, J.; Stathopoulos, J.; Marosis, K.; Michalopoulou, P. Comparison of Liposomal Cisplatin versus Cisplatin in Non-Squamous Cell Non-Small-Cell Lung Cancer. *Cancer Chemother Pharmacol* **2011**, *68*, 945–950, doi:10.1007/S00280-011-1572-5.

124. Serpico, L.; Zhu, Y.; Maia, R.F.; Sumedha, S.; Shahbazi, M.A.; Santos, H.A. Lipid Nanoparticles-Based RNA Therapies for Breast Cancer Treatment. *Drug Delivery and Translational Research 2024 14:10* **2024**, *14*, 2823–2844, doi:10.1007/S13346-024-01638-2.

125. Cheng, Z.; Fobian, S.F.; Gurrieri, E.; Amin, M.; D'Agostino, V.G.; Falahati, M.; Zalba, S.; Debets, R.; Garrido, M.J.; Saeed, M.; et al. Lipid-Based Nanosystems: The next Generation of Cancer Immune Therapy. *Journal of Hematology & Oncology 2024 17:1* **2024**, *17*, 1–39, doi:10.1186/S13045-024-01574-1.

126. Conti, L.; Lanzardo, S.; Iezzi, M.; Montone, M.; Bolli, E.; Brioschi, C.; Maiocchi, A.; Forni, G.; Cavallo, F. Optical Imaging Detection of Microscopic Mammary Cancer in ErbB-2 Transgenic Mice through the DA364 Probe Binding Avβ3 Integrins. *Contrast Media Mol Imaging* **2013**, *8*, 350–360, doi:10.1002/CMMI.1529.

127. Bowerman, C.J.; Byrne, J.D.; Chu, K.S.; Schorzman, A.N.; Keeler, A.W.; Sherwood, C.A.; Perry, J.L.; Luft, J.C.; Darr, D.B.; Deal, A.M.; et al. Docetaxel-Loaded PLGA Nanoparticles Improve Efficacy in Taxane-Resistant Triple-Negative Breast Cancer. *Nano Lett* **2017**, *17*, 242–248, doi:10.1021/ACS.NANOLETT.6B03971.

128. Tran, P.; Nguyen, T.N.; Lee, Y.; Tran, P.N.; Park, J.S. Docetaxel-Loaded PLGA Nanoparticles to Increase Pharmacological Sensitivity in MDA-MB-231 and MCF-7 Breast Cancer Cells. *Korean Journal of Physiology and Pharmacology* **2021**, *25*, 479–488, doi:10.4196/KJPP.2021.25.5.479.

129. Rafiei, P.; Haddadi, A. Docetaxel-Loaded PLGA and PLGA-PEG Nanoparticles for Intravenous Application: Pharmacokinetics and Biodistribution Profile. *Int J Nanomedicine* **2017**, *12*, 935–947, doi:10.2147/IJN.S121881.

130. Xiong, X.B.; Huang, Y.; Lu, W.L.; Zhang, X.; Zhang, H.; Nagai, T.; Zhang, Q. Intracellular Delivery of Doxorubicin with RGD-Modified Sterically Stabilized Liposomes for an Improved Antitumor Efficacy: In Vitro and in Vivo. *J Pharm Sci* **2005**, *94*, 1782–1793, doi:10.1002/jps.20397.

131. Gao, T.; Zou, C.; Li, Y.; Jiang, Z.; Tang, X.; Song, X. A Brief History and Future Prospects of Cest Mri in Clinical Non-brain Tumor Imaging. *Int J Mol Sci* **2021**, *22*, doi:10.3390/IJMS222111559.

132. Cai, K.; Singh, A.; Poptani, H.; Li, W.; Yang, S.; Lu, Y.; Hariharan, H.; Zhou, X.J.; Reddy, R. CEST Signal at 2ppm (CEST at 2ppm) from Z-Spectral Fitting Correlates with Creatine Distribution in Brain Tumor. *NMR Biomed* **2015**, *28*, 1–8, doi:10.1002/nbm.3216.

133. Zhang, L.; Bu, P. The Two Sides of Creatine in Cancer. *Trends Cell Biol* 2022, *32*, 380–390.

134. Mccoy, M.G.; Nascimento, D.W.; Veleeparambil, M.; Murtazina, R.; Gao, D.; Tkachenko, S.; Podrez, E.; Byzova, T. V *Endothelial TLR2 Promotes Proangiogenic Immune Cell Recruitment and Tumor Angiogenesis*; 2021; Vol. 14;.

135. Long, Y.; Tao, H.; Karachi, A.; Grippin, A.J.; Jin, L.; Chang, Y.; Zhang, W.; Dyson, K.A.; Hou, A.Y.; Na, M.; et al. Dysregulation of Glutamate Transport Enhances Treg Function That Promotes VEGF Blockade Resistance in Glioblastoma. *Cancer Res* **2020**, *80*, 499–509, doi:10.1158/0008-5472.CAN-19-1577.

136. Dornier, E.; Rabas, N.; Mitchell, L.; Novo, D.; Dhayade, S.; Marco, S.; MacKay, G.; Sumpton, D.; Pallares, M.; Nixon, C.; et al. Glutaminolysis Drives Membrane Trafficking to Promote Invasiveness of Breast Cancer Cells. *Nat Commun* **2017**, *8*, doi:10.1038/S41467-017-02101-2.

137. Hasegawa, M.; Takahashi, H.; Rajabi, H.; Alam, M.; Suzuki, Y.; Yin, L.; Tagde, A.; Maeda, T.; Hiraki, M.; Sukhatme, V.P.; et al. Functional Interactions of the Cystine/Glutamate Antiporter, CD44V and MUC1-C Oncoprotein in Triple-Negative Breast Cancer Cells. *Oncotarget* **2016**, *7*, 11756–11769, doi:10.18632/ONCOTARGET.7598.

138. Briggs, K.J.J.; Koivunen, P.; Cao, S.; Backus, K.M.M.; Olenchock, B.A.A.; Patel, H.; Zhang, Q.; Signoretti, S.; Gerfen, G.J.J.; Richardson, A.L.L.; et al. Paracrine Induction of HIF by Glutamate in Breast Cancer: EglN1 Senses Cysteine. *Cell* **2016**, *166*, 126–139, doi:10.1016/j.cell.2016.05.042.

139. Dixon, S.J.; Patel, D.; Welsch, M.; Skouta, R.; Lee, E.; Hayano, M.; Thomas, A.G.; Gleason, C.; Tatonetti, N.; Slusher, B.S.; et al. Pharmacological Inhibition of Cystine-Glutamate Exchange Induces Endoplasmic Reticulum Stress and Ferroptosis. *Elife* **2014**, *2014*, doi:10.7554/ELIFE.02523.

140. Linares, V.; Alonso, V.; Domingo, J.L. Oxidative Stress as a Mechanism Underlying Sulfasalazine-Induced Toxicity. *Expert Opin Drug Saf* **2011**, *10*, 253–263, doi:10.1517/14740338.2011.529898.

141. Robe, P.A.; Martin, D.H.; Nguyen-Khac, M.T.; Artesi, M.; Deprez, M.; Albert, A.; Vanbelle, S.; Califice, S.; Bredel, M.; Bours, V. Early Termination of ISRCTN45828668, a Phase 1/2 Prospective, Randomized Study of Sulfasalazine for the Treatment of Progressing Malignant Gliomas in Adults. *BMC Cancer* **2009**, *9*, 372, doi:10.1186/1471-2407-9-372.

142. Jacca, S.; Rolih, V.; Quaglino, E.; Franceschi, V.; Tebaldi, G.; Bolli, E.; Rosamilia, A.; Ottonello, S.; Cavallo, F.; Donofrio, G. Bovine Herpesvirus 4-Based Vector Delivering a Hybrid Rat/Human HER-2 Oncoantigen Efficiently Protects Mice from Autochthonous Her-2+mammary Cancer. *Oncoimmunology* **2016**, *5*, doi:10.1080/2162402X.2015.1082705.

143. Siegel Mph, R.L.; Tyler, |; Kratzer, B.; Giaquinto, A.N.; Hyuna, |; Phd, S.; Ahmedin, |; Dvm, J. Cancer Statistics, 2025. *CA Cancer J Clin* **2025**, *75*, 10–45, doi:10.3322/CAAC.21871.

144. Tarone, L.; Giacobino, D.; Camerino, M.; Maniscalco, L.; Iussich, S.; Parisi, L.; Giovannini, G.; Dentini, A.; Bolli, E.; Quaglino, E.; et al. A Chimeric Human/Dog-DNA Vaccine against CSPG4 Induces Immunity with Therapeutic Potential in Comparative Preclinical Models of Osteosarcoma. *Molecular Therapy* **2023**, *31*, 2342–2359, doi:10.1016/J.YMTHE.2023.06.004.

145. Ruiu, R.; Barutello, G.; Arigoni, M.; Riccardo, F.; Conti, L.; Peppino, G.; Annaratone, L.; Marchiò, C.; Mengozzi, G.; Calogero, R.A.; et al. Identification of TENM4 as a Novel Cancer Stem Cell-Associated Molecule and Potential Target in Triple Negative Breast Cancer. *Cancers (Basel)* **2021**, *13*, 1–25, doi:10.3390/CANCERS13040894.

146. Liu, J.; Xia, X.; Huang, P. XCT: A Critical Molecule That Links Cancer Metabolism to Redox Signaling. *Molecular Therapy* **2020**, *28*, 2358, doi:10.1016/J.YMTHE.2020.08.021.

147. Garcia-Manero, G.; Jabbour, E.J.; Konopleva, M.Y.; Daver, N.G.; Borthakur, G.; DiNardo, C.D.; Bose, P.; Patel, P.; Komrokji, R.S.; Shastri, A.; et al. A Clinical Study of Tomaralimab (OPN-305), a Toll-like Receptor 2 (TLR-2) Antibody, in Heavily Pre-Treated Transfusion Dependent Patients with Lower Risk Myelodysplastic Syndromes (MDS) That Have Received and Failed on Prior Hypomethylating Agent (HMA) Therapy. *Blood* **2018**, *132*, 798–798, doi:10.1182/BLOOD-2018-99-119805.

148. Shitara, K.; Doi, T.; Nagano, O.; Imamura, C.K.; Ozeki, T.; Ishii, Y.; Tsuchihashi, K.; Takahashi, S.; Nakajima, T.E.; Hironaka, S.; et al. Dose-Escalation Study for the Targeting of CD44v+ Cancer Stem Cells by Sulfasalazine in Patients with Advanced Gastric Cancer (EPOC1205). *Gastric Cancer* **2017**, *20*, 341–349, doi:10.1007/S10120-016-0610-8.

149. Mastall, M.; Roth, P.; Bink, A.; Fischer Maranta, A.; Läubli, H.; Hottinger, A.F.; Hundsberger, T.; Migliorini, D.; Ochsenbein, A.; Seystahl, K.; et al. A Phase Ib/II Randomized, Open-Label Drug Repurposing Trial of Glutamate Signaling Inhibitors in Combination with Chemoradiotherapy in Patients with Newly Diagnosed Glioblastoma: The GLUGLIO Trial Protocol. *BMC Cancer* **2024**, *24*, doi:10.1186/S12885-023-11797-Z.

150. Otsubo, K.; Nosaki, K.; Imamura, C.K.; Ogata, H.; Fujita, A.; Sakata, S.; Hirai, F.; Toyokawa, G.; Iwama, E.; Harada, T.; et al. Phase I Study of Salazosulfapyridine in Combination with Cisplatin and Pemetrexed for Advanced Non-Small-Cell Lung Cancer. *Cancer Sci* **2017**, *108*, 1843–1849, doi:10.1111/cas.13309.

151. Rovero, S.; Amici, A.; Carlo, E. Di; Bei, R.; Nanni, P.; Quaglino, E.; Porcedda, P.; Boggio, K.; Smorlesi, A.; Lollini, P.-L.; et al. DNA Vaccination Against Rat Her-2/Neu P185 More Effectively Inhibits Carcinogenesis Than Transplantable Carcinomas in Transgenic BALB/c Mice . *The Journal of Immunology* **2000**, *165*, 5133–5142, doi:10.4049/JIMMUNOL.165.9.5133.

152. Liu, S.; Chen, H. Isolation of Primary Breast Cancer Cells from HER2 Transgenic Mice. *Iss* **2016**, *6*, doi:10.21769/BioProtoc.1956.

153. Geninatti Crich, S.; Cadenazzi, M.; Lanzardo, S.; Conti, L.; Ruiu, R.; Alberti, D.; Cavallo, F.; Cutrin, J.C.; Aime, S. Targeting Ferritin Receptors for the Selective Delivery of Imaging and Therapeutic Agents to Breast Cancer Cells. *Nanoscale* **2015**, *7*, 6527–6533, doi:10.1039/C5NR00352K.

154. Lee, S.-J.; Kim, H.-J.; Huh, Y.-M.; Kim, I.W.; Jeong, J.H.; Kim, J.-C.; Kim, J.-D. Functionalized Magnetic PLGA Nanospheres for Targeting and Bioimaging of Breast Cancer. *J Nanosci Nanotechnol* **2017**, *18*, 1542–1547, doi:10.1166/JNN.2018.14220.

155. Ferrauto, G.; Tripepi, M.; Di Gregorio, E.; Bitonto, V.; Aime, S.; Delli Castelli, D. Detection of U-87 Tumor Cells by RGD-Functionalized/Gd-Containing Giant Unilamellar Vesicles in Magnetization Transfer Contrast Magnetic Resonance Images. *Invest Radiol* **2021**, *56*, 301–312, doi:10.1097/RLI.0000000000000742.

156. Grange, C.; Geninatti-Crich, S.; Esposito, G.; Alberti, D.; Tei, L.; Bussolati, B.; Aime, S.; Camussi, G. Combined Delivery and Magnetic Resonance Imaging of Neural Cell Adhesion Molecule-Targeted Doxorubicin-Containing Liposomes in Experimentally Induced Kaposi's Sarcoma. *Cancer Res* **2010**, *70*, 2180–2190, doi:10.1158/0008-5472.CAN-09-2821/655702/P/COMBINED-DELIVERY-AND-MAGNETIC-RESONANCE-IMAGING.

157. Abraham, S.A.; Waterhouse, D.N.; Mayer, L.D.; Cullis, P.R.; Madden, T.D.; Bally, M.B. The Liposomal Formulation of Doxorubicin. *Methods Enzymol* **2005**, *391*, 71–97, doi:10.1016/S0076-6879(05)91004-5.

List of publications related to this thesis

1. "The Role of the Toll-like Receptor 2 and the cGAS-STING Pathways in Breast Cancer: Friends or Foes?" Chiara Cossu, **Antonino Di Lorenzo**, Irene Fiorilla, Alberto Maria Todesco, Valentina Audrito, Laura Conti. Int J Mol Sci. 2023 Dec 29;25(1):456. doi: 10.3390/ijms25010456

2. "RGD_PLGA Nanoparticles with Docetaxel: A Route for Improving Drug Efficiency and Reducing Toxicity in Breast Cancer Treatment" Di Gregorio Enza Di, Romiti Chiara, **Di Lorenzo Antonino**, Cavallo Federica, Ferrauto Giuseppe, Conti Laura (2022). CANCERS, vol. 15, p. 1-24, ISSN: 2072-6694, doi: 10.3390/cancers15010008

3. "Immunotherapy against the Cystine/Glutamate Antiporter xCT Improves the Efficacy of APR-246 in Preclinical Breast Cancer Models" Barutello Giuseppina, **Di Lorenzo Antonino**, Gasparetto Alessandro, Galiazzi Chiara, Bolli Elisabetta, Conti Laura, Cavallo Federica (2022). BIOMEDICINES, vol. 10, p. 1-17, ISSN: 2227-9059, doi: 10.3390/biomedicines10112843

4. "Toll-like receptor 2 promotes breast cancer progression and resistance to chemotherapy" **Antonino Di Lorenzo**, Elisabetta Bolli, Roberto Ruiu, Giuseppe Ferrauto, Enza Di Gregorio, Lidia Avalle, Aurora Savino, Pietro Poggio, Irene Fiore Merighi, Federica Riccardo, Mara Brancaccio, Elena Quaglino, Federica Cavallo & Laura Conti (2022), OncoImmunology, 11:1, DOI: 10.1080/2162402X.2022.2086752

5. "Are Cancer Stem Cells a Suitable Target for Breast Cancer Immunotherapy?" Roberto Ruiu, **Antonino Di Lorenzo**, Federica Cavallo and Laura Conti. Front. Oncol., 21 April 2022 | https://doi.org/10.3389/fonc.2022.877384

6. "Toll-Like Receptor 2 at the Crossroad between Cancer Cells, the Immune System, and the Microbiota" **Di Lorenzo, A.**; Bolli, E.; Tarone, L.; Cavallo, F.; Conti, L. Int. J. Mol. Sci. 2020, 21, 9418. doi.org/10.3390/ijms21249418

7. "Immunotargeting of the xCT Cystine/Glutamate Antiporter Potentiates the Efficacy of HER2-Targeted Immunotherapies in Breast Cancer" Laura Conti, Elisabetta Bolli, **Antonino Di Lorenzo**, Valentina Franceschi, Francesca Macchi, Federica Riccardo, Roberto Ruiu, Luca Russo, Elena Quaglino, Gaetano Donofrio and Federica Cavallo. Cancer Immunol Res August 1 2020 (8) (8) 1039-1053; DOI: 10.1158/2326-6066.CIR-20-0082

List of publications not related to this thesis

1. "Cross-Reactive Immune Response of Bovine Coronavirus Spike Glycoprotein to SARS-CoV-2 Variants of Concern" Chiara Cossu, Valentina Franceschi, Antonino Di Lorenzo, Elisabetta Bolli, Sergio Minesso, Camilla Cotti, Laura Conti, Gaetano Donofrio. Int J Mol Sci. 2024 Oct 26;25(21):11509. doi: 10.3390/ijms252111509.

2. "A Magnetic Resonance Imaging - Chemical Exchange Saturarion Transfer (MRI-CEST) method for the detection of water cycling across cellular membranes" Enza Di Gregorio, Chiara Papi, Laura Conti, **Antonino Di Lorenzo**, Eleonora Cavallari, Marco Salvatore, Carlo Cavaliere, Giuseppe Ferrauto, Silvio Aime. Angew. Chem. Int. Ed.2023, e202313485 doi.org/10.1002/anie.202313485

3. "Assessment of BoHV-4-based vector vaccine intranasally administered in a hamster challenge model of lung disease" Seok-Chan Park, Laura Conti, Valentina Franceschi, Byungkwan Oh, Myeon-Sik Yang, Gaeul Ham, **Antonino Di Lorenzo**, Elisabetta Bolli, Federica Cavallo, Bumseok Kim, Gaetano Donofrio (2022) Front Immunol. 2023 Jul 6;14:1197649. doi: 10.3389/fimmu.2023.1197649

List of activities performed during the PhD program

Abstracts presented in conference proceedings

- **(2024) –** "How to improve the efficacy of breast cancer immunotherapy? A TLR2 targeting approach" **Antonino Di Lorenzo**, Chiara Cossu, Elisabetta Bolli, Enza Di Gregorio, Chiara Romiti, Alessandro Amaolo, Lidia Avalle, Valentina Franceschi, Federica Cavallo, Gaetano Donofrio, Giuseppe Ferrauto, Laura Conti. 24th international conference in vaccination against cancer (PIVAC-24) September 26-28 2024, Prague, Czech Republic. (Abstract selected for oral presentation)

- **(2024) –** "Targeting Toll-like Receptor 2 improves therapy efficacy in breast cancer by disrupting the pro-tumoral crosstalk between cancer cells and tumor microenvironment" **Antonino Di Lorenzo**, Chiara Cossu, Elisabetta Bolli, Valentina Franceschi, Giuseppe Ferrauto, Enza Di Gregorio, Chiara Romiti, Alessandro Amaolo, Gaetano Donofrio, Federica Cavallo, Laura Conti.

European Association for Cancer Research (EACR) Conference "The tumor ecosystem: cellular interactions and therapeutic opportunities" 19-21 March 2024, Bergamo, Italy (Abstract selected for poster presentation)

- **(2023) –** "Exploiting TLR2 and the cystine/glutamate antiporter xCT to develop a new combined therapy for breast cancer" **Antonino Di Lorenzo**, Elisabetta Bolli, Federica Cavallo, Laura Conti. European Association for Cancer Research (EACR) Congress 12-15 June 2023, Turin, Italy (Abstract selected for poster presentation)

- **(2022) –** "Targeting the crosstalk between TLR2 and the cystine/glutamate antiporter xCT as a new strategy to improve breast cancer treatment" **Antonino Di Lorenzo**, Elisabetta Bolli, Federica Cavallo and Laura Conti. Department of Molecular Biotechnology and Health Sciences, University of Turin, Turin, Italy. 21st international conference in vaccination against cancer (PIVAC-22) 26-28 September 2022. (Abstract selected for poster presentation)

- **(2022) –** "Toll-like Receptor 2 promotes breast cancer progression and resistance to chemotherapy" **Antonino Di Lorenzo**, Elisabetta Bolli, Federica Cavallo, Laura Conti. European Association for Cancer Research (EACR) 28th Congress 20-23 June 2022, Seville, Spain (Abstract selected for poster presentation)

- **(2022) –** "Targeting the crosstalk between TLR2 and the cystine/glutamate antiporter xCT to design a new strategy for breast cancer treatment" **Antonino Di Lorenzo**, Elisabetta Bolli, Federica Cavallo, Laura Conti. 33rd Pezcoller Symposium 13-14 June 2022, Trento, Italy (Abstract selected for poster presentation)

- **(2022) –** "Toll-like Receptor 2 promotes breast cancer progression and resistance to chemotherapy" **Antonino Di Lorenzo**, Elisabetta Bolli, Federica Cavallo, Laura Conti. Società Italiana di Immunologia Clinica e Allergologia (SIICA) congress 2022 National Congress 23-26 May 2022, Naples, Italy (Abstract selected for poster presentation)

- **(2021) –** "Targeting the crosstalk between TLR2 and the cystine/glutamate antiporter xCT as a new combined therapy for breast cancer" **Antonino Di Lorenzo**, Elisabetta Bolli, Federica Cavallo, Laura Conti. Virtual XIX NIBIT (Network Italiano per la Bioterapia dei Tumori) meeting, 14-15 October 2021. (Abstract selected for oral presentation)

- **(2021) –** "Toll-like Receptor 2 upregulates the cystine-glutamate antiporter xCT in breast cancer, and their combined inhibition synergistically hinders cancer progression" **Antonino Di Lorenzo**, Elisabetta Bolli, Federica Cavallo, Laura Conti. European Association for Cancer Research (EACR) 2021 Virtual Congress 9-12 June 2021. (Abstract selected for e-poster presentation)

- **(2021)** – "Targeting the cystine/glutamate antiporter xCT and Mutant-p53 synergistically hinders breast cancer progression" **Antonino Di Lorenzo**, Giuseppina Barutello, Alessandro Gasparetto, Federica Cavallo, Laura Conti. Società Italiana di Immunologia Clinica e Allergologia (SIICA) 2021 National Congress, Virtual event 26-28 May 2021. (Abstract selected for e-poster presentation)

- **(2021) –** "Toll-Like Receptor 2 targeting impairs breast cancer progression and overcomes resistance to chemotherapy" **Antonino Di Lorenzo**, Elisabetta Bolli, Elena Quaglino, Roberto Ruiu, Federica Cavallo, Laura Conti. CancerTo 2021, Webinar Unito-Polito conference series, Nanosciences in cancer immunotherapy 9-11 March 2021. (Abstract selected for oral presentation)

- **(2021)** – "Anti-xCT vaccination targets cancer stem cells (CSCs) improving HER2-targeted immunotherapies efficacy in breast cancer" **Antonino Di Lorenzo**, Elisabetta Bolli, Valentina Franceschi, Francesca Macchi, Federica Riccardo, Roberto Ruiu, Luca Russo, Elena Quaglino, Gaetano Donofrio, Federica Cavallo, Laura Conti. European Association for Cancer Research Conference "Defence is the Best Attack: Immuno-Oncology Breakthroughs" Virtual event, Worldwide, 16 - 17 February 2021. (Abstract selected for e-poster presentation)

Abstracts in conference proceedings (presented by co-author)

- **(2023)** – "Exploiting the crosstalk between TLR2 and the cystine/glutamate antiporter xCT for the development of a new combined therapy for breast cancer" Chiara Cossu, **Antonino Di Lorenzo**, Elisabetta Bolli, Valentina Franceschi, Gaetano Donofrio, Federica Cavallo and Laura Conti. PIVAC23, Athens, 28-30 September 2023.

- **(2023) –** "Targeting Toll-Like Receptor 2 and the cystine-glutamate antiporter xCT for enhanced immunotherapy in preclinical models of breast cancer" **Antonino Di Lorenzo**, Chiara Cossu, Elisabetta Bolli, Valentina Franceschi, Ilaria Badoglio, Giulia Dessì, Gaetano Donofrio, Laura Conti. Seventh International Cancer Immunotherapy Conference: Translating Science into Survival. SEPTEMBER 20-23, 2023. MILAN, ITALY

- **(2023)** – "Nanoparticles containing chemotherapeutic drugs and TLR2 inhibitors improve drug efficiency and reduce toxicity in preclinical models of mammary cancer" Chiara Cossu, Enza Di Gregorio, Chiara Romiti, **Antonino Di Lorenzo**, Alessandro Amaolo, Federica Cavallo, Giuseppe Ferrauto and Laura Conti. EACR 2023 Congress: Innovative Cancer Science, Turin, 12-15 June 2023

- **(2023)** – "Toll-like Receptor 2-targeted therapies ameliorate the efficacy of chemo- and immunotherapies in breast cancer models" **Antonino Di Lorenzo**, Elisabetta Bolli, Giuseppe Ferrauto, Enza Di Gregorio, Lidia Avalle, Chiara Cossu, Valentina Franceschi, Gaetano Donofrio, Federica Cavallo, Laura Conti. Società Italiana di Immunologia Clinica e Allergologia (SIICA) congress 2023 National Congress 22-25 May 2023, Verona, Italy

- **(2023)** – "Innovative targeted nanosystems for diagnosis and treatment of triple negative breast cancer" Alessandro Amaolo, Chiara Romiti, **Antonino Di Lorenzo**, Laura Conti, Giuseppe Ferrauto, Enza Di Gregorio. 18th European Molecular Imaging Meeting | EMIM 2023, Salsburg, Austria, March 14-17, 2023

- **(2022)** – "Targeting Toll-like Receptor 2 to tackle breast cancer resistance to therapy" Chiara Cossu, Laura Conti, **Antonino Di Lorenzo**, Elisabetta Bolli. 21st International Conference on Progress In Vaccination Against Cancer (PIVAC-22), Turin 26-28 September 2022

- **(2022)** – "Targeting Toll-like Receptor 2 to tackle breast cancer resistance to therapy" **Antonino Di Lorenzo**, Elisabetta Bolli, Roberto Ruiu, Giuseppe Ferrauto, Enza Di Gregorio, Lidia Avalle, Aurora Savino, Pietro Poggio, Irene Fiore Merighi, Federica Riccardo, Mara Brancaccio, Elena Quaglino, Federica Cavallo, Laura Conti. 33rd Pezcoller Meeting. Trento 13 - 14 June 2022

- **(2021)** – "Toll-Like Receptor 2 Promotes Breast Cancer Progression and Resistance to Chemotherapy" Laura Conti, **Antonino Di Lorenzo**, Elisabetta Bolli, Giuseppe Ferrauto, Enza Di Gregorio, Elena Quaglino, Federica Cavallo XIX Virtual NIBIT Meeting, October 14-15 2021

- **(2021)** – "Targeting Toll-like Receptor 2 to tackle breast cancer resistance to therapy" Laura Conti, **Antonino Di Lorenzo**, Elisabetta Bolli. EACR 2021 Congress, Innovative Cancer Science: Better Outcomes through Research. 09 - 12 June 2021.

- **(2021)** – "Targeting Toll-like receptor 2 (TLR2) to impair breast cancer progression and resistance to chemotherapy" **Antonino Di Lorenzo**, Elisabetta Bolli, Elena Quaglino, Roberto Ruiu, Federica Cavallo, Laura Conti. XII SIICA 2021 NATIONAL CONGRESS, Virtual Edition, 26-28 May 2021

- **(2020)** – "Immunotargeting of the xCT cystine/glutamate antiporter potentiates the efficacy of Her2-targeted immunotherapies in breast cancer" Laura Conti, Elisabetta Bolli, **Antonino Di Lorenzo**, Valentina Franceschi, Francesca Macchi, Federica Riccardo, Luca Russo, Roberto Ruiu, Elena Quaglino, Gaetano Donofrio and Federica Cavallo. CANCERTO: Nanosciences in Cancer Immunotherapy. Turin November 16-18, 2020

Seminars and trainings attended during the PhD course

- "Basics of project writing" 2 hours, Università di Torino (01/02/2021)

- "Corso di formazione in materia di igiene e sicurezza" 12 hours, Università di Torino (21/06/2021)

- "Beyond immune checkpoint blockade: emerging strategies. Prof. Tak W. Mak, F.P. of Immunology Toronto" Prof. Paola Cappello (07/09/2021)

- "On the control of female fidelity – How p63 controls female germline fidelity. Prof. Gerry Melino, F.P. of Biochemistry, Rome" Prof. Paola Cappello (07/09/2021)

- Online seminar of prof. Sandra Demaria, 7th December, 2021. Title: "Radiation-induced re-programming of the tumor immune contexture"

- Online seminar of prof. Raffaele De Palma, 10th March, 2022. Title: "Notch derived signals determine tissue inflammation in COVID-19"

- Seminar of prof. Nadia Carlesso, 27th April 2022, MBC Aristotele room. Title: "Reacting to Inflammatory Stimuli: Notch and TLR4 Tailor Hematopoiesis in the Bone Marrow Niche"
- Webinar "Guido Tarone symposium", 16th May, 2022.

- "Metodologia delle Revisioni Sistematiche-Meta Analisi" 8 giugno 2023 (h 14-18) Università di Torino, Via Accademia Albertina 13 (room C), by Dr. Carlo Di Pietrantonj

- “Course for PhD students – Hallmarks of aging” May 2nd, h 14-17, Leonardo hall, May 5th, h 14-17 Galileo hall, Molecular Biotechnology Center, University of Turin, by Marco Demaria

Acknowledgments

At the end of this journey, I can confidently say that pursuing a PhD is a true challenge. My PhD story is a blend of experiences and emotions. I began this journey with great motivation, curiosity, and excitement about growing as a scientist. I consider myself fortunate because, for most of these years, I did not encounter major crises and things generally went well. Nevertheless, the PhD remains a demanding period, and towards the final stages, I often felt really tired. However, I have never regretted this choice, and I am proud to be closing this chapter. A PhD is not only a profound scientific training experience but also a significant personal growth journey. It has taught me to always seek solutions in the face of challenges and to persist despite repeated failures. It has shown me that perseverance and dedication are essential to achieving meaningful results. In the end, I am proud not only of my successes but also of every single failure, as they were necessary steps along the path to greater achievements.

One of the most important aspects of this experience is that I was never alone. For this reason, I would like to express my heartfelt gratitude to all the people who have accompanied me on this journey.

I sincerely thank my supervisors, Prof. Federica Cavallo and Prof. Laura Conti.
Thank to Prof. Federica Cavallo for giving me the opportunity to be part of her research group, first as a master's student and then as a PhD candidate. Her trust, guidance, and support have been invaluable throughout this journey.
I am grateful to Prof. Laura Conti, who has been there with me every step of the way. Every day in the lab, I knew I could rely on her for help, encouragement, and advice. Working with her has truly been one of the best parts of these past years.

My PhD experience would not have been the same without my colleagues. I want to thank my lab mates and friends, Giulia, Lidia, Chiara, and Antonella. Together, we are like a family, always supporting one another, sharing both the toughest and the happiest moments. I feel lucky to have you in my life.

I thank the other members of our research group: Prof. Elena Quaglino, Dr. Irene Merighi, Dr. Federica Riccardo, Dr. Elisabetta Bolli, Dr. Giuseppina Barutello, Zobia Arshad, and Dr. Roberto Ruiu, who was part of our team for most of this journey.

A special thank you goes to my family, whose unwavering support has been fundamental in every aspect of my life. I am also grateful to my friends and to everyone outside the lab who has been part of my journey.

Finally, my deepest thanks to Giulia, for standing by my side with love in every single moment.